In vitro and in cellulo profiling of a novel phosphorylated form of RAD51 at serine 97

Mohamad Alaouid

THESE DE DOCTORAT

NANTES UNIVERSITE

ECOLE DOCTORALE N° 605
Biologie-Santé
Spécialité : Biologie Moléculaire et Cellulaire, Biochimie

Par
Mohamad ALAOUID

Etude des mécanismes moléculaires et cellulaires de la modulation de la réparation de l'ADN par recombinaison homologue

La caractérisation *in cellulo* d'un nouveau site de phosphorylation, le résidu sérine 97 de RAD51

Thèse présentée et soutenue à Nantes, le 15 décembre 2023
Unité de recherche : US2B - Unité en Sciences Biologiques et Biotechnologies UMR CNRS 6286

Rapporteurs avant soutenance :

Mauro MODESTI	Directeur de Recherche, CRCM, Université Aix-Marseille, France
Josée GUIROUILH-BARBAT	Chargée de Recherche à l'Institut Cochin, Paris, France

Composition du Jury :

Président :	Mauro MODESTI	Directeur de Recherche, CRCM, Université Aix-Marseille, France
Examinateurs :	Masayuki Takahashi	Directeur de Recherche, Institut de technologie de Tokyo, Japon
	Stéphane SUPIOT	Professeur à l'Institut de Cancérologie de L'Ouest, Nantes, France
Dir. de thèse :	Fabrice FLEURY	Professeur d'Université à Nantes Université
Co-dir. de thèse :	Houda BENHELLI	Maitre de Conférence à Nantes Université

I dedicate this thesis to my late mother, father, my wife and my son, Jad Alaouid..!

Acknowledgments

I'd like to begin by thanking **Collège de France** for funding my three-year PhD studies under the PAUSE program. I would also like to thank **l'École Doctorale Biologie-Santé** of Nantes and the **University of Nantes** for enabling me to conduct this thesis.

I would like to express my sincere appreciation to **Dr. Houda Benhelli-Mokrani**, a senior lecturer at the University of Nantes, and **Pr. Fabrice Fleury**, the team head of the DNA repair team at U2SB lab UMR CNRS 6286, for giving me the chance to pursue my Ph.D. I am grateful for their respect and trust in allowing me to lead my project, which motivated me to strive for success. Their unwavering care, kindness, understanding, and encouragement will always be remembered.

I express my gratitude to **Dr. Josée Guirouilh-Barbat** and **Dr. Mauro Modesti** for accepting to be the rapporteurs for my thesis. I also extend my thanks to the other members of my jury, **Pr. Stephane Supiot** and **Pr. Masayuki Takahashi**. I am grateful to all of them for their valuable contribution to evaluating my work.

I would like also to express my gratitude to all the members of Pr. Fabrice Fleury's team. It is no exaggeration to say that they are more than just a research team to me; they are like family in every sense of the word. I would like to extend a special thanks to **Franck**, **Pierre**, **Yvonnick**, **Cathy**, **Vanessa**, **Céline**, **Gwennina**, **Carine**, **Damien**, and **Pascal** for their care and support. Additionally, I would like to thank my previous officemates, **Thomas Chabot** and **Alexandre Demeyer**, who were kind, brilliant, and optimistic Ph.D. candidates. Their fun mood and valuable advice were greatly appreciated.

I would like to express my gratitude to my dear colleagues and lab partners, **Lucie Fonteneau** and **Nizar Ayadi**. They have been my constant companions on every lab journey, sharing in both my successes and failures. Thank you for your unwavering support and the wonderful memories we shared. I hope that you have a prosperous future ahead of you.

Furthermore, I extend my heartfelt thanks to my mom's pure spirit, great father, and dear sisters and brothers. Despite the suffering and brutality of the war in Syria that you lived in, you did not abandon my encouragement.

I would like to thank all the members of US2B Unite, especially Professor **Bernard Offmann**, the unit director, for his recommendation of Program PAUSE, besides Professor **Fabrice Fleury**.

I would like to express my deepest gratitude to my soulmate, dear wife, **Asmaa**, for her unwavering support and patience. Thank you for always being there for me. I am also grateful for my dear son **Jad Alaouid**, who is currently 22 months old. I wish him a wonderful life ahead. My wife and my son, thank you. I could not have done it without you.

Nantes, 08/10/2023

Table of Contents

List of Abbreviations

(6-4)PP	pyrimidine-pyrimidone (6-4) photoproducts
53BP1	Tumor protein p53 binding protein 1
8-oxo-dG	8-oxo-7,8-dihydro guanine
AAG	Alkyl Adenine DNA Glycosylases
Alt-NHEJ	Alternative End-Joining
AP sites	(Apurinic or Apyrimidinic sites)
APC/C	Anaphase-Promoting Complex/Cyclosome
APE1	(AP Endonuclease1)
ARG	ABL-related gene
AS	Alternative Splicing
ATM	(Ataxia telangiectasia, mutation)
ATP	Adenosine TriPhosphate
ATR	(ATM and Rad3-related)
AURKA	Aurora kinase A
AURKB	Aurora kinase B
AURKC	Aurora kinase C
BER	Base Excision Repair
BIR	Break-Induced Replication
BLM	Bloom syndrome protein
BRCA1	(Breast cancer type 1 susceptibility protein)
BRCA2	(Breast cancer type 2 susceptibility protein)
BRD4	Bromodomain-containing protein 4
CACClnc	(Chemoresistance Associated Colorectal Cancer lncRNA)
CBs	Cajal Bodies
Cdh1	Cadherin-1
CDKs	Cyclin-Depended Kinases
CFSs	Common Fragile Sites
CHAMP1	Chromosome Alignment-Maintaining Phosphoprotein 1
CHD4	Chromodomain Helicase DNA Binding Protein 4
CHK1	Checkpoint Kinase 1
CHK2	Checkpoint Kinase 2
Cisplatin	(cis-diamminedichloroplatinum(II))
CK2	Casein Kinase 2
C-NHEJ	Canonical non-homologous end-joining
CPC	Chromosomal Passenger Complex
CPT	Camptothecin
CRC	Colorectal Cancer
CTD	C-terminal domain
CtIP	C-terminal binding protein interacting protein
DBD	DSS1-binding domain
dHJs	double Holliday Junctions
D-loop	Displacement loop

DMC1	Disrupted Meiotic cDNA1
DNA-PKcs	DNA-dependent protein kinase, catalytic subunit
dNTP	deoxyribonucleoside triphosphate
DSBR	Double-Strand Break Recognizing
DSBs	Double-Strand Breaks
DSCs	DNA Structure Checkpoints
dsDNA	Double-stranded DNA
DSS1	Deleted in Split Hand/Split Foot Protein 1
E2F1	E2F transcription factor 1
EGR1	Early Growth Response 1
EMI1	Early Mitotic Inhibitor 1 protein
ETC	Electron Transport Chain
FANCR	Fanconi anemia of Complementation Group R
FRET	Fluorescence Resonance Energy Transfer
GPS	Group-based Prediction System
HDR	Homology-Directed Repair
HhH	Helix-hairpin-Helix motif
HRR	Homologous Recombination Repair
IGC	Interchromatin granule clusters
INCENP	Inner Centromere Protein
MCC	Mitotic Checkpoint Complex
MDC1	Mediator of DNA damage checkpoint protein 1
MEKK2	Mitogen-Activated Protein Kinase Kinase Kinase 2
MiDAS	Mitotic DNA synthesis
MMR	Mismatch repair
MRMV2	Congenital Mirror Movements-2 disorder
MRN complex	(MRE11, RAD50, NSB1)
MS	Mass spectrometry
NBS1	Nibrin
NE	Nuclear Export Signal motif
NEBD	Nuclear Envelope BreakDown
NER	Nucleotide Excision Repair
NLS	Nuclear Localization Signal motif
NS	Nuclear Speckles
NPF	NucleoProtein Filament
NTD	N-terminal domain
P53	Tumor protein p53
PALB2	(Partner and Localizer of BRCA2)
PARP-1	(poly(ADP ribose) polymerase-1)
PCC	Pearson Correlation Coefficient
PDB	Protein Data Bank
PIKKs	PhosphoInositide-3-Kinase-related Kinases
PLK1	Polo-Like Kinases-1
PM	Polymerization Motif

PNKP	PolyNucleotide Kinase/Phosphatase
POGZ	Pogo transposable element derived with ZNF domain
POI	Premature Ovarian Insufficiency
PTIP	Pax transactivation domain-interacting protein
PTMs	Post-Translational Modifications
RAD51	Radiation sensitive protein 51
RB	Retinoblastoma protein
RBPs	RNA-binding proteins
RecA	Recombinase A
RNAPII	RNA polymerase II
rNTPs	ribonucleoside tri-phosphate
ROCK1	Rho Associated Coiled-Coil Containing Protein Kinase 1
RPA	Replication Protein A
SACs	Spindle Assembly Checkpoints
SAM	S-AdenosylMethionine
SDSA	Synthesis-Dependent Strand Annealing
SF2	helicases superfamily 2
SF3B	Splicing factor 3B
SRM	Subunit Rotation Motif
snRNP	small nuclear RiboNucleoProtein
SSA	Single-Strand Annealing
SSBs	Single-Strand Breaks
SUMO	Small Ubiquitin-like Modifier
SWSAP1	SWIM-Type Zinc Finger 7-Associated Protein 1
TERRA	Telomeric-repeat-containing RNA
Tdp1	Tyrosyl DNA phosphatase1
TdT	Terminal Transferase
TNBCs	Triple-Negative Breast Cancer
TODRA	Transcribed in the Opposite Direction of RAD51
TOP 1	DNA Topoisomerase type I
TopIIIα	Topoisomerase IIIα
TOPORS	Topoisomerase 1-binding arginine/serine-rich protein
TSSs	Transcriptional Start Sites
Ub	Ubiquitin
UCHL3	Ubiquitin C-terminal Hydrolase L3
UDG	Uracil-DNA Glycosylase
UPS	Ubiquitin-Proteasome System
VRK1	Vaccinia-Related Kinase 1
WEE1	WEE1 G2 checkpoint kinase
XRCC2 / XRCC3	X-ray repair cross-complementing 2/ 3

List of figures

List of Tables

List of Appendices

I- Introduction

Chapter 1 DNA damage

1. Causes and types of DNA damage

It is estimated that each human cell is subjected to approximately 70,000 to 100,000 events of DNA damage per day [1,2]. Several reports have emphasized that DNA damage plays a crucial role in causing mutagenesis, carcinogenesis, and aging [3,4]. Generally, the factors that can cause damage to DNA fall under two main classes comprise endogenous and exogenous agents.

Endogenous factors originate from routine cellular processes, such as oxidative reactions involving Reactive Oxygen Species (ROS) [5]. Other sources of endogenous DNA damage include spontaneous base deamination, and the endogenous alkylating agents such as S-adenosylmethionine (SAM), a methyl donor in cellular methylation reactions [6]. Additionally, replication mistakes, replication stress, and DNA base mismatches during DNA replication are considered as sources of endogenous DNA damage [7].

Exogenous factors are external agents that include environmental and physical agents such as Ionizing Radiation (IR) and Ultraviolet radiation (UV). Chemical agents that come from dietary sources, tobacco smoke, industry, biomass burning, and chemotherapy agents such as alkylating agents (Cisplatin), radio mimetics (Bleomycin), and topoisomerase inhibitors (Camptothecin) are also considered exogenous factors [7–10].

Both internal and external factors can cause various types of DNA damage, including abasic sites, base deamination, base alkylation, DNA cross-linking, and single- and double-strand breaks [7,11].

In this section, I will discuss in more detail some of the well-known sources and types of DNA damage. Farther, I will also talk in greater detail about DNA double-strand breaks (DSBs) and the pathways for repairing them, represented by Non-Homologous End Joining (NHEJ), and Homologous Recombination (HR), in the subsequent sections.

Before delving into the details of DNA damage, a general overview can be obtained from Figure 1, which illustrates the causes and types of DNA damage along with pathways for repairing every kind of damage.

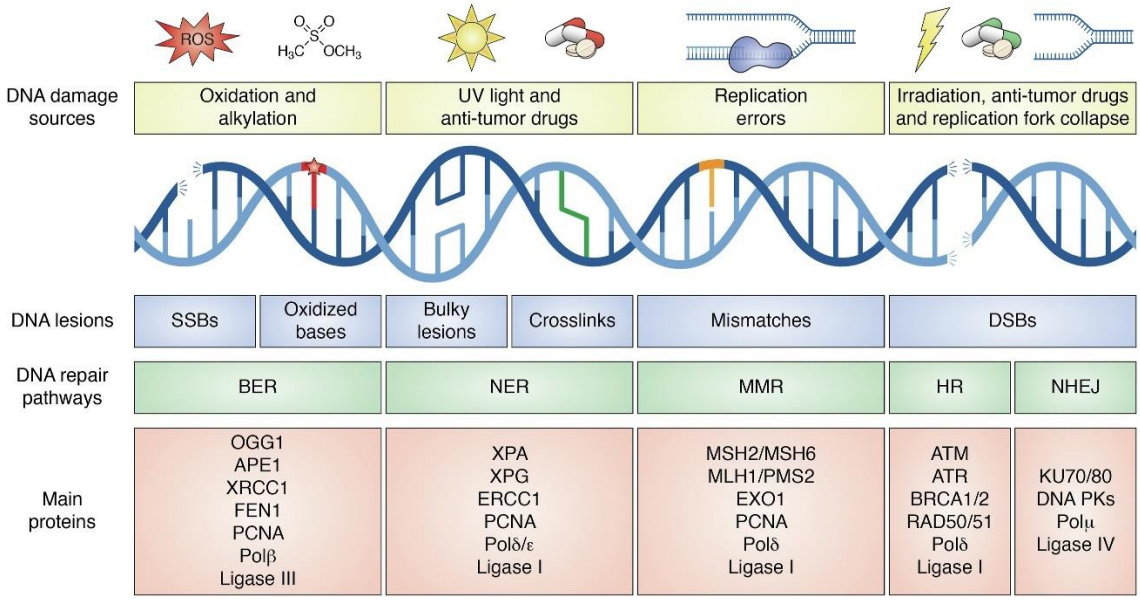

Figure 1 An overview of major DNA repair pathways and their significant proteins.

From the left to the right. The Base Excision Repair pathway (BER). A specific enzyme, OGG1, removes oxidized 8-oxoG bases, leaving an AP site. AP-endonuclease 1 processes AP sites into single-strand breaks. Polymerase delta, epsilon, and PCNA replace the base and additional nucleotides in long patch repair. Short patch repair involves Polβ replacing the missing base, LigIII ligates the DNA backbone, and XRCC1 aiding the process [12,13]. Next, the Nucleotide Excision Repair pathways (NER). This pathway involves excising 24-32 nucleotide DNA fragments containing the damaged lesion accurately, followed by reparative synthesis using the undamaged strand as a template, and ligation of the single strand break. NER has two pathways for initial damage recognition: transcription-coupled nucleotide excision repair (TC-NER) and Global genome nucleotide excision repair (GG-NER). TC-NER operates when damage to a transcribed DNA strand limits transcription activity, activated by the stalling of RNA polymerase II at the damaged sites. In contrast, GG-NER eliminates bulky damage in the entire genome [14,15]. After, the Mismatched repair (MMR) pathway involves several proteins that work together to recognize, excise, and resynthesize mismatched DNA base pairs. The MSH2/MSH6 complex identifies base-base mismatches, while the MLH1/PMS2 complex is responsible for nicking the mismatched base's 3'- or 5'-side on the discontinuous strand. The DNA segment resulting from this process is subsequently excised by the EXO1 exonuclease in collaboration with the single-stranded DNA-binding protein RPA. The DNA strand is then resynthesized by DNA polymerase δ and DNA ligase I [16,17]. On the Right, the HRR pathway and NHEJ repair the Double-Strand breaks (DSBs) will be discussed with more detail in Chapter 2. This figure was taken from [18].

1.1 Causes of DNA Damage

1.1.1 Oxidative DNA damage

During cellular respiration, the Electron Transport Chain (ETC) can generate Reactive Oxygen Species (ROS), including singlet oxygen ($^1O_2$), superoxide $(O_2)^{\bullet -}$, hydroxyl radicals ($^{\bullet}OH$), and hydrogen peroxide (H_2O_2). External causes like ionizing or UV radiation can also generate ROS (Section 1.1.2). Oxidative stress is an imbalance between ROS production and cellular antioxidant defense systems, damaging macromolecules like DNA, proteins, and lipids [19].

For example, hydroxyl radicals (•OH) caused the most common type of oxidative base damage by hydroxylation of the C-8 residue of guanine, forming 8-oxo-7,8-dihydro guanine (8-oxo-dG) adduct, each cell's DNA may experience up to 100,000 8-oxo-dG lesions per day, making this modification an oxidative stress marker. Elevated levels of 8-oxo-dG have been seen in some rare human diseases associated with impaired DNA repair mechanisms, including xeroderma pigmentosum, ataxia telangiectasia, Fanconi anemia, and Bloom's syndrome as reviewed in (*Cooke, M. S., et al.*) [5].

Moreover, ROS radicals can also lead to AP sites and harm the DNA's structural integrity, creating approximately 2300 single-strand breaks every hour per human cell [7].

Both BER and NER pathways remove oxidized damage before replication. BER eliminates single damage with a glycosylase enzyme, while NER removes an oligonucleotide containing the lesion [19] (Figure 1).

1.1.2 Radiations (IR and UV)

1.1.2.a- Ionizing radiation (IR)

Radiations are prevalent in our surroundings and comprise ionizing and non-ionizing radiations, which are fundamental parts of our environment. There are two types of ionizing radiation (IR): those that cause significant ionization (alpha and beta) are known as direct ionizing radiation; the radiation, here, directly impacts the DNA structure, causing DNA breaks, mainly Double-Strand Breaks (DSBs). Whereas the second type is indirect ionizing radiation, such as gamma, x-ray, and neutrons. In this type, radiation leads to radiolysis of the surrounding water or other molecules, creating a group of ROS that can damage DNA through oxidative stress, as explained earlier. Besides, this type of IR could induce Single-Strand Breaks (SSBs). It is worth noting that approximately 65% of the DNA damage caused by radiation is due to indirect damage from (•OH) radicals [7,20,21]. The SSBs are repaired through a process known as Single-Strand Break Repair (SSBR). This pathway is considered a specialized sub-pathway of the BER pathway, as it often involves proteins dedicated to BER [22]. In contrast, HR and NHEJ (Figure 1) are the main pathways to repair DSBs, as we will see in Chapter 2.

1.1.2.b- Ultraviolet radiation

Alternatively, non-ionizing forms (radio waves, microwaves, infrared, visible light, and ultraviolet light) do not eliminate electrons; thus, they do not disrupt atomic structures. However, ultraviolet light (UV) is radiation from the sun and other artificial sources. UV radiation targets cellular DNA,

causing photo-induced damage and mutations. However, DNA lesions' formation and chemical composition is heavily influenced by the wavelength of incoming photons.

On the one hand, UVB radiation is the most potent and mutagenic component of solar radiation. It is absorbed directly by DNA and leads to the creation of two primary types of damage: Cyclobutane pyrimidine dimers (CPD) account for 75% of the damage, while pyrimidine-pyrimidone (6-4) photoproducts ((6-4)PP) form the remaining 25%. On the other hand, UVA radiation cause oxidative DNA damage, primarily 8-oxo-dG [7].

However, cells have different repair pathways for UV lesions based on the type of lesion. These pathways include direct reversal of UV-damaged bases, interstrand cross-link repair, and NER, that can effectively repair the lesions (Figure 1) [23].

1.1.3 Replication stress

Replication stress occurs when the replication fork slows or stops, leading to stretches of single-stranded DNA due to polymerase stalling. Meanwhile, the replicative helicase continues to unwind the parental DNA [24,25]. Several factors can cause replication stress, including DNA lesions or adducts resulting from mutagens, UV radiation, ROS, and metabolic by-products. These factors can disrupt the replication forks, leading them to run off [25]. In the event of a cell's replication process stalling, it attempts to restart, but sometimes it fails and collapses. The collapse of the replication fork leads to DSBs, which can be repaired through HR with the help of CtIP and RAD51 [25,26] (will be addressed in Chapter 2).

1.1.4 Replication errors and DNA base mismatches

Three significant errors can occur during DNA replication: Base substitutions (mismatches), Deletions, and Insertions [27]. As a general rule, Proofreading allows DNA polymerases to check each base they add during DNA replication. Approximately one nucleotide is misincorporated in every 10^8 insertion events [28]. The occurrence of accidental incorporation of rNTPs (ribonucleoside tri-phosphate) is even higher due to their higher concentration (30-200 times) compared to dNTP (deoxyribonucleoside triphosphate) [29].

Moreover, most replication errors occur by tautomeric shifts. This arises because the purine and pyrimidine bases exist in different chemical forms, or tautomers, which have different proton positions in the molecule. Adenine and cytosine can be found in amino or imino forms. In contrast, guanine, thymine, and uracil can exist in lactam or lactim (enol) forms (detailed in Figure 2A).

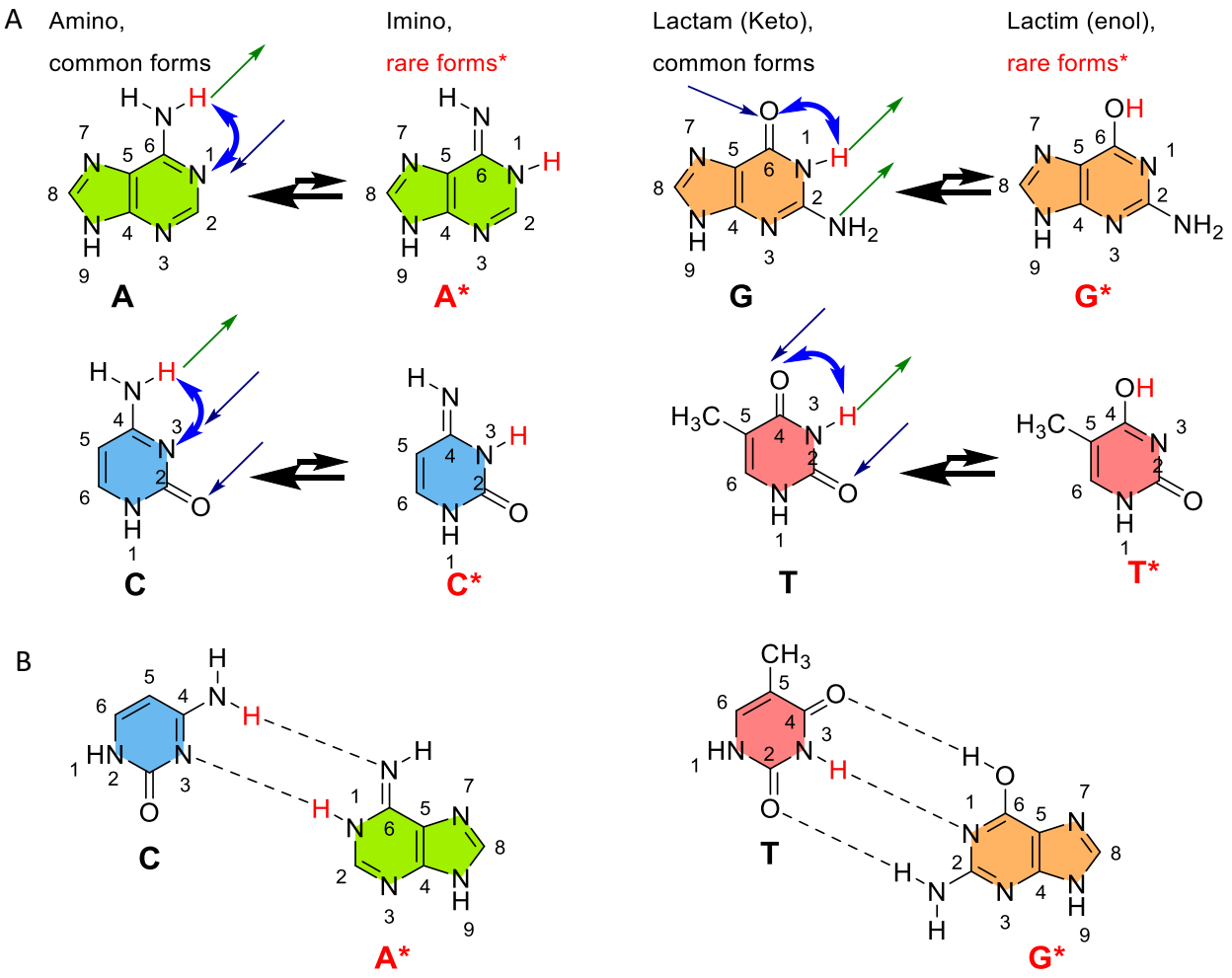

Figure 2 Base pair mismatching with the rare tautomeric forms of the four bases of DNA.

A) The purine and pyrimidine DNA bases can exist in at least two tautomeric forms. Adenine and cytosine shift from their common forms (amino) to their rare forms (imino), whereas guanine and thymine exist in either lactam (keto), common forms, or lactim (enol) rare forms. B) Rare base-pairing arrangements, adenine's rare form binds with cytosine's common form instead of guanine, while guanine's rare form binds with thymine's common form instead of cytosine. Asterisks and red coloring indicate rare forms. Double-ended blue arrows show the proton shift between the two tautomeric forms. Hydrogen donors are represented by green arrows, and hydrogen acceptor atoms in each nitrogen base are indicated by blue arrows. (*Alaouid. M's thesis)*

However, when a nucleotide base shifts into its rarer tautomeric form, it can result in base-pair mismatching. For example, imino-adenine, a tautomeric form of adenine, cannot pair with thymine but with cytosine. Conversely, enol-guanine, guanine's tautomeric form, binds more readily with thymine than cytosine. (Figure 2B) [30–32]. Fortunately, cells have mechanisms to correct errors during DNA replication, with 99% being fixed immediately through Proofreading. DNA polymerase enzymes identify and replace wrongly inserted nucleotides, while the mismatch

repair pathway corrects errors after replication. Uncorrected errors can lead to mutations, genetic disorders, aging, and cancer [30,33].

1.2 Types of DNA Damage

1.2.1 Abasic sites

Abasic sites, also called AP sites (Apurinic or Apyrimidinic sites), are DNA regions lacking either a purine or a pyrimidine base (Figure 3). They are ubiquitous DNA lesions that naturally form by spontaneous depurination, DNA deglycosylation, or as a step in the Base Excision Repair (BER) pathway [34]. Human cells form approximately 10,000 apurinic and 500 apyrimidinic sites every day. However, extreme pH and high temperatures favorably impact their synthesis [7,35,36].

Fortunately, isolated AP sites can be quickly repaired using BER. Alternatively, BER-resistant AP lesions can be effectively removed *via* the Nucleotide Excision Repair pathway (NER) [37,38].

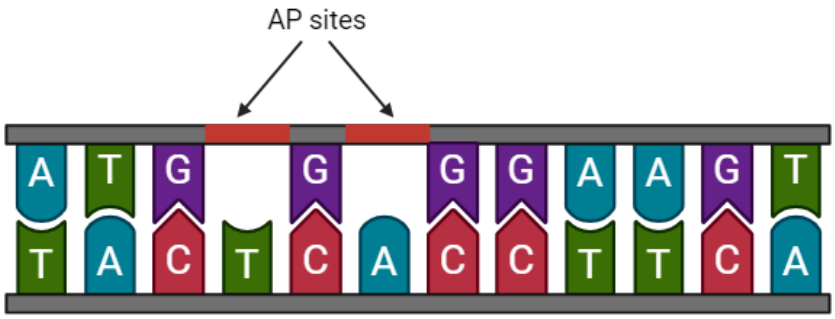

Figure 3 Representation of Apurinic and Apyrimidinic (AP) sites

(Alaouid. M's thesis)

1.2.2 Base deamination

Spontaneous base deamination is a significant cause of random mutations in human cells. It is a process in which nitrogenous bases (cytosine, adenine, guanine, and 5-methyl cytosine) are converted to other bases (uracil, hypoxanthine, xanthine, and thymine, respectively) by removing an amino group (Figure 4A). This process can also be triggered by deaminase enzyme activity, nitrosative stress, or other factors reviewed in (Shi K. *et al.)* [39].

Around 100-500 deoxycytidines undergo deamination in human cells daily, forming deoxyuridine (dU). However, adenine and guanine deamination rates are significantly slower than cytosine, with nearly 2-3% of cytosine deamination rate, making cytosine deamination appear more prominent. However, deoxyadenosine can transform into deoxyinosine (dI) (Figure 4B). During DNA replication, the (dI) base is misread as deoxyguanosine, causing a transition mutation by

inserting deoxycytidine. However, because (dI) and (dU) nucleosides are not part of DNA, they are removed from genomic DNA *via* BER, resulting in the formation of abasic sites (AP). DNA glycosylase enzymes such as Alkyl Adenine DNA Glycosylases (AAG) and Uracil-DNA Glycosylase (UDG) remove hypoxanthine and uracil, respectively (Figure 4B)[36,40,41].

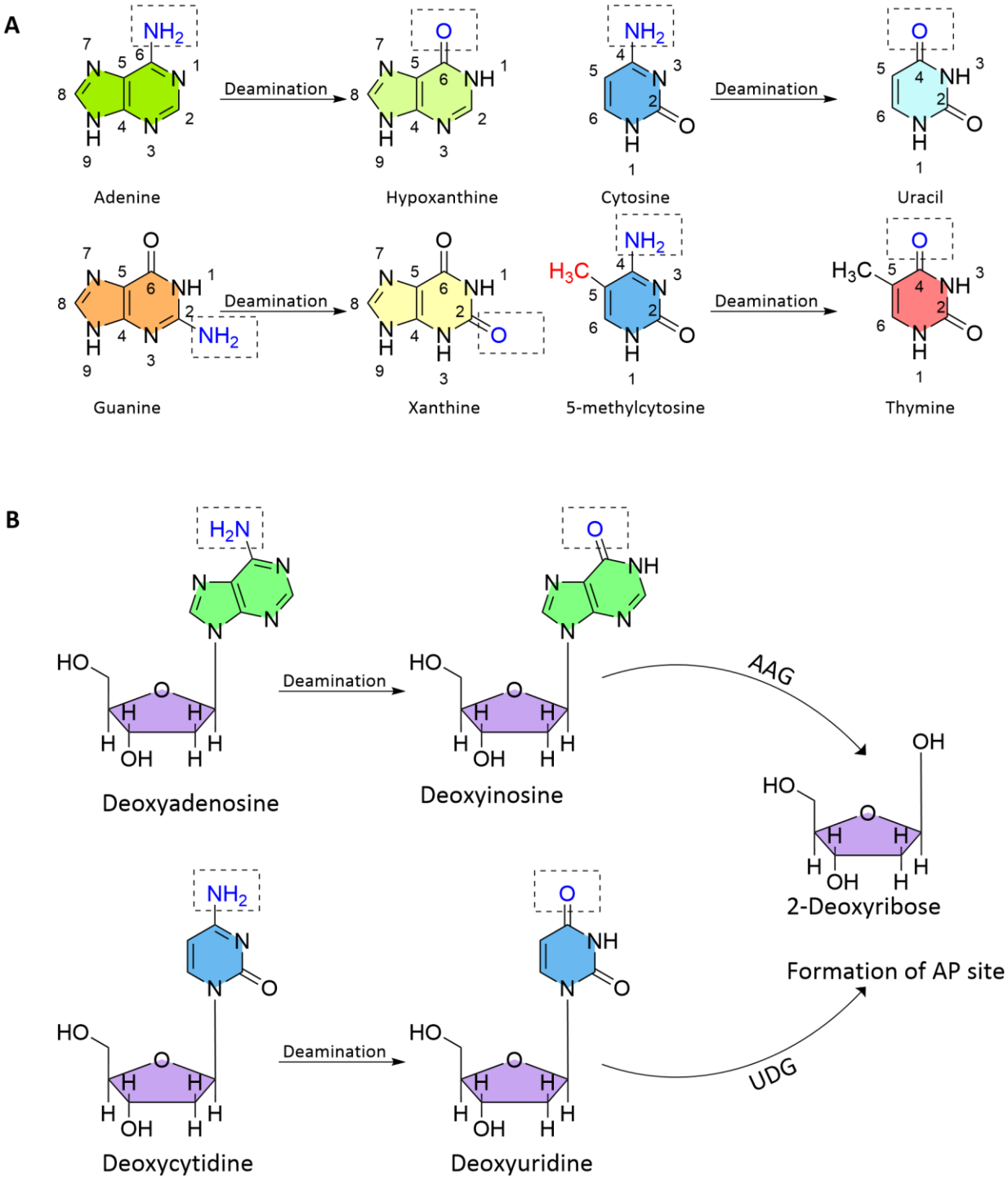

Figure 4 Spontaneous base deamination

A) DNA bases in their natural configuration include Adenine (A), guanine (G), cytosine (C), and 5-methylcytosine. Deamination converts them into hypoxanthine, xanthine, uracil, and thymine, respectively. B) Deoxyinosine and deoxyuridine are formed when deoxyadenosine and deoxycytidine are deaminated. The

Alkyl adenine DNA glycosylases (AAG) and uracil-DNA glycosylases (UDG) enzymes are used to eliminate these molecules, forming an AP site. (*Alaouid. M's thesis)*

1.2.3 Alkylation of bases

Alkylation is adding an alkyl group to nitrogenous bases, which can impair DNA or RNA's normal function. Alkylating agents are chemicals that can bond with electron-rich atoms. These agents can be produced by cellular metabolism, found in the environment, or synthesized for medical purposes such as cancer chemotherapy [5].

Alkylating agents, known as methylating agents, add a methyl group to biomolecules, such as DNA. Methyl transferases use S-AdenosylMethionine (SAM) as a methyl donor during typical methylation processes in mammals.

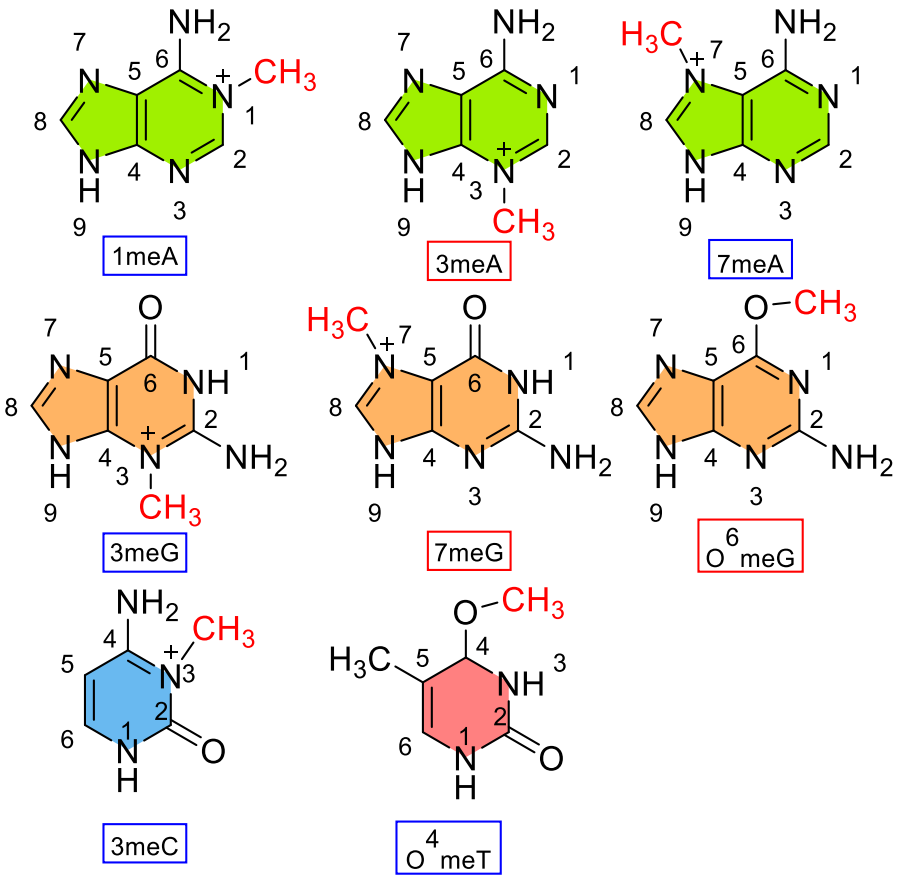

Figure 5 Methylated DNA bases.

Red boxes represent the three primary methylated bases, and blue boxes represent the minor ones (*Alaouid. M's thesis).*

Through this mechanism, SAM has the potential to spontaneously generate approximately 4000 N7-methylguanine (7meG), 600 N3-methyladenine (3meA), and 10-30 O^6-methylguanine (O^6meG) residues per cell daily. These alterations represent the three primary base changes introduced by methylating agents into double-stranded DNA, whereas N1-methyladenine (1meA) , N3-methylcytosine (3meC), N7-methyladenine (7meA), and O^4- methylthymine (O^4meT) are the more minor alterations. However, 1meA and 3meC are more common in single-stranded DNA than in double-stranded DNA[42] (Figure 5).

The O^6meG is the most mutagenic adduct that methylating agents may introduce into DNA because it could mispair with thymine during replication leading to G:C→A:T transition mutations [5,42]. However, methylated DNA adducts are eliminated through BER, NER, and Mismatch repair (MMR) pathways (Figure 1) [43].

1.2.4 DNA strand breaks

1.2.4.a- DNA single-strand breaks

DNA single-strand breaks (SSBs) are breaks in one double-helix strand. SSBs constitute about 10% of all DNA lesions in a genome. Approximately a mammalian cell experiences more than 10,000 SSBs daily under normal conditions. Unrepaired SSBs can develop into highly toxic double-strand breaks (DSBs) [44].

However, in a study on Chinese hamster fibroblasts, *Tounekti O. et al.* reported that SSBs are 300 times less toxic than DSBs, and more than 150 000 SSB lesions per cell are required to trigger apoptosis [44–46].

Huifen Cao et al. recently developed a genome-wide mapping technique with nucleotide-level resolution called SSiNGLe to identify SSB lesions [47]. This method directly tags 3'-OH termini of DNA breaks by adding polyA tails through Terminal Transferase (TdT). Interestingly, they uncovered that SSBs tend to occur more frequently in specific genome positions, creating SSBs hotspots (breakome). These hotspots appear in various cells of the same type and across different cell types. They also found that these hotspots tend to be enriched near Transcriptional Start Sites (TSSs) [47]. They thought that these hotspots could be generated by a novel mechanism, possibly involving preferential cleavage at cytosines. Alternatively, recent studies reviewed by (*Puc et al.,* 2017) [48] and (*Domingo-Prim et al.,* 2020) [49] have indicated a connection between DNA damage and gene expression regulation [47].

1.2.4.b- DNA double-strand breaks

When both complementary DNA strands break, it causes DSBs which cleave the helix into two halves. DSBs can occur due to exposure to external factors, like radiation and certain chemicals, or internal processes, such as DNA replication and repair. Besides, DSBs can occur naturally. For example, in meiosis I, cells intentionally create DSBs to prompt homologous recombination, which is crucial for proper chromosome segregation. T-lymphocytes and B-lymphocytes also undergo controlled DSB formation through V(D)J recombination mechanisms during T-cell receptor formation and immunoglobulin class switching (Reviewed by Cannan, W. J. et al. 2016) 50. Many CRISPR-Cas-based genome editing technologies also use Cas nucleases to cause DSBs at specific loci within a genome. The cellular DSB repair system must further process the DSBs to generate desirable mutations, sequence insertions, or gene deletions [51,52].

However, DSBs are the most dangerous type of DNA damage, and leaving it unrepaired can have serious consequences, including generating genomic instability, chromosomal abnormalities, and loss of genetic information, which often results in cell death [50]; hence, DSB repair reactions are strictly regulated, as will be described later in Chapter 2.

Moreover, In 1989, it was reported that the phosphorylation of H2AX on serine 139 (γ-H2AX) is a quick and sensitive cellular response to the presence of DSBs [53]. Since then, the γ-H2AX foci have been deemed essential for quantifying DSBs accurately. However, *Rybak et al.* (2016) found no correlation between low-level phosphorylation of γH2AX foci and the location of DSBs in cells exposed to topoisomerase I or II inhibitors. According to the results, low-level γH2AX formation is likely caused by factors other than DSBs and is characterized by small foci with few γH2AX moieties, while the larger foci likely indicate the presence of DSBs [54].

Notably, γH2AX can be detected in situations other than DNA damage response (DDR), such as apoptosis. However, the foci of γH2AX in the case of apoptosis are different from the well-known DDR γH2AX foci. In apoptosis, H2AX phosphorylation begins at the nuclear periphery within the nuclear envelope, whereas total H2AX remains dispersed throughout the nucleus. This mechanism is commonly called the "gamma-H2AX ring" and is apparent using immunofluorescence microscopy [55].

Recently, new methods have emerged to detect DSBs more accurately. One such technique is STRIDE, which uses BrdU, a synthetic thymidine analog, to detect DSBs through free 3'-OH DNA ends [56]. In 2023, Suh, J.-S. et al. created a DSB biosensor based on FRET (Fluorescence Resonance

Energy Transfer) that responds to γH2AX activity generated by medicine or radiation. This FRET biosensor-based imaging approach is highly accurate and enables real-time visualization of DSB events [57].

2. Induced damage for cancer treatment purposes and cancer resistance

2.1 Cancer and resistance to cancer therapy

Even before the structure of DNA was discovered, Dr. Theodor Boveri proposed in 1914 that cancer cells, which caused malignant tumors, came from the abnormal distribution of chromosomes in normal cells [58]. Later, during the 1980s, scientists described the process of carcinogenesis, where they identified that DNA mutations are caused by environmental mutagen exposure and the failure of effective DNA repair mechanisms [9].

Cancer cells can grow and spread by ignoring signals to undergo apoptosis. Genetic modifications in proto-oncogenes (such as Ras and Src genes), tumor suppressor genes (P53, BRCA1/2), and DNA repair genes (RAD51) can trigger abnormal cell growth and survival, known as "drivers" of cancer. For instance, P53 is dysfunctional in many cancer types; additionally, individuals who possess mutated variants in either the BRCA1 or BRCA2 genes are at a higher risk of developing various types of cancer, particularly breast and ovarian cancer, at a younger age [59]. Moreover, cancer cells can evade immune detection and have abnormal chromosomes [60].

The approach of using DNA damage to treat cancer has been in existence for more than a century. It began with radiation treatment for stomach cancer and DNA-damaging chemotherapy to treat childhood leukemia. Since then, the field of cancer treatment has advanced significantly. Radiotherapy and various anticancer chemotherapies have revolutionized the clinical management of cancer. Most cancer treatments still induce DNA damage, ultimately leading to cell death. Unfortunately, sometimes therapy-inducing DNA damage is not enough to kill cancer cells, where damage can be repaired through the DNA damage response and various pathways, leading to radio-chemotherapy resistance [61,62].

Healthy and cancer cells regulate responses to DNA damage and repair through gene expression, Post-Translational Modifications (PTMs), and controlling chromatin structure with DNA methylation and histone modifications. Cancer cells exploit these mechanisms to become resistant to treatment. Scientists are researching ways to overcome cancer cell resistance, including developing inhibitors that target critical DNA repair enzymes and studying the effects of

PTMs like phosphorylation on DNA repair. In the next section, I will discuss laboratory agents that commonly cause DNA damage and were used in my research.

2.2 DNA damage-inducing agents

2.2.1 Cisplatin

Platinum-based therapy is a highly effective treatment for many types of cancer [63]. Cisplatin (cis-diamminedichloroplatinum(II)) was discovered over 40 years ago and has been extensively researched to understand its mode of action. Cisplatin targets nuclear DNA by binding to purine bases at the N7 position, causing downstream effects such as inhibition of replication and transcription, cell cycle arrest, and triggering apoptosis in the fast-growing cancerous cells [64]. The primary cisplatin-DNA adducts are intrastrand cross-links, including approximately 65% 1,2-d (GpG), 25% 1,2-d (ApG), and 5–10% 1,3-d (GpNpG). In addition, a small percentage of interstrand cross-links are also formed, as shown in Figure 6 [63,65–67].

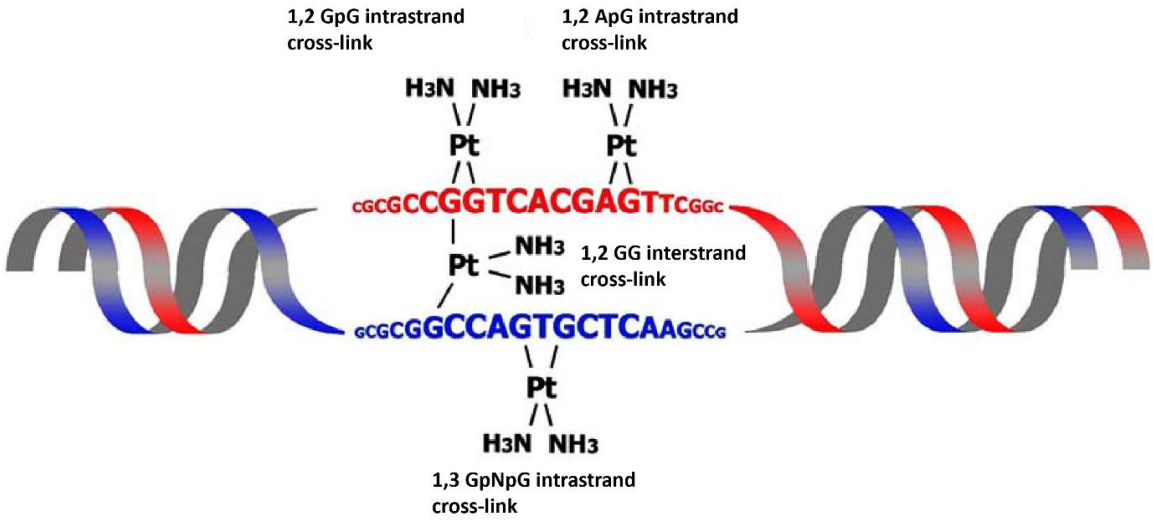

Figure 6 DNA interactions with Cisplatin.

When cisplatin [Pt(NH3)2Cl2] is introduced into the body, it undergoes aquation, where the chloride ions are replaced by water molecules, forming a highly electrophilic activated form. This form covalently binds to the N7 position of purine bases (adenine and guanine) in DNA. Purines located on the same strand can form an intrastrand crosslink, such as 1,2-d (GpG), 1,2-d (ApG), and 1,3-d (GpNpG). However, when they are on two different strands, they form an interstrand crosslink, known as 1,2 GG. The figure was taken from [67].

2.2.2 Camptothecin

Camptothecin (CPT), an alkaloid from the stem wood of the Chinese tree, *Camptotheca acuminata*, selectively inhibits DNA Topoisomerase type I (TOP 1) [68]. Topoisomerases are

enzymes that relieve torsional stress in DNA produced by replication, transcription, and other nuclear processes. Human TOP 1 cleaves a single DNA strand *via* transesterification of Tyr723 and forms a 3-phosphotyrosine linkage to DNA. The broken DNA strand can rotate around the unbroken strand and remove DNA supercoils after cleavage. CPT binds specifically to the covalent TOP 1-DNA complex (Figure 7), inhibiting religation and causing reversible accumulation of TOP 1-DNA adducts in vitro and *in-vivo* [69]. CPT stabilizes the enzyme-DNA complex, converting the TOP 1 enzyme into a DNA-damaging agent. Poisons from TOP 1 cause cytotoxic effects that are specific to the S-phase. In rapidly dividing cells, when the "trapped" TOP 1-DNA complex collides with the DNA replication fork, it leads to DSBs and apoptosis [70]. Moreover, CPT induces DSBs in non-dividing cells, such as neurons and normal lymphocytes, through a mechanism dependent on transcription rather than replication-mediated DNA damage [71,72].

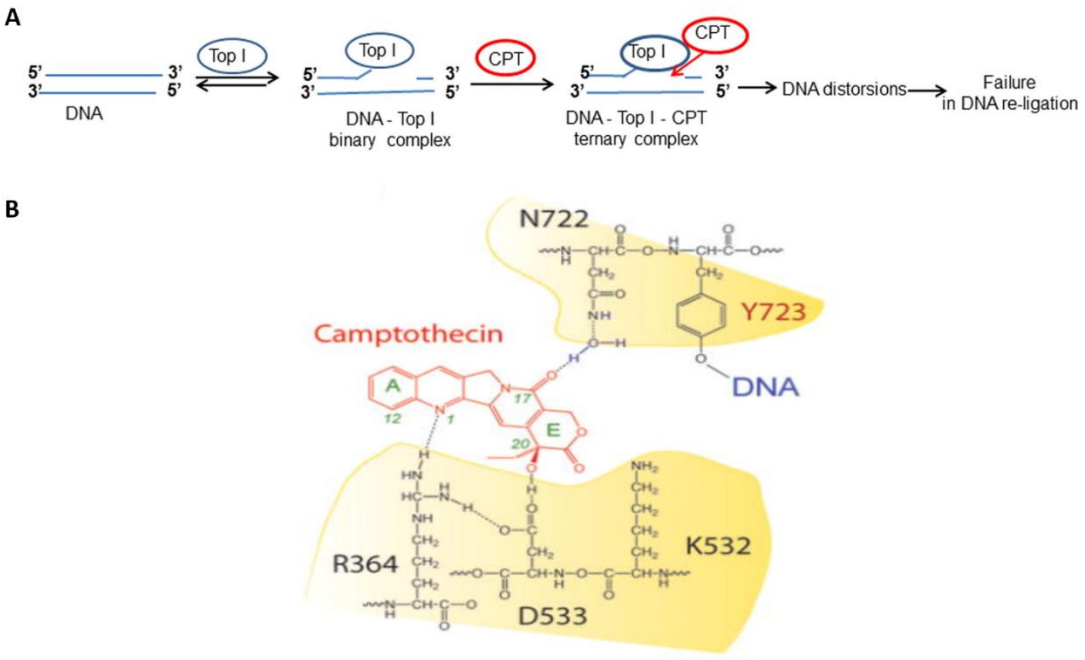

Figure 7 Mechanism of action of camptothecin.

A) Topoisomerase I (TOP I) normally cleave the phosphate backbone of the DNA strand, forming a transient binary TPO I-DNA complex. Camptothecin (CPT) binds to the DNA-TOP I complex through hydrogen bonding, forming a ternary complex (TOP I-DNA-CPT), which prevents both the re-ligation of the nicked DNA, causes a collision with the replication fork, and induces DNA double-strand breaks. B) Hydrogen bond network between TOP I amino acid residues (in yellow) and CPT. This figure was taken from [73,74].

Chapter 2 DNA DSBs Response and Repair

1. DSBs Response

As discussed in Chapter 1, Double-Stranded Breaks (DSBs) are the most harmful type of DNA damage. To combat this threat, cells have developed a surveillance system called DNA Damage Response (DDR), which comprises complex molecular pathways. In this Chapter, I will start by providing a short explanation of the cell cycle and its master mitotic kinases, as they are relevant to the findings of our work, which will be discussed in the results section. After that, I will briefly cover the DDR and repair pathways, focusing on DSBs.

1.1 Cell cycle and master mitotic kinases

The cell cycle is regulated by proteins called Cyclins and Cyclin-Depended Kinases (CDKs). Cyclins activate CDKs to move the cell cycle forward (Figure 10) [75]. However, Cyclin/CDK activity is triggered by mitogenic signals and inhibited by cell-cycle checkpoints in response to DNA damage [76].

Moreover, the Cell Division Cycle-25 (CDC25) family is a crucial group of cell cycle regulators. It includes three phosphatases: CDC25A, which facilitates the transition from G1 to S phase, and CDC25B and CDC25C, which play a major role in the progression from G2 to M phase. These phosphatases activate CDKs by removing inhibitory phosphorylation residues on the CDK active site (reviewed in [77]).

Furthermore, the regulation of mitotic events is realized by reversible phosphorylations mediated by master mitotic kinases, including CDKs, PLKs, and AURKs. These kinases work together to phosphorylate their substrates variably in space and time [78]. Here, I will briefly overview Aurora A kinase and Polo-Like Kinases-1 (Figure 8).

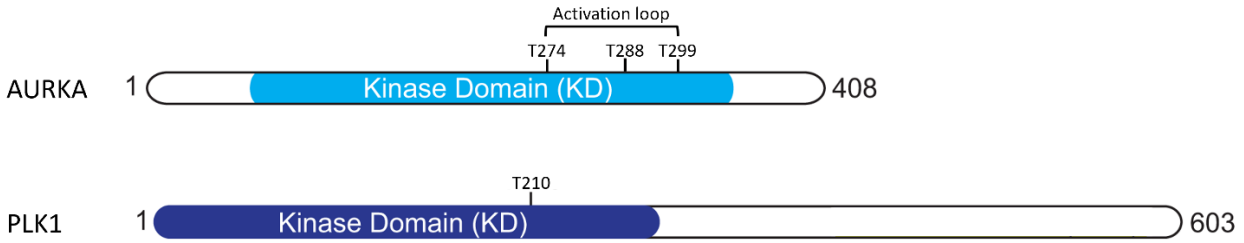

Figure 8 The domain structure of AURKA and PLK1

The activation loop phospho-regulatory sites of AURKA (T288) and Plk1 (T210) are labeled. This figure was derived from [79].

1.1.1 Aurora A kinase (AURKA)

Besides to CDKs, Aurora kinases are essential for cell cycle regulation, including spindle formation and chromosome segregation. The family has three members: Aurora-A, -B, and -C [80]. Aurora kinase A (AURKA) plays a crucial role in various mitotic events, such as mitotic entry, centrosome maturation, and spindle formation[81,82]. Moreover, AURKA overexpression or gene amplification has been observed in numerous human cancers, demonstrating their role as a potent oncogenes in carcinogenesis [83].

AURKA is activated in the G2 phase, localized into the centrosomes, and then translocated to mitotic spindles during prometaphase and metaphase [82]. After the metaphase-anaphase transition, it undergoes proteasome-dependent degradation by Cadherin-1 (Cdh1) /APC/C complex [84,85]. The activity of Aurora-A depends on its phosphorylation at Thr288 (and potentially Thr287) on the activation loop (Asp274-Glu299) of the kinase, which is also called the "T-loop." The effect of Aurora-A could be activated by co-factors Bora and Ajuba and deactivated by PP2A (protein phosphatase 2A) in human cancer [82,86].

Activated AURKA recruits proteins such as γ-tubulin ring complex (γ-TuRC), centrosomin, and TACC/MAP215 essential for microtubule nucleation, stabilization, and spindle assembly [87,88]. Moreover, AURKA phosphorylates Cyclin B1-CDK1 during late prophase, which activates the Ran GTPase pathway and provokes Nuclear Envelope BreakDown (NEBD)[89]. The Cyclin B1-CDK1 complex also activates the spindle assembly factor TPX2, which binds to AURKA and creates the bipolar mitotic spindle [90]. AURKA activates PLK1 by direct phosphorylation on Thr210, and Bora dramatically enhances the activity of AURKA towards PLK1 (Figure 10) [91].

1.1.1 Polo-like kinase-1 (PLK1)

Plk1 is a serine/threonine kinase that regulates mitosis and cytokinesis. PLK1 controls the activity of MPS1 kinase to start spindle checkpoint signaling, the histone kinases Aurora B (AURKB) and Haspin to determine centromere identity, the kinases BUB1 and its pseudokinase paralog BUBR1 to coordinate spindle checkpoint activation and inactivation (reviewed by *G Combes et al.*) [92]. Moreover, PLK1 triggers the G2/M transition and is activated shortly before CyclinB-CDK1 [93].

Activated PLK1 inhibits WEE1 kinase and activates CDC25C, leading to CDK1 activation. This first wave of Cyclin B-CDK1 activation is necessary for progression from G2 to the M phase after a checkpoint-dependent arrest [94]. Thereby, PLK1 activity play an important role in restarting the cell cycle after recovery from DNA damage (This will be made clearer in Section 1.2.2.a.) (Figure 10) [95]. Furthermore, besides the role of PLK1 in regulating the cell cycle, it directly participates in the regulation of DSB repair. It has been reported that PLK1 could phosphorylate BRCA1, an essential mediator protein in the HR repair pathway, on its Ser1164. This phosphorylation was found to be necessary for BRCA1 foci formation at DSB [96]. Additionally, PLK1 phosphorylates DNA polymerase theta (Polθ) to enable repair of mitotic DSBs by non-homologous end joining in mitosis [97].

1.2 DNA Damage response and cell cycle checkpoints

As previously mentioned, replication errors and/or replicative stress cause DSBs and threaten the genome's integrity. Cell cycle checkpoint pathways monitor critical cell cycle events, including replication, chromosome integrity, and proper chromosome segregation.

1.2.1 DNA damage response DDR

The DDR pathway is a complicated signal transduction mechanism that cells utilize to identify DNA damage. Depending on the type of damage and/or cell cycle phase, DDR can coordinate cell cycle arrest, DNA repair, and apoptosis [98]. The system operates in three stages: 1- damage sensing, 2- signaling cascade activation, and 3- checkpoint and repair effectors recruitment (Figure 9). All these components collaborate to guarantee accurate cell cycle regulation and DNA repair in response to DNA damage.

1.2.1-a- Damage sensing

In initiating DDR, a set of lesion-specific sensing molecules bind to their specific damaged DNA lesion, where each DNA lesion has its specific sensor proteins; for instance, DNA glycosylases sense damaged bases, and MutS proteins recognize mismatched bases [99,100]. While Replication Protein A (RPA) complex and PARP-1 (poly(ADP ribose) polymerase-1) or the MRN complex (MRE11, RAD50, NSB1) detect SSBs, and DSBs, respectively [101]. (Section 2.1 will go into more detail on this topic).

1.2.1-b- Signaling cascade activation

Upon MRN complex detection DSBs, a group of transducers are recruited. These transducers include members of the PhosphoInositide-3-Kinase-related Kinases (PIKKs) family, ATM (Ataxia

Telangiectasia, Mutation), and ATR (ATM and Rad3-related) kinases. These kinases play a crucial role in regulating checkpoint proteins, particularly in the case of DSBs and SSBs (Figure 10) [102]. Interestingly, DNA-PKcs, a member of the PIKKs family and the apical kinase implicated in DSB signaling and repair *via* c-NHEJ, has been shown to influence the G2/M DNA damage checkpoint in ATM-deficient cells. Whereas inhibiting DNA-PK or using RNAi to knock down DNA-PKcs weakens the G2 checkpoint and reduces the phosphorylation of CHK2 on Thr68 [103]. Once DSBs are detected, ATM undergoes autophosphorylation on Serine (S) S1981. However, ATM activation is also contributed by additional autophosphorylation sites at S367 and S1893, while acetylation by TIP60 may also play a role (as reviewed by Smith et al., 2010) [101]. Moreover, PIKK family kinases phosphorylate histone variant H2AX (γ-H2AX) at DSBs.

This histone modification recruits DDR factors like MDC1, promoting DDR amplification through ATM activation and consequent γ-H2AX spreading [104]. In addition to H2AX, ATM phosphorylates BRCA1, 53BP1, and MDC1 as well as checkpoint proteins CHK1 and CHK2. These processes stop the cell cycle and activate proteins for DNA repair (Figure 9), as explained below [105].

1.2.2 Cell cycle checkpoints

The checkpoints in the cell cycle are categorized into two types: 1- DNA Structure Checkpoints (DSCs), including G1 pre-DNA replication, S phase checkpoint, and G2 post-DNA replication, and 2- Mitotic Checkpoint Complex (MCC) and Spindle Assembly Checkpoints (SACs) during mitosis or meiosis. These checkpoints monitor all cell cycle stages, and in the case of detection of any damaged DNA or spindle structure disruption, they pause cell cycle progression at several cell cycle stages: termed G1/S arrest, S-phase arrest, G2/M arrest, M-phase arrest, and spindle checkpoint arrest allowing time for DNA repair [106,107].

1.2.2-a- DNA structure checkpoints

In the G1 phase, the Retinoblastoma (RB) gene binds with transcription factor E2F to form a dimer, inactivating E2F. Cyclin D is synthesized once the cell enters the cycle, activating CDK4/6. CDK4/6 then phosphorylates the RB protein, causing pRB to change conformation and release E2F. This promotes the transcription of G1-S target genes required for DNA synthesis [108,109]. In response to DNA damage, pRB is dephosphorylated and inhibits E2F causing G1/S arrest; thus, RB protects cells from genotoxic stress by impeding the G1/S transition (Figure 10) [110].

In the G2/M phase, cell cycle checkpoint proteins such as Checkpoint Kinase 1 (CHK1) and Checkpoint Kinase 2 (CHK2) are phosphorylated and activated by ATR and ATM [76]. The activity of

CHK2 is linked to arrests in the G1-S and G2-M phases, while CHK1 activity is mainly involved in the intra-S phase cell cycle checkpoint and the G2-M transition [111]. CHK2 activates p53, which inhibits cyclin E/CDK2 and upregulates DNA repair machinery in the early G1 phase, promoting DNA repair [76,112].

On the other hand, the phosphorylation of CDC25 by CHK1 and CHK2 can inhibit it, leading to cell cycle arrest. CHK1 phosphorylates CDC25C at serine 216, preventing entry into mitosis [113].

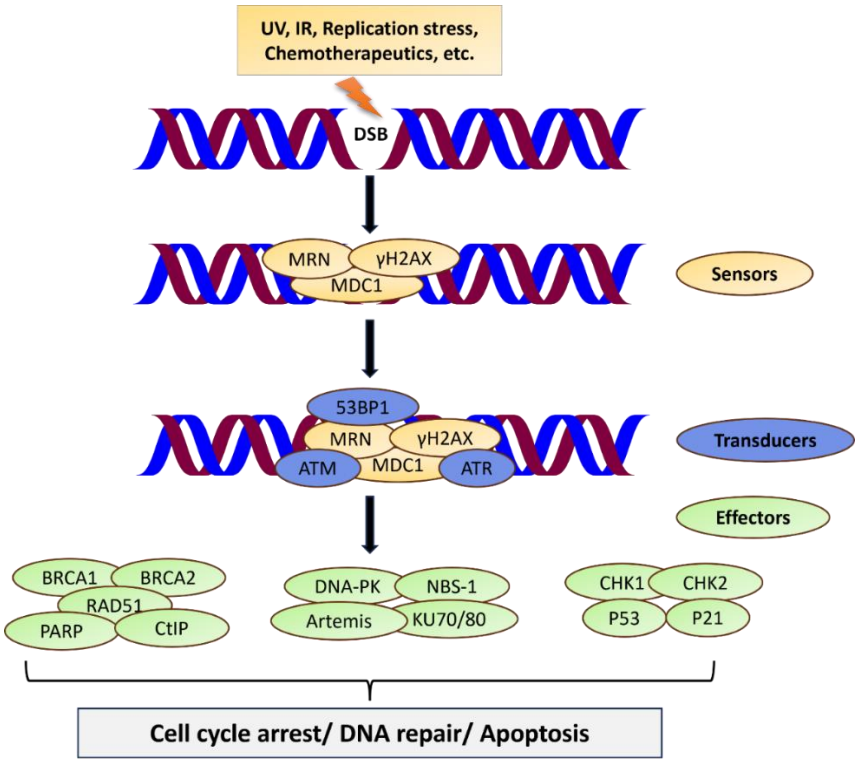

Figure 9 An overview of the DNA double-strand break (DSB) damage response.

Sensor proteins, such as the MRN complex, MDC1, and gamma H2AX, detect DSB. They then activate downstream transducer proteins, including ATM, ATR, and 53BP1, which in turn activate effector proteins. Depending on the extent of damage, the effector proteins can result in cell cycle arrest, DNA damage repair, or apoptosis. Figure was adapted from [114].

In addition, the Phosphorylation of CDC25A by CHK1 sends it to degradation and prevents the activation of downstream signaling pathways required for entry into the G2/M phase [115]. Moreover, CHK1 activates WEE1, a tyrosine kinase and G2 checkpoint regulator, which inhibits CDK2 and CDK1, causing cell-cycle blockage in the G2 phase (Figure 10) [111,116].

However, it has been reported that CDC25 and WEE1 are dose-dependent mitotic activators and inhibitors, respectively [113]. Furthermore, in response to DNA damage, CHK1 represses AURKA to prevent mitotic entry [117]. If DNA is repaired, CHK1 is inhibited, allowing AURKA activation,

followed by PLK1 and CDC25B stimulation [118]. Activation of CHK1 in mitotic cells also inhibits AURKB, causing delays in H3 phosphorylation. This results in delays in chromosome replication and condensation [94].

Concerning the S phase checkpoint, if DNA damage happens during the S phase, either due to stalled replication forks, nucleotide excision/repair process, or DSB resolution intermediates, the intra-S phase checkpoint is triggered to stop further replication; however, the S phase checkpoint is regulated by ATR/CHK1 pathway, inducing CDCD25A proteasomal degradation (as explained above) and blocking further progression through the S phase [119]. Furthermore, ATM plays a crucial role in regulating S-phase checkpoints through three distinct signaling pathways: ATM/CHK2/CDC25A/CDK2, ATM/MRN/SMC1, and ATM/MRN/RPA [106].

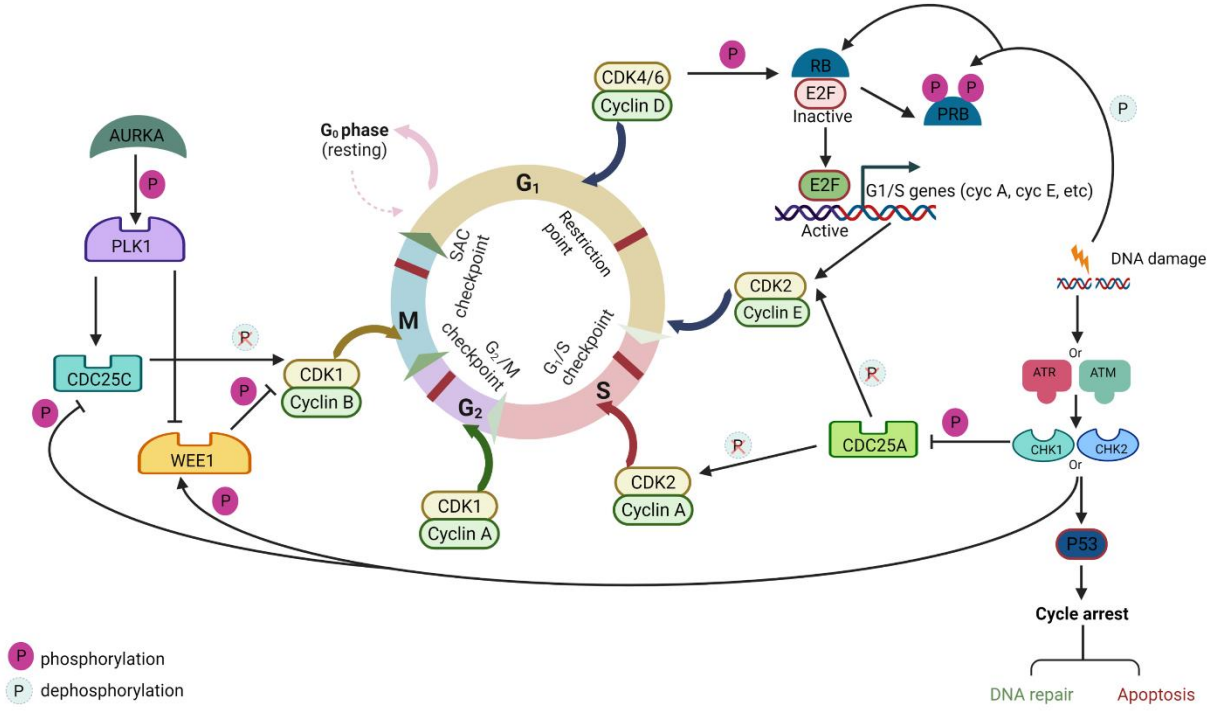

Figure 10 Cell cycle Checkpoints.

Activation of ATM and ATR kinases causes checkpoint cascades *via* CHK1 and CHK2. These kinases inhibit CDC25, a phosphatase required for CDK activation, leading to cell cycle arrest. In G1/S, p53 prevents DNA replication in damaged cells and induces cell cycle arrest for DNA repair. Unrepairable damage leads to apoptosis. AURKA activates PLK1, restarting the cycle after recovery from DNA damage-induced cell cycle arrest [76]. *(Alaouid.M's thesis).*

1.2.2-b- Spindle assembly checkpoints

During mitosis, proper chromosome segregation is regulated by the Mitotic Checkpoint Complex (MCC) and the Spindle Assembly Checkpoint (SAC). Unattached kinetochores activate the SAC [120]. The SAC delays the degradation of cyclin B and securin until all chromosome pairs are successfully

attached in a bipolar manner by inhibiting the function of the ubiquitin ligase Anaphase-Promoting Complex/Cyclosome (APC/C) [119]. Alternatively, The MCC consists of BubR1, Bub3, Mps1 , AURKB, and Mad2 checkpoint proteins linked to the CDC20 coactivator of the APC/C [56,57]. It is activated when chromosomes are not correctly attached to the spindle and deactivated once all kinetochores are correctly attached. The MCC is essential for the maintenance of the SAC [123].

Moreover, *Courtheoux, T. et al.* (2018) showed that AURKA helps regulate SAC by keeping Mad2 protein on unattached kinetochores. Losing AURKA activity affects SAC function, causing Mad2 to relocalize to centromeres and potentially leading to chromosome missegregation and aneuploidy [122].

However, when DNA is damaged, ATM and ATR not only halt cell cycle progression by triggering checkpoint events but also trigger DNA repair by phosphorylating multiple substrates, as will be seen in the upcoming section.

2. DSB Repair pathways

As mentioned in Section 1, DNA replication in the presence of DNA lesions and exposure to ionizing radiation or chemical products may cause DSBs. Nevertheless, unrepaired DSBs can lead to extreme genetic consequences [51]. Fortunately, cells possess various methods to repair DSBs, which we can gather into two main groups: 1- Canonical non-homologous end-joining (C-NHEJ) and 2- Homologous Recombination Repair (HRR).

2.1 DSB repair pathway choice

The choice of the DSB repair pathway is highly dependent on 1- DSB detection, 2- DSB resection, and 3- the cell cycle phase.

2.1.1 DSB detection

During the detection phase, the repair pathway is chosen very early to respond to DNA damage. Several studies suggest that pre-existing histone modifications are crucial for DDR [124]. Histone modifications, including acetylation, phosphorylation, and methylation, can modify the electrostatic interactions between histones and DNA, thus affecting the DDR factor's accessibility to DSB sites [125].

For example, Histone acetylation neutralizes positively charged lysine residues, modifying intra- and inter-nucleosomal chromatin fibre interactions to enable decondensation and improve access to nucleosomal DNA [126]. Moreover, ATM and ATR phosphorylate H2AX on Ser139, forming

γ-H2AX foci at the DSB sites [125]. γ-H2AX is required for subsequent foci formation by DDR factors like 53BP1, NBS1, BRCA1, and MDC1 [124].

Furthermore, repair proteins such as 53BP1 require methylation histone H3 Lys79 (H3K79) or H4 Lys20 (H4K20) for focus formation at DNA damage sites [127]. The 53BP1 is one of the first proteins involved in DNA damage detection, and it guides the repair process towards the NHEJ pathway (Figure 11)[128]. However, in contrast, BRCA1 plays a role in removing 53BP1 during the S phase, facilitating resection through the recruitment of CtIP (As will be discussed further in the 2.4 section). This ultimately leads to the selection of the HRR pathway for repair (Figure 11) [129,130]. Interestingly, It has been reported that when 53BP1 is silenced, it triggers resection, leading to an increase in Single-strand annealing (SSA) that requires longer resection than HRR [131].

2.1.2 DSB resection

DSB resection is a nuclear process that transforms the ends of the DSBs into 3'- single-stranded DNA (ssDNA) overhangs [132]. Creating 3' ssDNA is vital for HRR and triggers ATR activation. Various factors, such as MRN/X, CtIP/Sae2, EXO1, BLM/Sgs1, DNA2 nuclease/helicase, and chromatin remodelers, work together to finish end resection (reviewed in [132]). C-NHEJ does not require a 3' ssDNA tail, where 53BP1, PTIP, or RIF1-shieldin protects the broken DNA end.

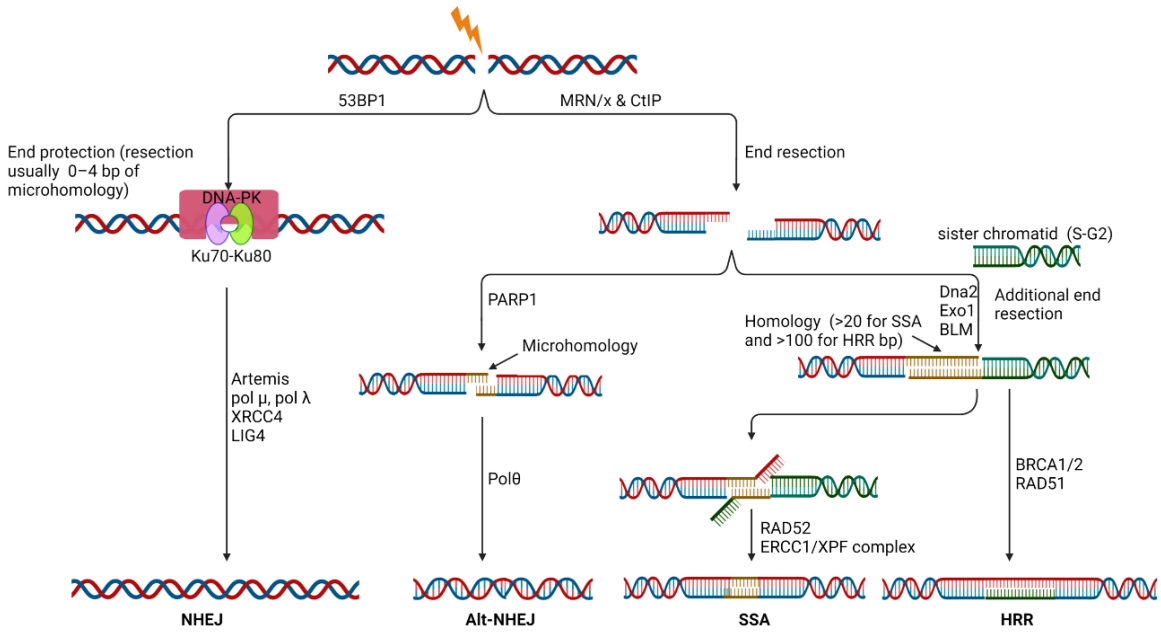

Figure 11 An overview of ends DNA breaks and DSB repair pathway choice.

DSBs can be repaired by different pathways such as C-NHEJ, Alt-NHEJ, SSA, or HRR, depending on the extent of DNA end resection needed. The figure is modified from Derived from [133,134]. *(Alaouid.M's thesis).*

This inhibits long-range end resection, promoting NHEJ and inhibiting HRR [135]. Conversely, CHAMP1 interacts with POGZ to enhance BRCA1's HRR function by promoting DNA end resection at DSB sites, counteracting 53BP1's inhibitory effect [136].

Moreover, *Gómez-Cabello, D et al.* (2022) reported that RNA synthesis by RNA polymerase II (RNAPII) is necessary to initiate DNA end resection, which favors the more accurate HRR pathway over C-NHEJ. Additionally, CtIP reactivates RNAPII paused by RNA: DNA hybrids during early DSB response, promoting DNA resection and skewing repair towards HRR [129]. However, the significance of RNA in DNA repair is yet unclear and requires further investigation.

2.1.3 Cell cycle phase:

The presence of an undamaged sister chromatid is crucial in determining the repair pathway. C-NHEJ does not require a template, so it can occur at any point during the cell cycle. However, HRR is dominant in the late S and G2 phases due to the presence of a sister chromatid that can be used as a repair template, which is why HRR is a relatively error-free repair pathway [137,138].

2.2 Non-homologous End-Joining (C-NHEJ):

In the C-NHEJ pathway, KU70/80 heterodimer begins with recognizing DSB sites, followed by end processing by DNA-PKcs and Artemis, DNA strand synthesis by Polymerases X family (pol μ and pol λ), and finally, resealing of breaks by Ligase IV/XRCC4/XLF complex (Figure 12) [139].

The heterodimer of Ku70 and Ku80 initially attaches to the DSB ends, forming a ring that encircles the duplex DNA and protects the ends from degradation. Ku70 and Ku80 are DNA-dependent ATP-dependent helicases, specific for single-strand DNA, and function as regulatory subunits of DNA-PK [140]. DNA-PK phosphorylates and activates other C-NHEJ proteins like the endonuclease Artemis, XRCC4-XLF complex, and DNA ligase IV to join the broken DNA ends [103,133]. The pathway contains other processing-related enzymes, PNKP (PolyNucleotide Kinase/Phosphatase), APE1 (AP Endonuclease1),and Tdp1 (Tyrosyl DNA phosphatase1) [9].

Different sets of NHEJ proteins align DNA ends in an end-to-end configuration. The degree of microhomology affects DNA end joining. Some DNA ends can be joined using only ligase complex, while others require polymerases or nucleases, forming different NHEJ subpathways [134]. For example, in the case of blunt DNA ends (which do not share any nucleotide of homology), Ku70-80 heterodimer along with XRCC4 and DNA ligase IV proteins are sufficient for efficient joining by direct ligation sub-pathway.

On the other hand, certain DSB ends, like the ones with incompatible 5' or 3' overhanging ends that possess a certain level of microhomology, employ sub-pathways that necessitate the presence of additional nuclease or polymerase proteins beside Ku70-80 heterodimer and ligase for successful joining [134].

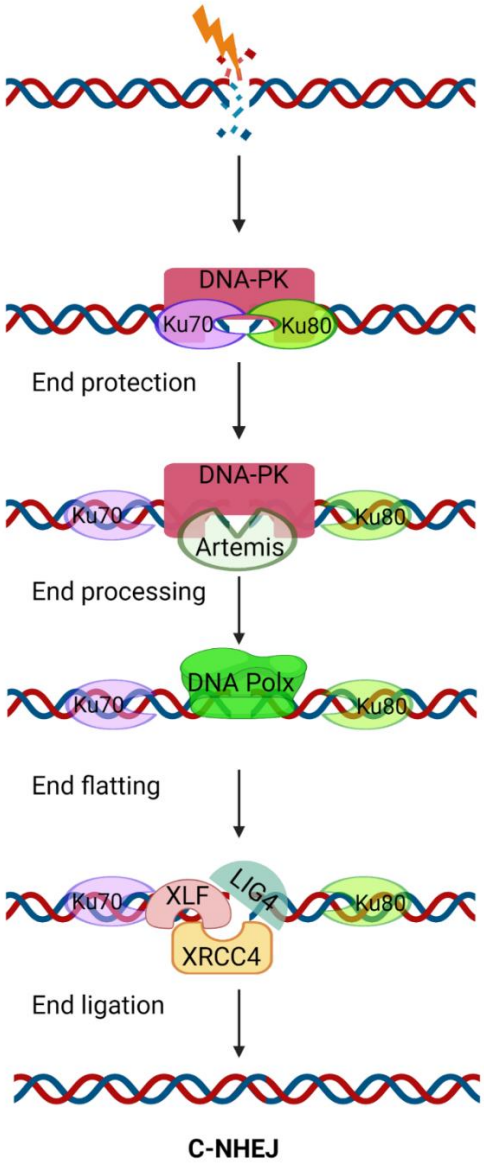

Figure 12 Schematic representation of the mechanism of Canonical non-homologous end-joining (C-NHEJ).

(Alaouid. M's thesis)

2.3 Alternative End-Joining (Alt-NHEJ) pathway

In addition, when one or more key protein components of C-NHEJ are lacking, other Alternative End-Joining (Alt-NHEJ) pathway become active. This pathway involves resection of DNA ends to

reveal sequence homology, which is annealed to stabilize the two ends of a break and allow for more efficient joining and ligation. The Alt-NHEJ pathway functions as backup mechanism initiated at DSBs only after C-NHEJ or HRR have engaged but failed to complete processing successfully. Alt-NHEJ is more error-prone than C-NHEJ and is a major source of genomic instability (Figure 11) [134,141,142].

2.4 Homologous Recombination Repair Pathway (HRR):

HRR acts *via* several successive phases, including the first presynaptic step. MRN complex and CtIP endonuclease recognize the DSB site and generate 3' single-strand DNA (ssDNA) overhangs [143]. The triple MRN complex includes RAD50, MRE11 (a dimer), and NBS1. NBS1 contains an NLS motif that enables it to localize the MRN complex in the nucleus. Additionally, it interacts with γH2AX to bring MRE11 and RAD50 near the DSB site [144].

It has been reported that NBS1 is required to recruit and activate ATM, ATR, and probably DNA-PKcs after UV or IR induction of DNA damage [145–147]. The RAD50 binds to the DNA duplex with its ATPase motifs and holds the broken ends together with its coiled-coil arms aiding in locating homology regions for recombination [148]. The MRE11 protein possesses 3'-5' exonuclease activity that primes the DNA duplex's broken ends [149].

In addition, CtIP (C-terminal-binding protein interacting protein) works with the MRN complex to begin short-range resection by creating a gap in the 5' DNA strand at the break ends blocked by the NHEJ factor Ku. Meanwhile, a long-range 5' strand resection is catalyzed by exonuclease EXO1, supported by endonuclease DNA2, which works along with BLM (a RecQ helicase) that unwinds DNA, producing 3' ssDNA overhangs [143].

These ssDNA overhangs become quickly covered by the replication protein A (RPA) complex, which protects them from the nucleases' activity and prevents the formation of the secondary structure. In addition, RPA inhibits spontaneous annealing between microhomologies, hence avoiding the Alt-NHEJ [150].

Moreover, the MRN complex mediates the activation and the recruitment of the upstream ATM serine/threonine kinase, which phosphorylates 'Ser-139' of histone variant H2AX at DSBs; it is believed that γH2AX plays a significant role in signaling by enhancing DNA accessibility. This chromatin modification enables the accumulation of repair proteins in the damaged areas. Additionally, γH2AX aids DSB rejoining by bringing broken ends together through nucleosome repositioning at damaged sites and decreasing chromatin density [151,152].

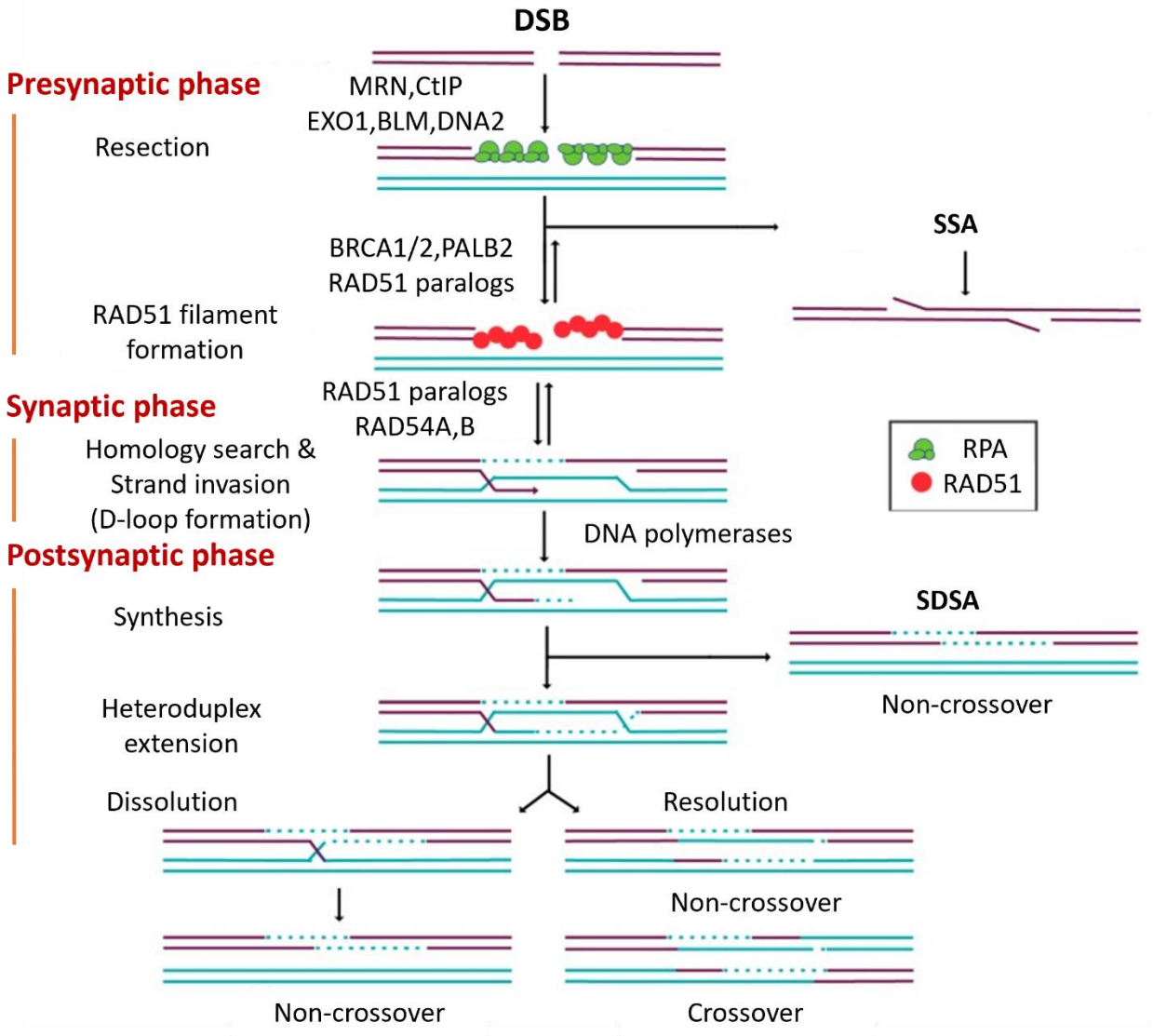

Figure 13 Schematic representation of the mechanism of homologous recombination.

After a double-strand break (DSB) occurs (represented by purple lines), cells can repair the damage through homologous recombination (HR) using a homologous template (represented by turquoise lines). The MRN complex (MRE11-RAD51-NBS1), CtIP, EXO1, BLM, and DNA2 perform resection, which creates 3' single-stranded DNA (ssDNA) overhangs. These overhangs are then coated by the trimeric replication protein A (RPA) complex (represented by green circles). During canonical HR (DSBR), RAD51 (represented by red circles) replaces RPA. Alternatively, RAD51-independent repair can occur by Single-Strand Annealing (SSA), where complementary DNA sequences anneal the overhang, flap endonucleases cut the overhang, and the DNA ends are subsequently ligated together. The RAD51 paralogs and RAD54A,B govern RAD51-mediated homology search and strand invasion. Besides, D loops mediated by RAD51 are formed. The missing information is then copied from the homologous template (indicated in turquoise). The D loop is displaced during the Synthesis-Dependent Strand Annealing (SDSA), and the DNA is resolved into a non - crossover product. In the event of a heteroduplex extension and a double Holliday junction creation. The DNA intermediates can be resolved by dissolution or resolution. This figure was adapted from [153].

In addition, the protein BRCA1(breast cancer type 1 susceptibility protein) directly interacts with the MRN complex and CtIP during the beginning stages of resection events. It also indirectly

interacts with RAD51 through BRCA2. RAD51 paralogs, including RAD51B-C-D and XRCC2/3 along with BRCA2 act as recombination mediators to assist in loading RAD51 onto RPA-coated ssDNA, replacing RPA in the process. This promotes the formation of RAD51 nucleoprotein filaments.

It's important to mention that the Partner and Localizer of BRCA2 (PALB2) recruits BRCA2 to DSB sites. Additionally, reports indicate that PALB2 and the BRCA1-BARD1 complex are necessary to stabilize RAD51 nucleoprotein filaments and facilitate strand exchange during recombination [154,154].

During the second phase, the synaptic or DNA synthesis step, the RAD51/ssDNA filament searches the homologous duplex sequence and then proceeds to invade it. This invasion leads to a Displacement loop (D-loop) between the invading 3' overhang and the homologous strand. It has been reported that RAD54 works together with RAD51 to facilitate and stabilize the formation of strand D-loops. After the formation of a D-loop structure from pairing homologous templates, three distinct sub-pathways of HRR could take place: Synthesis-Dependent Strand Annealing (SDSA), Break-Induced Replication (BIR), and Double-Strand Break Recognizing (DSBR), which is considered the classic pathway. Repair modes differ in each sub-pathway where the D-loop becomes stable in DSBR, extends and matches in SDSA, and forms a replication fork in BIR [9,133].

In the case of the DSBR pathway, a DNA polymerase initiates the replication process using the homologous template and creates a cross-shaped structure known as double Holliday Junctions (dHJs). In the final step (post-synaptic), in humans, Topoisomerase IIIα (TopIIIα) and BLM work on the HJs to produce a non-crossover product through dissolution. Alternatively, an endonuclease called Resolvase (like MUS81-EME1 or GEN1) [155] cuts the DNA at the HJs to create either non-crossover or crossover products through resolutions (Figure 13) [156].

2.5 Single-strand annealing (SSA) pathway

It is important to note that disruption of RAD51 or RAD51 mediator proteins (e.g., BRCA2 and RAD54) substantially increases the frequency of the SSA (Single-strand annealing), which is a type of non-conservative Homology-Directed Repair (HDR) pathways. SSA requires more than 20 bp of homology. However, Both Alt-NHEJ and SSA pathways anneal flanking repeats to repair DSBs. The HRR pathway is a conservative HDR pathway and generally requires lengths of homology longer than 100 bp (Figure 11 & 13) [134,157,158].

Chapter 3 The RAD51 recombinase

In the previous chapter, I highlighted the importance of RAD51 in repairing DSBs *via* the HRR pathway. This chapter will provide a more detailed analysis of the recombinase's structure and functions. I will also give a general overview of the different regulation levels that it undergoes.

1. RAD51 origin and structure.

1.1 A conserved *recA/RAD51* genes

RAD51 is a conserved gene found in all life domains, including archaea, bacteria, and eukaryotes. It belongs to the conserved recombinase superfamily, RecA/RAD51, which facilitates strand exchange between homologous DNA molecules in an ATP-dependent manner [159]. The RecA/RAD51 superfamily dates back to an ancient common ancestor before the appearance of Archaea and Eukarya [160]. This family is divided into three subfamilies: RecA, RADα, and RADβ (Figure 14A) [161].

The recA subfamily consists of bacterial and eukaryotic recA genes found in bacteria, protists, and certain fungi [160].

The RADα subfamily comprises the main recombinases in eukaryotes (RAD51 and DMC1) and Archaea (radA) [162]. The vertebrate RAD51 is 99% similar in mice and humans; however, it only shares 83% and 74% of its amino acid sequence with yeast and plants, respectively [163,164].

Finally, the RADβ subfamily includes the eukaryotic RAD51 paralogs, which are known as RAD51B, RAD51C, RAD51D, XRCC2, and XRCC3 in vertebrate animals and plants, as well as Rad55 and Rad57 in yeast, besides to the archaeal radB [164–166] (Figure 14B).

The RecA/RAD51 family proteins are essential for the cell's survival in many species; for instance, in bacteria, if the recA gene is knocked out, the accumulation of harmful mutations leads to cell death [167]. Similarly, knocking out the *RAD51* gene in mice results in cell death and early embryonic lethality [168]. Moreover, the absence of the *DMC1* gene in mice causes disrupted meiosis and truncated oogenesis [169]. Also, mutations in the Rad51 gene (spn-A) in Drosophila can disrupt both somatic and meiotic repair of DSBs [170]. Furthermore, In *C. elegans,* rad51 RNAi lines exhibit defective chromosome morphology and an accumulation of meiotic DSBs in oocytes [171]. Thus, the recA/RAD51 proteins play a vital role in the survival of cells in all life domains.

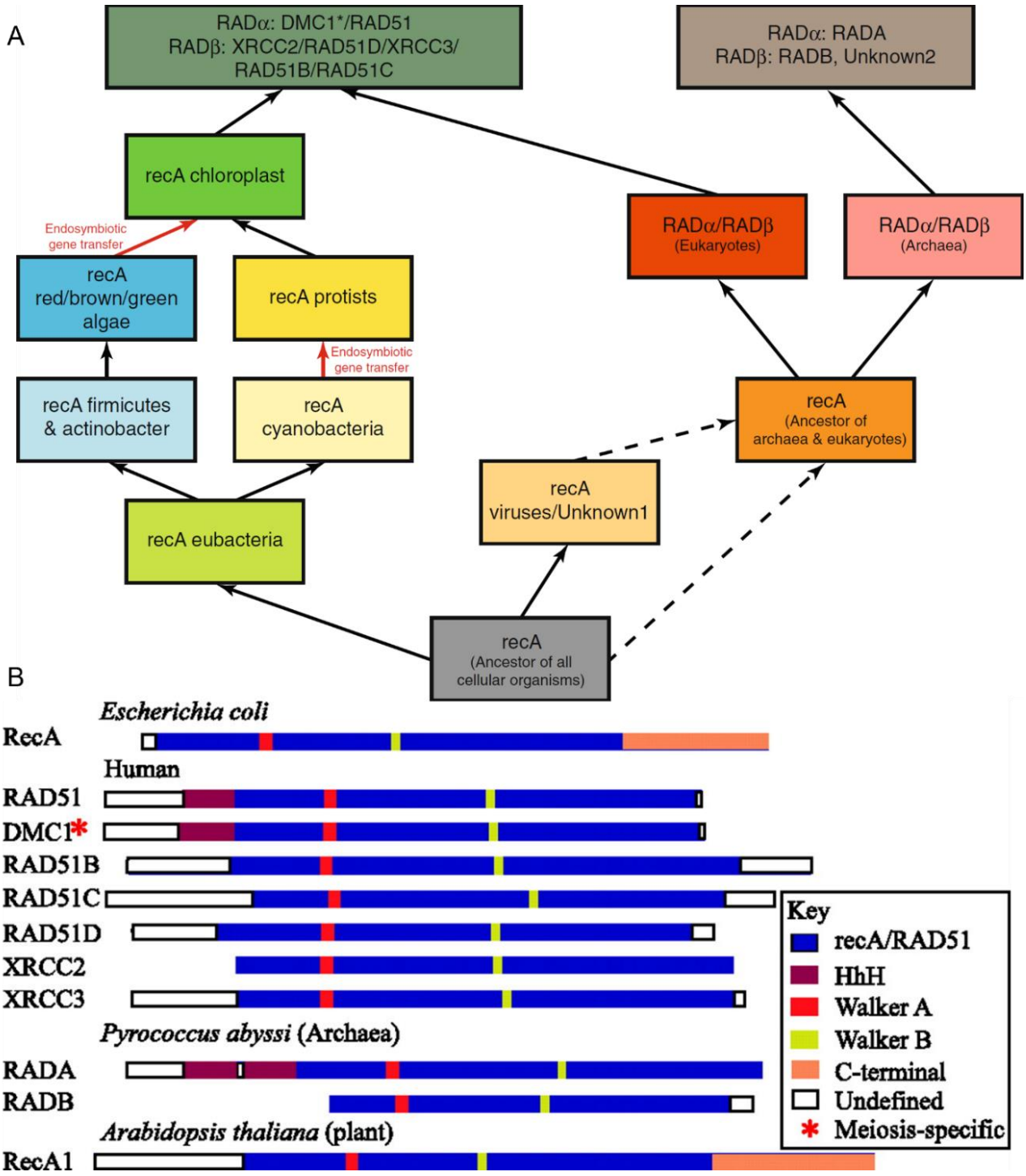

Figure 14 Model of the recA/RAD51 superfamily's evolutionary history

A) A graphical representation of the recA/RAD51 family's evolutionary model, as determined by phylogenetic trees. Events of cyanobacterial to protist and algae to plant endosymbiotic gene transfer are identified. (*) denotes a gene specific to meiosis (According to [161]). B) A schematic diagram presents RecA/RAD51-like proteins' domain structures. The domain names are labeled in the illustration (Taken from [160]).

1.2 Homo sapiens *RAD51* gene

RAD51 is a gene that belongs to the RAD52 epistasis group (A set of genes involved in the repair of DSBs)[172]. It was named after a genetic screening analysis of budding yeast that revealed its sensitivity to radiation [172,173].

In 1993, *Shinohara et al.* mapped the Homo sapiens *RAD51* gene (Hs*RAD5*1) to chromosome 15 [163]. Later, in 1994, *Takahashi et al.* confirmed this result and assigned the *RAD51* gene to the 15q15.1 location on chromosome 15 through FISH analysis [174]. Some RAD51 mutations have been found in several forms of sporadic cancer, but is unknown whether they promote tumorigenesis [175,176]. (For the upcoming sections, I will refer to the RAD51 gene and protein of Homo sapiens without the prefix Hs.).

It is worth noting that several observed phenotypes have been linked to mutations in *RAD51* gene, such as Fanconi anemia of Complementation Group R (FANCR), which is associated with a missense mutation in the *RAD51* gene [177]. Additionally, a truncating mutation in the *RAD51* gene (R254X) has been reported in Norwegian and French families with congenital Mirror Movements-2 (MRMV2) disorder [178,179]. In 2020, *Luo et al.* identified a missense variant in *RAD51* (E68G) in a Premature Ovarian Insufficiency (POI) patient. Furthermore, they discovered that this variant is only present in the cytoplasm and impaired DSB repair [180].

1.3 RAD51 structure

RAD51 recombinase is a protein of 37 kDa composed of 339 amino acid residues. This protein is composed of two domains. The first is the N-terminal domain (NTD) which has five α-helices beside a β-strand that facilitates interactions between RAD51 protomers. The second domain is the C-terminal domain (CTD) which has α/β ATPase core domain with Walker motifs for nucleotide binding and loops for interacting with DNA [181,182]. These two domains are connected by a linker, which enables them to rotate relative to each other [183] (Figure 15 and Appendix 1).

The N-terminal domain (NTD) is a compact region consisting of five short helices formed by approximately 84 residues [184,185]. The NTD is highly conserved in eukaryotic Rad51 proteins, but it is missing in RecA. RecA, on the other hand, has an additional C-terminal domain that forms the DNA-binding surface [185,186]. In 1999, Aihara and colleagues' work highlighted the significance of the NTD as a DNA binding site, which they found to be located on the outer surface of the RAD51 filament. Their findings offer a possible explanation for the results of Yuan et al. in 1998, which suggested phosphorylation on Tyr54 by c-ABL inhibited DNA binding. According to Aihara

et al., this inhibition is due to electrostatic repulsion or perturbation of the NTD's structure at the DNA binding site. They also noted that the NTD can replace RecA's C-terminal domain and function in DNA binding [185,187]. Moreover, the NTD has been shown to interact with dsDNA through its Helix-hairpin-Helix motif (HhH) [182].

Through analysis of the G103E mutation in yeast Rad51's NTD and the missing 62 N-terminal residues of RadA (RadA-Δ62), *Galkin et al.* concluded that the NTD of both yeast Rad51 and RadA is essential for coordinating the ATPase activity of the catalytic core, which requires rotations of the core inside the filaments [188].

Furthermore, in a study by *Subramanyam et al*., they used three glutamate-to-alanine mutants of RAD51, (E42A, E59A, and E237A), to explore the unknown interactions between the BRC4 peptide of BRCA2 and RAD51 (for further information on BRCA2, see Section 2.2.2.). They discovered critical BRC4-RAD51 contacts involving the RAD51 NTD. Where they found that the mutants have reduced affinities for the BRC4 peptide but maintain the biochemical characteristics of wild-type RAD51. Their findings revealed how the interaction between the BRC4 peptide and the neighboring monomer within the RAD51 oligomer contributes to RAD51 oligomer instability and ssDNA selectivity [189].

The linker, consisting of residues 85-99, is a flexible helix [183,190] with a short β-strand (residues 85-GFTT-88) called the Polymerization Motif (PM) (Figure 15). This motif forms an interaction protomer-protomer interface [182,190]. In addition, the ability of RAD51 to form nuclear foci and self-associate is dependent on the integrity of Phe 86 and Ala 89 within the linker domain. Where, mutants of RAD51 F86E and A89E, have been shown to impair foci formation and decrease the ability of RAD51 to form filaments [184]. Furthermore, the hydrophobic residue in the PM (phenylalanine in RadA, Rad51, and Dmc1, and isoleucine in RecA) was found to dock into a hydrophobic pocket on the neighboring core domain. The same connection was found in the combined structures of the RAD51 and BRC4 peptide of BRCA2 [184,190,191].

In a study on *Sulfolobus solfataricus* (*Sso*) RadA using Electron Microscopy (EM) imaging and comparing with *Pyrococcus furiosus* (*Pf*) Rad51, *Chen et al.* Identified a hinge region located directly after the α5 helix. They donate it as Subunit Rotation Motif (SRM). Based on our knowledge, their work is the only report of this RAD51 motif. In human RAD51, this region corresponds to amino acid residues (95-RRSEI-99) [190]. The SRM undergoes sequential conformational changes leading to the different conformations of Rad51. It may have enough

flexibility to enable Rad51 filaments to rotate axially by 360°. This motif also controls the protomer-protomer interface for ATP binding and modulates DNA binding [190].

Moreover, they found that the Arg83 (donated as R0) in the SRM of SsoRadA is an evolutionarily conserved amino acid. The equivalent amino acid residue of human RAD51 is Arg69. This arginine residue was found to form salt bridges with two conserved glutamate residues, Glu96 and Glu157 (donated as E1 and E2, respectively), which correspond to the Glu 118 and Glu 169 of human RAD51 (Refer to Appendix 1). They found that conformational changes of SRM could be coupled to ATP binding, hydrolysis, and DNA binding. In the right-handed filament of *Methanococcus voltae* RadA with AMP-PNP, they found that the E1-R0-E2 triad stabilizes the binding of AMP-PNP between two protomers. This reflects that the SRM is most likely crucial in controlling ATP binding and/or hydrolysis. In addition, while Loop1 and Loop2 of the core domain align with the filament axis, E1, and E2 are excluded to avoid repulsion between their acidic groups and phosphate groups in ssDNA. The ATP binding site opens after ATP hydrolysis and the two glutamates shift away from R0, as seen in the left-handed RadA-ssDNA filament. In this conformation, the exposure of residues E1 and E2 may interfere with DNA binding due to their placement on the path of L1 and L2. The alignment of L1, L2, E1, and E2 residues is crucial for extruding ssDNA and, as a result, stabilizing the heteroduplex DNA after homologous pairing [190,192,193].

Furthermore, by making a series of point mutations on the SRM residues of yeast Rad51, *Chen et al* have shown that the SRM is essential for yeast Rad51 to function properly *in vivo*. Their study found that the mutant proteins were unable to make cells resistant to the DNA-damaging reagent methyl methanesulfonate (MMS), in contrast to the wild-type Rad51, which was able to make cells resistant to MMS [190].

Their structural analyses have shown that the SRM is conserved in RecA family proteins across all evolutionary stages in archaeal and eukaryotic organisms [190]. In our current work, we have identified a previously unknown phosphorylation site, serine 97, within the SRM of RAD51 5 (This subject will be addressed in the results chapter) . Multiple sequence alignment has indicated that this serine residue is conserved in eukaryotic Rad51 proteins (except the Danio rerio (Dr) Rad51) and archaeal RadA and bacterial RecA (Figure 15).

The CTD consists of approximately 240 residues, known as the core domain [183]. Within the core domain, potential ssDNA binding motifs are located in the L1 (**232-YSGRGEL-238**) and L2 (**269-VVAQVDGAAMFAADPKKPI-287**) loops [194,195]. This domain also contains the ATP binding motifs

Walker A (**127-GEFRTGKT-134**) and Walker B (**218-LLIVD-222**) [182,196,197] (Appendix 1). Moreover, this core domain contains the Nuclear Export Signal motif (NES) that spans amino acids **245-LARFLRMLLRLADEFG-260**. The NES can become masked by the interaction with the BRC repeats of BRCA2, which enables RAD51 nuclear localization [198,199] (this will be covered later in a separate section).

However, thanks to multiple high-resolution X-ray and EM crystallography studies, we now better understand the 3D structure of RAD51 and its filaments. Currently, 16 structures of eukaryotic RAD51 are available in the Protein Data Bank (PDB), presented in Appendix 2.

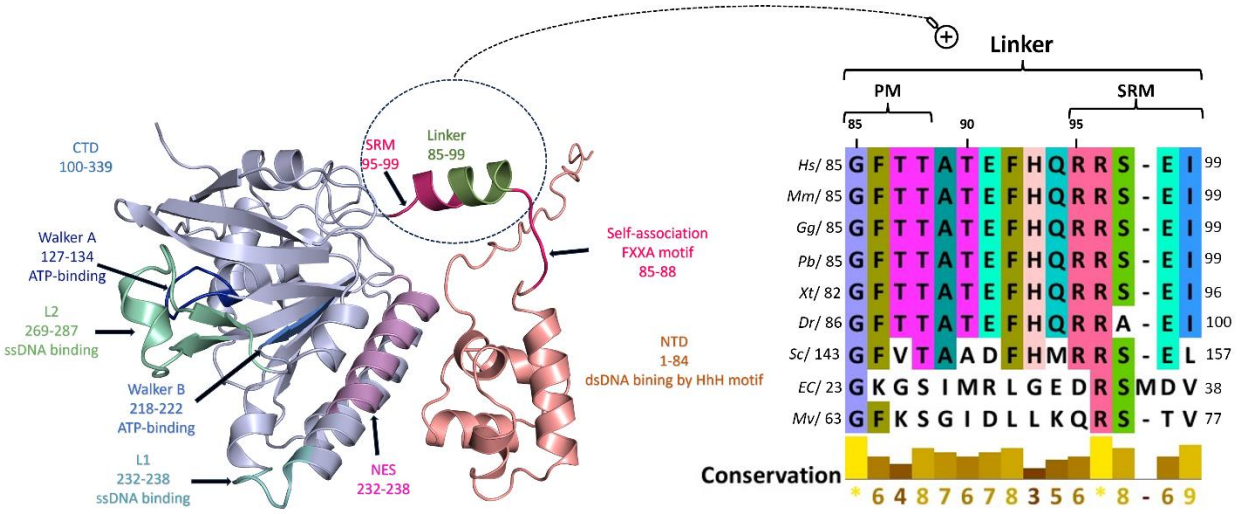

Figure 15 Human RAD51 3D structure besides sequence alignment of RecA family proteins' linker regions.

On the left 3D sttructur of Human RAD51, the N-terminal DNA binding domain (NTD) (residues 1-84) is visible in red, followed by a small linker domain (residues 85-99) in green, and finally, the C-terminal ATPase domain (CTD) (residues 100-339) in blue. This structure was created with pyMOL using the previously computed AlphaFold RAD51 3D structure, AF-Q06609-F1-model_v4 [200,201]. On the right, multiple sequence alignments of linker regions in recA family proteins were performed using the MUSCLE algorithm of alignment tools version 7.0.3 provided by SnapGene (www.snapgene.com). The results were displayed and edited using Jalview version 2.11.2.0 (https://www.jalview.org/) [202]. The protein sequences were provided by UniProtKB (https://www.uniprot.org/) in FASTA format. The accession code for each protein is provided just before the species name. For instance, Q06609 represents the human RAD51 protein. Hs: Homo sapiens (RAD51), Mm: Mus musculus (Rad51), Gg: Gallus gallus (Rad51), Pb: Python bivittatus (Rad51), Sc: Saccharomyces cerevisiae (Rad51), Xt: Xenopus tropicalis (Rad51), Dr: Danio rerio (Rad51), Ec: Escherichia coli (RecA), Mv: Methanococcus voltae (RadA). The alignment conservation annotation is a quantitative numerical index that reflects the conservation of the alignment's physicochemical attributes for each column. Below the histogram is the score for each column. '*' indicates conserved columns with a score of 11 [202]. (*Alaouid. M's thesis*).

2. RAD51 function

2. 1 RAD51 plays a catalytic role in the HRR

In Chapter II I described the different players and steps in the HRR. Here, I will focus on RAD51. How do the RAD51 monomers assemble to form protein filaments? Moreover, how does this filament interact with ssDNA to generate NucleoProtein Filament (NPF)?

However, we saw that when DSBs occur, a long tail of 3'-OH ssDNA ends is generated by nucleolytic resection. This is then quickly coated by an RPA complex. Afterward, RAD51 polymerizes on the ssDNA overhang (also known as the invading or incoming strand) with the help of BRCA2 [203]. This process creates an NPF in a right-handed helical shape, formed in an ATP-dependent manner. The structure produced is referred to as the presynaptic filament [204,205]. During the process, the NPF performs the strand invasion of the target homologous dsDNA template to create a three-strand intermediate (Synapsis) called, as we saw, D-loop, where the search for homology and strand exchange occurs [206,207]. Finally, in the postsynaptic stage, RAD51 dissociates from the resultant heteroduplex DNA, enabling the replication machinery to re-synthesize resected DNA [208] (Figure 16 Schematic diagram illustrating RAD51 nucleoprotein filament formation (NPF).Figure 16). Below, I will examine how RAD51 operates in the presynaptic, synaptic, and postsynaptic stages of the HRR in more detail.

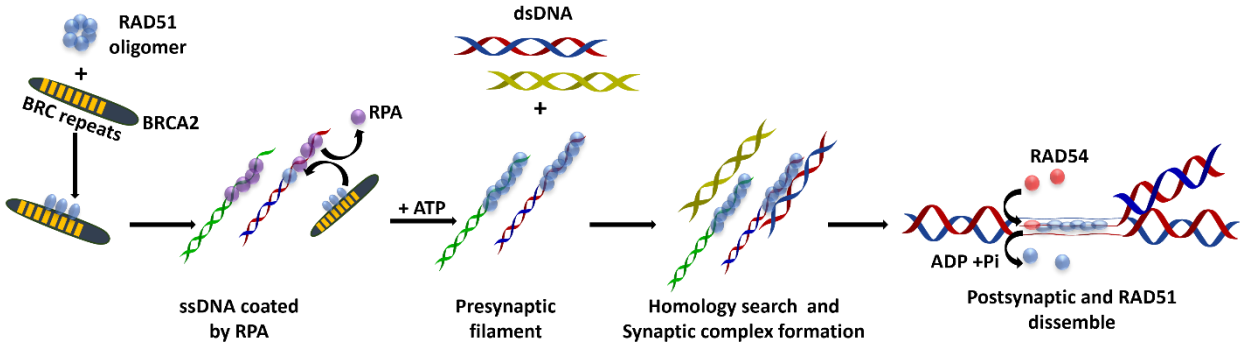

Figure 16 Schematic diagram illustrating RAD51 nucleoprotein filament formation (NPF).

In the nucleoplasm, around 40% of RAD51 exists as either self-assembled oligomers or bound to the BRC repeats of BRCA2 [209,210]. When DSBs are present, BRCA2 assists in loading RAD51 onto the coated ssDNA.. RAD51 replaces RPA protein. By binding to ATP, RAD51 polymerize on the ssDNA and form NPF [211]. After being formed, NPF searches for matching sequences in double-stranded DNA (dsDNA). When a match is found, a strand exchange occurs, resulting in the formation of hybrid dsDNA within a "displacement loop" (D-loop). When two complementary DNA strands recognize each other, they can exchange segments of genetic material without using ATP hydrolysis. This happens because the exchange reaction is energetically favorable and causes the distorted strand to find a more comfortable position near the filament axis. This process does not require any chemical energy and is driven by the stability of the final product. Following strand exchange, ATP hydrolysis and RAD54 remove RAD51 from the D-loop [212]. This figure was inspired by [209,213,214]. *(Alaouid.M's thesis)*

2.1.1 Presynapsis

RAD51 has been shown to be capable of forming NPF on either ssDNA or dsDNA. There is one RAD51 monomer for every three nucleotides or DNA base pairs (bp) [205,215]. Moreover, studies involving Biochemical *in-vitro* assays have revealed that RAD51 displays a preference for ssDNA [216].

The nucleation phase is the initial step in RAD51 filament formation, and it involves assembling a small number of RAD51 monomers on the ssDNA [217,218]. In a cryo-EM analysis of human RAD51, *Xu J. et al.* showed that the RAD51 protomers connect in a helical arrangement through three main interfaces [182].

The first interface is supported by an ATP molecule fixed between two adjacent protomers. Using a non-hydrolyzable ATP analog (AMP-PNP), the EM map displays that the Walker A motif holds together AMP-PNP with conserved residues K133 and T134 encircling the phosphates [182,219]. Additionally, E163 and D316, which are essential for RAD51's recombinase activity, were present surrounding AMP-PNP [182] (Figure 17A).

In the second interface, a short β-strand (residues 85-GFTT-88) in the linker region is packed against the central β-sheet of the ATPase domain in the adjacent protomer [182] (Figure 17A).

In the third interaction interface, there is an aromatic packing between residue Y54 in the N-terminal domain of one protomer and residue F195 in the ATPase domain of the adjacent protomer [182] (Figure 17A).

When ATP is absent, RAD51 forms a shorter and inactive filament with a helical pitch of around 65-85 Å [220]. However, when ATP or non-hydrolyzable ATP analogs are present, the filament stretches out into an active conformation with 6.3 protomers per turn and a helical pitch of 100 Å [221,222]. The C-terminal region of BRCA2 directly interacts with the interfaces formed by two adjacent RAD51 protomers. These interactions stabilize filaments so that they cannot be separated by the connection between BRC repeats and RAD51 monomers [223] (as will be seen later when discussing BRCA2).

In the presynaptic complex, the residues in two loop regions, L1 and L2, of RAD51, bind to the phosphate backbone of the DNA (Figure 17B). The DNA backbone will be inside the protein sheath of the NPF, while the stacked bases will be exposed and pointing in the axial direction. Through these interactions, the RAD51 filament increases the length of the ssDNA to roughly 1.5 times that of the B-form DNA [182,224]. These interactions collectively prepare the presynaptic complex to initiate the Synapsis by invading intact dsDNA for searching the homology.

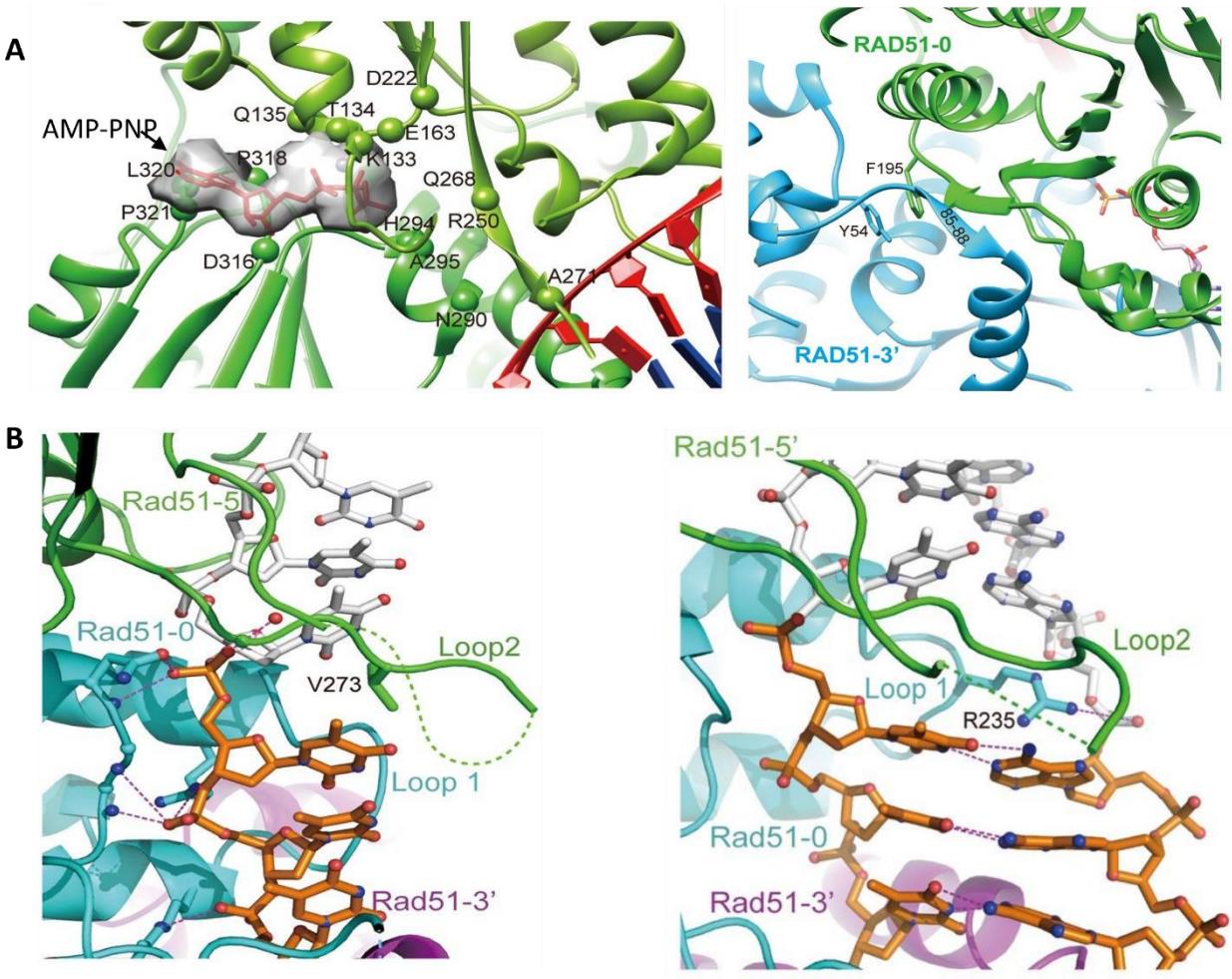

Figure 17 RAD51 protomer-DNA interaction in presynaptic and postsynaptic complexes

A) The interface between RAD51 protomers structure analysis. The Left panel characterizes the first protomer-protomer interface, where the AMP-PNP is buried in two neighboring RAD51 protomers that bind to dsDNA (red and blue). Labeled spheres indicate key residues that play a role in these interactions. The right panel represents the residues involved in the other two protomer-protomer interfaces. **B) RAD51-DNA interaction in presynaptic and postsynaptic complexes.** The left panel represents the presynaptic complex; each nucleotide triplet connects from the 5' to 3' with three RAD51 protomers (RAD51-5', RAD51-0, and RAD51-3') are shown in green, cyan, and purple. V273 in Loop 2 of the middle RAD51 separates and stabilizes the adjacent nucleotide triplets. RAD51 mainly interacts with the backbone of ssDNA (in red), while the stacked bases are exposed and oriented in the axial direction. The right panel represents the postsynaptic complex with the interaction of R235 and the complementary strand in blue color. The invading strand is red. The figure shown is adapted from [182].

2.1.2 Synapsis

During the synaptic stage, the NPF searches for homology and examines the dsDNA template to identify a matching region. If a matching region is found, the invading strand forms a limited base pairing with the complementary strand in the dsDNA [203,225].

As sister chromatids are quite long molecules, it can take a lot of searching to find the right sequence that matches. [226]. However, the cell uses enhanced search methods to speed up the process and complete the homology search within the cell cycle time frame [227].

The duration required to compare two DNA sequences is called synapse lifetime [206]. In order to do an efficient search homology, the lifetime of synapses that do not result in strand exchange must be very short [228]. Thus, if the DNA strands are entirely different, their synapse lifetime can be as short as 10 seconds. In contrast, the lifetime can be much longer if they are somewhat similar. Moreover, if the invading strand has an area longer than 30 bases with a complete homology, the synapse lifetime increases quickly [206,229]. However, even a few mismatches can shorten the synapse's lifetime [206,230].

Once the strand exchange is finished, the filament can be disassembled through ATP hydrolysis [207]. This allows DNA synthesis to begin with DNA polymerase, ultimately completing the HRR process. The removal of RAD51 take place in the postsynaptic step.

2.1.3 postsynapsis

CryoEM studies by the Sung lab showed that the interaction between RAD51 and the invading strand in the postsynaptic complex is very similar to that of the presynaptic complex. However, the L 1 and L 2 regions are more clearly resolved in the postsynaptic complex, which suggests that extra protein-DNA interactions help stabilize the exchanged product [182] (Figure 17B). The residue in the L1 of the RAD51-0 protomer enters the gap between two consecutive nucleotide triplets and interacts with the phosphate backbone of the complementary strand. Additionally, it seems to have an electrostatic interaction with the L2 of the neighboring RAD51-5' protomer [182] (Figure 17B).

The process of ATP hydrolysis helps break down filaments by decreasing the affinity of RAD51, which is attached to ADP, for DNA [205]. It is important to note that there is a distinction between RAD51 and RecA. While once ATP hydrolysis happens, RecA dissociates from dsDNA [231]. In contrast, RAD51 remains attached to dsDNA even after ATP hydrolysis. This may be due to its slow intrinsic ATP hydrolysis [205]. Therefore, more accessory proteins are required to dissociate RAD51 completely from the newly formed heteroduplex DNA. For instance, it has been demonstrated that RAD54 removes RAD51 from dsDNA [232,233].

2. 2 RAD51 partners

Several proteins help with the removal of RPA and the polymerization of RAD51 onto the exposed ssDNA overhangs. These include RAD51 mediators (such as BRCA1, BRCA2, PALB2, and RAD52) besides to RAD51 paralogs (such as RAD51B, RAD51C, RAD51D, XRCC2, XRCC3, and SWSAP1) [164,234] (Table 1 Regulators of RAD51.Table 1). Here I will introduce some of them.

2.2.1 BRCA1

BRCA1 (BReast CAncer type 1 susceptibility protein) is a 220 kDa tumor suppressor protein that participates in various cellular processes through its diverse protein complexes [235,236]. It contains two main domains that serve different functions. Firstly, The RING domain is located at the N-terminus and mediates protein-protein interactions [237,238]. The RINK domain forms a heterodimer with its partner protein, BRCA1-Associated RING Domain 1 (BARD1) [239]. Secondly, Tandem BRCT repeats at the C-terminus that have regulatory functions by recognizing phosphorylated proteins such as 53BP1, Abraxas, and CtIP [240–242] (Figure 18).

Interestingly, *Zhao et al*. used affinity pull-down to report that the BRCA1-BARD1 complex interacts with human RAD51 but not with yeast Rad51. Additionally, they used a DR-GFP reporter and the CRISPR/Cas9-stimulated gene targeting assay to reveal a new cellular role of the BRCA1-BARD1 complex. This complex enhances the DNA strand invasion step of HR [243].

Moreover, BRCA1 is essential for regulating the DDR process and is directly engaged in HR-mediated DSB repair. Using phospho-peptide affinity proteomic analysis, *Wang et al* were able to identify Abraxas, a novel protein that directly binds the BRCA1 BRCT repeats *via* a phosphor-SXXF motif. Besides they showed that BRCA1 binds to phosphorylated Rap80, a ubiquitin interacting motif (UIM) protein. Interaction between BRCA1, Abraxas, and Rap80 forms a macro-complex, which binds to ubiquitylated histones at DNA DSBs [242,244].

Furthermore, BRCA1 interacts with the MRN complex *via* its N terminus and with CtIP through its BRCT repeats. However, in vivo, BRCA1 requires a direct interaction between CtIP and NBS1 for association with MRN. This BRCA1·CtIP·MRN complex is formed in a cell cycle-dependent manner, and it is essential for producing single-stranded DNA required for HR-mediated DSB repair in S and G2 phases [245].

In addition, BRCA1 is necessary for recruiting RAD51 to DNA damage sites *via* interaction with PALB2 (Partner and Localizer of BRCA2) and BRCA2. The formation of the BRCA1- PALB2- BRCA2 complex requires the phosphorylation of S988 on BRCA1 by CHK2 [246].

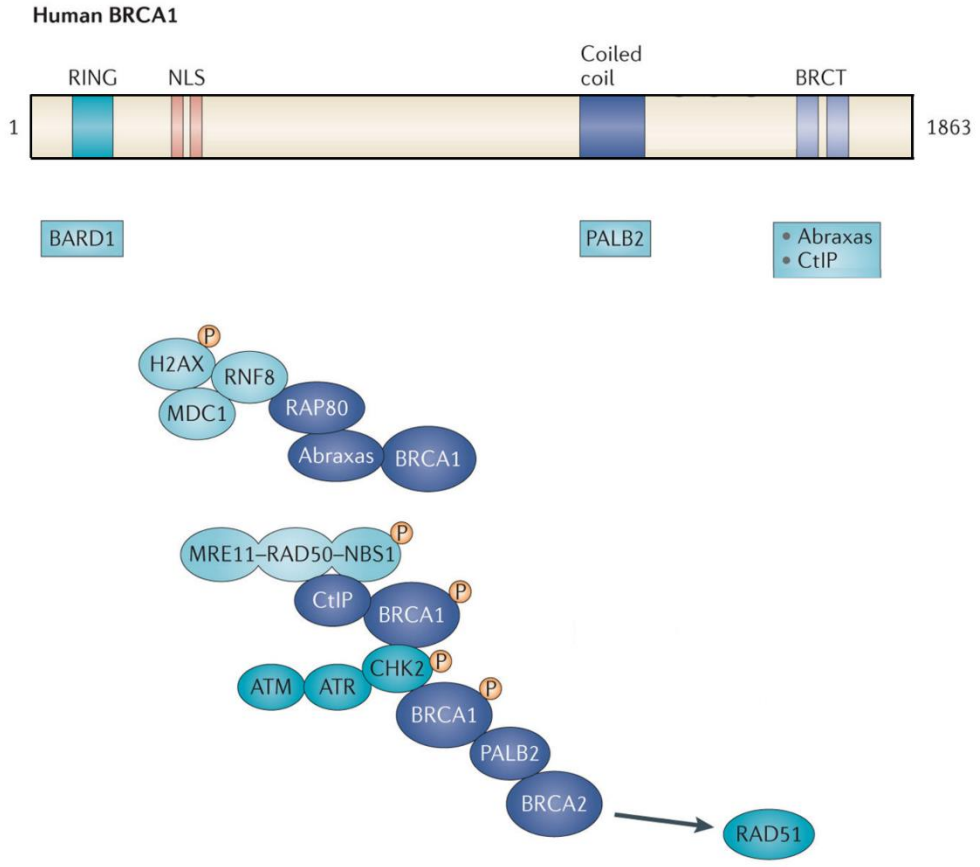

Figure 18 Functional domains of BRCA1 and its partners.

The upper panel of the figure illustrates the domain structure of BRCA1. At the N terminal of BRCA1, there is a nuclear localization sequence (NLS) and a RING domain that interacts with BRCA1-associated RING domain protein 1 (BARD1). At the carboxyl terminus of BRCA1, there is a coiled-coil domain that interacts with PALB2 and a BRCT domain that binds to ATM-phosphorylated Abraxas and CtBP-interacting protein (CtIP). The lower panel displays the various complexes that are formed by BRCA1. The figure was modified from [247].

Several kinases have been found to phosphorylate BRCA1 at specific residues during different cell cycle checkpoints in response to genotoxic stress. These kinases function at different stages of the cell cycle, suggesting that BRCA1 plays a role in regulating cell cycle checkpoints. Among these kinases are ATM, ATR, and CHK2which were reviewed by [248].

2. 2.2 BRCA2

BRCA2 (BReast CAncer type 2 susceptibility protein) is a 384 kDa tumor suppressor protein and is the main mediator protein responsible for RAD51 loading onto ssDNA [184,249]. BRCA1 and PALB2 direct BRCA2 to the DSB sites [250].

BRCA2 has two distinct regions that play a role in binding with RAD51. The first region is composed of eight repeated sequences are known as BRC motifs, each of which is approximately 35 amino acids in length [251]. The second RAD51 interaction motif is located at the protein's C-terminus and spanned from position 3270 to position 3305 (36 residues), which is known as the C-Terminal RAD51- interaction Domain (CTRD; previously referred to as TR2) [184,252,253] (Figure 19).

The results of individual BRC repeats biochemical investigations indicated that BRC1,2,3 and 4 strongly bind to RAD51 monomers and stabilize the RAD51-ssDNA complex. This is due to their ability to inhibit RAD51's DNA-dependent ATPase activity and prevent RAD51 from binding to dsDNA[254]. Besides, it has been reported that the BRC4 repeat inhibits the formation of the NPF of RAD51 by interfering with a critical contact between RAD51 subunits, where *via* its FxxA motif, BRC4 mimics the conformation of the RAD51 segment involved in protomers contact [184,255]. On the other hand, BRC5, 6,7, and 8 cannot bind to free RAD51 and do not affect its ATPase activity. However, they stabilize RAD51-ssDNA nucleoprotein filaments [254].

Esashi F et al., demonstrated that BRCA2's C-terminal region, which interacts with recombination protein RAD51, has a site (serine 3291) phosphorylated by CDKs. This phosphorylation prevents interactions between BRCA2 and RAD51. They also found that During the S phase, when recombination is active, the pSer3291 level is low; however, it increases as cells move toward mitosis [256].

After, *Davies et al.,* discovered that the TR2 motif interacts with RAD51 by specifically recognizing oligomerized RAD51 ATPase domains. This interaction stabilizes the RAD51 nucleoprotein filament against disassembly by BRC4. When the CDKs phosphorylate Ser3291, this eliminates TR2 protection for RAD51 filaments created on single-stranded DNA, causing them to be disrupted by the BRC repeats [252,257] (Figure 19).

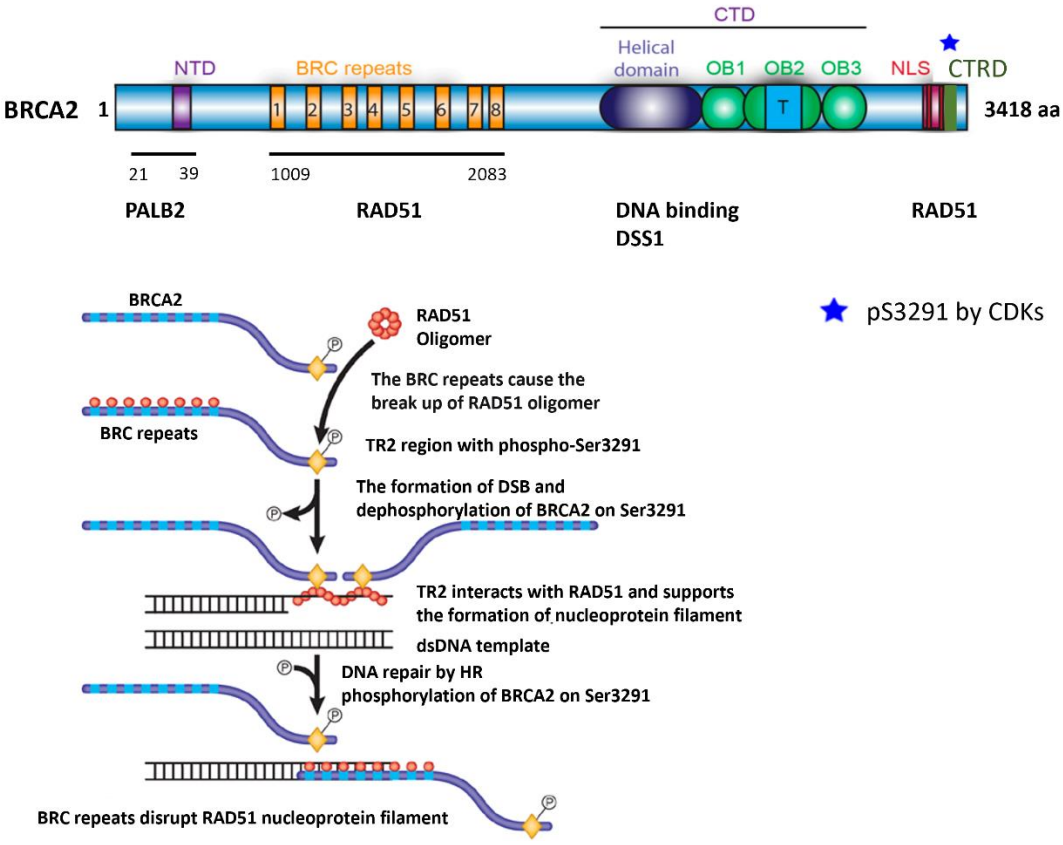

Figure 19 Structure of Human BRCA2 protein

Domain structures with mapped binding partner and phosphorylation sites. The N-terminal DNA-binding domain (NTD) of BRCA2 comprises a protein-interaction site for PALB2 and a DNA-binding site. BRCA2's core domain spans nearly one-third of the protein and contains eight BRC repeats, which are the key RAD51 interaction sites. The C-terminal DNA-binding domain (CTD) is a complex DNA-binding domain capable of binding both ssDNA and dsDNA. The C-terminus additionally contains two nuclear localization signals (NLS) and another RAD51 interaction site (CTRD also known as TR2) that interacts exclusively with RAD51 filaments. The TR2 domain, on the other hand, stabilizes RAD51 coupled to both ssDNA and dsDNA. This figure is adapted from [209,257].

2. 2.2 RAD52

As stated in Chapter 2, RAD52 is crucial for the SSA pathway of DSB repair. The human RAD52 has two domains of equal size (about 209 aa for each one of them): the N-terminal domain (NTD) and the C-terminal domain (CTD). The NTD is responsible for RAD52's oligomerization ability and binding to both ssDNA and dsDNA. In contrast, the CTD interacts with RPA and RAD51 and contains a Nuclear Localization Signal motif (NLS) [258–260] (Figure 20).

Rad52 in *S. cerevisiae* stimulates Rad51 filament formation on RPA-coated ssDNA and stabilizes them *via* protein-protein interactions [261]. However, its ortholog RAD52 in vertebrates plays a secondary role in recombination, where it has been reported that human RAD52 can compensate for the activity of BRCA 1/2 and keep BRCA-deficient cells alive [262]. According to previous studies

on the human breast cancer cell lines, RAD52 knockdown is synthetically lethal in the presence of BRCA2 deficiency [263,264]. Furthermore, it has been reported that RAD52 promotes the MiDAS pathway following replication stress [265] (to get further details about the MiDAS pathway, refer to section 3.2.1-b).

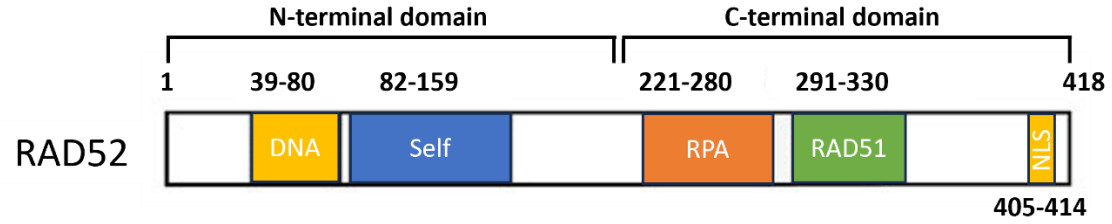

Figure 20 Structure of Human RAD52 protein

The functional domain map of human RAD52. The DNA binding region and a self-associating region are found in the N-terminal domain (NTD), while the RPA and RAD51 interaction regions and a nuclear localization signal are found in the C-terminal domain (CTD).This figure is adapted from [258].

2. 2.3 RAD54

RAD54 is a highly conserved gene that belongs to the RAD52 epistasis group [172]. The protein RAD54 is a member of the SWI2/SNF2 class of the helicases superfamily 2 (SF2) [266,267] (Figure 21). This class's proteins are DNA-binding proteins that participate in gene-specific transcriptional activation or repression by controlling the remodeling of chromatin complexes [267]. Moreover, the RAD54 is a translocase protein that moves along dsDNA in an ATP-dependent manner [268].

In vitro, yeast Rad54 protein significantly increases yeast Rad51 protein's DNA strand exchange activity [269]. Moreover, RAD54 is involved in all three stages of the HRR (presynaptic, synaptic, and postsynaptic). Its role includes stabilizing the NPF onto the ssDNA by interacting with RAD51, remodeling chromatin during the homology search and strand exchange [233,270], and being involved in the dissociation of RAD51 from dsDNA [232].

Additionally, the RAD54 family contains other translocase proteins like RAD54A and RAD54B, chromatin remodelers that enable strand exchange [271].

Collectively, it seems that RAD54 plays a role in DNA repair by helping to maintain the connection between RAD51 and ssDNA before RAD51 initiates the strand exchange process. After that, RAD54 helps to remove RAD51 from the final dsDNA product.

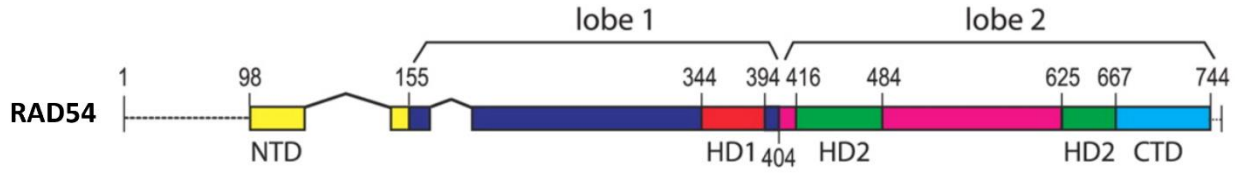

Figure 21 Structure of Human RAD54 protein

Yellow and blue represent the N-terminal domain (NTD) and C-terminal domain (CTD), respectively. The helical domains of Snf2 are shown in red (HD1) and green (HD2). The RecA-like / domains are depicted in blue (lobe 1, which contains motifs I, IA, II, III) and magenta (lobe 2, which contains motifs IV, V, VI). This figure was derived from [266].

2. 2.4 RAD51 paralogs

RAD51 has five canonical paralogs : (RAD51B, RAD51C, RAD51D, XRCC2, XRCC3) and SWSAP1, a non-canonical paralog, has been recently discovered [272]. RAD51 paralogs have ~25% protein identity with RAD51, mainly in the ATP-binding Walker A and B domains, and are similar to each other [273]. In human cells, the five paralogs assemble in two distinct complexes, both of which contain RAD51C. The first complex is (BCDX2) and consist of RAD51B–RAD51C–RAD51D–XRCC2 and the second one is (CX3) is comprised of RAD51C–XRCC3 [274].

Chun et al. reported that in response to DNA damage, the BCDX2 and CX3 complexes function at different points of the HR pathway. The BCDX2 complex comes into action after the recruitment of BRCA2 and just before the recruitment of RAD51. In contrast, the CX3 complex operates after RAD51 recruitment [275].

In a recent study it has been reported that BCDX2 stimulates RAD51 filament nucleation and extension in an ATP-dependent manner; besides, BCDX2 has exhibited a strong affinity towards binding with ssDNA, which was induced by the joined RAD51B and RAD51C ATPases [276].

SWSAP1 was found first as a protein that interacts with SWS1, a human homolog of the fission yeast Sws1 and the budding yeast Shu2 [272]. According to a recent study, SWSAP1 interacts with RAD51 through its conserved Phe-X-X-Ala (FxxA) BRC-like motif. This interaction is required for RAD51-focus formation after DNA damage [277].

Table 1 provides a summary of the functions of each paralog protein.

3. RAD51 regulation

We have seen that RAD51 is highly conserved in all life domains. It plays a crucial role in repairing DSBs through the HRR pathway.

Besides, as mentioned earlier, knockout for the *RAD51* gene causes early embryonic lethality in mouse and chicken embryos, reflecting its importance for cell viability during development. On the other hand, high levels of this recombinase are involved in stimulating genomic instability due to elevating the HRR rate, which contributes to the development of cancers and favors their resistance to chemo and radiotherapy [278,279]. Thus, normal levels of RAD51 are essential for maintaining genomic stability and the survival of cells.

The cell has strict control over the levels and activity of RAD51 at various stages, from regulating the transcription of the *RAD51* gene and post-transcriptional processes to regulating the post-translational modifications (PTMs) and the cellular distribution of RAD51. This section will provide detailed information on the various methods of RAD51 regulation. Additionally, Table 1 will summarize the key RAD51 regulators.

3.1 Regulation of RAD51 expression

The expression of RAD51 is tightly regulated in normal cells. However, In cancer cells, RAD51 mRNA and protein levels are approximately elevated by four and six times, respectively [280].

In this explanation, I will introduce some of the different regulation levels that cells use to control the expression of RAD51.

3.1.1 Transcriptional regulation at the promoter level

Orhan et al. reviewed the various factors that regulate *RAD51* transcription. They classified these factors into three groups. The first group consists of transcription factors like E2F1 and EGR1 along with the CDK12/13, which activate the RAD51 promoter.

The second group includes transcription factors like E2F4/7 and the P53 protein, which exhibit a repressive impact on the RAD51 promoter.

The third group consists of proteins such as BRD4 and CHD4, which activate chromatin remodeling to promote RAD51 gene expression [281] (Figure 22).

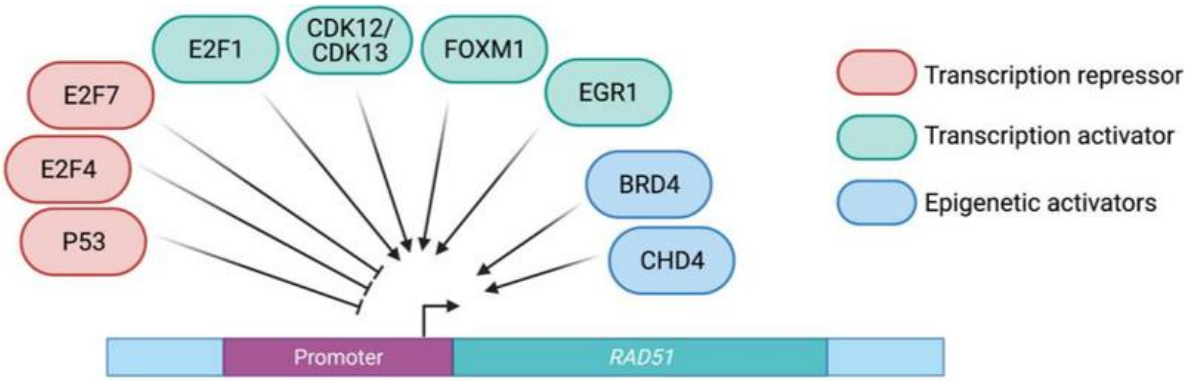

Figure 22 The transcriptional regulators of RAD51

The RAD51 promoter and gene DNA sequences are shown as purple and green boxes, respectively. This figure is taken from [281].

3.1.2 Post-transcriptional regulation of RAD51 by ncRNAs

Non-protein coding RNAs (ncRNAs) are RNA molecules that do not produce proteins but have important cellular functions [282]. They are classified into small ncRNAs and long ncRNAs (lncRNAs). Small ncRNAs include microRNAs (miRNAs), and small interfering RNAs (siRNAs), which are associated with genes and have implications in carcinogenesis [283]. LncRNAs are mRNA-like transcripts that are longer than 200 nucleotides and may contribute to tumorigenesis. They are reviewed by [283].

In this discussion, I will focus on miRNAs and lncRNAs and their role in the post-transcriptional regulation of RAD51.

3.1.2-a- Regulation of RAD51 by miRNAs

MiRNAs are single-stranded RNA molecules encoded by endogenous genes and typically consist of 18-25 nucleotides in length [284]. MiRNAs can indirectly or directly regulate RAD51 expression and influence HRR [285]. Research has shown that miR-34 family members (miR-34a, miR-34b, and miR-34c) can inhibit the expression of RAD51 in human colon adenocarcinoma cells [286].

In addition, Piotto et al. conducted a study that demonstrated the radiosensitizing effect of miR-96-5p in Non-Small Cell Lung Cancer cell line (NSCLC) A549. The study revealed that miR-96-5p targets the 3'-UTR of the RAD51 gene, causing a decrease in the expression level of RAD51. As a result, miR-96-5p increased the radiosensitivity of NSCLC by 20%, similar to chemical inhibitors of HR repair [287].

Moreover, a recent study has identified the loss of miR-214-5P in Triple-Negative Breast Cancer (TNBCs). This loss was only in cell lines derived from African- American women compared to

Caucasian-American (CA) women. According to the study, RAD51 expression is notably elevated in AA TNBC patients compared to other TNBC patients. This was correlated with a higher mortality rate since AA TNBC is resistant to cancer therapy [288]. Additionally, their study found that transfection with miR-214-5P resulted in decreased expression of RAD51, impairing HRR and enhancing the efficacy of chemical treatments [289].

3.1.2-b- Regulation of RAD51 by lncRANs

lncRNAs can act as molecular sponges of miRNAs (lncRNAs have been reviewed by [290]).

In 2015, *Gazy, I. et al.* explored the involvement of a lncRNA known as TODRA (Transcribed in the Opposite Direction of *RAD51*) in RAD51 transcription regulation. TODRA is transcribed just 69bp upstream of *RAD51* [291].

The study discovered that TODRA has a role in regulating the expression of *RAD51* through E2F1 and TPIP, which is a part of the PTEN phosphatase family, where TODRA induces the expression of TPIP. The TPIP, in turn, co-activates RAD51 induction by E2F1. This shows that RAD51 expression and activity are regulated by a feedback loop in which TODRA participates. Moreover, The researchers observed that overexpressing of TODRA increases DSB repair through the HR and also improves the formation of RAD51 foci following DNA damage [291] (Figure 23A).

In 2018, *Shen et al*., found that a type of lncRNA called ionizing radiation-inducible lncRNA (lnc-RI) helps to keep RAD51 mRNA stable by competing with microRNA called miR-193a-3p. The results showed that miR-193a-3p target both RAD51 mRNA and lnc-RI, causing RAD51 mRNA degradation to be accelerated, hence decreasing *RAD51* expression [292] (Figure 23B). They also demonstrated that knocking down the lnc-RI resulted in a sharp decrease in *RAD51* expression. Additionally, there was a noticeable increase in spontaneous DSB levels along with a decrease in the effectiveness of the HHR in lnc-RI-depressed cells [292].

In 2023, *Zhang, X. et al.* documented the mechanism by which lncRNA is known as CACClnc (Chemoresistance Associated Colorectal Cancer lncRNA) controls *RAD51* expression and promotes Colorectal Cancer (CRC) chemoresistance. Their findings revealed that CACClnc binds specifically to two proteins, Y-box binding protein 1 (YB1, a splicing factor) and U2AF65 (a subunit of U2AF splicing factor), which in turn promotes their interaction and modulates the Alternative Splicing (AS) of *RAD51* mRNA (Figure 23C). As a result, the biology of CRC cells is altered. They found that CACClnc can prevent abnormal alternative RNA splicing of *RAD51* [293].

When they knocked down the CACClnc in cells, they observed a significant increase in a transcript variant of RAD51 (RAD51-204) that lacked exon 6 (exon 6-). This variant could not be translated into protein. In contrast, the CACClnc knockdown was combined with reducing RAD51 transcript with exon 6 (exon 6+) (Figure 23C). Therefore, CACClnc upregulates *RAD51* expression by preventing exon 6 exclusion (exon 6-) [293].

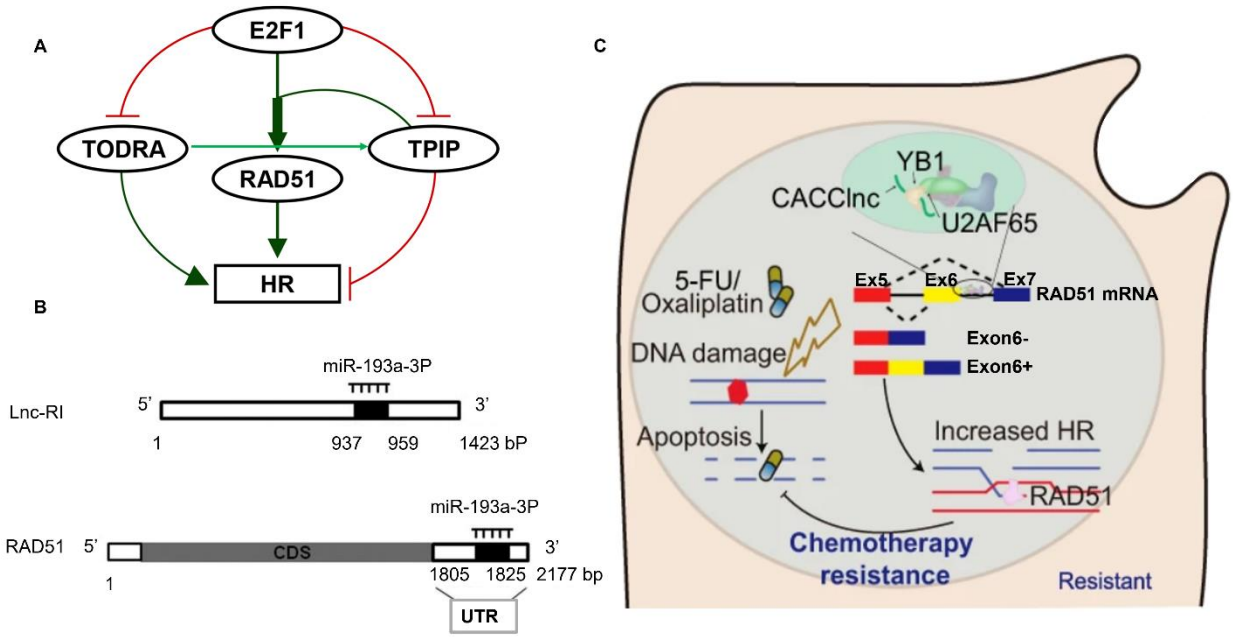

Figure 23 The lncRNA regulates the *RAD51* expression.

A) **The TODRA lncRNA mediates a novel feedback loop that controls the expression and activity of RAD51**. When E2F1 is induced, it causes an increase in RAD51 expression while at the same time decreasing the expression of lncRNA TODRA and TPIP. In addition, the induction of RAD51 by E2F1 is made even stronger by TPIP (shown by the thick green arrow). E2F1 induction decreases TPIP expression, possibly by impacting TODRA expression, which promotes TPIP expression. This feedback regulation of RAD51 expression helps to finely control its expression and facilitate HR-DSB repair. The green arrows indicate an enhancement of expression or activity, while the red arrows indicate a suppression of expression or activity. B) Predicted miR-193a-3p target locations in lnc-RI and the RAD51 mRNA 3'UTR .C) The CACClnc/YB1/U2AF65 axis functions as a switch to control the alternate splicing of the RAD51 pre-mRNA, which in turn controls chemoresistance in human CRC.

3.2 Regulation of RAD51 by Post-translational Modifications

Protein properties can be altered through post-translational modifications (PTMs), which involve covalent processing events. These modifications include proteolytic cleavage and the addition of a modifying group like acetyl, phosphoryl, glycosyl, or methyl to one or more amino acids [294]. In the upcoming section, I will highlight the impact of ubiquitination/ SUMOylation and phosphorylation on RAD51 activity.

3.2.1 Regulation of RAD51 by Ubiquitination

Ubiquitination (or Ubiquitylation) is a type of PTMs that involves attaching ubiquitin (Ub), a 76-amino acid protein, to a specific target protein. Multiple ubiquitin molecules binding to a target protein can make it a proteasome target for degradation. However, ubiquitination may have non-proteolytic purposes, including controlling signaling cascades and protein-protein interactions [295,296]. Three enzymes are involved in the ubiquitination pathway, including ubiquitin-activating enzyme (E1), ubiquitin-conjugating enzyme (E2), and ubiquitin-protein ligase (E3) [297].

The Ubiquitin-Proteasome System (UPS), notably E3 ligases, serve as a link between cellular metabolism and DDR by regulating the enzymes involved in both processes [298]. The E3 Ub ligases (E3s) catalyze the formation of an iso-peptide bond between the substrate's lysine-amino group and the C-terminal carboxyl group of Ub [299].

It has been reported that the RFWD3 E3 ubiquitin ligase can physically interact with RAD51 and polyubiquitinates it *in-vitro* and *in-vivo*. As a result of the RFWD3-dependent ubiquitination process, RAD51 undergoes degradation through the proteasome [300].

A recent study on stem and progenitor cells revealed that the protein PUMA (p53 upregulated modulator of apoptosis) can prevent RAD51 nuclear translocation and the HRR by interacting with the Early Mitotic Inhibitor 1 protein (EMI1) that promotes the degradation of cytoplasmic RAD51 through ubiquitination. Furthermore, the study found that cells lacking PUMA have higher DSB DNA repair activity *via* the HRR [301]. Moreover, RAD51 ubiquitination hinders RAD51-BRCA2 contact, whereas RAD51 deubiquitination mediated by UCHL3 enhances RAD51-BRCA2 binding and facilitates RAD51 recruitment to DSBs [302].

3.2.2 Regulation of RAD51 by SUMOylation

Alternatively, Small Ubiquitin-like Modifier (SUMO) proteins bind to specific lysine residues in target proteins through the process of SUMOylation, which controls many aspects of protein function, including transcription, subcellular localization, cell cycle, and DNA repair [303].

According to a recent study, the topoisomerase 1-binding arginine/serine-rich protein (TOPORS) induces RAD51 SUMOylation at lysine residues K57 and K70 in response to DNA damage. The results demonstrated that knocking down TOPORS or expressing SUMOylation-deficient RAD51 mutants reduced the ability of RAD51 to support normal HRR activities. These were linked to

RAD51's reduced ability to interact with BRCA2, which explains why it is less effective in supporting HRR [304].

Another study showed that the Hepatocyte Growth Factor (HGF) can induce RAD51 transcription and SUMOylation at K70 in human Mesenchymal Stem Cells (hMSCs). This process leads to an increase in telomere length and mtDNA replication, resulting in higher ATP generation and preventing hMSC senescence [305].

3.2.1 Regulation of RAD51 by Phosphorylation

Phosphorylation is the most studied PTM. It is a reversible modification in which a protein kinase adds a covalently bonded phosphate group to the serine, threonine, or tyrosine residues. The phosphorylation leads to significant conformational changes in the protein 3D structure, which can activate or inactivate its function [306]. The phosphorylation of RAD51 plays a crucial role in regulating its activity and ability to be recruited to DSB sites [307]. In the following section, I will review the reported phosphorylated RAD51 sites in more detail (Figure 25).

3.2.1-a- Sequential phosphorylation of Tyr315 and Tyr54 residues

In 1998, *Yuan, Z.-M. et al*. conducted a study that showed for the first time that phosphorylation regulates RAD51 [187]. Based on their research using mass spectrometry, they discovered that a target of c-ABL kinase is tyrosine 54 (Y54) residue. Their results were validated *in-vitro* and *in-cellulo, showing* inhibitory effects on RAD51 activities [187]. A year later, *Chen, G. et al.* reported that c-ABL phosphorylates tyrosine 315 (Y315). Their studies, both *in-vitro* and *in- cellulo*, revealed that RAD51 phosphorylation mediated by c-ABL is likely to promote repair through homologous recombination [308].

Furthermore, later studies confirmed the phosphorylation of Y54 and Try315 by c-ABL or its oncogenic fusion protein BCR/ABL [309,310]. According to a study conducted *in-vitro* using a phosphomimetic method, it was found that the phosphorylation of Y54 enhances RAD51's ability to exchange DNA strands. This occurs through a change in the properties of the nucleoprotein filament. However, the phosphorylation of Y315 appears to have little effect on RAD51's functions [311].

Studies in our laboratory have demonstrated that this dual phosphorylation is linked to a sequential phosphorylation mechanism. C-ABL kinase phosphorylates RAD51 on Y315, which in turn promotes the second phosphorylation at position Y54 [310,312].

Moreover, during a co-immunoprecipitation of RAD51 from cells that were overexpressing RAD51 and ABL-related gene (ARG), a member of the c-ABL family, it was found that ARG could interact with RAD51. An anti-phosphoTyrosine antibody indicated that ARG phosphorylates RAD51, which appears to be more effective than the phosphorylation by c-ABL. However, the exact location of the phosphorylation was not determined [313].

3.2.1-b- Sequential phosphorylation of Ser14 and Thr13 residues

In 2012, *Yata, K. et al.* reported that RAD51 is phosphorylated during the cell cycle in response to DNA damage at serine 14 (S14) by Polo-Like Kinase 1 (PLK1). The S14 phosphorylation enables subsequent RAD51 phosphorylation at threonine 13 (T13) by Casein Kinase 2 (CK2) [314]. T13 phosphorylation of RAD51 by CK2 results in direct contact with the Forkhead-associated (FHA) domain of the MRN component, NBS1. Moreover, this subsequent dual phosphorylation, which occurs in the N-terminal regulatory domain of RAD51, appears vital for accurate HRR and cellular resistance to genotoxic stresses [314].

Another study reported that having functional BRCA2 impacts the level of phosphorylated S14 in the nuclear soluble fraction. Whereas, the research revealed that the phosphorylation of Threonine 77 (T77) of BRCA2 by CDKS facilitates the binding to PLK1, which results in BRCA2 acting as a platform to aid in RAD51 phosphorylation by PLK1 [315,316] (Figure 24).

Moreover, during mitosis, under-replicated DNA, which is often seen at Common Fragile Sites (CFSs), can cause problems with chromosome separation and prevent SAC satisfaction [317,318]. It has been suggested that under-replicated CFSs finish replicating during early mitosis through a process called Mitotic DNA synthesis (MiDAS), which resembles break-induced replication (BIR) [319,320]. Upon cells entering the mitotic phase, MiDAS is initiated by the cleavage of stalled replication forks, leading to DSBs [265,318]. It has been documented that the S14/T13 phosphorylation peaks during mitosis and assists in recruiting RAD51 to under-replicated DNA, promoting MiDAS. Additionally, the S14/T13 phosphorylation plays a crucial role in promoting cellular proliferation [318].

A study published in July 2021 examined the role of AURKA and CHK1 in activating PLK1 [321]. The researchers focused on whether AURKA or CHK1-mediated PLK1 activation was essential for RAD51 phosphorylation. Their findings indicate that while activated CHK1 can phosphorylate and activate PLK1 to phosphorylate RAD51 at S14, AURKA does not play a significant role in this

process. Interestingly, it was shown that CHK1 directly promotes RAD51 phosphorylation at T309 [321].

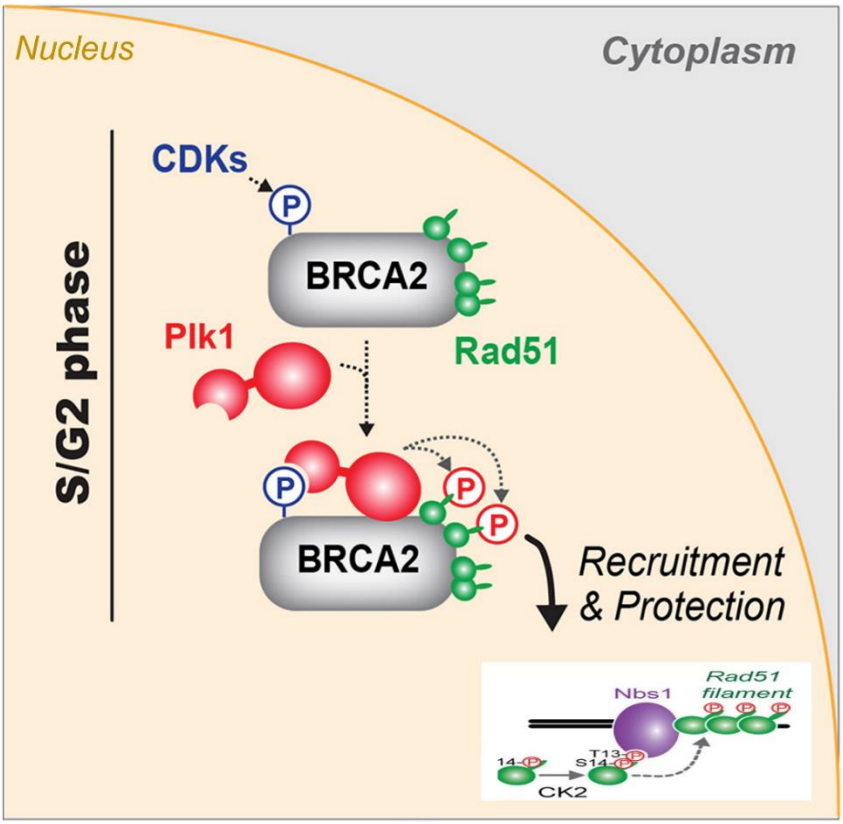

Figure 24 Phosphorylated RAD51 at S14 and T13.

The model demonstrates that BRCA2 serves as a platform to aid in the S14 RAD51 phosphorylation by PLK1. Sequential RAD51 phosphorylation, mediated by CK2 on T13, is necessary for RAD51 recruitment to DSB sites through 50 phosphor-dependent binding to NBS1. The figure was adapted from [315].

3.2.1-c- Phosphorylation of RAD51 on Threonine 309

According to a study by *Sørensen, C. S. et al.* CHK1 interacts with RAD51 and leads to the phosphorylation of RAD51 on Threonine 309 (T309) in a CHK1-dependent manner [322].

It has been suggested that the CHK1 kinase plays a role in developing RAD51 foci after genotoxic therapy. However, when siRNA transfection was used to reduce CHK1 expression, the development of RAD51 foci in response to UV light irradiation was significantly reduced. In contrast, CHK2 inhibition had no effect [323]. Thus, the development of RAD51 foci depends on its phosphorylation at T309, a consensus CHK1 phosphorylation site [322,324].

In addition, it has been demonstrated that overexpression of T309A, a non-phosphorylatable mutant form of RAD51, led to sensitizing cells to chemotherapy agents by inhibiting HRR [325].

3.2.1-d- Phosphorylation of RAD51 on Y159, Y191, Y205, and Y315 tyrosine residues

In previous research conducted by our laboratory, *Chabot, T. et al.* discovered that RAD51 could be phosphorylated *in-vitro* at four specific tyrosine residues - Y159, Y191, Y205, and Y315 - by the receptor tyrosine kinase, c-MET. These tyrosine sites are located at the interfaces of RAD51 monomers and play a significant role in promoting the formation of RAD51 oligomers [326].

Additionally, these modifications also regulate the interaction between BRCA2 and RAD51, as the molecular modeling of RAD51-BRC4 reveals that the Y159, Y191, and Y205 residues are in direct contact with the BRC4 peptide [326].

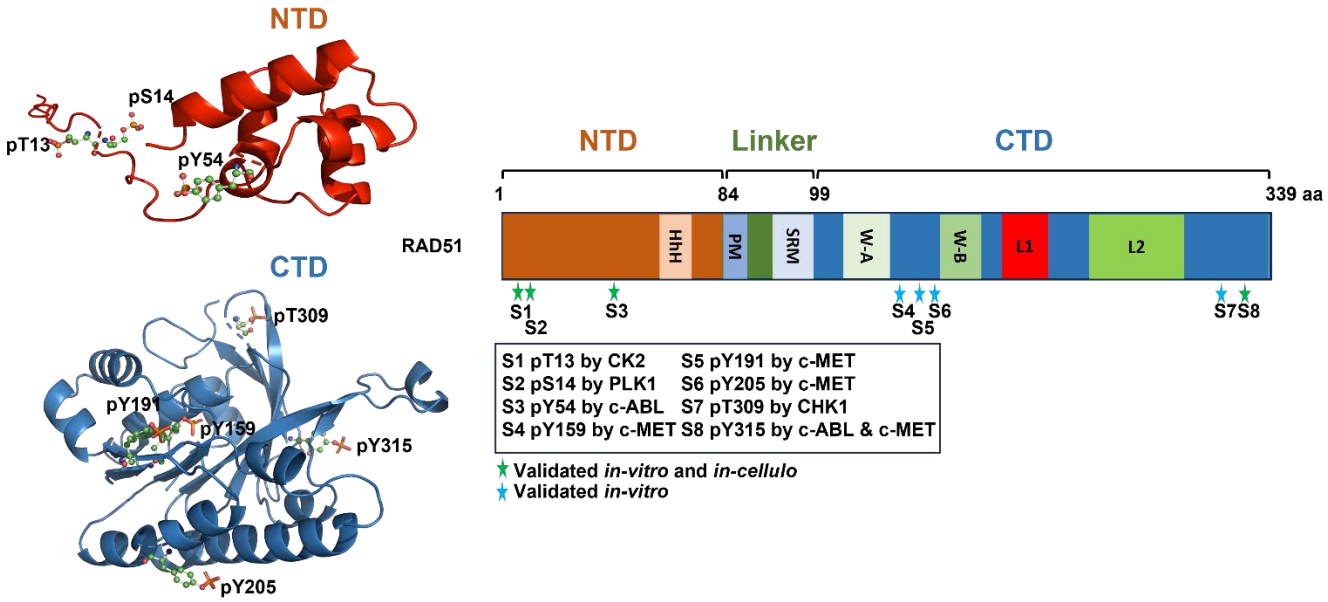

Figure 25 Phosphorylation sites of RAD51

The right panel represents the domain structures of RAD51 with mapped motifs and phosphorylation sites; RAD51 has two different domains: The residues 1–84 form the N-terminal Domain (NTD) within the Helix-hairpin-Helix motif (HhH) motif. The C-terminal Domain (CTD) is formed by residues 100-339 and contains the Walker-A (W-A), Walker-B (W-B), Loop1 (L1), and Loop2 (L2). The Linker (residues 85-99) binds between the NTD and the CTD and contains the polymerization motif (PM) and the Subunit Rotation Motif (SRM). The known phosphorylation sites are distributed in the NTD and CTD and are indicated by stars. **The left panel** displays the phosphorylated residues in their 3D configuration. This panel was created with pyMOL using the AlphaFold RAD51 3D structure, AF-Q06609-F1-model_v4 [200,201] *(Alaouid. M's thesis)*.

3.3 RAD51 cellular distribution

In 1995, *Haaf et al.* utilized antibodies produced against RAD51 to determine its distribution within human somatic cells. They discovered that only a small percentage (10% or less) of cells exhibited detectable nuclear immunolabeling. The RAD51 protein was focal and clustered in distinct sites throughout the nucleoplasm of these immune-positive cells, varying from several dozen to several hundred. Moreover, it was mostly absent from the nucleoli and cytoplasm.

Furthermore, when cells were exposed to DNA-damaging agents, most nuclei in treated cells exhibited a significant increase in RAD51 foci [327]. However, their Western blot analysis revealed no net increase in RAD51 protein in irradiated cells. Thus, they suggested that DNA damage primarily impacts RAD51's nuclear distribution [327].

In their laser microirradiation experiments on a human fibroblast cell line GM02063, *Tashiro et al.* found that RAD51 foci disappeared in non-irradiated nuclear areas in a dose-dependent manner. This resulted in the exclusive accumulation of RAD51 at microirradiated nuclear sites, indicating that RAD51 was selectively redistributed to damaged DNA sites [328].

Moreover, RAD51 foci are present in undamaged S-phase cells and are believed to indicate sites where stalled or damaged replication forks undergo repair [329]. However, the formation of RAD51 foci in non-irradiated S-phase cells does not seem to require BRCA2, suggesting that the assembly of RAD51 foci during the S phase and in response to ionizing radiation occurs through different pathways, each with specific protein requirements [330].

Thereby, to repair DNA damage, RAD51 must be nuclear translocated and redistributed to damaged sites. In this section, I will attempt to summarize existing knowledge on this topic.

3.3.1 RAD51 nuclear translocation:

The nuclear translocation of RAD51 is highly dynamic and regulated, particularly in response to DNA damage [331]. RAD51 monomer, with its mass of 37 kDa, could freely travel across nuclear pores, which generally accommodate substrates ≤ 60 kDa [332]. However, for a protein such as RAD51, things do not happen like that because uncontrolled levels of RAD51 inside the nucleus may lead to genome instability *via* random and harmful recombination events. Hence, the cell must strictly regulate this process, as we will see.

Although the RAD51 protein has a Nuclear Export Sequence (NES), it does not possess a Nuclear Localization Signal (NLS). Additionally, due to the possibility of RAD51 forming polymers, it may not be able to traverse the nuclear pores if present in the cytoplasm as dimers (74 kDa) or multimers. These facts imply that the RAD51 protein requires active assistance to move from the cytoplasm to the nucleus highlighting the significance of RAD51 cellular distribution as a mechanism of RAD51 regulation.

However, previous studies showed that RAD51 interacts with other proteins comprising a functional NLS [199,333].

A study conducted by *Tarsounas et al* in 2003 found that cells with a BRCA2 truncating mutation were unable to form RAD51 foci when exposed to IR. However, these cells still formed S-phase foci normally [330]. One year later, they reported a good co-localization between RAD51 and BRCA2 in the IR-induced foci. Besides, using band-shift assays and electron microscopy they demonstrated that BRC4 prevented RAD51 from binding to DNA and forming nucleoprotein filaments. Additionally, they found that single amino acid changes in the BRC motifs eliminated the inhibitory effect, allowing RAD51 to bind to DNA normally in the presence of mutant peptides. Based on their findings, they concluded that BRCA2 plays an essential role in the accumulation of RAD51 at damage-induced foci. BRCA2 acts as a scaffold that maintains RAD51 inactive until DNA damage occurs. Once the damage occurs, BRCA2 and RAD51 relocate to repair foci, where RAD51 is released to form a nucleoprotein filament [334].

In fact, BRCA2's nuclear localization is maintained *via* its interaction with a protein named DSS1 *via* its DSS1-binding domain (DBD). This interaction hides the BRCA2's NES, thus preventing it from binding to CRM1, the nuclear exportin protein. Furthermore, it has been observed that mutations in the DBD of BRCA2 impair its binding to DSS1, causing BRCA2 to become cytoplasmic [199]. In the case of RAD51, the interaction between BRCA2's BRC4 repeat and RAD51 prevents CRM1 protein from binding to RAD51's NES [199]. Thereby, both BRCA2-DSS1 and BRC4-RAD51 interactions cause NES masking, which is crucial for preserving the nuclear localization of BRCA2 and RAD51.

On the other hand, using a series of mutant RAD51 proteins that exhibit a disruption in self-assembly and/or to bind BRCA2, *Yu et al*. demonstrated that the proteins with mutations that affect both self-association and BRCA2 binding have shown a capability for nuclear entry. In contrast, those with a defect only in BRCA2 binding did not show the ability to enter the nucleus [210].

Gildemeister et al. experiments with Capan-1 cells have shown that nuclear RAD51 levels increased following DNA damage induction simultaneously with an increase in nuclear foci of RAD51C, a paralog of RAD51, which interacts directly with it during HRR. RAD51C has a functional NLS that allows it to nuclear entry. The Capan-1 cell transfection with RAD51C siRNA induces a significant reduction of the nuclear RAD51 levels in both steady state and after induction of DNA damage [335].

Moreover, according to *Garcin et al*., the five classical RAD51 paralogs (RAD51B, RAD51C, RAD51D, XRCC2, and XRCC3) are crucial in the formation of stable RAD51 nuclear foci, both

	Regulator	Level of Regulation	Function
Positive Regulators	CDK12/CDK13	*RAD51* transcription	RNA polymerase II Regulator
	E2F1	*RAD51* transcription	Transcription Factor
	FOXM1		
	EGR1		
	BRD4	*RAD51* transcription	Transcription Activator
	CHD4	*RAD51* transcription	Chromatin Remodeler
	TODRA	*RAD51* post-transcription	lncRNA
	lnc-RI		
	CACClnc		
	PLK1	PTM	Kinase
	CK2		
	CHK1		
	RAD51B; RAD51C	RAD51 protein and NPF	The RAD51 paralogs serve as a recombination mediator and help stabilize the filament.
	RAD51D; XRCC2		
	XRCC3; SWSAP1		
	BRCA2	RAD51 monomers and NPF	Recombination mediator
	RAD52	ssDNA,dsDNA, RPA and RAD51	Recombination mediator, SSA, and MiDAS
	RAD54	dsDNA and NPF	The ATP-dependent dsDNA translocase is responsible for stabilizing the RAD51 filament and a dissociation of RAD51 after completing HRR.
Negative Regulators	E2F4	*RAD51* transcription	Transcription Factor
	E2F7		
	P53		
	MiR-34 a,b, and c	*RAD51* post-transcription	MicroRNAs
	miR-214-5P		
	miR-96-5p		
	miR-193a-3p		
	FBH1	PTM	Ubiquitin ligase
	FBX05		
	RFWD3		
	BLM	NPF	DNA helicase has multiple roles in HR and DNA replication, including resolution dHJ.
	RPA	Resected ssDNAends	Competition with RAD51

Table 1 Regulators of RAD51.

Abbreviation: post-translational modification (PTM), NucleoProtein filament (NPF) and long-non-coding RNA (lncRNA). Adapted from [281,336].

spontaneously and due to IR. They conducted a study to investigate the role of RAD51 paralogs in forming spontaneous and IR-induced RAD51 nuclear foci using immunofluorescence in U2OS lines that were either wild-type or RAD51 paralog-deficient. They observed that the number of positive cells (cells with at least five foci per nucleus) was markedly reduced in the paralog-deficient cells and was completely restored when each RAD51 paralog was re-expressed [337].

The previous findings suggest that RAD51 nuclear translocation can occur through distinct pathways involving both BRCA2 and RAD51 paralogs.

Objectives

During previous *in-vitro* investigations conducted in our laboratory, *Benhelli et al.* discovered that Aurora-A, a mitotic serine/threonine kinase, has the ability to phosphorylate RAD51 at the serine 97 residue that is located within the linker domain. Therefore, my Ph.D. research aims to investigate the presence of this newly phosphorylated form of RAD51 in a cellular context.

Additionally, I want to investigate whether Aurora A or other kinases are involved in the phosphorylation of Ser97 in the cells. My work also aims to understand how phosphorylation at Ser97 affects RAD51 activity.

II- Materials and methods

1. *In-Vitro* Methods

1.1 Proteins production and purification

1.1.a- Protein production

Human Wild type (WT) RAD51 DNA sequence was cloned into the pET15b vector (Novagen-Merck, Darmstadt). This plasmid was used as a template for site-directed mutagenesis to obtain two pET-15b plasmids for RAD51 mutants: S97D (phosphomimetic) and S97A (non-phosphorylatable). The plasmids encoding His-tagged RAD51, both wild-type and mutated versions (S97A, S97D), were transformed into Chloramphenicol-resistant (CmpR) Escherichia coli BL21-DE3 strain.

The transformed bacteria were then grown in one litter of Lysogeny Broth (LB) containing ampicillin (100µg/mL) and Chloramphenicol (20µg/mL) to select transformed bacteria. The culture was agitated until an OD600nm of 0.6 was obtained. Then, the induction was carried out at 30°C overnight by adding IPTG (Isopropyl β-D-1-thiogalactopyranoside) to the final concentration of 1 mM. (1 ml of culture was saved before and after induction as a control). The bacteria were centrifuged for 25 min at 4100 rpm, and the pellets were lysed in a lysis buffer containing (Tris-HCl pH 8 50 mM, NaCl 500 mM, glycerol 10%, imidazole 5 mM, β-mercaptoethanol 5 mM) supplemented with lysozyme (1 mg/mL), and DNAse (5µg/mL). For effective bacterial lysis, the solutions underwent three freeze and thawing cycles at -80°C for 15 minutes each. They were followed by two cycles of sonication (5 minutes, pulse 5s on/5s off, amplitude 80%). The Supernatant fraction (contains the His-tagged RAD51 proteins) and the insoluble fraction were separated after 30 minutes of centrifugation at 12000rpm, at 4°C. Before proceeding purification, the effectiveness of induction was investigated using a gel electrophoresis on 1 mL samples of bacteria before and after induction.

1.1.b- Protein purification

The supernatant was incubated in a column of Ni-NTA Resin (#P6611, Sigma-Aldrich, Saint-Louis, MO, USA) for 1 hour at 4° C on the rotating mixer. The supernatant was allowed to pass through the resin. The flow-through fraction (FT) was saved for additional control procedures. The nickel resin was then washed using the washing buffer: Tris HCl 50 mM, NaCl 500 mM, glycerol 10%, β-mercaptoethanol 5 mM, (and increasing concentrations of imidazole 20 mM, 60 mM, and 80

mM). Afterward, the proteins were eluted using a 300 mM imidazole solution in 2 mL fractions. The most concentrated fraction is determined by quantifying the eluted fractions using the Bradford protein assay, after which it is dialyzed. Dialysis was performed over two days at 4°C in order to eliminate the imidazole (dialysis buffer: Tris HCl pH8 50mM, NaCl 500mM, Glycerol 10%, EDTA 1mM, Dithiothreitol (DTT) 1mM, with decreasing imidazole concentration). The dialyzed fraction is then aliquoted in a microtube. The aliquots are numbered, labeled, and stored at -80°C. To check the purity of the proteins, the obtained fractions were migrated on Sodium Dodecyl Sulfate PolyAcrylamide Gel Electrophoresis (SDS-PAGE) and stained with Coomassie blue.

1.2 RAD51 *in vitro* Phosphorylation

Recombinant Aurora A protein from SIGMA (A1983) or recombinant Aurora B from ProQinase(0190-0000-1) were used to phosphorylate recombinant RAD51 *in-vitro*. The phosphorylation reaction was conducted using 5 µg of RAD51 and 200 ng of Aurora enzymes at 37°C for 20 minutes in a solution containing 50 mM Tris HCL pH=7.5, 10 mM MgCl2, 50 µM DTT, 50 µM ATP. The products of phosphorylation were separated using a 12% acrylamide gel electrophoresis.

1.3 Identification of Phosphorylated Sites Using Mass Spectrometry (MS)

Proteins were colored by the BIO-SAFE Coomassie stain reagent (BIORAD, 1610786) according to the manufacturer's recommendations. Gels slices were maintained in 1% acetic acid solution at room temperature before their digestion and analysis. MS/ORBITRAP analysis was performed by the 3P5 core facility (Institut Cochin, Paris). Two independent experiments were conducted and gave the same results.

1.4 Interferometry analysis of RAD51's DNA/RNA binding

1.4. a- The Principle

BLItz by Molecular Devices, San Jose, CA, USA, is an instrument that uses the Biolayer Interferometry (BLI) technology to study biomolecular interactions. This optical biosensing technology provides a label-free analysis and allows for real-time measurement of binding/dissociation kinetics and affinity. During this method, one biomolecule (DNA or RNA in our case) is immobilized on a fiber optic sensor (tip) surface, and an optical signal is used to detect the binding partner (RAD51 protein) from the solution as it associates with the immobilized biomolecule [338] (Figure 26).

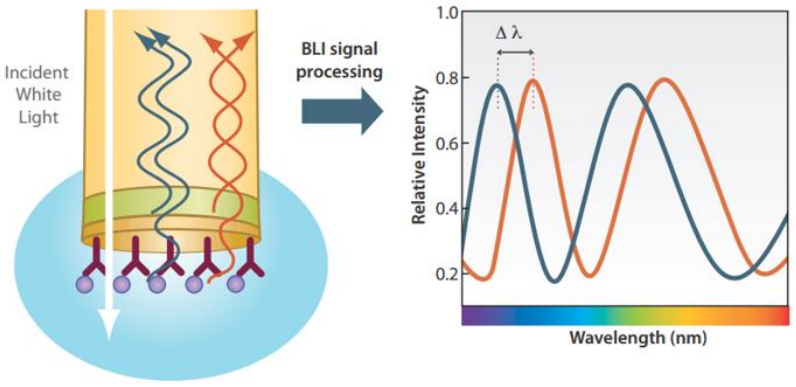

Figure 26 Principles of biolayer interferometry (BLI)

Schematic view of a BLI biosensor. The BLItz device emits white light through the biosensor and gathers any reflected light. The thickness of the coating on the optical layer influences the wavelengths reflected. Certain wavelengths exhibit constructive interference (blue), whereas others exhibit destructive interference (red). A spectrometer detects this interference as a distinct spectral signature and reports it in relative intensity units (nm). Any change in the amount of molecules bound to the biosensor creates a real-time shift in the interference pattern (Δλ). This wavelength shift is a direct measure of the change in optical thickness (nm) of the biological layer. This figure was taken directly from the BLITZ user guide of Fortebio.

1.4.b- Basic protocol of BLITZ

100 mM of 5' biotinylated 33 mer of DNA or RNA bound on a streptavidin-coated biosensor. DNA and RNA sequences are given below. WT and mutants RAD51 (S97D and S97A) recombinant proteins were diluted at different concentrations (0.5 µM, 1 µM, 2 µM, 3 µM and 4 µM) in PBS buffer 1× and ATP 2 mM. The streptavidin tips were hydrated before use and then used to immobilize biotinylated DNA or RNA. After the BLITZ was programmed for three kinetic steps as follows: The buffer baseline was measured for 10 sec, then the association step between ssDNA or ssRNA and RAD51 at different indicated concentrations from 0,5 to 4 µM was monitored for 200 sec, and finally, the dissociation step of the bound RAD51 was monitored for 200 sec. The tip was regenerated in NaOH (50 mM) twice for 40 sec before reuse.

Nucleic acids sequences:

33m DNA: 5' TCCTTTTGATAAGAGGTCATTTTTGCGGATGGC 3'

33m RNA: 5' GCCAUCCGCAAAAAUGACCUCUUAUCAAAAGGA 3'

1.5 D-loop assay

1.5.a- The principle

The D-loop assay involves the formation of D-loops by proteins involved in homologous recombination, such as RAD51 and DMC1. These proteins bind to a labeled ssDNA and promote

the invasion of a homologous dsDNA molecule provided by a supercoiled plasmid containing a homologous sequence (Figure 27).

The D-loop structure involves labeled ssDNA and the plasmid, meaning it migrates less far than labeled DNA alone during agarose gel analysis, allowing for later quantify it after gel scanning.

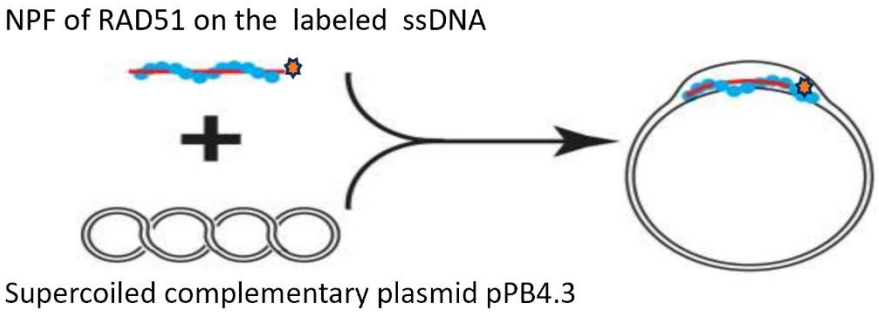

Figure 27 D-loop reaction formation

In-vitro incubation of RAD51 (in blue) with a labeled ssDNA (in red) to form the nucleofilament (NPF). The formed NPF catalyzes D-loop formation with supercoiled plasmid dsDNA pPB4.3. The D-loop complex could be measured thanks to the labeled probe, which is detectable at 700nm. The figure was modified from [339].

1.5.b- Basic protocol of D-loop

Following the D-loop protocol of our lab, 0.5 µM of the recombinant RAD51 protein was incubated with 1 µM ssDNA of 100 nucleotides and labeled with IRD700 (Integrated DNA Technologies, Coralville, IA, USA) at 37°C for 5 min in 10µL of reaction buffer, containing 25mM of Tris-HCl pH 7.5, 1mM of CaCl2, 1mM of ATP, 1 mM DTT and 2 µL 100-ss-IRD700 DNA (1 µM). Supercoiled Plasmid pPB4.3 DNA was added at a final concentration of 200 µM to start the strand exchange reaction. After incubating for 30 minutes at 37°C, the reaction was stopped by adding 10 mM Tris HCl pH=8, 10 mM MgCl2, and 1% SDS (final concentrations). Proteinase K (1mg/mL) was used to deproteinize the reaction for 15 minutes at 37°C. Electrophoresis on a 1% agarose gel in 0.5x TAE buffer (20 mM Tris, 10 mM acetic acid, and 1 mM EDTA) at 100 V for 2 hours separated the reaction products. The detection of the IRD-700 dye with the Odyssey Infrared Imager (LI-COR Biosciences) with the 700 nm infrared fluorescent detection channel allowed us to detect and quantify the ssDNA and D-loop structures.

2. *In-Cellulo* Methods

2.1 Cell culture

The human basal-like TNBC cell line, HCC1806, and HeLa were grown in 100 mm x 20 mm dishes (for sub-fractionation experiments) or six-well plates (for total extract experiments) at 37 °C

under a humidified atmosphere containing 5% CO2. RPMI 1640 medium 1X (Life Technologies, Carlsbad, CA, USA) and DMEM medium 1X (Dulbecco's Modified Eagle Medium) were used as growth media for HCC1806 and HeLa, respectively. Each growth medium was supplemented with 10% fetal bovine serum and 1% penicillin /streptomycin (REF15140-122, Gibco).

2.2 Cellular treatment

Cells were treated with 10 µM Camptothecin (C9911-100MG, Sigma), or (5 or 10 µM) Pladienolide B (SC-391691, Santa Cruz Biotechnology) for 4 or 24 hours. Alisertib (cat.# HY-10971/CS-0106, Medchemexpress) was used to suppress Aurora-A activity at various concentrations (10, 50, 100, or 500 nM). Additionally, either 50 or 100 nM of KU55933 or NU7441 from Selleckchem, (Cat.no.S1092 or Cat.no.S2638, respectively), or AZ20 (TargeMOl CAS No. : 1233339-22-4) at a concentration of 5 or 50 nM, were used to inhibit ATM, DNA-PK, and ATR respectively, were applied to the cells. Dimethylsulfoxide (DMSO) was initially used to dilute the kinase inhibitors and prepare stock solutions. The stock solutions were stored at -20°C, and additional dilution steps were carried out, if necessary, with growth media to treat the cells with concentrations of the nM range.

Pladienolide B (PlaB) is a macrocyclic splicing modulator that selectively binds to splicing factor 3B (SF3B) and inhibits pre-mRNA splicing (Figure 28). By acting like a wedge within a hinge, PlaB stalls SF3B in an open conformation, modulating SF3 B's transition to the closed conformation needed for correct splicing activity. PlaB also inhibits tumor cell proliferation [340].

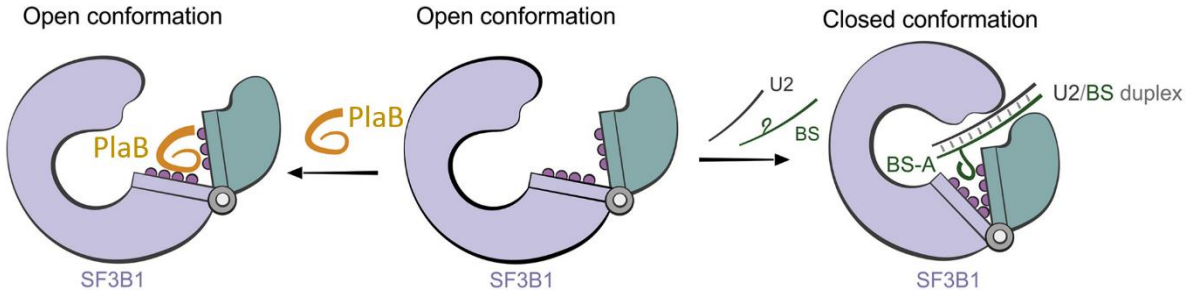

Figure 28 Schematic diagram represents the mechanism of action of PlaB.

SF3B is a multi-protein complex that plays a crucial role in recognizing and selecting Branch Sites (BS) during pre-mRNA splicing. U2 is a ribonucleoprotein composed of U2 snRNA and splicing factors SF3A and SF3B, which recognize BS during splicing. Subunits of the SF3B complex stabilize the U2/BS interaction by contacting intron nucleotides flanking the BS adenosine (BS-A). Modulating SF3B's transition to the closed conformation is necessary to form the adenosine-binding pocket of the BS and stably accommodate the BS/U2 duplex. PlaB (orange) binds to SF3B1 in an "open" state, inhibiting stable accommodation of the U2/BS helix and BS-A, which need a "closed" protein conformation [340]. This figure was taken from [340].

In both cancer cells and non-transformed cells, splicing inhibition by PlaB impairs the assembly of repair factors, including WRAP53β, RNF168, 53BP1, BRCA1, and RAD51 at double-strand breaks and interferes with the DNA damage response.[341]

After treatment, cells underwent protein total extract or sub-fractionation experiments as described below.

2.3 Total extract

HeLa and HCC1806 cells were cultured in six-well plates. After different treatments, the cells were washed twice with room temperature PBS (Gibco, REF 14190-094). Proteins were extracted by treating the plates with RIPA buffer (25 mM Tris•HCl pH 7.6, 150 mM NaCl, 1% NP-40, 1% sodium deoxycholate, 0.1% SDS) (#89900, Thermo scientific) supplemented with 1mM Phosphatase inhibitor cocktail3, 1mM PMSF, 1/100 Protease inhibitor Cocktail and 1/1000 DNAse. All extraction steps were carried out on the ice.

2.4 Subcellular fractionation:

After applying the desired treatments, the cells were rinsed twice with room temperature PBS, trypsinized, and collected in 1 ml Eppendorf tubes. They were again washed with buffer A (10 mM HEPES pH 7.9, 1.5 mM MgCl2, 10 mM KCl, 0.5 mM DTT), and centrifuged for 5 minutes at 1000 rpm. They were then homogenized in buffer A supplemented with (0.1% NP-40, 1mM Phosphatase inhibitor cocktail3, 1mM PMSF, 1/100 Protease inhibitor Cocktail) and incubated on ice for 10 minutes. The cytoplasmic fractions correspond to the supernatants obtained after 5 minutes of centrifugation at 5000 rpm. The pellets were then washed twice with 1 ml of buffer A and centrifuged at 5000 rpm for 5 minutes. Following, they were agitated for 15 minutes in buffer B (20 mM HEPES pH 7.9, 25% glycerol, 0.42 M NaCl, 1.5 mM MgCl2, 0.2 mM EDTA, 0.5 mM DTT) complemented with (1 mM Phosphatase inhibitor cocktail3, 1 mM PMSF, 1/100 Protease Inhibitor Cocktail) and centrifuged at 14000 rpm for 15 minutes. The collected supernatants correspond to the nuclear fractions. The pellets were then washed twice with 1 ml of buffer B and centrifuged at 14,000 rpm for 15 minutes. Depending on the pellet volume, 50 to 75 µl of Buffer B with (1 mM Phosphatase inhibitor cocktail3, 1 mM PMSF, 1/100 Protease Inhibitor Cocktail) were added. Finally, the pellets were sonicated at 70% amplitude for 1 min with a sonication pulse rate of 1 second on/ 1 second off. The obtained fractions represent the proteins bound to chromatin. Throughout the process, the samples were stored on ice. Furthermore, all centrifugations were conducted at 4 °C. The workflow steps are represented in Figure 29.

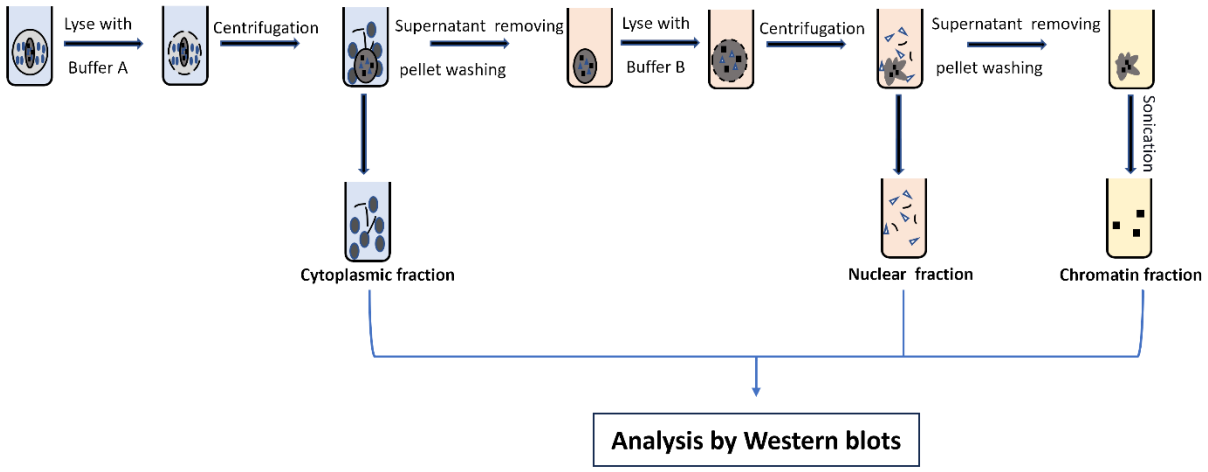

Figure 29 The workflow steps of subcellular fractionation protocol.

2.5 Overexpression of Aurora by transfection

2.5.a- Aurora A plasmid purification

E. coli strain DH5α was transformed with 100 ng of the Aurora plasmid, pCMV6-XL5. The transformed bacteria were inoculated in 15 mL of LB supplemented with Ampicillin (100 µg/mL) and incubated overnight at 37 °C with shaking at 180 RPM. Finally, the plasmids were purified using the NucleoSpin Plasmid Miniprep Kit from Macherey-Nagel.

2.5.b- Aurora A plasmid transfection

The transfection was performed using Lipofectamine 2000 (#11668019, Invitrogen, Carlsbad, CA, USA) according to the manufacturer's instructions with a ratio of DNA/lipo2000 of 1:1. HeLa and HCC1806 cells were seeded in 6-well plates and allowed to reach 70-90% confluence prior to transfection. The transfection mix was added dropwise to 2 mL of culture medium and incubated for 24-48 hours, followed by a PBS wash and total extract.

2.6 Si-RNAs transfection

The si-RNAs targeting RAD51 and VRK1 proteins were designed using Horizon Discovery's Custom siRNA design tool (Dharmacon). The sequence targets are listed below. A negative control was used, "ON-TARGETplus Non-targeting siRNA," from Dharmacon. Commercial si-RNAs were also purchased from OriGene for RAD51 Oligo Duplex (Locus ID 5888) CAT#: SR321568. The indicated si-RNAs were transfected at a concentration of 20 nM using Lipofectamine 2000 Reagent from Invitrogen, following the manufacturer's instructions with a ratio of si-RNA/lipo2000 of 1:1. The mock controls were transfected only with Lipofectamine 2000 without si-RNAs.

si-RAD51#3: 5’ GACTCGCTGATGAGATTGTAT 3’

si-VRK1-02: 5’ CAAGGAACCTGGTGTTGAA 3’

2.7 Cell Synchronization

HeLa cells were grown in a T75 flask until they reached 35-40% confluency. Next, 2 mM of thymidine (Sigma, T9250-1G) was added and incubated for 18 hours. Then, thymidine was removed, and cells were rinsed twice with fresh DMEM. Subsequently, fresh DMEM supplemented with 24 µM deoxycytidine was added for 11 hours. The second blockade was obtained by incubating cells in 2 mM thymidine for 14 hours. Afterward, thymidine was removed, and cells were rinsed twice with fresh DMEM. A second turn of 24 µM of deoxycytidine in DMEM was performed, followed by cell harvesting after 0h -2h -6h -8h -10h -12h. The cells were washed twice with PBS. Then, they were divided into two portions. One portion underwent total protein extraction, while the other was analyzed by flow cytometry, as described below.

2.8 Cell cycle analysis by flow cytometry

Cell cycle analysis by flow cytometry identifies cells in different stages of division based on changes in DNA content. The flow cytometry protocol was performed as follows: The cells were fixed in 70 % ethanol at -20°C for 1 hour, then rinsed twice with PBS (after this step, cells could be conserved at 4°C). Permeabilization was performed with 0.25% Triton X100 in PBS on ice for 20 minutes. Blockage was achieved with 1% PBS-BSA. Centrifugation was done for 10 minutes at 1500 rpm after every step. The nuclear DNA was stained with 25 µg/mL of propidium iodide (PI) in PBS for 30 minutes. All steps were performed at 4°C. The acquired data were analyzed using FlowJo™ v10.9.

2.9 RAD51 Immunoprecipitation

HeLa and HCC1806 cells were seeded in 100 mm x 20 dishes until they had reached around 80% of confluence. They then were collected and lysed with Pierce® IP lysis buffer (87787, Thermo), which contains: (25 mM Tris-HCl pH 7.4, 150 mM NaCl, 1% NP-40, 1 mM EDTA, 5% glycerol) and supplemented with 1 mM Phosphatase inhibitor cocktail3, 1 mM PMSF, 1/100 Protease Inhibitor Cocktail. The lysate was then clarified by centrifugation (14,000 rpm, 15 min) and divided into two tubes, one of which received 100 µg/ml of RNase A (EN0531, Thermo Fisher), and the other of which served as a control, the tubes were then incubated at 37 °C for 20 minutes. After that, one milligram of proteins was overnight incubated with 10 µg of anti-pser97 RAD51 antibody (Gene Cast). The resulting immune complex was then incubated for 1 h with 40 µl of protein A/G plus agarose beads (sc-2003, Santa Cruz). Following, the beads were washed four times with IP lysis buffer, and proteins were then eluted by heating the beads for 5 min at 95 °C in 50 µl of 2x SDS

buffer (Laemmli 2x ref S3401-1VL, Sigma). Finally, the IP fractions underwent Western blot analysis as described below.

2.10 Gel electrophoresis and Western blot analysis

Proteins from cell lysates were separated on 12% SDS-polyacrylamide gels by electrophoresis. For Western blot analysis, the proteins were transferred onto nitrocellulose membranes (GE Healthcare, Little Chalfont, UK) by wet transfer method for 1 hour at 250 mA (4 °C). Membranes were blocked for 30 min at room temperature with agitation using 5% non-fat dry milk (w/v) in PBST (1x PBS, 0.1% Tween 20) (v/v).

Name of antibody	Host	# of Reference	Furnisher	Experiment	Dilution
Anti-p Ser 97	Rabbit	Specifically produced	GeneCast	WB	1:1000
Anti-RAD51	Mouse	MA5-14419	Invitrogen	WB	3:1000
Anti-α-tubulin	Mouse	MA1-19162	Invitrogen	WB	1:1000
Anti-ATM	Rabbit	Ab82512	Abcam	WB	1:1000
Anti- p ATM	Mouse	Ab2793244	Abcam	WB	1:1000
Anit- p DNA-PK	Rabbit	Ab124918	Abcam	WB	1:1000
Anti-Aurora-A	Mouse	A1231	Sigma	WB	1:2000
Anit- p Aurora-A	Rabbit	SAB4503898	Sigma	WB	1:500
Anti-Histone H3	Rabbit	PA5-16183	Invitrogen	WB	1:1000
Anti-γ H2AX	Mouse	JBW301	Merck Millipore	WB	1:1000
IRDye® 800CW	Goat anti-Rabbit	D00804-07	LI-COR	WB	1:20000
IRDye® 680RD	Goat anti-Mouse	D00804-13	LI-COR	WB	1:10000

Table 2 Primary and secondary antibodies that were used in Western blots.

Rinse 2 times for 5 min in PBST, after which the membranes were incubated with the primary antibody overnight with agitation at 4 °C. Then, they were incubated with the secondary antibody for 30 min in the dark at room temperature and washed (3X, 5 min) with PBST. The Odyssey infrared imaging system (LI-COR Biosciences, Lincoln, NE, USA) was used to visualize immunoreactive bands. Image Studio Lite software version 5.2 (LI-COR) was used to quantify and normalize protein of interest signals to loading controls (α-tubulin and H3). The primary and secondary antibodies that were used are summarized in Table 2

2.11 Immunofluorescence (IF):

Cells were grown in 24-well plates with 1 cm diameter coverslips in appropriate medium media until they reached a cell density of approximately 1 x 10^4 cells per well. 24 hours post cell seeding, coverslips were rinsed using 500 µL of 1X DPBS, then Fixed using 500 µL of 3.7% paraformaldehyde for 15 min at room temperature (RT). They were washed three times with DPBS and kept at 4°C. Cells were incubated for 20 minutes in PBS 0.1 M glycine to eliminate any unreacted aldehyde sites after fixation. Cells were then permeabilized for 15 minutes with 0.5% Triton X100. Next, they were blocked for 30 minutes with 1% DPBS-BSA before immunostaining with primary antibodies for 2 to 3 hours. Then, they were incubated for 30 minutes with desired secondary antibodies coupled with Alexa 555 fluorophores (# A32732, Life Technologies-Invitrogen). The cells were washed with 1% DPBS-BSA three times between each manipulation step, and all steps after fixation were carried out at room temperature. The coverslips were then placed on slides with a drop of ProLong (#P36930, Invitrogen, Carlsbad, CA, USA). The slides were left to dry for at least 24 hours in the dark before observation under a NIKON epifluorescence microscope (Nikon, Tokyo, Japan) or a NIKON confocal microscope. Confocal microscopy acquisitions were made at the IBISA MicroPICell facility (Biogenouest), a member of the national infrastructure France-Bioimaging supported by the French national research agency (ANR-10-INBS-04). The analysis of images and creation of figures was done using the FIJI and Figure J plugin.

3. Statistical Analysis

A paired Student's t-test or one-way ANOVA was employed in the statistical analysis using Microsoft Excel 2016 and GraphPad Prism 8.0.1. Statistical significance was considered to be present when $p \leq 0.05$ (*), $p \leq 0.01$(**), $p \leq 0.001$(***), $p \leq 0.0001$(****), or not significant (ns) when $p > 0.05$. Each error bar represents the standard deviation.

4. In-Silico Methods

4.1 Kinase prediction

The FASTA sequence of the RAD51 protein (Q06609 – https://www.uniprot.org/)[342] was subjected to Kinase prediction websites. Three bioinformatics websites were used to predict the kinase responsible for phosphorylation RAD51 at Ser97: 1- GPS 5, and GPS 6 (http://gps.biocuckoo.cn/online.php) [343], 2- Kinexus PhosphoNET (http://www.phosphonet.ca/) The scores of Kinase Predictor V2 are grouped into two sets. The first set is based on analysis of the phosphosite alone, and the maximum score possible is 1000. While the second set considers neighboring phosphosites and is not scaled to a maximum of 1000 [344].

4.2 RAD51-Kinase docking

RAD51-Kinase docking was performed using the ClusPro 2.0 web server (https://cluspro.bu.edu/login.php) [345]. ClusPro is a popular protein-protein docking website that supports direct and template-based docking approaches [346,347]. The 3D structures of the proteins were obtained from the protein data bank (PDB, https://www.rcsb.org/). The docking calculations were performed using the default parameters. ClusPro generates clusters of docked protein conformations ranked by their binding energy. Generally, the Cluspro algorithm generates four sets of models using the scoring schemes called 1- balanced, 2- electrostatic-favored, 3- hydrophobic-favored, and 4-van der Waals + electrostatics [347].

As a brief explanation (Figure 30): The docking was performed using the ClusPro web service with default settings. The docked proteins with RAD51 are shown in (Table 3).

Protein	RAD51	AURKA	AURKB	AURKC	VRK1	VRK2	PLK1	PLK2	CK1
PDB code	5JZC	1OL7	4AF3	6GR8	2RSV	8Q1Z	2OWB	4I5M	6GZD

Table 3 PDB codes of docked proteins

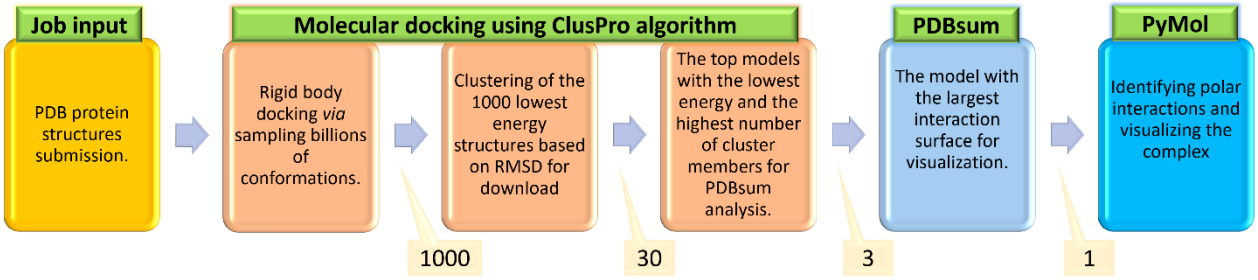

Figure 30 Outline of the RAD51-kinases docking workflow

After every step, the number of structures retained is given in a yellow box. RMDS stands for Root-Mean-Square Deviation. This figure is adapted from [347].

To prioritize interactions involving Ser97 of RAD51 during the docking process, we enabled the "search attraction" option for Ser97 in ClusPro's advanced settings. Based on Cluspro guide recommendations, the models from the balanced energy set with the largest number of clusters and lowest energy were selected.

The selected models were then analyzed using PDBsum for protein-protein interactions (http://www.ebi.ac.uk/thornton-srv/databases/pdbsum/Generate.html), and the ones with the largest interaction surface were chosen for visualization of polar contacts using the open-source PyMOL version 2.5. https://github.com/schrodinger/pymol-open-source

III- Results

Chapter 1 – Article: Aurora A mediated new phosphorylation of RAD51 is observed in Nuclear Speckles

Aurora A mediated new phosphorylation of RAD51 is observed in Nuclear Speckles

Mohamad Alaouid, Parfait Kenfack Ymbe, Vanessa Philippot-Ménil, Gwennina Cueff, Alexandre Demeyer, Damien Marquis, Nizar Ayadi, Fabrice Fleury, Houda Benhelli-Mokrani*

From Nantes Université, US2B, DNA repair team, UMR 6286 CNRS, 44000 Nantes, France

*To whom correspondence should be addressed: Houda Benhelli-Mokrani, US2B, Faculté des Sciences et Techniques, 2 rue de la Houssinière BP 92208, 44322 Nantes, Cedex 3. Houda.benhelli@univ-nantes.fr; tel 33 251 125 753

ABSTRACT

To maintain its genome integrity, the cell uses complementary and orchestrated processes, among which is the DNA Damage Response. Pre mRNA maturation is an essential step of the DNA damage response that provides an adapted proteome in order to face genotoxic stress. We describe here a new phosphorylation of the RAD51 recombinase, on its Ser97 residue. This new Aurora A mediated RAD51 phosphorylation modulates its *in vitro* activity evaluated by D-loop and polymerization assays. Using recombinant proteins, we show that RAD51 is an RNA binding protein and that the Ser97 phosphorylation modulates its RNA binding affinity *in vitro*. Using a specifically generated antibody we revealed that this Ser97 phosphorylation is correlated with RAD51 localization into the RNA maturation membrane less organelles, Nuclear Speckles. We describe here for the first time the presence of RAD51 DNA repair factor within the Nuclear Speckles, raising the hypothesis of a possible role for RAD51 in splicing modulation. This point is of particular interest in the context of splicing profile modulations associated with radio and/or chemoresistance.

INTRODUCTION

Repair of DNA damages is essential for genomic stability and a miss-regulation of this essential DNA metabolism can cause cancer. The cell response to DNA damages includes a cell cycle arrest in G1/S or G2/M, depending on the cell cycling and the DNA damage, to provide the time needed to repairing its genome before cycling again [348]. In the case of a large amounts of damages, the cell undergoes apoptosis and this is the principle used in chemo- and radiotherapies to kill cancer cells (for review [349]). Aurora A is a well-known kinase implicated in mitosis orchestration and its kinase activity has been described as diminishing after DNA damages [350].

The RAD51 recombinase is implicated in the strand exchange mechanism during the DSB repair by the Homologous Recombination (HR) pathway. In the absence of DNA Damage (DD), RAD51 is predominantly cytoplasmic and translocates to the nucleus during the DNA Damage Response (DDR) to manage HR repair [351] [335]. Since it needs the undamaged sister chromatid as a template, the HR repair pathway occurs mainly in the late S, G2 phases of the cell cycle [352] [353]. However, it has been documented that HR repair can also occur during early S phase, and in this case, the undamaged template used for the repair could be the homologous chromosome or an RNA transcript [354]. These mechanisms of sister chromatid-less HR repair may induce a Loss Of Heterozigosity (LOH) which is frequently observed in cancer development [355] [356]. Thus, RAD51 localization and activity must be controlled and finely regulated in order to maintain genomic stability. For that purpose, RAD51 is post-translationally modified by multiple phosphorylations which affect its auto-polymerization, DNA binding capacities, and D-loop formation [357–359].

When considering the DDR, we usually direct our thoughts to the cascade of post-translational modifications (PTMs), and in particular the phosphorylation which is the most studied. These PTMs thus regulate protein/protein and protein/DNA interactions in the context of chromatin remodeling and DNA repair. This view is completed by the consideration of protein variant adaptation. Indeed, the response to DD is also regulated at the post-transcriptional level by a modulation of pre-mRNA maturation making possible the production of proteins isoforms [360] [361]. Active splicing machinery is essential during the DDR, allowing the cell to repair its DNA damages and maintain its genomic stability. That is why alternative splicing deregulation could be implicated in carcinogenesis as supposed by many studies showing abnormal alternative

splicing profiles in cancer cells compared to the non-pathological cells [362,363]. We know from Pederiva's work that inhibiting splicing before DNA damage induction impedes the recruitment of DNA repair factors to the damaged sites [364]. We must consider that the splicing modulation occurring after DNA damages takes part of the DDR itself. In this sense, some well-known players in the signaling cascade that allow DNA damage repair have been described as also being implicated in splicing modulation in the context of the DDR. Thanks to the work of Katzenberger, we know that ATM and ATR kinases and their respective targets, CHK2 and CHK1 checkpoint kinases, are essential for the splicing modulation of the TAF1 factor after DNA damage [365]. The work of Matsuoka, consisting of identifying ATM and ATR targets after IR, using the SILAC approach, revealed new pathways activated during the DDR. Of them, there is the RNA metabolism where many proteins implicated in pre mRNA maturation are phosphorylated by ATM or ATR [366]. Even the number of studies showing a link between DNA repair and RNA splicing is growing, (for review [367]), we are still in the identification process for the connections between these two branches of the cell response to DNA damage.

Here, we identified an Aurora A mediated new phosphorylation of RAD51 that is located into nuclear structures that are not γ–H2AX DNA repair foci. We showed that this new phosphorylation of RAD51 is located into Nuclear Speckles, the RNA maturation sites. In this work, we also demonstrated that RAD51 is an RNA binding protein and that this Ser97 phosphorylation affects its *in vitro* RNA binding affinity.

MATERIAL AND METHODS

RAD51 recombinant protein production

WT and RAD51 mutants (S97D phosphomimetic), (S97A non phosphorylable) were produced according to the previously described protocol [358]. Briefly, pet15b plasmids encoding His-tagged RAD51, WT and (S97A, S97D) mutated versions were used in the E coli BL21 DE3 strain at 37°C. After IPTG induction, the bacteria were lysed with Tris HCl 50 mM, NaCl 500 mM, glycerol 10%, β-mercaptoethanol 5 mM, imidazole 5 mM and recombinant RAD51-proteins were purified on a NiNTA resin (#P6611, Sigma, St Louis, MO, USA) using the washing buffer: Tris HCl 50 mM, NaCl 500 mM, glycerol 10%, β-mercaptoethanol 5 mM, (and increasing

imidazole concentrations). A dialysis step was then added (dialysis buffer: Tris HCl 50 mM, NaCl 500 mM, glycerol 10%, EDTA 1 mM, DTT 1 mM). A Bradford assay was used to determine protein concentrations and SDS- PAGE followed by Coomassie staining were used to check the purity of the protein fractions.

In vitro phosphorylation assay and MS analysis

Recombinant Aurora A active protein was purchased at SIGMA (A1983). 5 µg of recombinant RAD51 were phosphorylated *in vitro* at 37°C for 30 minutes in 50 mM Tris HCL pH=7,5, 10mM MgCl2, 50uM DTT, 50uM ATP, and 200 ng of Aurora A enzyme. Phosphorylation products were separated using 12% acrylamide gel electrophoresis.

Proteins were colored with the BIO-SAFE Coomassie stain reagent (BIORAD, 1610786) according to the manufacturer's recommendations. Gels slices were maintained in 1% acetic acid solution at room temperature before their digestion and analysis. MS/ORBITRAP analysis was performed by the 3P5 core facility (Institut Cochin, Paris).

D-loop assay

As described previously in Chabot et al [358]: 100-ssDNA labeled IRD700 (1 µM) (Integrated DNA Technologies, Coralville, IA, USA) was incubated with 0.5 µM RAD51 in 10 µL of standard reaction buffer containing 20 mM Tris HCl pH=8, 1 mM ATP, 1 mM DTT and 1 mM CaCl2 at 37 °C for 20 min. Supercoiled complementary plasmid pPB4.3 DNA was added at a final concentration of 200 µM (in bp), to initiate the strand exchange reaction. After an incubation time of 30 min at 37 °C, the reaction was stopped by the adding 10 mM of Tris HCl pH=8, 10 mM MgCl2 and 1% SDS (final concentrations) to the reaction. 1 mg/mL of proteinase K was used to deproteinize the reaction for 15 min at 37 °C. The reaction products were then separated by electrophoresis on a 1% agarose gel, in 0.5× TAE buffer (20 mM Tris, 10 mM acetic acid and 1 mM EDTA) at 100 V for 2 h. Detecting the IRD-700 dye with the 700 nm infrared fluorescent detection channel of the Odyssey Infrared Imager (LI-COR Biosciences) allowed us to detect and quantify the ssDNA and D-loop structures.

DNA /RNA binding activity

Blitz technology was used with 100 mM of 5' biotinylated 33 nt DNA or RNA bound on a streptavidin coated biosensor. DNA and RNA sequences are given below. WT and mutants RAD51 recombinant proteins were diluted at the indicated concentration in PBS buffer 1× and ATP 2 mM. Three steps kinetics were made. The buffer baseline was measured for 10 sec, then the association step between ssDNA or ssRNA and RAD51 at different indicated concentrations from 0,5 to 4 μM was monitored for 200 sec. Finally, the dissociation step of the bound RAD51 was monitored for 200 sec in buffer. Tip was regenerated in NaOH (50 mM) twice for 40 sec before reuse. Nucleic acids sequences:

33m DNA: 5' TCCTTTTGATAAGAGGTCATTTTTGCGGATGGC 3'

33m RNA: 5' GCCAUCCGCAAAAAUGACCUCUUAUCAAAAGGA 3'

Antibodies

Rabbit antiPSer97 RAD51antibody was specifically produced by Genecust. Mouse anti-RAD51 antibody is from Invitrogen, ref: MA5-14419. Rabbit anti-RAD51 antibody is from Invitrogen, ref: MA5-32789. Anti-tubulin antibody is from Invitrogen, ref: MA1-19162. Anti-histone H3 antibody is from Invitrogen, ref: PA5-16183. Anti-gH2AX antibody is from Merck Millipore, ref: JBW301. Goat anti rabbit secondary antibody is from LI-Cor, ref: D00804-07, Goat anti mouse secondary antibody is from LI-Cor, ref: D00804-13.

Immunofluorescence labelling/Microscope acquisitions

Cells were seeded on a 1cm diameter glass. At the indicated time, the cells were washed twice with PBS then fixed for 15min in 3.7% formaldehyde in PBS. After 3 PBS washes, slides were kept at 4°C before immunolabelling. Briefly, cells were permeabilized in triton 0.01%, washed with PBS 1% BSA and incubated with primary antibodies diluted in PBS 1% BSA for 2 hours. After 3 washes, the cells were incubated with an Alexa conjugated secondary antibodies for 30 min. After 3 washes, the cells were mounted in Prolong DIAMOND+DAPI mounting medium

(Thermofisher, P36962). Image acquisitions were made on a NIKON epifluorescence microscope and on a NIKON confocal microscope. Confocal microscopy acquisitions were made at the IBISA MicroPICell facility (Biogenouest), member of the national France-Bioimaging infrastructure supported by the French national research agency (ANR-10-INBS-04). Image analysis and figures realization were made using Fiji and the Figure J plugin. Colocalization studies were performed in accordance with the recommendations of Dunn Practical guide to evaluation of colocalization in biological microscopy [368]. JACoP tool on Fiji was used to calculate the Pearson's Correlation Coefficient (PCC). This analysis was performed in a cell-by-cell ROI (regions of interest) PCC determination. Two signals are colocalized when a PCC value is positive, and they are anti-colocalized which means an exclusion when the PCC value is negative. A null PCC value means a random distribution of the two signals. We used the Zinchuk et al., 2013 methodology to interpret PCC colocalization values. It proposes a classification of 5 degrees of colocalization: PCC from 0 to 0.12: very weak/ PCC from 0.13 to 0.39: weak, PCC from 0.4 to 0.6: moderate, PCC from 0.49 to 0.84: strong, PCC from 0.85 to 1: very strong [369]. As recommended by the Mcdonald et al. work, the comparative analysis of two conditions, (Ctl and plaB treatment for example) was made using a unilateral t-test [370].

Cell culture and treatments

The human basal-like TNBC cell line, HCC1806, and HeLa were grown in 100 mm x 20 mm dishes (for sub-fractionation experiments) or six-well plates (for total extract experiments) at 37 °C in a humidified atmosphere containing 5% CO2. RPMI 1640 medium 1X (Life Technologies, Carlsbad, CA, USA) and DMEM medium 1X (Dulbecco's Modified Eagle Medium) were used as growth media for HCC1806 and HeLa, respectively. Each growth medium was supplemented with 10% fetal bovine serum and 1% penicillin /streptomycin (REF15140-122, Gibco). Cells were treated with 10 µM camptothecin (C9911-100MG, Sigma), 5 µM Pladienolide B (SC-391691, Santa Cruz Biotechnology) for 4 hours, or 50 nM alisertib (cat.# HY-10971/CS-0106, Medchemexpress®) for 24h to inhibit Aurora-A activity (alisertib was dissolved in DMSO and then stored at -20°C). The cells then underwent protein total extract or sub-fractionation experiments as described below.

Total cell extracts

HeLa and HCC1806 cells were cultured in six-well plates. After different treatments, the cells were washed twice with room temperature PBS (Gibco, REF 14190-094). Proteins were extracted by treating the plates with RIPA buffer (25 mM Tris HCl pH=7.6, 150 mM NaCl, 1% NP-40, 1% sodium deoxycholate, 0.1% SDS) (#89900, Thermo scientific), All extraction steps were carried out on ice.

Subcellular fractionation

Following application of the desired treatments, the cells were rinsed twice with room temperature PBS, trypsinized, and collected in 1 ml Eppendorf tubes. They were washed again with buffer A (10 mM HEPES pH=7.9, 1.5 mM MgCl2, 10 mM KCl, 0.5 mM DTT), and centrifuged for 5 minutes at 1000 rpm. They were then homogenized in buffer A supplemented with (0.1% NP-40, 1mM phosphatase inhibitor cocktail3, 1mM PMSF, 1/100 protease inhibitor cocktail) and incubated on ice for 10 minutes. The cytoplasmic fractions correspond to the supernatants obtained after 5 minutes of centrifugation at 5000 rpm. They were then washed twice with 1 ml of buffer A and centrifuged at 5000 rpm for 5 minutes. Following, they were agitated for 15 minutes in buffer B (20 mM HEPES pH=7.9, 25% glycerol, 0.42 M NaCl, 1.5 mM MgCl2, 0.2 mM EDTA, 0.5 mM DTT) complemented with (1 mM phosphatase inhibitor cocktail3, 1 mM PMSF, 1/100 Protease Inhibitor Cocktail) and centrifuged at 14000 rpm for 15 minutes. The supernatants collected correspond to the nuclear fractions. The pellets were then washed twice with 1 ml of buffer B and centrifuged at 14,000 rpm for 15 minutes. Depending on the pellet volume, 50 to 75 µl of buffer B with (1 mM phosphatase inhibitor cocktail3, 1 mM PMSF, 1/100 Protease Inhibitor Cocktail) were added. Finally, the pellets were sonicated at 70% amplitude for 1 min, with a sonication pulse rate of 1 second on/ 1 second off. The fractions obtained represent the proteins bound to chromatin. Throughout the process, the samples were stored on ice and the centrifugations were conducted at 4 °C.

Cell transfections

HeLa and HCC1806 cells were transfected for the time indicated (24 or 48h) with purified Aurora-A plasmid, or indicated siRNA, using Lipofectamine 2000 (Invitrogen) according to the manufacturer's instructions with a ratio of DNA (or RNA)/lipo2000 of 1/1. Scramble and RAD51 siRNA were purchased from Origene technologies, ref: SR321568.

Western blot assay

Proteins from cell lysates were separated on 12% SDS-polyacrylamide gels by electrophoresis. For western blot analysis, we transferred the proteins onto nitrocellulose membranes (GE Healthcare, Little Chalfont, UK) using the wet transfer method for 1 hour at 250 mA (4 °C). Membranes were blocked for 30 min at room temperature with agitation using 5% non-fat dry milk (w/v) in PBST (1x PBS, 0.1% Tween 20) (v/v). They were rinsed twice for 5 min in PBST, after which the membranes were incubated with the primary antibody overnight with agitation at 4 °C. Then, they were incubated with the secondary antibody for 30 min in the dark at room temperature and washed (3X, 5 min) with PBST. The Odyssey infrared imaging system (LI-COR Biosciences, Lincoln, NE, USA) was used to visualize immunoreactive bands. Image Studio Lite software version 5.2 (LI-COR) was used to quantify and normalize protein of interest signals to loading controls (α-tubulin and H3).

Dot blot assay

Phospho and non-phospho ser97 peptides were spotted on nitrocellulose membrane (GE Healthcare, Little Chalfont, UK). Membranes saturation, antibodies incubation and scanning were performed in the same way as for western blot assays.

Statistical analysis

A paired Student's t-test was used in the statistical analysis using Microsoft Excel 2016 and GraphPad prism 8. Statistical significance was considered to be present when $p \leq 0.05$ (*), $p \leq 0.01$(**), $p \leq 0.001$(***), or not significant (ns) when $p > 0.05$. Each error bar represents the standard deviation.

Cell synchronization

HeLa cells were grown in a T75 flask until they were around 35–40% confluent. After that, 2 mM of thymidine (Sigma, T9250-1G) was added, and the cells were incubated for 18 hours. Following this, thymidine was removed, and the cells were washed twice in fresh DMEM. After that, fresh DMEM supplemented with 24 µM deoxycytidine was added for 11 hours. The second blockade was obtained by incubating cells in thymidine 2 mM for 14 h. Then the thymidine was removed, and the cells were washed twice in fresh DMEM. The second turn of 24 µM of deoxycytidine in DMEM was then done, followed by cell harvesting after 0h -2h -6h -8h -10h and12h.

After ethanol fixation and IP staining, cells were passed in a FACS. Cell cycle analysis were done using FlowJo ® software.

RAD51 immunoprecipitation

HCC1806 cells were collected and lysed with Pierce® IP lysis buffer (87787, Thermo), which contains: (25 mM Tris-HCl pH 7.4, 150 mM NaCl, 1% NP-40, 1 mM EDTA, 5% glycerol) and supplemented with 1 mM phosphatase inhibitor cocktail3 (Sigma, P0044), 1 mM PMSF, 1/100 protease inhibitor cocktail (Sigma, P8340). The lysate was then clarified by centrifugation (14,000 rpm, 15 min), and divided into two tubes, one of which received 100 µg/ml of RNase A (EN0531, Thermo Fisher), and the other of which served as a control, the tubes were then incubated at 37 °C for 20 minutes. After that, one milligram of proteins was then incubated overnight with 10 µg of anti-pSer97 RAD51 antibody (GeneCust). The resulting immune complex was then incubated for 1 h with 40 µl of protein A/G plus agarose beads (sc-2003, Santa Cruz). After this, the beads were washed four times with IP lysis buffer, and the proteins were then eluted by heating the beads for 5 min at 95 °C in 50 µl of 2x SDS buffer (Laemmli 2x ref S3401-1VL, Sigma), Finally, IP fractions were subjected to electrophoresis.

Computational mutagenesis

The 3D structure of RAD51 used is a nucleofilament consisting of a trimer of HsRAD51 and a dsDNA; it is available in the Protein Data Bank under accession code 5H1C.

The analysis and the 3D rendering are achieved on the open-source Pymol 2.5 software (https://github.com/schrodinger/pymol-open-source).

The mutagenesis of HsRAD51 from S97 to S97A or S97D was performed using the "Mutagenesis" tool in Pymol.

Polymerization assay

20 µM HsRAD51 was incubated in 20 mM HEPES pH=7.5, 150 mM KCl, 20 mM DTT for 30 min at 4°C. HsRAD51 complexes were cross-linked by incubation with 0.5 or 10 mM of BS3 (Sigma-Aldrich) at 22°C for 30 min. BS3 allows reticulation between different amines located on the residues side chains and terminal amin functions of RAD51 monomeres. Cross-linking was terminated by adding 80 mM Tris pH=8.0 for 15 min at 22°C and analyzed with SDS-PAGE. The gels were colored with Coomassie-Blue staining and the Odyssey infrared imaging system (LI-COR Biosciences, Lincoln, NE, USA) was used to visualize immunoreactive bands. Image Studio Lite software version 5.2 (LI-COR) was used to quantify and analyze band intensity signals.

RESULTS

Aurora A kinase phosphorylates RAD51 *in vitro* within its subunit rotation motif

Recombinant HsRAD51 protein was used to perform an Aurora A kinase mediated *in vitro* phosphorylation. Figure 1A shows a Coomassie-Blue stained SDS-PAGE, with a shift in the last well corresponding to the RAD51 with ATP and Aurora A kinase condition. Differential MS analysis in comparison with the unphosphorylated form allowed us to identify a unique phosphorylated site on the Serine 97 (see Supplemental Figure 1). This residue is located in the linker region of RAD51, between the N-terminal domain (Nter) and the Core domain (Core), within the Subunit Rotation Motif (SRM) as shown in figure 1A. In this same figure, the sequence alignment of RAD51 linker regions from different species shows the conservation of the phosphorylated residue, represented in bold. The 3D structure of HsRAD51 was used to visualize the Ser97 residue within the RAD51 nucleofilament. We can see in figure 1B that this residue

remains exposed at the surface of the nucleofilament and thus, is available for potential modulation of the interactions of RAD51 with its partners. Recombinant S97A and S97D, respectively non phosphorylable and phosphomimetic mutants, were produced and used to test the effect of this phosphorylation on RAD51 activity. Figures 1B2 and 1B3 show the S97A and S97D mutations respectively. The side chains of these mutants are free like that of the Ser of the WT RAD51. We used these recombinant mutants RAD51 to explore their molecular phenotype and predict the impact of the phosphorylation of the Ser97 residue on RAD51 activity.

The S97D RAD51 phosphomimetic mutant shows increased *in vitro* strand invasion capacity

To evaluate the effect of the Ser97 phosphorylation on RAD51 activity, we performed a D-loop assay experiments and evaluated the strand invasion capacity of WT, S97A and S97D-RAD51 recombinant proteins. This assay allows to quantify the RAD51 enzymatic activity which favors the strand invasion of a free labelled probe within a plasmid containing the same sequence, to form a displacement loop, (refer to figure 1C illustration of this technique). We observed that the phosphomimetic mutant, S97D has an increased D-loop formation ability. Relatively to the D-loop activity of the WT RAD51, set as 100%, the S97D-RAD51 activity was more than two-times higher. This difference was statistically significant. We noticed that the S97A-RAD51 mutant also had increased activity, about 50% more than the WT one. These results highlight the importance of the Serine 97 on RAD51 activity.

The S97D RAD51 phosphomimetic mutant has a decreased polymerization rate

In order to evaluate the impact of the Ser97 mutations on RAD51 protein/protein interactions, we performed a polymerization assay without the presence of DNA. RAD51 was incubated at different concentrations with or without the amine reticulating agent BS3, then loaded in an acrylamide gel. (BS3 is used here to stabilize, proteinic interactions. Refer to the materiel section for more details). The gels were stained with Coomassie-Blue and the band intensities of monomeric or polymeric RAD51 were quantified and analyzed. We can see, in Figure 1D that the Ser97 mutations affects the RAD51 polymerization state. Both S97A and S97D mutants showed a statistically significant decreased ability to polymerize, meaning that RAD51/RAD51

interaction without nucleic acids are affected by the Ser97 Phosphorylation. These results highlight the importance of the Ser97 residue in RAD51 self-association ability, in accordance with the already described role of the SRM (that includes the Ser97 residue) on RAD51 polymerization.

RAD51 Ser97 is phosphorylated *in cellulo*

We generated a specific antibody directed against the phosphorylated Ser97 form of RAD51 (PSer97-RAD51). This rabbit raised phosphospecific antibody was validated by different complemental techniques presented in the figure 2A panel. Using dot-blot assay, the phosphospecific antibody was tested for its ability to recognize two peptides corresponding to the RAD51 SRM region, with only one of them phosphorylated on its Ser97. The results are presented in the figure 2A.1 and show that the generated antibody recognizes only the peptide with the phosphorylated Ser97. Peptide competition assays were also used in order to validate the phospho-antibody specificity. Results are shown in figure 2A.2. The PSer97-RAD51 signal almost disappeared after PSer97-RAD51 peptide competition assay, while it is maintained after the competition with the Ser97-RAD51 non-phosphorylated peptide. Bovine Intestine Phosphatase (BIP) was also used to treat half of a membrane, before its immunoblotting was performed. We observe in the figure 2A.3, that on the BIP treated part of the membrane, we see only a little remaining PSer97-RAD51 signal and more non-specific signals. This experiment prove that the signal detected by this antibody is a phosphorylation. BIP was also used directly after Aurora A mediated *in vitro* phosphorylation of recombinant RAD51 protein, before performing a western blot. Results are shown in the figure 2A.4, in which the comparison of the wells n°5 and 10 allows us to see that the BIP treatment strongly diminished the signal detected by the anti-PSer97-RAD51 antibody. We also used siRNA mediated RAD51 depletion to test the antibody specificity. The results from n=3 experiments, illustrated in figure 2A.5 showed that RAD51 siRNA induced a 60% diminution of RAD51 protein level and a 47% diminution of PSer97-RAD51 level.

Finally, we performed immunoprecipitation experiments using our specifically generated anti-PSer97-RAD51 antibody raised in rabbits, and a western-blot analysis using a commercial anti-

RAD51 antibody raised in mice. Immunoprecipitation of PSer97-RAD51 was difficult to perform and we observed very low levels of immunoprecipitated proteins. We made a first scan of the membrane after its incubation with the secondary antibodies alone, to reveal non-specific signals (cf. upper part of the figure 2A.6). We observe in this figure that RAD51 was revealed after the precipitation with the anti-PSer97-RAD51 antibody and that we slightly improved this experiment by pretreating our whole cell extracts with RNaseA.

All the presented results allowed us to conclude that this generated antibody recognize specifically the Ser97 phosphorylated form of RAD51. This antibody was then used for the *in cellulo* analysis of the PSer97-RAD51using HeLa and HCC1806 cells.

PSer97-RAD51 is detected at all stages of the cell cycle

HeLa double thymidine-bloc synchronized cells, were used to follow the presence of Ser97-RAD51 phosphorylation by western blotting using whole cell extracts. The cell cycling progression was followed by cytometric analysis of the cells genetic material content and are presented in figure 2B.1. The H3Ser10 phosphorylation was also used to detect mitosis phase. The western blot results are shown in Figure 2B.2. First, we observed that this phosphorylation could be detected throughout the cell cycle. We secondly noticed that the PSer97-RAD51/RAD51 ratio seems to vary a little during the cell cycle progression, but with a statistically non-significant way. We conclude that the PSer97-RAD51 signal is present at all stages of the cell cycle.

The PSer97-RAD51 is enriched in the nucleus

To evaluate the sub-cellular localization of this new RAD51 phosphorylation, we performed cytoplasmic/nuclear cell extracts fractionations from HeLa and HCC 1806 cell lines. We can see in Figure 2C.1 that the PSer97-RAD51 is observed only in the nuclear fraction of both cells, while the RAD51 signal is mainly cytoplasmic. We also noticed that the PSer97-RAD51 band is below that of RAD51. This point was considered with the recurrent observation made in the lab, of the existence of an undersized nuclear form of RAD51. The figure 2C.2 shows a western blot assay made with a RAD51 directed commercial antibody and illustrates this observation. We can

hypothesize that this weaker but recurrent signal corresponds to a cleaved form of RAD51. We then tested the co-incubation of HeLa and HCC1806 whole cell extracts with a RAD51 directed commercial antibody and the PhosphoSer97 antibody. In the figure 2C.3, when observing the results of the HeLa cells, in which the signal is higher, we see clearly that the PSer97 signal is superposed to the undersized RAD51. We concluded that the PSer97-RAD51 is present in the nuclear fraction of HeLa and HCC1806 cell lines.

We then evaluated the subnuclear localization of the PSer97-RAD51 by performing a cytoplasmic/nuclear soluble/chromatin linked fractionation. The results are presented in the figure 2C.4 in which we observed that in the two tested cell lines, the PSer97-RAD51 form is present in both nuclear fractions but is predominantly localized (2 to 3-times more) in the chromatin linked fraction. To validate these results, we used immunofluorescence labelling and confocal microscopy to evaluate the sub-cellular distribution of the PSer97-RAD51 on the same cell lines. The results are presented in Figure 2D. We observed that PSer97-RAD51 (in red) is predominantly localized in the nucleus. The labelling is granular, with a pan-nuclear distribution with nucleolar exclusion and some foci of different sizes that are localized throughout the nucleus. This labeling is shown in figure 2E, for 3 other human cell lines of breast cancers and showed similar results. All these results were obtained under control conditions, meaning in the absence of exogenous DNA damaging agents, and show that the RAD51 Ser97 phosphorylated form is always present in the nucleus. We also used RAD51 directed siRNA to create a RAD51 deficient context in order to validate the anti PSer-RAD51 antibody by immunofluorescence. The results are shown in the figure 2F, in which we observe under RAD51 siRNA condition, the presence of cells without any RAD51 nor PSer97-RAD5 labelling (see the cells labelled with an arrow with two stars). We also observed cells with a diminution of both RAD51 and PSer97-RAD51 labellings (see the cells labelled by an arrow with one star). This experiment validates the use of the PSer97-RAD51 antibody *in cellulo*.

The phosphorylated Ser97-RAD51 is affected by camptothecin treatment

Camptothecin is an inhibitor of the topoisomerase I that causes replicative stress and DNA damages that are managed by the HR pathway. We tested the effect of a camptothecin-induced

DDR on RAD51 Ser97 phosphorylation. We performed western blot experiments using whole cell extracts. We can see in the figure 3A, that the DNA damages induce a decrease of PSer97-RAD51/RAD51 ratio in both cell lines. This decrease was statistically significant only for the HeLa cell line. Therefore, the PSer97-RAD51 decreases after DNA damage induction.

In this context, we performed immunofluorescence experiments to evaluate the effect of camptothecin on PSer97-RAD51 sub-cellular localization. Here again, we labelled the PSer97 in red and the γ-H2AX DNA damages foci in green. For reminder, the DNA double strand breaks are classically marked by the presence of a phosphorylated form of the histone H2AX variant, called γ-H2AX which is found enriched on several kb around the DNA breaks [371]. The results are shown in figure 3B. We were very surprised to observe that the PSer97 foci were not colocalized with the γ-H2AX foci. This was true for the control condition, in which we observed dsDNA breaks due to the replicative stress, and the camptothécine treatment condition. We used confocal images and a line scan analysis to illustrate that observation. We can see in the figure 3B that the two labelings are completely different, meaning that PSer97-RAD51 is not located in DNA damage "repair centers". To validate these atypical results, we performed a labelling of RAD51 using a commercial antibody and checked if there were some RAD51 foci that do not colocalize with γ-H2AX foci. The results are shown in Figure 3C and we can see that there are indeed some RAD51 foci that are not colocalized with γ-H2AX foci. Here again, we used confocal microscopy and line scan analysis tool to illustrate this observation. We easily see in the figure 3C that some RAD51 foci are not colocalized to γ-H2AX foci.

Aurora A kinase is implicated in the phosphorylation of RAD51 on its Ser97 residue

We identified the Ser97-RAD51 phosphorylation *in vitro*, under the action of the Aurora A kinase, but the complexity of the *in cellulo* mechanisms regulating protein phosphorylation and the multiple redundancy observed between kinases, do not allow us to consider that Aurora A kinase is necessarily also responsible for this phosphorylation *in cellulo.* We explored the implication of the Aurora A kinase in the *in cellulo* phosphorylation of RAD51 by using two approaches to enhance or diminish Aurora A kinase activity. On the one hand we used alisertib, a known specific Aurora A inhibitor, and on the other hand we performed an Aurora A over-

expression, and we assessed the effect of these two conditions on RAD51-Ser97 phosphorylation. The results of Aurora A inhibition are shown in Figure 4A, in which we see the PSer97RAD51/RAD51 ratio for all conditions. The Aurora A inhibition induced a statistically significant decrease of PSer97-RAD51 in the HCC1806 cell line, while it had no effect on the HeLa cells.

Aurora A over-expression by transient transfection was performed and the total extracts were used to evaluate the PSer97-RAD51/RAD51 ratio. In figure 4B, we observe that Aurora A over-expression induced an enhancement of the PSer97-RAD51/RAD51 ratio in both cell lines, and the statistical analysis allowed us to conclude that this enhancement is significant in the HCC1806 cell line. Therefore, the aurora A inhibition or overexpression experiments performed in the HCC1806 cell line allowed us to conclude that Aurora A is implicated in the *in cellulo* phosphorylation of RAD51 on its Ser97 residue. The absence of a statistically significant effect in the HeLa cell line underlines the probability of a complex regulation of RAD51 Ser97 phosphorylation in this cell line. This point will be developed in the discussion part.

The phosphorylated Ser97-RAD51 is located in the Nuclear Speckles

To identify the structures in which we observe the PSer97-RAD51 foci, we performed immunofluorescence experiments and labelled different nuclear organelles. Nuclear Speckles (NS) are membrane less organelles, also called interchromatin granules, which contain RNA, RNA binding proteins (RBP) and splicing factors. These structures are the location of alternative splicing and mRNA maturation. Using immunofluorescence co-labelling and confocal microscopy, we showed that the PSer97-RAD51 foci are colocalized with Sc35, a Nuclear Speckles component.

We show in the figure 5A a colocalization analysis of the Sc35 and the PSer97-RAD51 labelling on confocal images. The line scan analysis along the arrow shows that maximal pics intensities of the two signals are perfectly colocalized. We used confocal microscopy acquired images to quantify the colocalization of the Sc35 and PSer97-RAD51 signals using JACoP tool on Fiji. We used the Pearson's Correlation Coefficient (PCC) analysis that is classically used to address this type of question. For reminder, the PCC value varies from -1: which means exclusion of the two

signals, to +1: which means a total colocalization of the signals. A PCC equal to 0 means a random distribution of the two signals. According to the interpretation standards detailed in the material section, PCC values were used to interpret more finely the colocalization [369]. We obtained a PCC=0.608+/- 0.05 for HeLa cells and a PCC=0.555+/- 0.04 for HCC1806 cells. These results allowed us to conclude to a high colocalization of these two signals in the two cell lines, which signifies the colocalization of the PSer97-RAD51 within NS. To answer if this RAD51 localization within the Nuclear Speckles is linked or not to a splicing activity, we performed experiments in which we inhibited the pre-mRNA maturation. Pladienolide B (plaB) is a splicing-inhibitor that interacts with the SF3b1 subunit of the spliceosome. This drug leads to the accumulation of incompletely spliced or unspliced pre-mRNA, and provokes modifications of the Nuclear Speckles that become larger in size with a modified shape [372]. We treated HeLa and HCC1806 cells with plaB to evaluate the effect on the PSer97-RAD51 foci.

We can see in the figure 5B that the PSer97 signal is still present with large foci which remain co-localized with the Nuclear Speckles after plaB treatment. Here again, we quantified the colocalization of PSer97-RAD51 and Sc35 in control and plaB conditions, using the PCC indicator. Results are shown in the figure 5B. We found that the PCC values after plaB treatment were still typical to a colocalization of the two analyzed labelings. However, we noticed that the plaB treatment induces a statistically significant decrease of theses PCC values. For the HeLa cell line, the PSer97-RAD51/SC35 colocalization is strong in control condition (PCC= 0,608+/- 0.05) and moderate after plaB treatment (PCC= 0.468+/- 0.06). For HCC1806 cell line too, the colocalization is strong in the control condition (PCC= 0.555+/- 0.04) and moderate after plaB treatment (PCC= 0.388+/- 0.07). Meaning that PSer97-RAD51 stays colocalized within NS even when splicing is inhibited.

To evaluate the impact of this treatment on the PSer97-RAD51 level we used western-blot analysis and signal quantifications. The results presented in the figure 5C show that there was no statistically significant difference after plaB treatment. Meaning that the PSer97-RAD51 signal quantity at the cellular level is not affected by plaB induced splicing inhibition.

In order to evaluate the *in cellulo* interaction between RAD51 and Sc35, we performed immunoprecipitation assays of HeLa nuclear extracts using a commercial anti-RAD51 antibody. The western blot membrane was scanned a first time just after its incubation with the secondary antibody alone. The obtained signals are non-specific and are shown in the upper part of the figure 5D. After that, a classical immunoblot was performed to reveal Sc35 factor. The results in the lower part of the figure 5D and show (at the level of the arrow) that Sc35 factor is co-immunoprecipitated with RAD51. These results confirm the immunofluorescence experiments showing that RAD51 exits in the same structure as Sc35 within Nuclear Speckles.

RAD51 overexpression affects the Nuclear Speckles

To pursue our investigation of the presence of RAD51 within the Nuclear Speckles, we tested the effect of RAD51 overexpression on these structures. We used plasmids coding the HA-tagged RAD51 protein, either Wild Type (WT) or mutated on the Ser97 residue, (S97A non phosphorylable mutant, and S97D phosphomimetic mutant). HeLa and HCC1806 cell lines were transfected with these plasmids for 24h before their use for immunofluorescence labelling of the HA-tag or Sc35 epitopes. The results obtained with the HeLa and HCC1806 cells are shown in figure 6 panels A and B respectively. In the HeLa cells, we observed that exogenous WT and mutated RAD51 were translocated into the nucleus. RAD51 overexpression and its nuclear translocation had a strong effect on the Nuclear Speckles. We can see that the transfected cells, visualized by the HA-labelling and white arrows, had an abnormal Sc35 labeling. Indeed, in these transfected cells, the Nuclear Speckles number were strongly diminished, and some cells had no NS at all. This effect was observed for the WT as well as for the two mutants. The same experiment was performed in the HCC1806 cells, in which we observed that the exogenous WT and mutant RAD51 were expressed, but maintained in the cytoplasm. Besides this difference in exogenous RAD51 sub-cellular localization, we observed that RAD51 overexpression in HCC1806 cells had no “eye visible” strong effect on NS and we observed no cell without NS. Using Image J, we quantified the NS number for the different conditions in order to determine the average NS number per cell. The results are presented in the figure 6C. In HeLa cells, consistently with our observations, after the overexpression of exogenous RAD51, the average

NS number/cell is strongly diminished in a statistically highly significant manner, with the presence of cells without NS. Concerning the Ser97 residue, we noticed that the S97A mutant has the lower average NS number per cell, while the S97D and WT RAD51 gave the same phenotype. Surprisingly, in the HCC1806 cell line, the NS quantification revealed that the WT and S97D overexpression had also a diminution of the average NS number /cell that is statistically significant. In this same cell line, the S97A overexpression had no effect at all.

Taken together, these results showed that exogenous RAD51 overexpression induces a decrease of the average Nuclear Speckles number per cell, in the two cell lines, but with a more pronounced way in the HeLa cells, where exogenous RAD51 is localized within the nucleus. The most striking difference between the two cell lines concerns the presence of cells without NS. A phenotype that is observed only in HeLa cells and particularly those overexpressing the S97A non phosphorylable RAD51 mutant. In comparison, within the HCC1806 cell line, the S97A overexpression maintained within the cytoplasm had no effect on average NS number per cell. Thus, nuclear translocation of the exogenous non phosphorylable RAD51 is an essential point associated with a NS destabilization.

RAD51 is an RNA binding protein and its Ser97 phosphorylation affects its binding to RNA

After the finding of RAD51 colocalization within nuclear structures highly enriched in RNA, we pursued our investigations by testing RAD51 ability to bind RNA. In the context of DNA damage repair *via* the HR pathway, RAD51 is a well-known DNA binding protein, that has also been described as promoting DNA/RNA hybrids structures called R-loops, with the TERRA long non coding RNA in the context of telomeric maintenance [373]. In this same work, they showed that RAD51 binds the TERRA RNA *in vitro*. Little is known about RAD51 affinity to bind RNA. Using Blitz technology, we performed *in vitro* experiments to compare RAD51 binding to ssDNA *vs* ssRNA and evaluate the impact of the phosphorylation on the Ser97 residue on these bindings. For this, we used the phosphomimetic and non phosphorylable recombinant proteins described in the materials section. The results are presented in the figure 7A and B, in which association and dissociation curves are presented for 33 nt sized DNA and RNA respectively. Different RAD51 concentrations were used in order to determine the equilibrium dissociation

constant KD of the WT and mutant RAD51 proteins for DNA and RNA binding. The curves are presented in the fig 7C for DNA and fig 7D for RNA, the estimated KD values are presented in the figure 7E.

We show in the figure 7A, the effects of the Ser97 mutations on ssDNA binding capacity. In comparison to the WT RAD51, the S97D RAD51 phosphomimetic mutant showed different association and dissociation curves, with a higher binding capacity and a slightly more rapid dissociation profile. However, the resulting KD evaluation (that takes into account the dissociation/association parameters) showed that the S97D mutant has a ssDNA binding affinity similar to that of the WT (with a KD=3.63 μM for the S97D-RAD51 *vs* a KD=3.84 μM for the WT RAD51). Concerning, the S97A mutant comparison to the WT RAD51, we observed modified association and dissociation curves, with a lower binding capacity and a slower dissociation profile. The resulting KD evaluation showed a higher affinity to ssDNA for the S97A mutant (with a KD=0.34 μM for the S97A-RAD51 *vs* a KD=3.84 μM for the WT RAD51). We can conclude that in our *in vitro* conditions, the Ser97 phosphorylation has no impact on RAD51 affinity for ssDNA, while the S97A mutation provokes a 10-fold higher ssDNA binding affinity. This effect of the S97A mutation will be discussed later.

We next evaluated RAD51's ability to bind RNA, and the effects of the Ser97 mutations on this ssRNA binding capacity. First, we can see in the figure 7B, that WT and mutants RAD51 are all able to bind RNA. In comparison to the WT RAD51, the S97D mutant showed very different association and dissociation profiles with a higher binding capacity and a faster dissociation profile. These marked differences result in a lower ssRNA binding affinity for the S97D mutant in comparison to the WT RAD51, (with a KD=1.73μM for the S97D *vs* a KD=0.53 μM for the WT RAD51).

Concerning the comparison between the S97A mutant, and the WT RAD51, it shows similar association curves with comparable binding capacities but different dissociation curves. Indeed, the S97A mutant shows a slower dissociation profile. Logically, the resulting KD evaluation showed a slightly higher affinity for ssRNA for the S97 mutant (with a KD=0.32 μM for the S97A *vs* a KD=0.53 μM for the WT RAD51).

All these data showed that RAD51 binds DNA and RNA. The Ser97 mutants highlight the impact of the Ser97 residue as a major modulator of RAD51 affinity for RNA and DNA.

DISCUSSION

In this work, we identified a new phosphorylation of RAD51 recombinase, the key player in the Homologous Recombination DNA repair pathway. This *in vitro* Aurora A mediated phosphorylation targets the Subunit Rotation Motif of RAD51 at the Ser97 residue. This region is a putative anchoring platform for many other proteins and remains accessible at the surface of the RAD51 nucleofilament. The RecA family SRM, with is evolutionarily conserved, is described as being important in the 3D structure of RecA monomers and is crucial for regulating RecA enzymatic activity [374]. According to these results, we showed here that the Ser97 phosphorylation has a strong effect on *in vitro* RAD51 D-loop activity, self-association and RNA binding affinity. We showed that RAD51 is an RNA binding protein and that its Ser97 phosphorylation affects strongly its binding to RNA, while it has no effect on its affinity for DNA (WT KD= 3.84 µM and S97D KD=3.63 µM). Indeed, blitz experiments showed that the phosphomimetic RAD51 dissociation from ssRNA is more rapid than that of the WT RAD51 and it lowers its affinity for RNA by a 3-fold factor (KD=1.73µM for the S97D *vs* KD=0.53µM for the WT). This result may seem in contradiction with the *in cellulo* observed presence of PSer97-RAD51 within the nuclear Speckles, but we must consider the difference between the *in vitro* and *in cellulo* conditions where the presence of many partners and PTM of RAD51 can regulate its RNA binding and/or dissociation. Moreover, it is interesting to notice that the S97D phosphomimetic mutant, has a higher binding affinity for ssRNA (KD=1.73 µM) than for ssDNA (KD=3.63µM). Even though the S97D mutant has the same ssDNA affinity than the WT RAD51, it has a higher D-loop activity. The D-loop assay, being a combined evaluation of RAD51/DNA interactions and RAD51 strand exchange activity, we can hypothesize that RAD51 strand exchange activity is enhanced by its phosphorylation on the Ser97 residue. Concerning the S97A mutant comparison to the WT RAD51, we observed that it has higher affinities for both ssDNA (KD= 0.34 µM) and ssRNA (KD= 0.32 µM) with the same affinity for both RNA and DNA. We

also observed that the S97A mutation has an effect on RAD51 D-loop activity. This enhanced D-loop activity may be due to a better ssDNA binding or a better strand exchange activity. Even if these results are *in vitro* and do not include physiological regulation of RAD51 activity, they highlighted the importance of the Subunit Rotation Motif and in particular the Ser97 residue in regulating RAD51's activity and affinity for nucleic acids.

Using a specifically engineered antibody, we also showed that this PSer97-RAD51 does indeed exist *in cellulo*. During RAD51 siRNA experiments, the diminution of RAD51 protein level (63%) is higher than that of the PSer97RAD51 (51%). This could be linked to the PTM effects on proteins half-life. Concerning RAD51, little is known about the effect of its PTMs on its half's life modulation. Genetic experiments should be performed, using CRISPR/Cas9 technology, in order to answer if the Ser97 phosphorylation affects RAD51 half-life.

Concerning the kinase implicated in this *in cellulo* phosphorylation, we showed that Aurora A overexpression drives a significant enhancement of the Ser97 phosphorylation of RAD51, thus showing that Aurora A is implicated in this new PTM of RAD51. Use of an aurora A inhibitor (alisertib) showed an effect only in the HCC1806 cell line and not in the HeLa cells. These cell line-dependent results point to possible redundancy and illustrate the miss-regulations that occur in different cancers. Therefore, it is possible that other kinases could also phosphorylate RAD51 Ser97 residue. Concerning the characterization of this phosphorylation, we showed that it is decreased after DNA damage induction. It is interesting to notice here that Aurora A kinase activity has been described as decreasing after DNA damage induction [350]. On the contrary, Aurora A overexpression has been described as inhibiting RAD51 recruitment to DNA breaks without affecting γ-H2AXfoci formation. This inhibition of RAD51 recruitment necessitates Aurora A kinase activity and led to a decrease of HR mediated DNA repair [375].

Surprisingly, immunofluorescence experiments showed that the Ser97 phosphorylation is distributed in nuclear foci structures that are not colocalized with γ-H2AX foci. Using a commercial antibody against RAD51, we indeed found that there are some RAD51 foci that are not colocalized with γ-H2AX. Our results revealed an atypical sub-cellular location for RAD51, linked to its Ser97 phosphorylation. Using immunofluorescence and confocal microscopy, we

identified these PSer97 foci and showed that they are located within the Nuclear Speckles. It is described in the literature that the use of the splicing inhibitor plaB has an effect on NS activity but keep their structure maintained with an enhancement of their size [376]. After PlaB treatment, we observed that PSer97-RAD51 foci were still within the Nuclear Speckles even if a slight decrease of the colocalization coefficient was observed. Then, RAD51 recruitment to the NS is independent of a functional splicing activity. Using transitory transfection experiments, we showed that exogenous RAD51 maintained in the cytoplasm had less effect on Nuclear Speckles number, than exogenous RAD51 translocated in the nucleus. Indeed, in HeLa cells, in addition to the decrease of NS number per cell we also observed cells without NS. This phenotype was particularly observed for the non-phosphorylable S97A-RAD51 overexpression. Meaning that the presence of exogenous non-phosphorylable RAD51 in the nucleus is deleterious for Nuclear Speckles. While in HCC1806 cell line, exogenous non-phosphorylable RAD51 maintained in the cytoplasm did not produce this extreme phenotype. The role of the Ser97 residue phosphorylation in RAD51/RNA interaction and NS colocalization needs to be pursued. For that purpose, a comparative analysis of PSer97-RAD51 *vs* RAD51 partners must be performed to understand the regulation of RAD51 binding to RNA within the Nuclear Speckles. Moreover, RAD51 IP showed a co-immunoprecipitation of Sc35. Taken together, our results allow us to consider a possible role of RAD51 in these splicing machineries: a new RAD51 function beyond DNA repair needs to be explored.

RAD51 binding to RNA has also been described by the work of Feretzaki et al. in the context of telomeric metabolism in which they showed that RAD51 is essential for the *in cellulo* recruitment of the TERRA RNA on telomeres and the R-loop formation. These results consolidate our finding of a new phosphorylated form of RAD51 that binds RNA and is found in Nuclear Speckles.

While writing this manuscript, we learned of the work by Damodaran that described a link between Aurora A activity and the splicing machinery. They showed that overexpressed Aurora A is partially colocalized with Sc35, within the Nuclear Speckles, and that Aurora A inhibition provokes splicing alterations. They also showed that Aurora A interacts with and phosphorylates

splicing factors [377]. These data strongly reinforce ours and particularly the implication of Aurora A in the *in cellulo* RAD51 Ser97 phosphorylation.

The DDR requires the orchestrated recruitment of different proteins intervening in chromatin remodeling, cell signaling, and DNA repair. This work provides a basis for further studies exploring more precisely the possible role of the RAD51 DNA repair factor within the Nuclear Speckles's structure or function, and reveals a new link between DNA repair and alternative splicing regulation. Understanding the regulation of pre mRNA splicing during the DDR is of particular interest as we know that splicing regulation in the context of chemo/radio-therapies is implicated in the development of treatment resistances [378] [372]

AUTHORS CONTRIBUTION

M.A. made the Cpt, Ali and PlaB cell treatments and WB experiments, Cell-cycle analysis, IP, siRNA experiments.

P.K.Y. made polymerization assays, Blitz DNA and RNA assays. NA made Blitz assay analysis. V.P.M and G. C made cell culture and protein extractions. A.D. made D-loop assay. D.M made recombinant protein production. HBM conceived, supervised all the study and wrote the manuscript. F.F as the team head made that possible.

AKNOWLEDGMENTS

This work was financed by the SATT grand-Ouest valorisation.

Figure 1

A

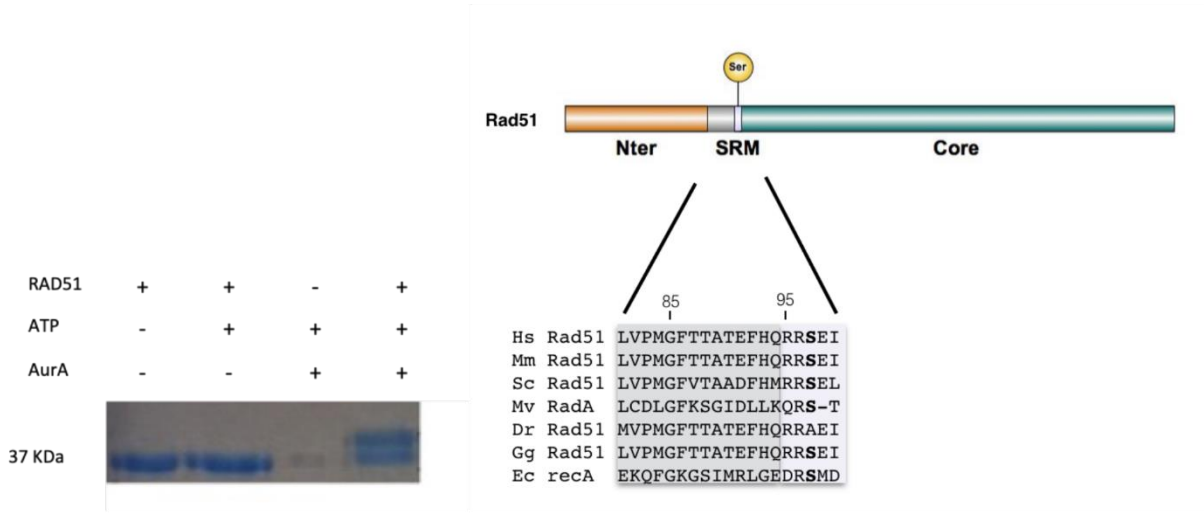
RAD51 + + - +
ATP - + + +
AurA - - + +
37 KDa
Ser
Rad51
Nter
SRM
Core
85
95
Hs Rad51 LVPMGFTTATEFHQRRSEI
Mm Rad51 LVPMGFTTATEFHQRRSEI
Sc Rad51 LVPMGFVTAADFHMRRSEL
Mv RadA LCDLGFKSGIDLLKQRS-T
Dr Rad51 MVPMGFTTATEFHQRRAEI
Gg Rad51 LVPMGFTTATEFHQRRSEI
Ec recA EKQFGKGSIMRLGEDRSMD

B

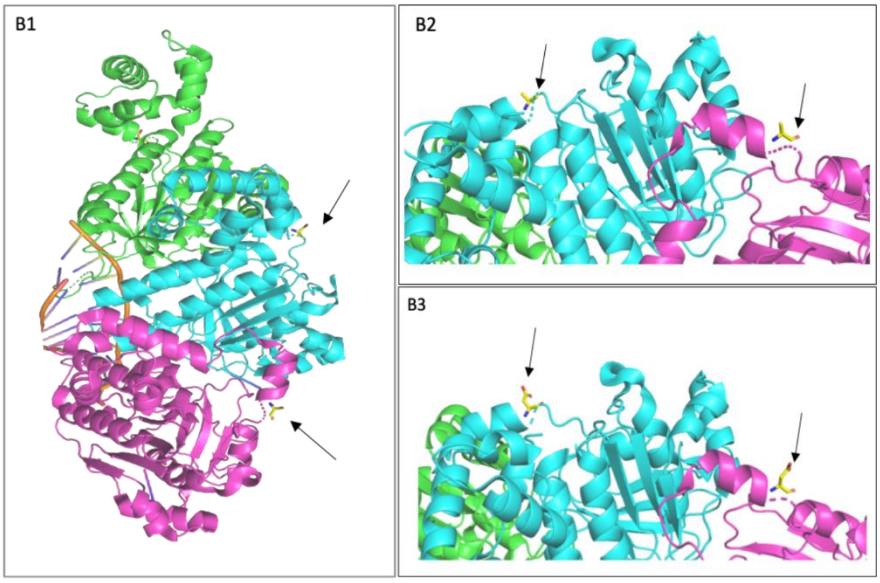
B1
B2
B3

C

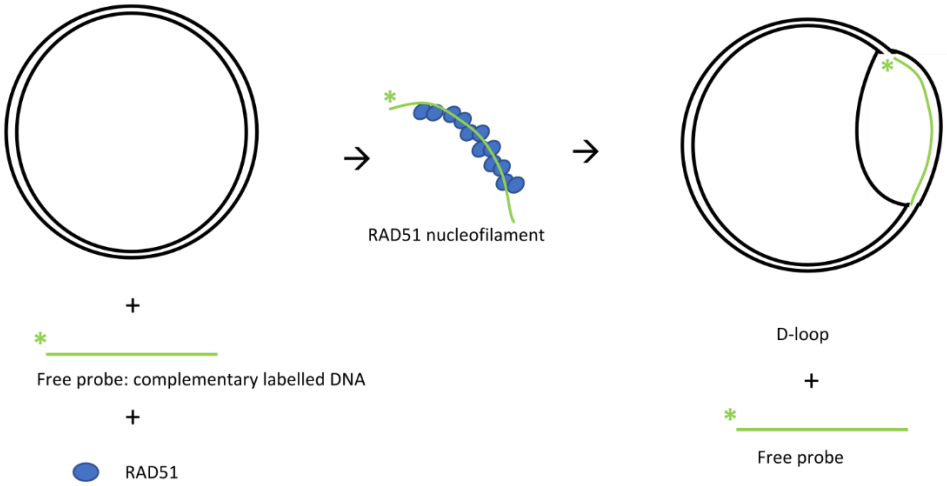
RAD51 nucleofilament
+
Free probe: complementary labelled DNA
+
RAD51
D-loop
+
Free probe

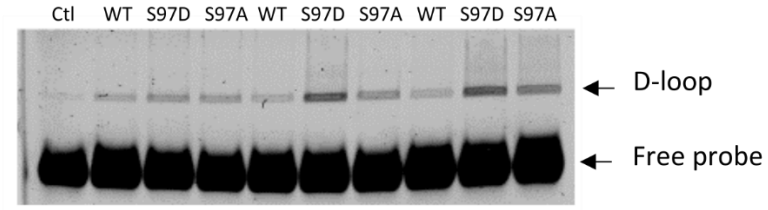
Ctl
WT
S97D
S97A
WT
S97D
S97A
WT
S97D
S97A
D-loop
Free probe

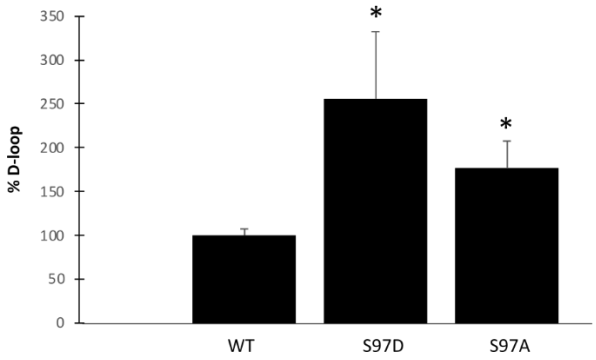
% D-loop
350
300
250
200
150
100
50
0
*
*
WT
S97D
S97A

D

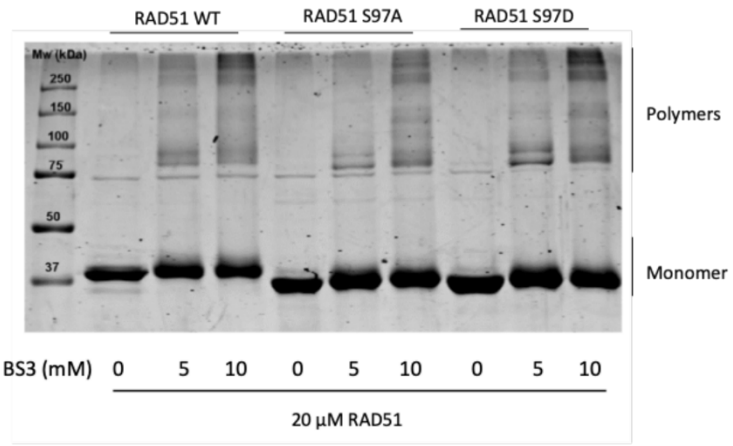

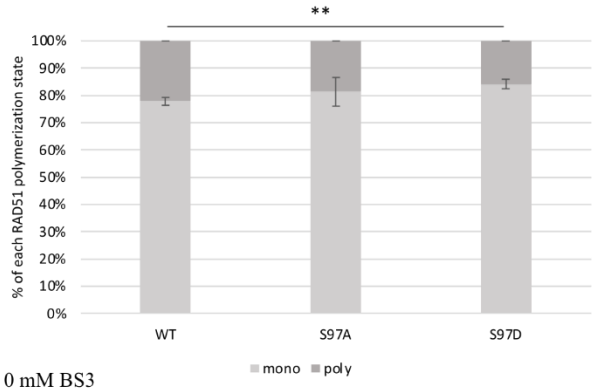

0 mM BS3

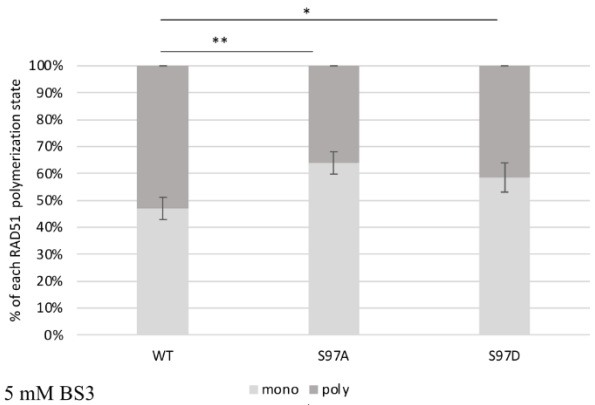

5 mM BS3

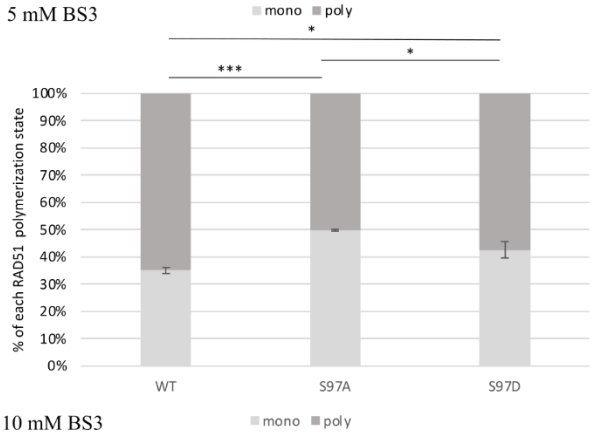

10 mM BS3

Figure 1

A: Aurora A kinase phosphorylates RAD51 *in vitro* on its Ser97 residue

Coomassie blue stained SDS-PAGE after *in vitro* phosphorylation of recombinant RAD51 by Aurora A kinase. Within the Subunit Rotation Motif, the Ser97-RAD51 residue is well conserved among species.

The AurA-phosphorylated residue is located within the Subunit Rotation Motif (SRM) of RAD51

Nter: N terminal domain, Core: Core domain.

Sequence alignment of RAD51 Linker Region (81 to 99). Light gray background corresponds to the Subunit Rotation Motif (95 to 99). S in bold corresponds to the residue phosphorylated in HsRAD51.

Hs: Homo sapiens, Mm: Mus musculus, Sc: Saccharomyces cerevisiae, Mv: Moloney virus, Dr: Danio rerio, Gg: Gallus gallus, Ec Escherichia coli.

B: Prediction of the effect of Ser97-phosphorylation on RAD51 structure

The 3D structure of HsRAD51 WT allows us to observe Ser97 which is located in a random coil on the linker region of each monomer precisely in the SRM (B1). By zooming in on a part of the nucleofilament where Ser97 has been mutated to Ala, S97A mutation (B2) or to Asp, S97D mutation (B3), we can see that the side chains of these residues are free like that of Ser97. Arrows indicate the residues located on the 97 position (Ser, Ala or Asp in the B1, B2 and B3 pictures respectively).

C: RAD51 phosphorylation mimetic on Ser97 affects its D-loop activity

The D-loop test was used to evaluate the D-loop formation capacity of the of WT, S97A and S97D-RAD51 recombinant proteins. Top figure: a scheme of the experimental D-loop assay. The intensities of the free probe and the D-loop were quantified by an IRD700 scan, then used to evaluate the D-loop formation. The activity of the WT-RAD51 was set as 100% and used for S97A and S97D activity standardization. T-test with alpha=0,05 was used: p-value WT *vs* S97D=0,025, pvalue WT *vs* S97A=0,014 (n=3 experiments).

D: RAD51 phosphorylation mimetic on Ser97 affects its polymerization rate

WT**,** S97D and S97A RAD51 recombinant proteins were used to evaluate the effect of RAD51 phosphorylation on its polymerization, by the *in vitro* polymerization assay. RAD51 was incubated with or without BS3 reticulating agent, then used to perform an acrylamide gel electrophoresis and a Coomassie blue staining. Intensities of n=3 experiments were quantified using a Lycor scan and used for statistical analysis (t-test with alpha= 0,05 was used: without BS3, Wt *vs*S97D, p-value= 0.008. For the 5mMBS3 condition, p-value WT *vs* S97A=0.007, p-value WT *vs* S97D= 0.04. for the10mM BS3 condition, p-value WT *vs* S97A=2.3 10^{-5}, p-value WT *vs* S97D= 0.015, p-value S97D *vs* S97A= 0.016).

Figure 2

A

1.

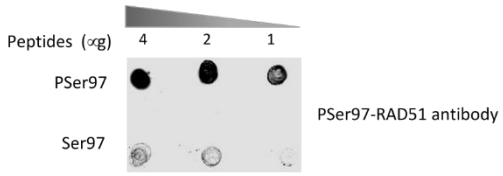

2.

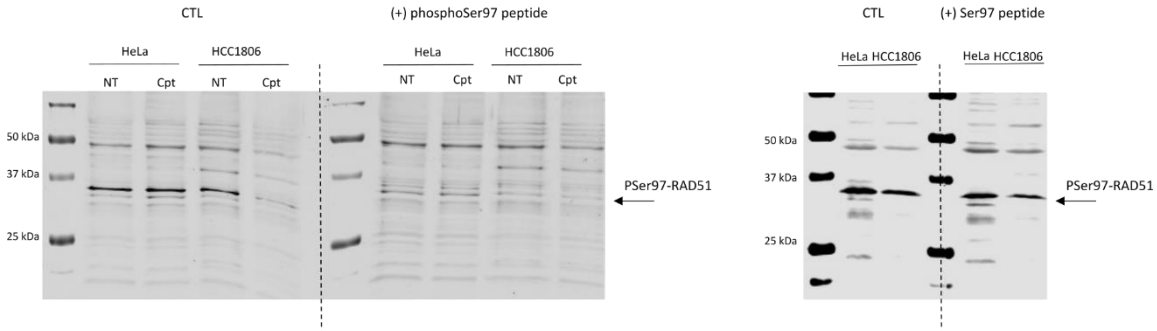

3.

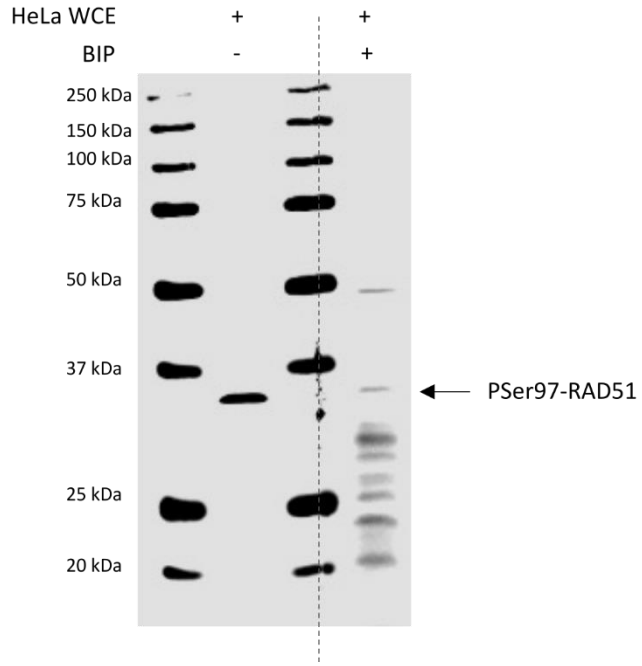

4.

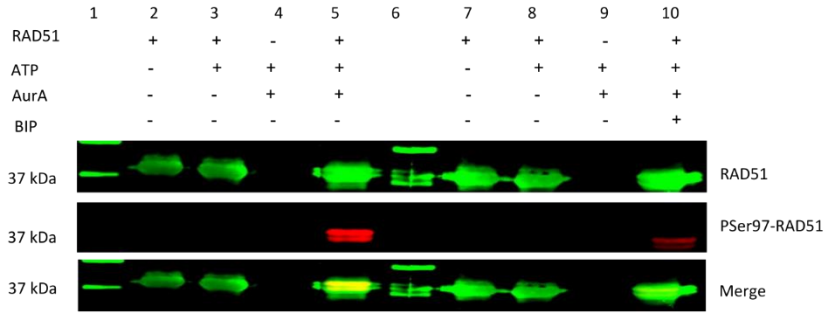
1 2 3 4 5 6 7 8 9 10
RAD51 + + - + + + - +
ATP - + + + - + + +
AurA - - + + - - + +
BIP - - - - - - - +
37 kDa
RAD51
37 kDa
PSer97-RAD51
37 kDa
Merge

5.

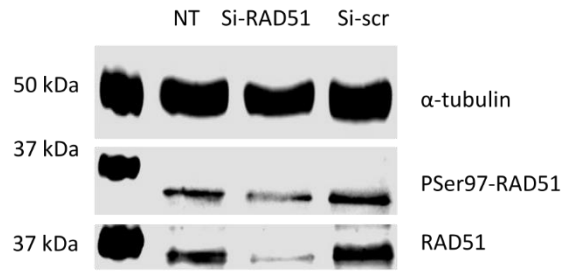
NT Si-RAD51 Si-scr
50 kDa
α-tubulin
37 kDa
PSer97-RAD51
37 kDa
RAD51

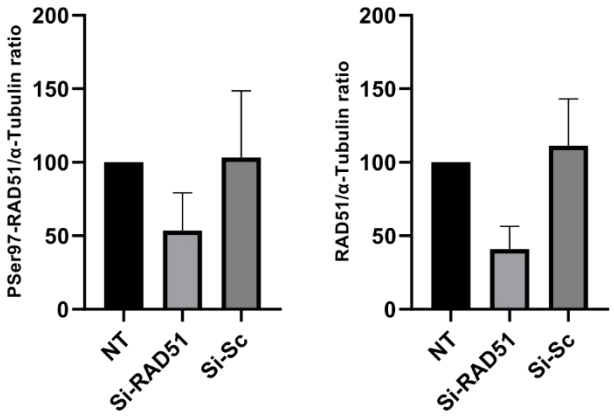
PSer97-RAD51/α-Tubulin ratio
200
150
100
50
0
NT
Si-RAD51
Si-Sc
RAD51/α-Tubulin ratio
200
150
100
50
0
NT
Si-RAD51
Si-Sc

6.

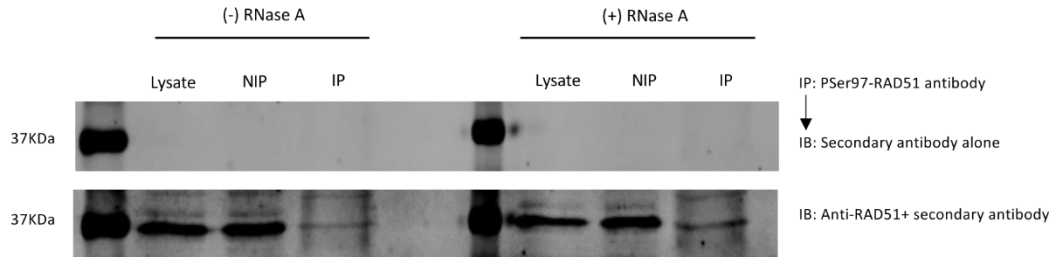
(-) RNase A
(+) RNase A
Lysate NIP IP
Lysate NIP IP
IP: PSer97-RAD51 antibody
37KDa
IB: Secondary antibody alone
37KDa
IB: Anti-RAD51+ secondary antibody

B

1.

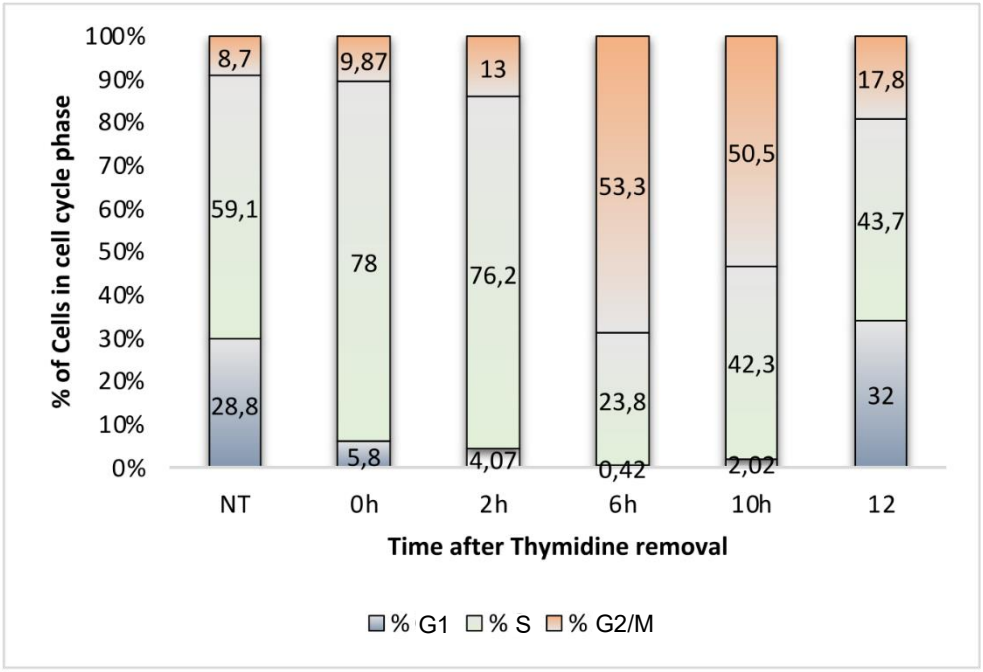
100%
90%
80%
70%
60%
50%
40%
30%
20%
10%
0%
% of Cells in cell cycle phase
8,7
59,1
28,8
9,87
78
5,8
13
76,2
4,07
53,3
23,8
0,42
50,5
42,3
2,02
17,8
43,7
32
NT
0h
2h
6h
10h
12
Time after Thymidine removal
% G1
% S
% G2/M

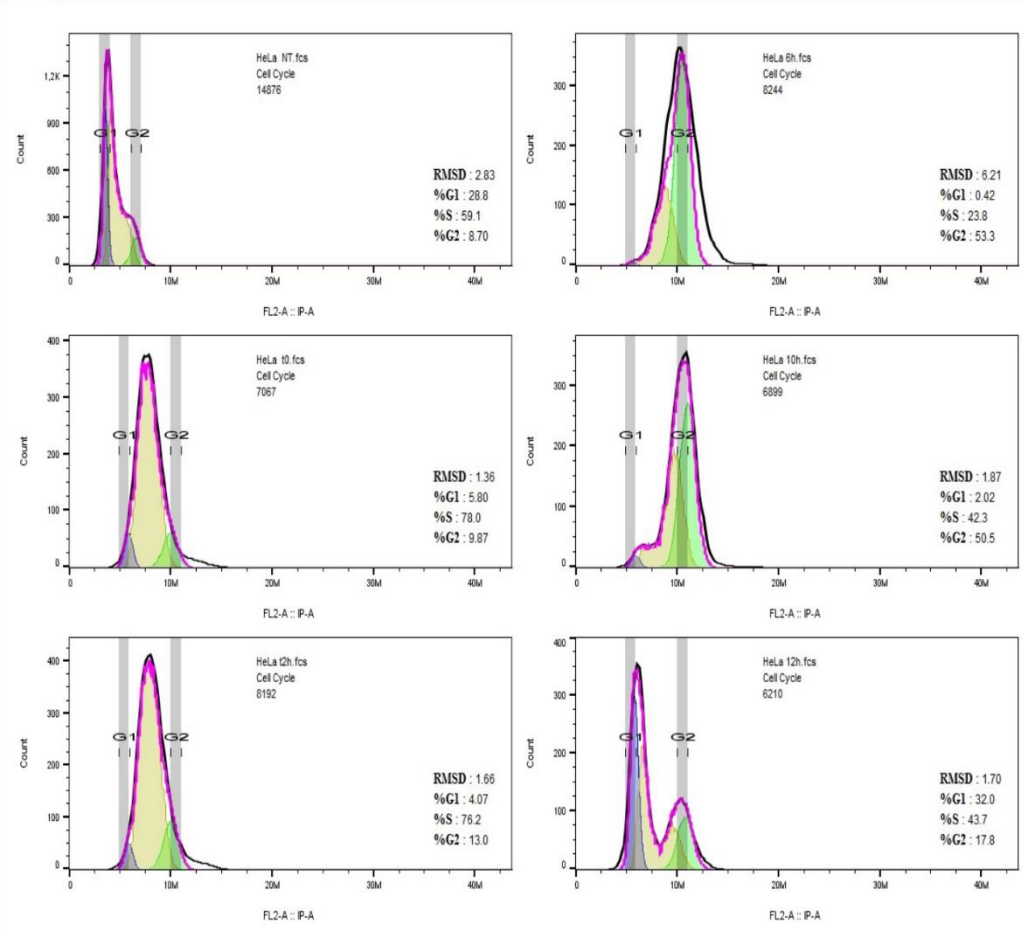
HeLa NT.fcs
Cell Cycle
14876
RMSD : 2.83
%G1 : 28.8
%S : 59.1
%G2 : 8.70
HeLa 6h.fcs
Cell Cycle
8244
RMSD : 6.21
%G1 : 0.42
%S : 23.8
%G2 : 53.3
HeLa t0.fcs
Cell Cycle
7067
RMSD : 1.36
%G1 : 5.80
%S : 78.0
%G2 : 9.87
HeLa 10h.fcs
Cell Cycle
6899
RMSD : 1.87
%G1 : 2.02
%S : 42.3
%G2 : 50.5
HeLa t2h.fcs
Cell Cycle
8192
RMSD : 1.66
%G1 : 4.07
%S : 76.2
%G2 : 13.0
HeLa 12h.fcs
Cell Cycle
6210
RMSD : 1.70
%G1 : 32.0
%S : 43.7
%G2 : 17.8
Count
FL2-A :: IP-A
G1
G2

2.

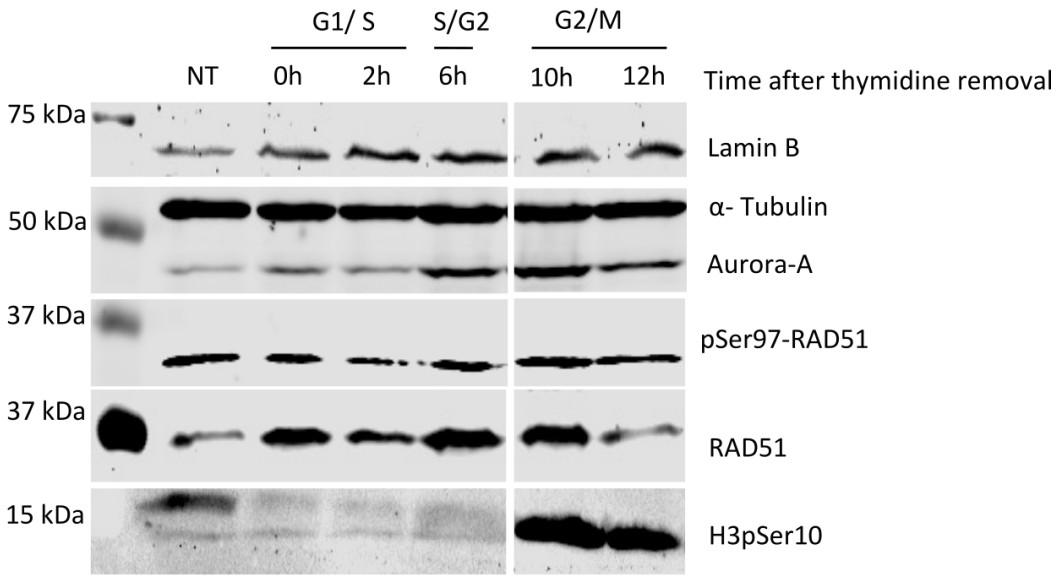
G1/ S
S/G2
G2/M
NT
0h
2h
6h
10h
12h
Time after thymidine removal
75 kDa
Lamin B
50 kDa
α- Tubulin
Aurora-A
37 kDa
pSer97-RAD51
37 kDa
RAD51
15 kDa
H3pSer10

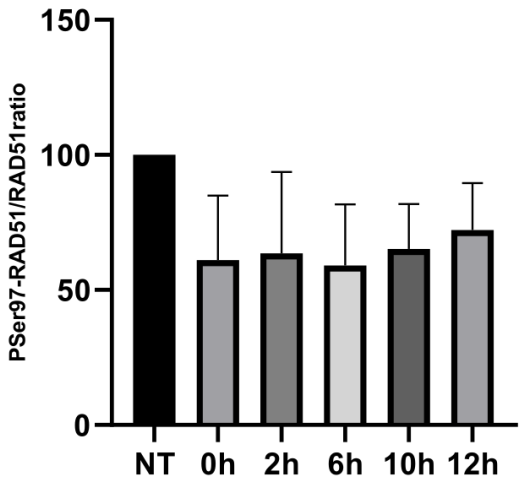
PSer97-RAD51/RAD51ratio
150
100
50
0
NT
0h
2h
6h
10h
12h

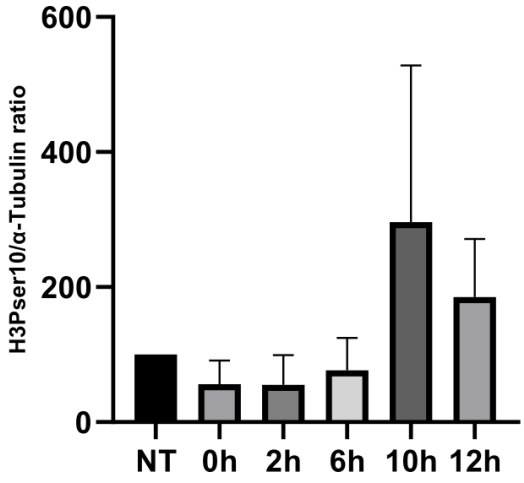
H3Pser10/α-Tubulin ratio
600
400
200
0
NT
0h
2h
6h
10h
12h

C

1.

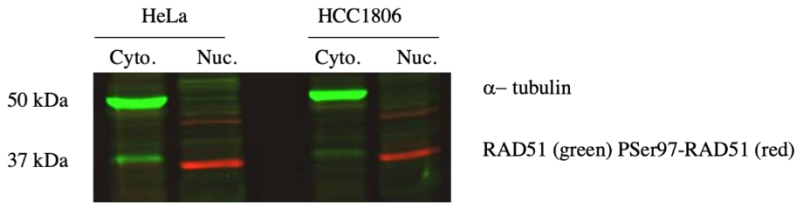
HeLa
HCC1806
Cyto.
Nuc.
Cyto.
Nuc.
50 kDa
37 kDa
α– tubulin
RAD51 (green) PSer97-RAD51 (red)

2.

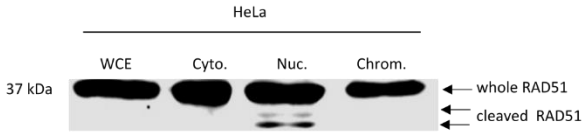
HeLa
WCE
Cyto.
Nuc.
Chrom.
37 kDa
whole RAD51
cleaved RAD51

3.

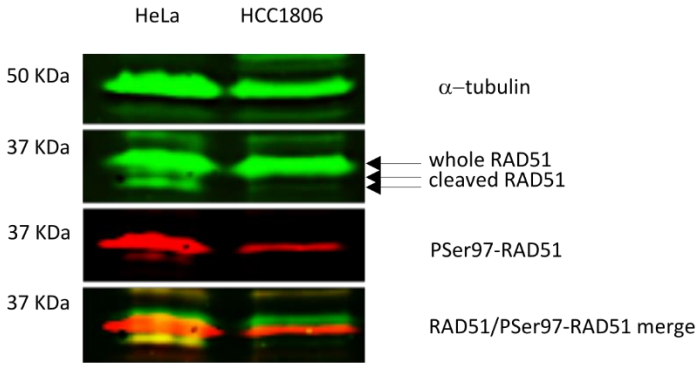
HeLa
HCC1806
50 KDa
37 KDa
37 KDa
37 KDa
α–tubulin
whole RAD51
cleaved RAD51
PSer97-RAD51
RAD51/PSer97-RAD51 merge

4.

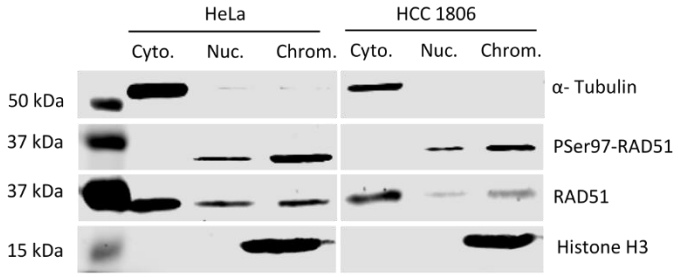
HeLa
HCC 1806
Cyto.
Nuc.
Chrom.
Cyto.
Nuc.
Chrom.
50 kDa
37 kDa
37 kDa
15 kDa
α- Tubulin
PSer97-RAD51
RAD51
Histone H3

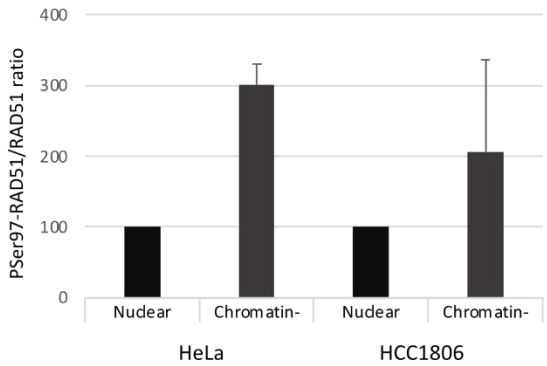
PSer97-RAD51/RAD51 ratio
400
300
200
100
0
Nuclear
Chromatin-
Nuclear
Chromatin-
HeLa
HCC1806

D

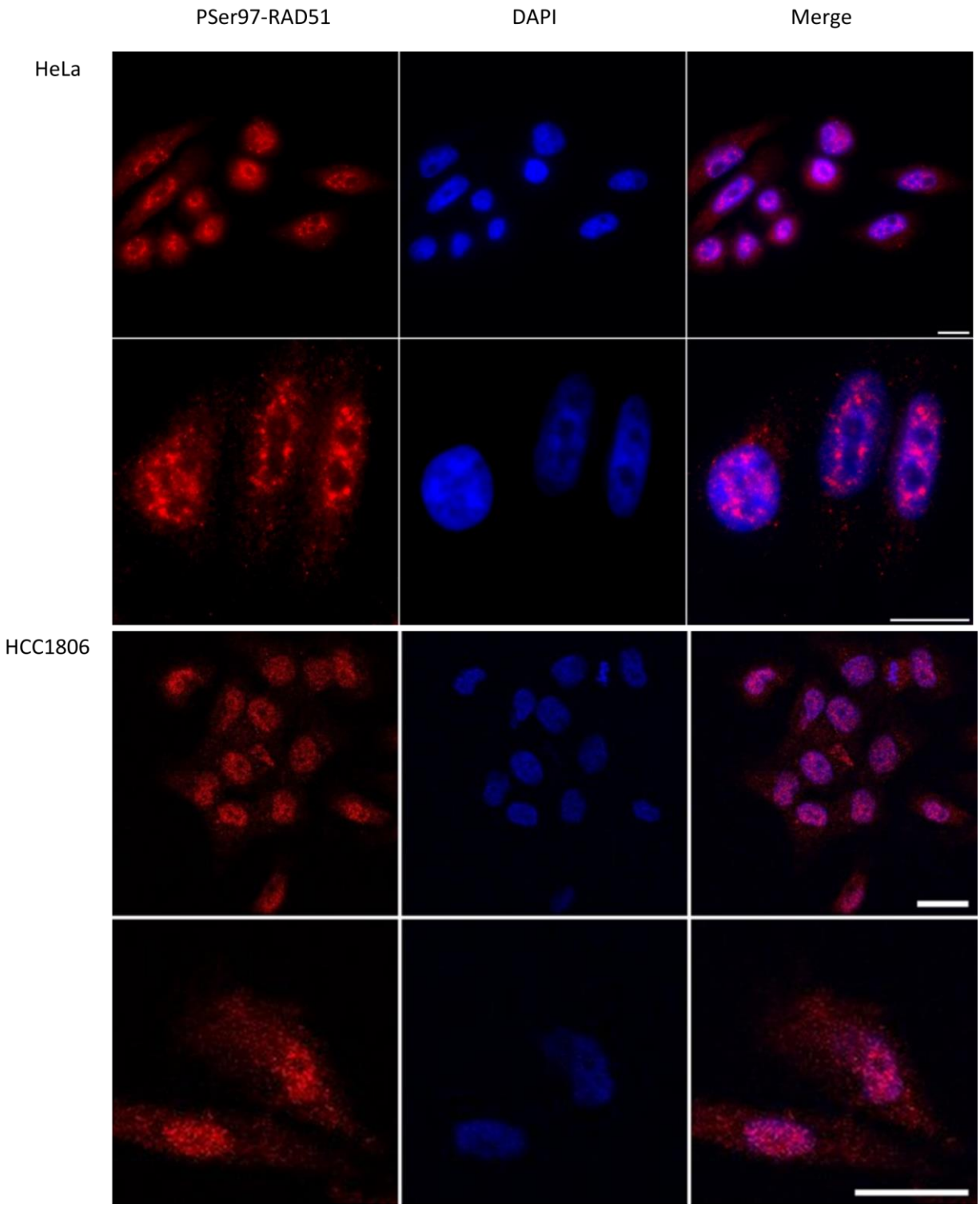

E

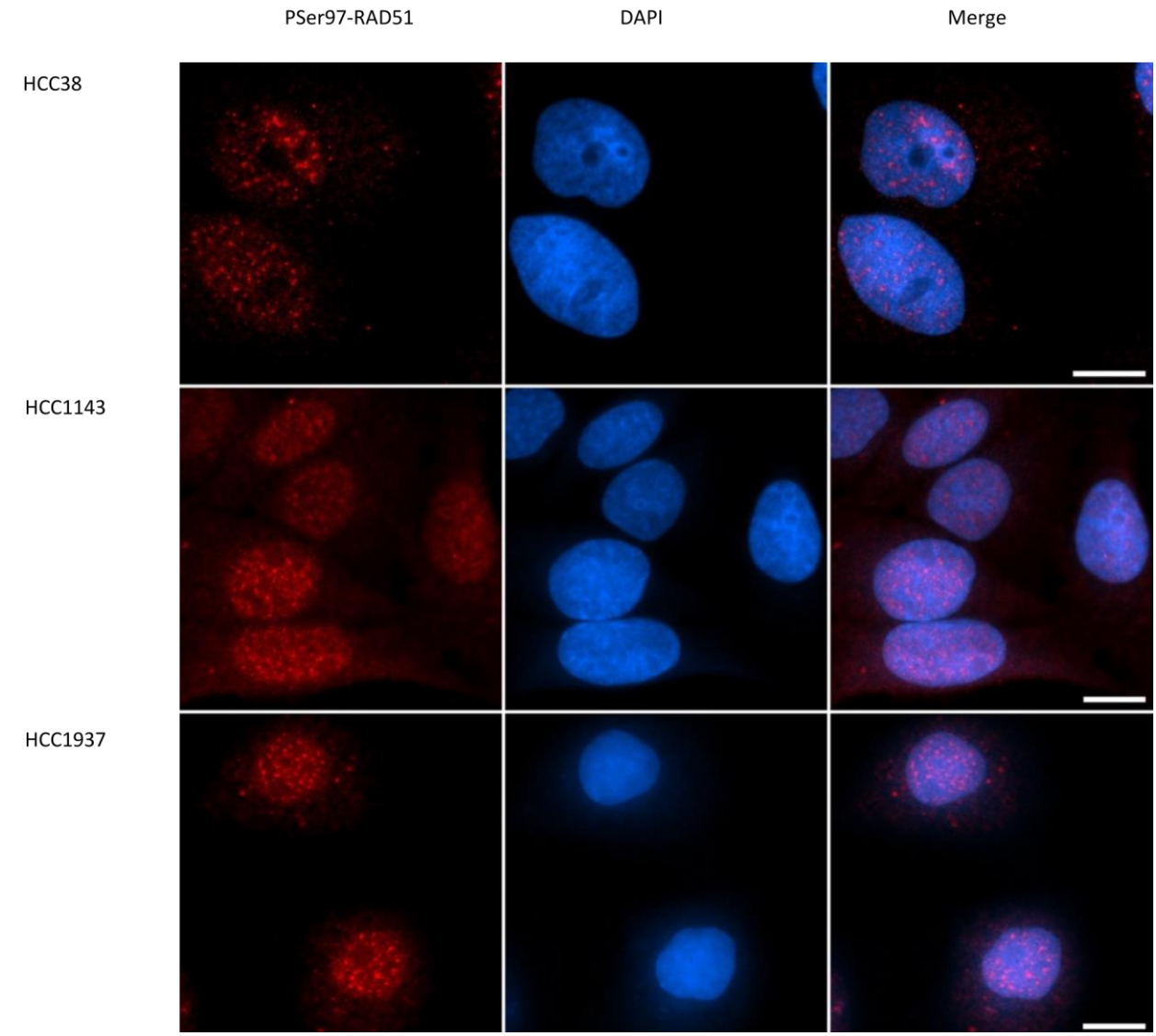

F

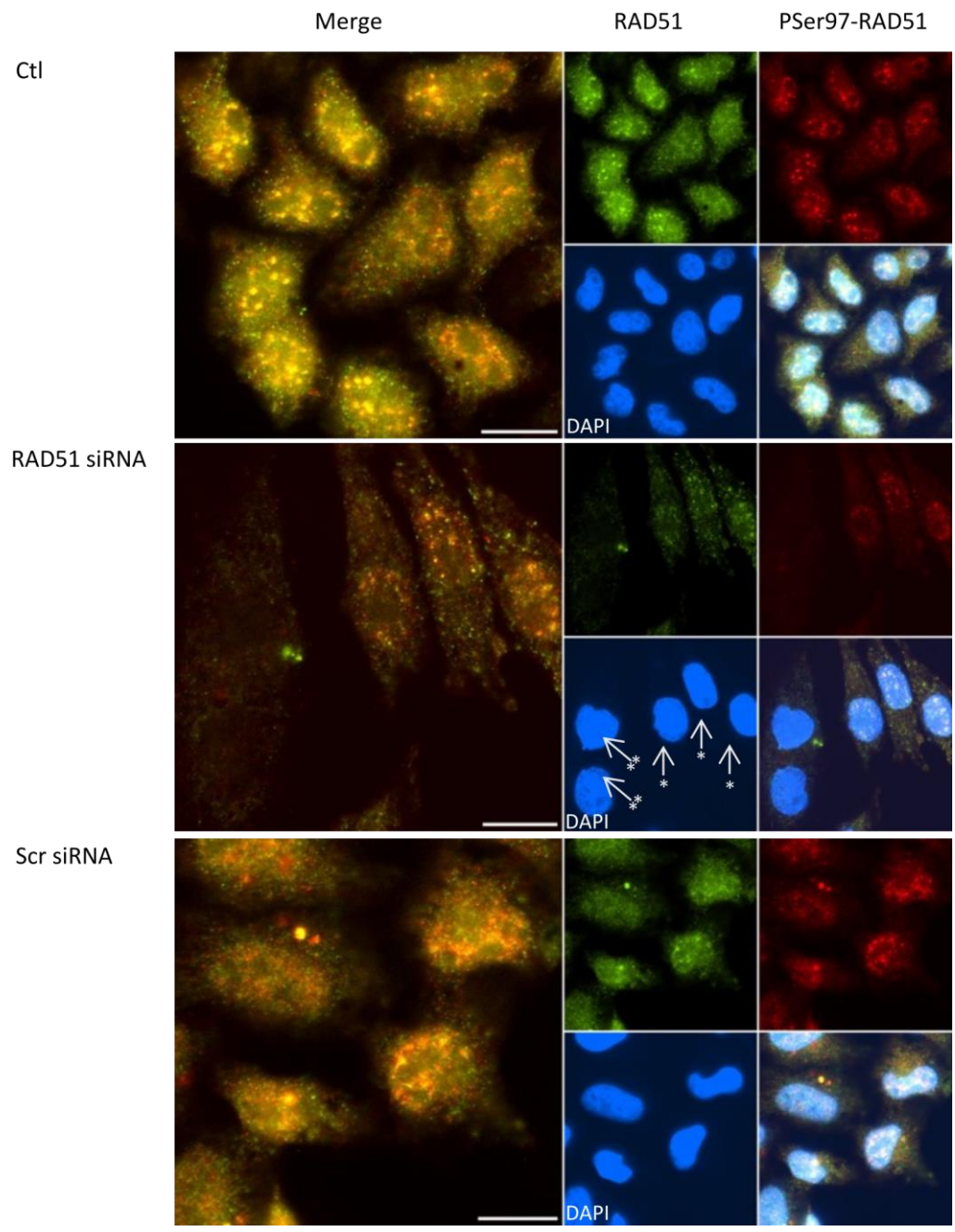
Merge
RAD51
PSer97-RAD51
Ctl
RAD51 siRNA
Scr siRNA
DAPI
DAPI
DAPI

Figure 2

A: anti PSer-RAD51 antibody validation and *in cellulo* exploration of PSer97-RAD51 presence

1.Dot blot assay showing the Pser-RAD51 antibody recognition of the PSer-RAD51 peptide and not the Ser-RAD51 peptide. 2. Western blot assay showing the PSer-RAD51 signal in HeLa and HCC1806 whole cell extracts in control condition or after a peptide competition. The dashed lines correspond to the membrane cutting for the two kinds of incubation (classical or with a peptide competition). Two peptides were used for the competition, the non-phosphorylated (Right gel) and the Ser97 phosphorytated one (left gel). Cpt for Camptothecin (10 µM for 4h) 3. HeLa whole cell extracts were used to perform a western blot in control condition and after the action of Bovine Intestine Phosphatase (BIP). The dashed line corresponds to the membrane cutting for the incubation with BIP of the right part of it. Western blot assay showing an *in vitro* phosphorylation assay of RAD51 by Aurora A kinase in control condition (lines 1-5) and after BIP action (lines 7-10). 5. Western blot assay with HeLa whole cell extracts in control condition and after 24h transfection with RAD51siRNA or scr siRNA. The Pser-RAD51 and RAD51 signals were quantified from n=3 experiments. 6. Immunoprecipitation of PSer97-RAD51 with the phosphospecific antibody, and Immunoblotting using a monoclonal antiRAD51 antibody. RNase A treatment ameliorates the precipitation of the PSer97-RAD51 form. NIP: Non Immuno Precipitated, IP: Immuno Precipitated.

B: PSer97-RAD51/RAD51 ratio is dynamic during the cell cycle progression

1. Cell cycle progression of HeLa cells after double thymidine block. Cytometer was used to count cells and follow their genomic material after PI (Propidium Iodide) labelling. Cell cycle distribution analysis was performed using FlowJo® software. 2. Western blot assay was used to the tracking of PSer97-RAD51 levels in HeLa cells during cell cycle progression after the double thymidine block. The H3pSer10 was used as a mitosis labelling.

C: PSer97-RAD51 is predominantly localized in the nucleus

Evaluation of the sub-cellular and subnuclear localization of PSer97-RAD51 in control condition in HeLa and HCC1806 cells. 1.Cytoplasmic/nuclear fractionation. Western blot using rabbit PSer97-RAD51 antibody in red and mouse RAD51 antibody in green. Alpha-tubulin was used as a loading control and fractionation quality indicator. 2. HeLa whole cell extracts, cytoplasmic, nuclear soluble and chromatin linked fractions were used to perform a western blot analysis using a commercial anti RAD51 antibody. Undersized RAD51 proteins are observed in the nuclear fraction. 3. The phospho-specific PSer97-RAD51 antibody (red signal) and a commercial antiRAD51 antibody (green signal) were used to check for the presence of this phosphorylation in whole cell extracts of HeLa and HCC1806 cell lines. 4. Western blot assay using PSer97-RAD51 and RAD51 antibodies was performed using cytoplasmic, nuclear soluble and chromatin linked fractions of HeLa and HCC1806 cells. Alpha-tubulin and H3 were used as loading controls and fractionation quality indicators. Signals were quantified and used to calculate the PSer97-RAD51 ratio relative to RAD51 in nuclear soluble and chromatin bound fractions (n=5 experiments).

D: *in cellulo* nuclear enrichment of PSer97-RAD51

Immunofluorescence staining of PSer97-RAD51 in HeLa and HCC1806 cells. PSer97-RAD51 is in red and the DNA DAPI staining is in blue. Scale Bar= 10µm.

E: PSer-RAD51 labelling in different human cell lines

PSer97-RAD51 labelling in HCC38, HCC1143 and HCC1937 breast cancer cell lines. PSer97-RAD51 is in red and the DNA DAPI staining is in blue. Scale Bar= 10µm.

F: *In cellulo* anti PSer-RAD51 antibody validation

HeLa cell line was used to follow the RAD51 and the PSer97-RAD51 signals in control condition and after RAD51-si RNA transfection. Scr siRNA was used as a negative control. In the RAD51 siRNA condition, arrows with one star indicate cells with a diminished RAD51 and PSer97 signals. Arrows with two stars indicate cells with a complete RAD51 and PSer97 RAD51 signal extinction. Scale Bar= 10µm. Image acquisitions properties and treatment were identical for all conditions.

Figure 3

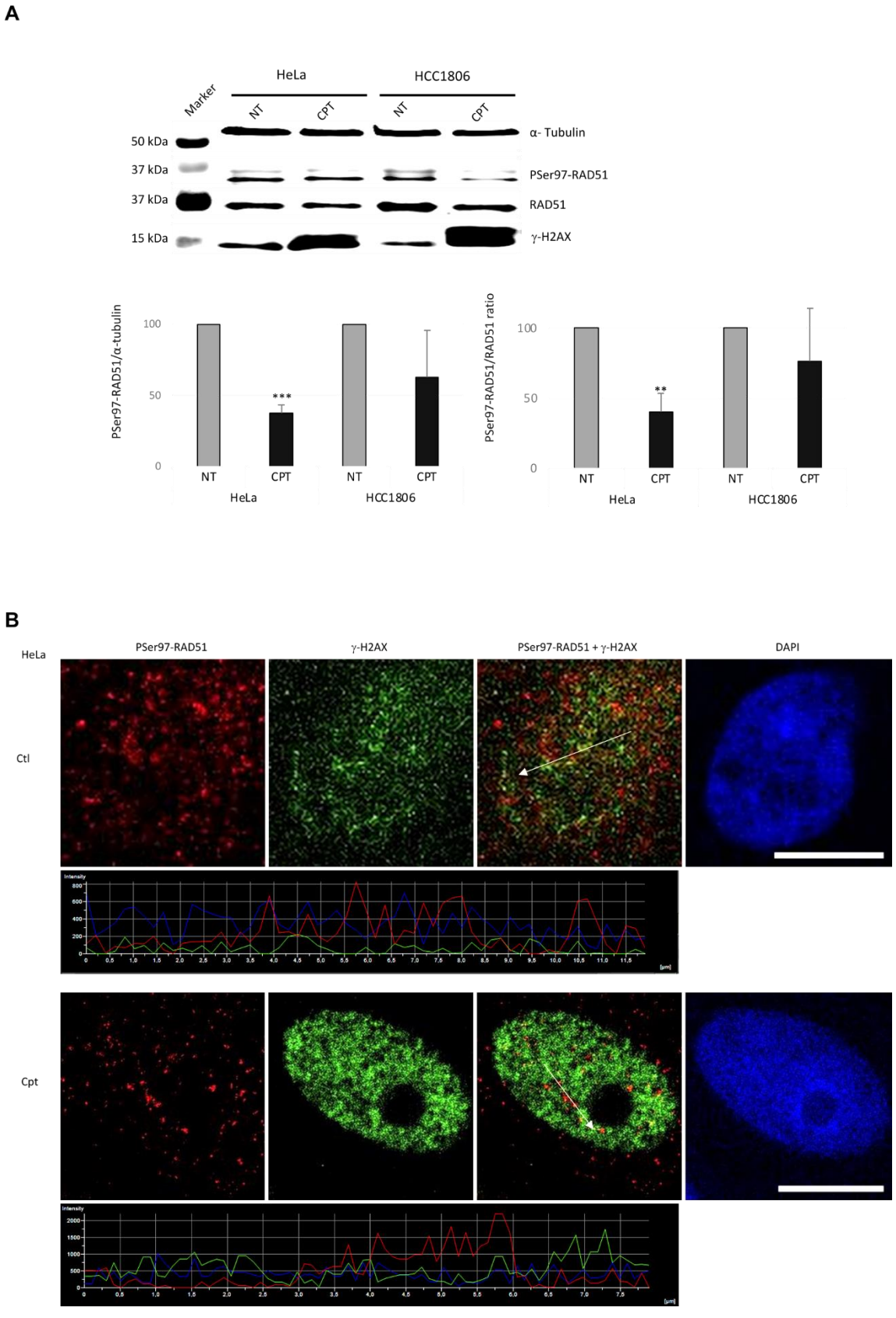
A
HeLa
HCC1806
Marker
NT
CPT
NT
CPT
50 kDa
37 kDa
37 kDa
15 kDa
α- Tubulin
PSer97-RAD51
RAD51
γ-H2AX
PSer97-RAD51/α-tubulin
100
50
0
***
NT
CPT
NT
CPT
HeLa
HCC1806
PSer97-RAD51/RAD51 ratio
100
50
0
**
NT
CPT
NT
CPT
HeLa
HCC1806
B
HeLa
PSer97-RAD51
γ-H2AX
PSer97-RAD51 + γ-H2AX
DAPI
Ctl
Intensity
Cpt
Intensity

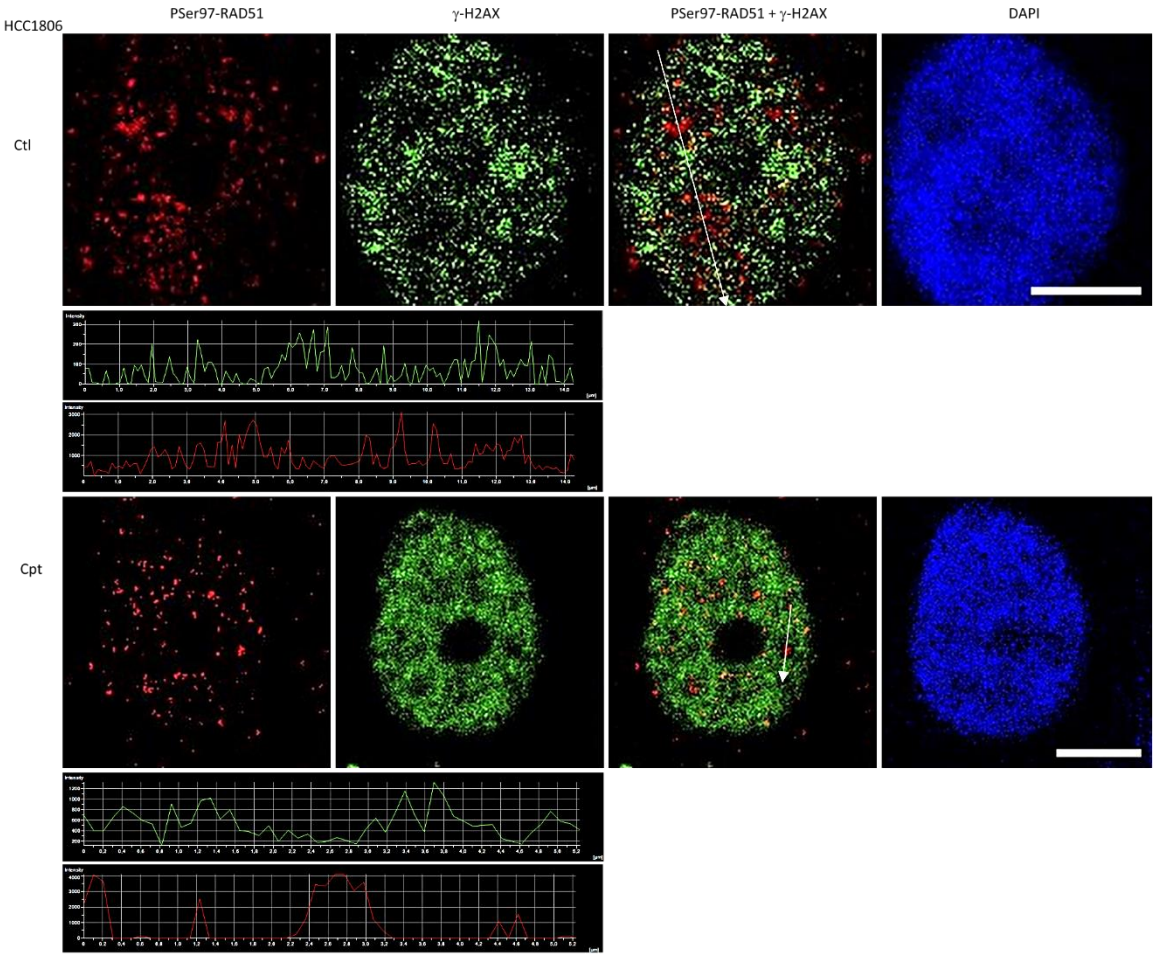
HCC1806
PSer97-RAD51
γ-H2AX
PSer97-RAD51 + γ-H2AX
DAPI
Ctl
Cpt

C

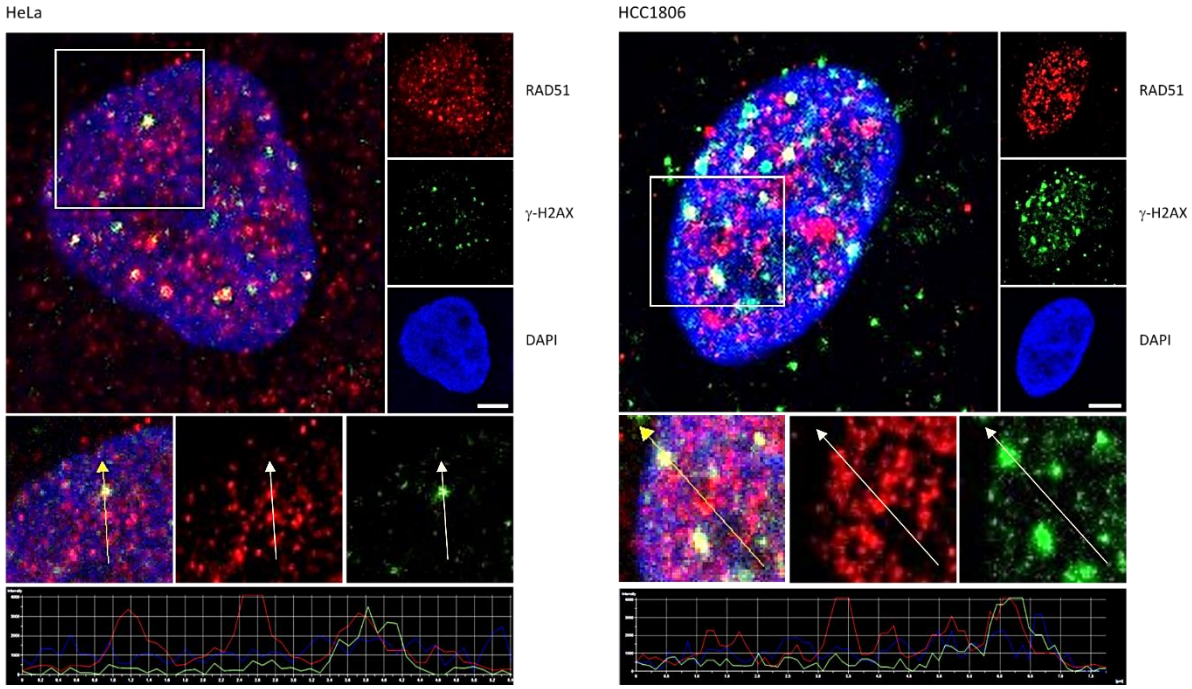
HeLa
HCC1806
RAD51
γ-H2AX
DAPI
RAD51
γ-H2AX
DAPI

Figure 3

A: PSer97-RAD51 is reduced after a camptothecin treatment

Evaluation of the Camptothecin-induced DDR effect on PSer97-RAD51 in HeLa and HCC1806 cells. The DDR was induced by a Camptothecin treatment during 4h at 10 μM final concentration. Western blot was performed using HeLa and HCC1806 whole cell extracts, n=4. We observe an enhancement of the g-H2AX signal after Camptothecin treatment, which induces double strand DNA breaks. PSer97-RAD51/a-tubulin ratio values are: HeLa Ctl: set as 100%, HeLa Cpt= 37.67+/-5.9. t-test p-value (Ctl *vs* Cpt = 0.0014). HCC1806 Ctl: set as 100%, HCC1806 Cpt= 62.6 +/- 32. T-test p-value (Ctl vs Cpt =0.095). PSer97-RAD51/RAD51 ratio values are: HeLa Ctl: set as 100%, HeLa Cpt= 40.5 +/- 13.28. t-test pvalue (Ctl *vs* Cpt = 0.008). HCC1806 Ctl: set as 100%, HCC1806 Cpt= 76.5 +/- 37.4 T-test p-value (Ctl vs Cpt =0.19).

B: PSer97-RAD51 foci are not localized in DNA damaged sites

HeLa and HCC1806 cells in control condition and after Camptothecin treatment (10 μM for 4h) conditions were used for immunofluorescence labelling of PSer97-RAD51. PSer97-RAD51 is in red, g-!2"# is in green and the DNA DAPI staining is in blue. Line scan analysis showing the PSer97-RAD51 and g-!2"# signals intensities along the arrow are below each image. Scale Bar= 10μm.

C: Some RAD51 foci are not DD sites

Confocal images of immunofluorescence labelling of RAD51 and g-H2AX with commercial antibodies in non treated HeLa and HCC1806 cells. RAD51 is in red, g-H2AX is in green and the DNA DAPI staining is in blue. Scale Bar= 10μm. The squares indicate magnified areas used for line scan analysis of the signal intensities along the arrows.

Figure 4

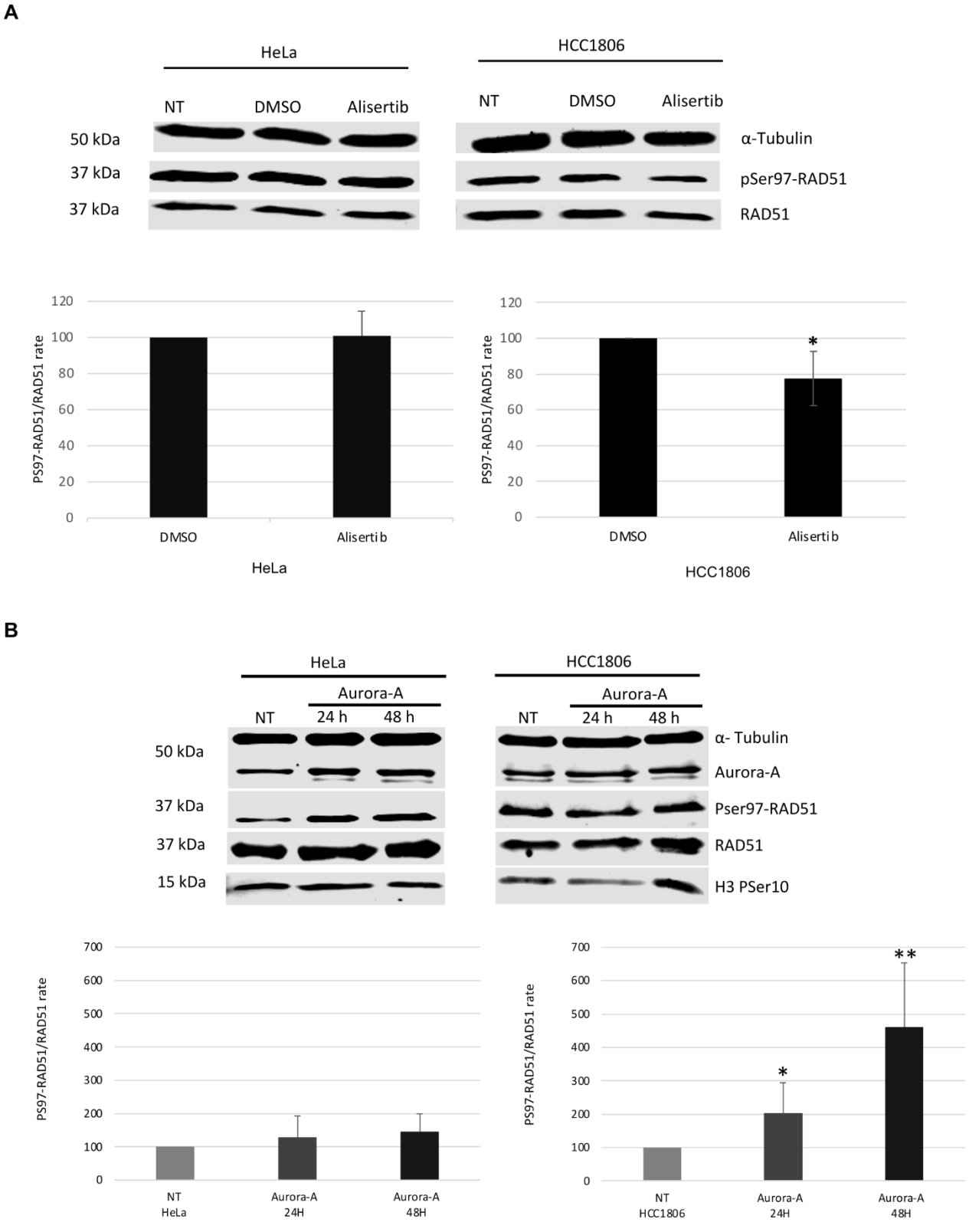
A
HeLa
HCC1806
NT
DMSO
Alisertib
50 kDa
37 kDa
37 kDa
α-Tubulin
pSer97-RAD51
RAD51
PS97-RAD51/RAD51 rate
120
100
80
60
40
20
0
DMSO
Alisertib
HeLa
HCC1806
*
B
HeLa
HCC1806
Aurora-A
NT
24 h
48 h
50 kDa
37 kDa
37 kDa
15 kDa
α- Tubulin
Aurora-A
Pser97-RAD51
RAD51
H3 PSer10
PS97-RAD51/RAD51 rate
700
600
500
400
300
200
100
0
NT
HeLa
Aurora-A
24H
Aurora-A
48H
NT
HCC1806
Aurora-A
24H
Aurora-A
48H
*
**

Figure 4: Aurora A inhibition/ overexpression affect PSer97-RAD51 cellular level
A. Evaluation of the use of Aurora A inhibitor on PSer97-RAD51. The Aurora inhibitor Alisertib was used at a 50nM final concentration for 24 hours in HeLa and HCC1806 cells. Statistical analysis was done for n=5 experiments, using a paired t-test. p-value (a= 0,05: *, a= 0,001: **, a= 0,001: ***). PSer97-RAD51/RAD51 ratio values: HeLa DMSO: set as 100%, HeLa Ali =100.7 +/- 13.7, (p-value DMSO *vs* Ali = 0.9). HCC1806 DMSO: set as 100%, HCC1806 Ali= 77.7 +/- 15.18, (pvalue DMSO *vs* Ali = 0.03).

B. Evaluation of the effect of Aurora A over-expression on PSer97-RAD51. Aurora A coding plasmid was transfected for 24h and 48 h in HeLa and HCC1806 cells. WB were done with whole cell extracts and the PSer97RAD51/RAD51 ratio was calculated. Statistical analysis (using a paired t-test) was done for n=3 experiments, p-value (a= 0,05: *, a= 0,01: **, a= 0,001: ***). PSer97-RAD51/RAD51 ratio values: HeLa NT: set as 100%, HeLa 24h =128.1 +/- 64, (p-value NT *vs* 24h = 0.2), HeLa 48h =145 +/- 54.4, (p-value NT *vs* 48h= 0.09). HCC1806 NT: set as 100%, HCC1806 24h = 203 +/- 90, (p-value NT *vs* 24h = 0.050), HCC1806 48h = 461+/- 191, (p-value NT *vs* 48h = 0.016).

Figure 5

A

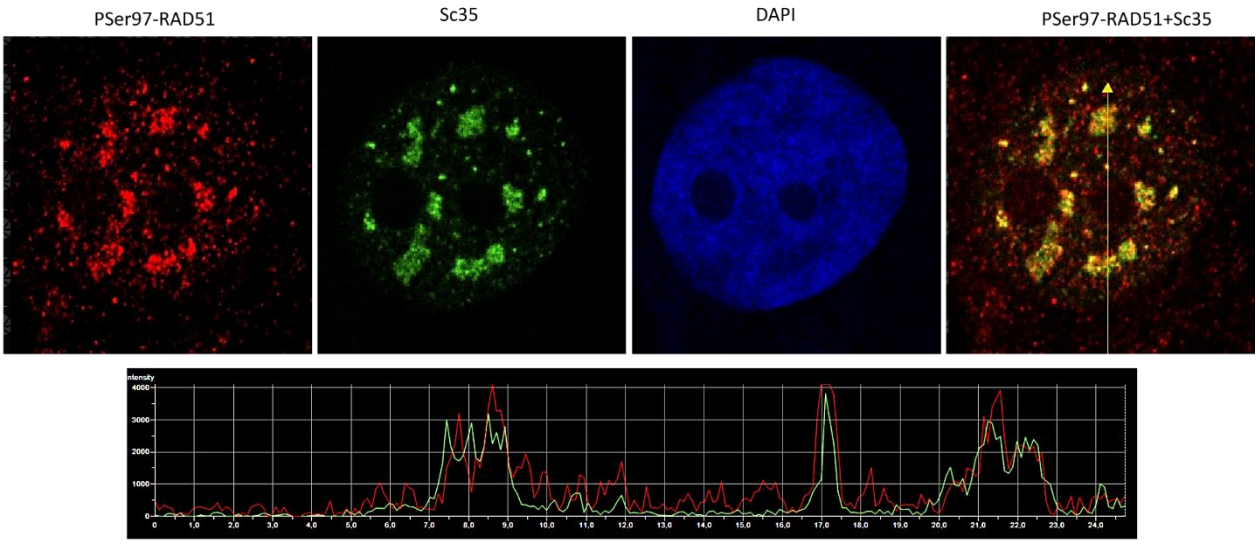
PSer97-RAD51
Sc35
DAPI
PSer97-RAD51+Sc35
Intensity
4000
3000
2000
1000
0
0
1,0
2,0
3,0
4,0
5,0
6,0
7,0
8,0
9,0
10,0
11,0
12,0
13,0
14,0
15,0
16,0
17,0
18,0
19,0
20,0
21,0
22,0
23,0
24,0

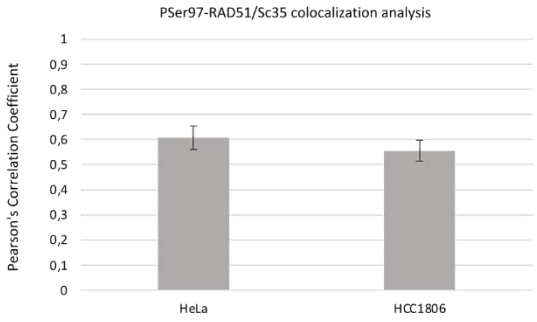
PSer97-RAD51/Sc35 colocalization analysis
Pearson's Correlation Coefficient
1
0,9
0,8
0,7
0,6
0,5
0,4
0,3
0,2
0,1
0
HeLa
HCC1806

B

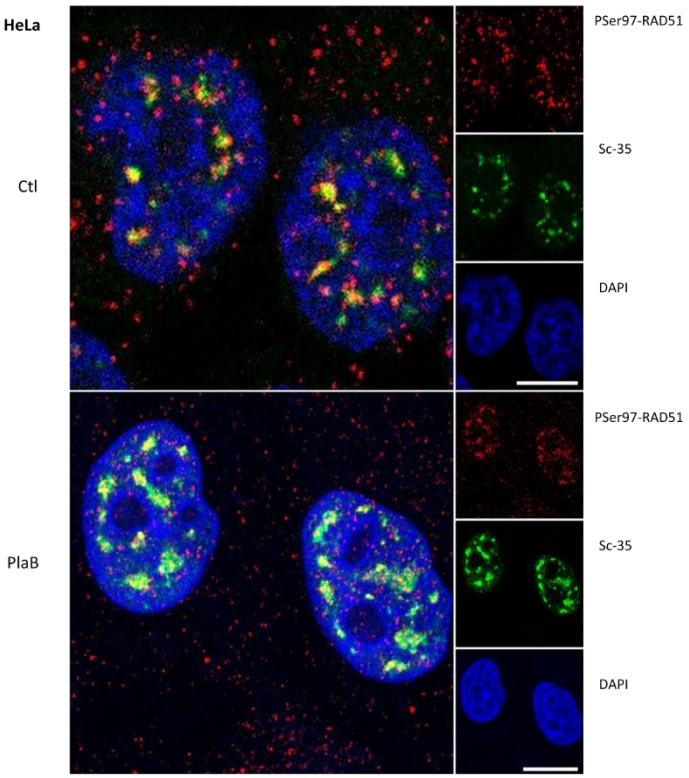
HeLa
Ctl
PlaB
PSer97-RAD51
Sc-35
DAPI
PSer97-RAD51
Sc-35
DAPI

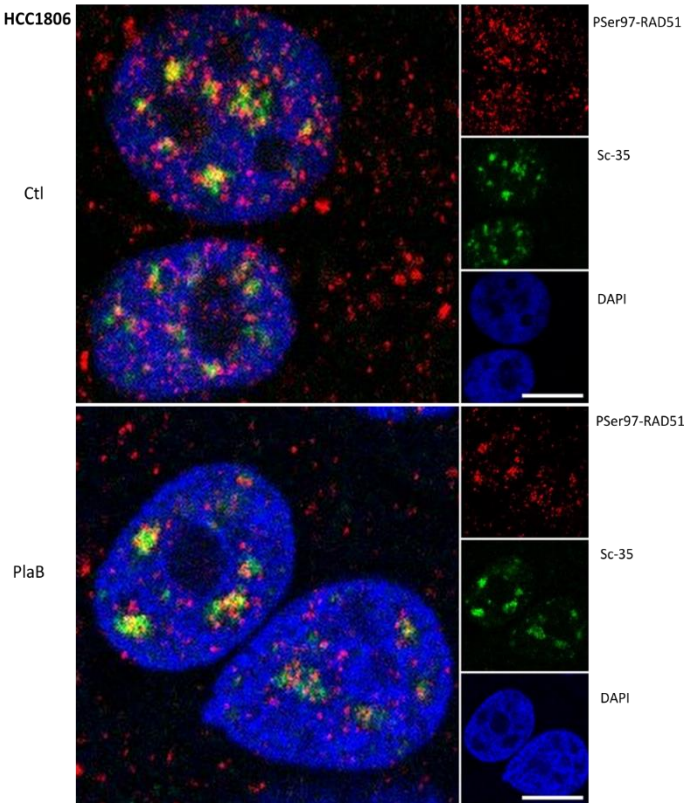
HCC1806
Ctl
PlaB
PSer97-RAD51
Sc-35
DAPI
PSer97-RAD51
Sc-35
DAPI

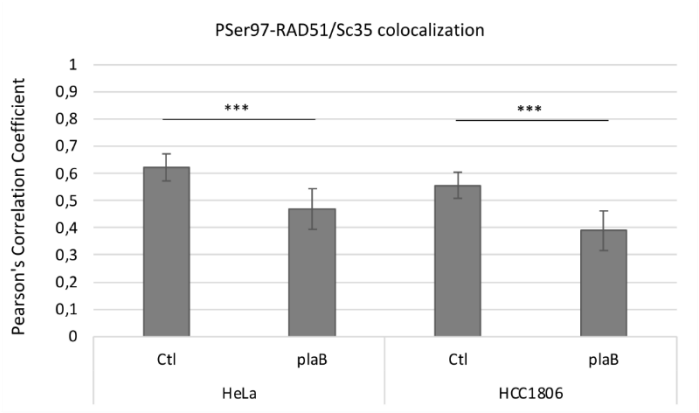
PSer97-RAD51/Sc35 colocalization
Pearson's Correlation Coefficient
1
0,9
0,8
0,7
0,6
0,5
0,4
0,3
0,2
0,1
0
***
***
Ctl
plaB
Ctl
plaB
HeLa
HCC1806

C

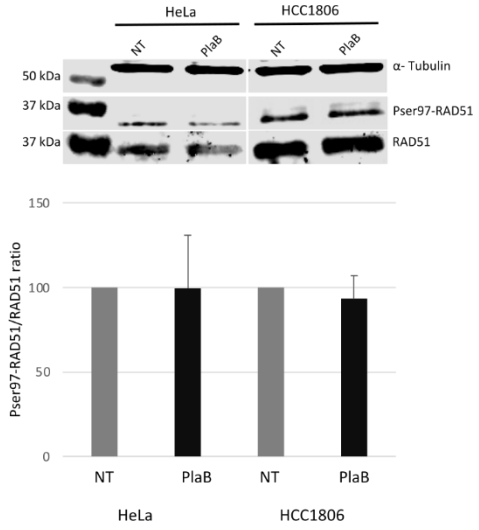
HeLa
HCC1806
NT
PlaB
NT
PlaB
50 kDa
37 kDa
37 kDa
α- Tubulin
Pser97-RAD51
RAD51
150
100
50
0
Pser97-RAD51/RAD51 ratio
NT
PlaB
NT
PlaB
HeLa
HCC1806

D

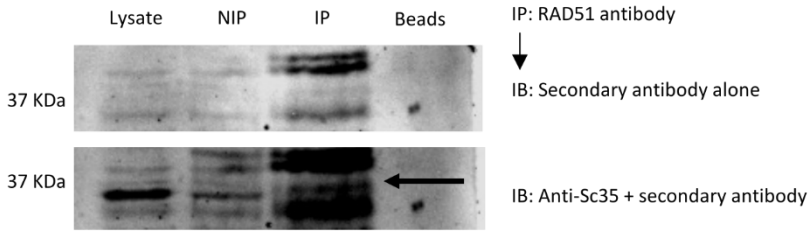
Lysate
NIP
IP
Beads
IP: RAD51 antibody
37 KDa
IB: Secondary antibody alone
37 KDa
IB: Anti-Sc35 + secondary antibody

Figure 5: PSer97-RAD51 nuclear foci are localized within Nuclear Speckles and remain there after pladienolide B treatment

A. Line scan analysis showing the PSer97-RAD51 and Sc35 signal intensities along the arrow, (HeLa cells). PSer97-RAD51/Sc35 colocalization was evaluated by a Pearson's Correlation Coefficient (PCC) analysis using confocal images and JACoP/Fiji. For HeLa: PCC= 0,608 +/- 0,05, n= 30 and for HCC1806, PCC= 0,555 +/- 0,04, n=35 cells. PCC: Pearson's Correlation Coefficient. Results are mean +/- sd (sd: standard deviation)

B. Immunofluorescence staining of PSer97-RAD51 in HeLa and HCC 1806 cells. PSer97-RAD51 is in red, the nuclear speckles component Sc35 is in green and the DNA DAPI staining is in blue. Confocal acquisitions. Scale Bar= 10μm. PlaB effect on PSer97-RAD51/Sc35 colocalization was evaluated by a Pearson's Colocalization Coefficient (PCC) analysis using confocal images and JACoP/Fiji. For HeLa ctl: PCC= 0,608 +/- 0,05, n= 30. For HeLa plaB: PCC=0.468 +/- 0.06, n=32. For HCC1806 ctl, PCC= 0,555 +/- 0,04, n=35. For HCC1806 plaB: PCC= 0.388 +/- 0.07, n=28. One tailed t-test was used to evaluate plaB effect on PCC values. For HeLa p-value= 1.17E-6 and for HCC1806 p-value= 5.04E-7. Results are mean +/- sd.

C. PSer97-RAD51 level is not affected by plaB treatment. HeLa and HCC1806 cells were treated by pladienolide B at 5μM, 4h. Whole cell extracts were used to evaluate the effect on PSer97-RAD51/RAD51 ratio by Western-Blot analysis. PSer97-RAD51/RAD51 values are: HeLa ctl : set as 100%, HeLa plaB= 99,4 +/- 31.7, HCC1806 Ctl: set as 100%, HCC1806 plaB= 93.3 +/- 13.5. Results are mean +/- sd.

D. Sc35 is co-immunoprecipitated with RAD51 from HeLa nuclear extracts. NIP: Non Immuno Precipitated, IP: Immuno Precipitated. The black arrow indicates the Sc35 signal.

Figure 6

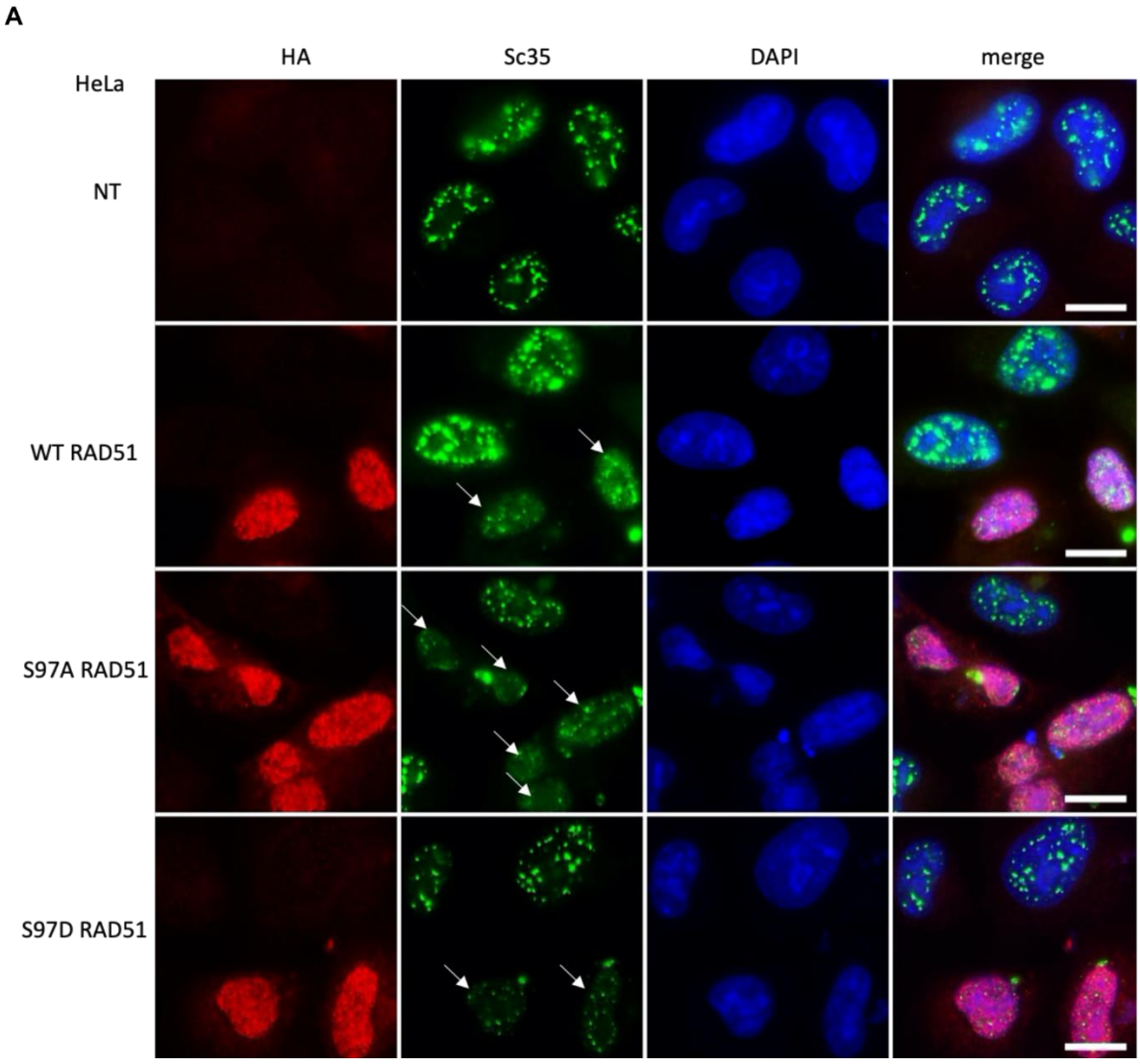

B

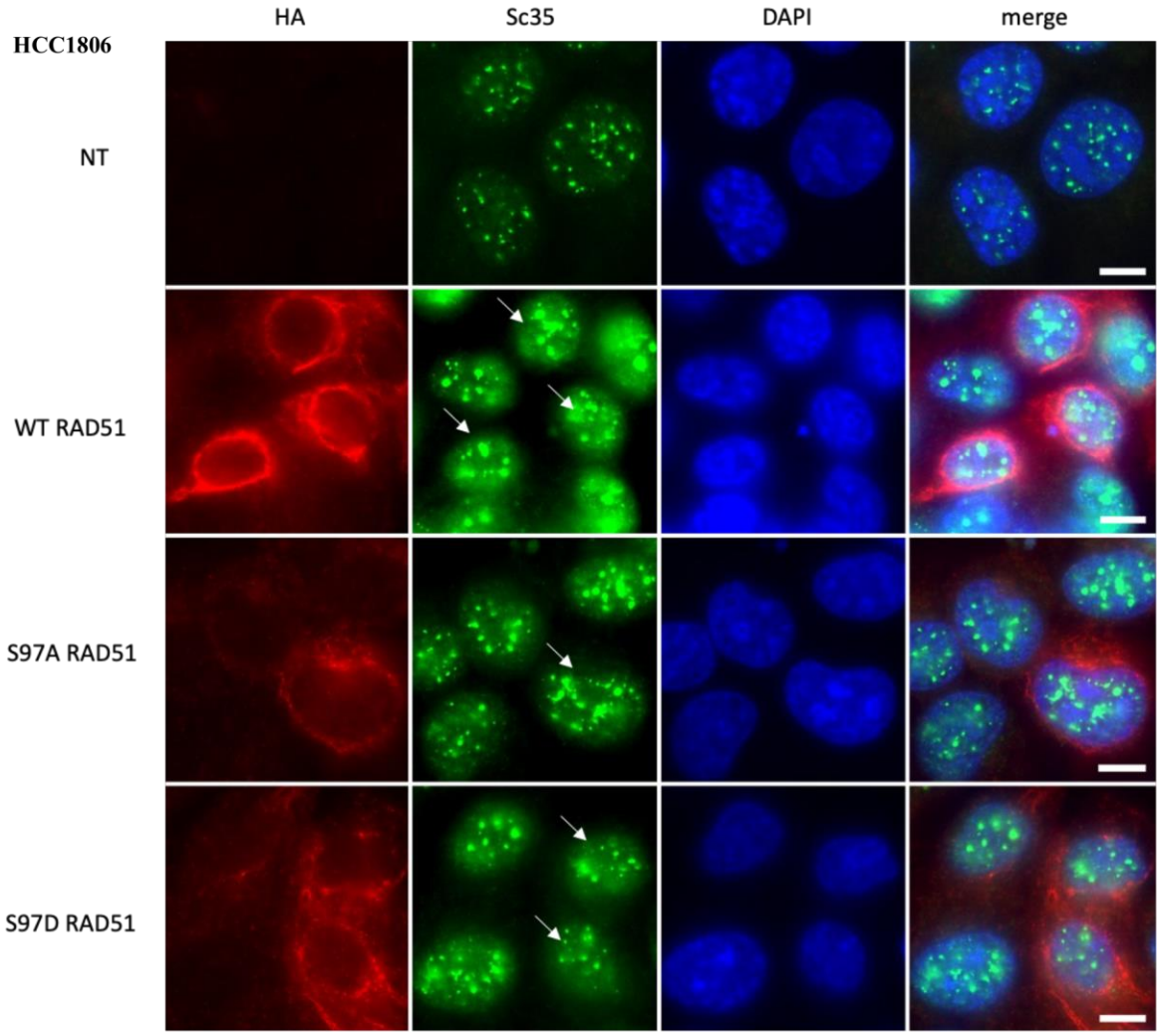

C

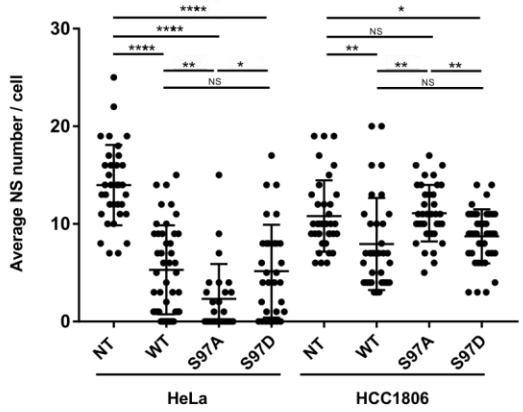

T-test p-values	HeLa			HCC1806		
	WT RAD51	S97A RAD51	S97D RAD51	WT RAD51	S97A RAD51	S97D RAD51
P-value *vs* NT	3.8 E-13	1.84 E-16	6.79 E-6	0.0062	0.696	0.030
P-value *vs* WT		0.0065	0.856		0.0013	0.415
P-value *vs* S97A			0.0164			0.007

Figure 6: RAD51 overexpression affects Nuclear Speckles number.
A, B: HA tagged WT, S97A and S97D RAD51 proteins were expressed during 24h in HeLa (panel A) and HCC1806 (panel B) cells. Exogenous RAD51, in red, was labelled with the anti-HA antibody. NT: Non-Treated. The arrows indicate the RAD51 overexpressing cells. The nuclear speckles component Sc35 is in green and the DNA DAPI staining is in blue. Epifluorescence microscope acquisitions. Scale bar= 10 μm. **C**: Average Nuclear Speckles number per cell was quantified using FiJi analysis tool with confocal images. (n=32 to 51 cells for Non-Treated (NT)and 24h transiently transfected HeLa and HCC1806 cells. Two tailed t-tests were performed to evaluate the statistical significance of the observed differences after WT, S97A and S97D RAD51 overexpression on average NS number/cell. Table of the obtained p-values.

Figure 7

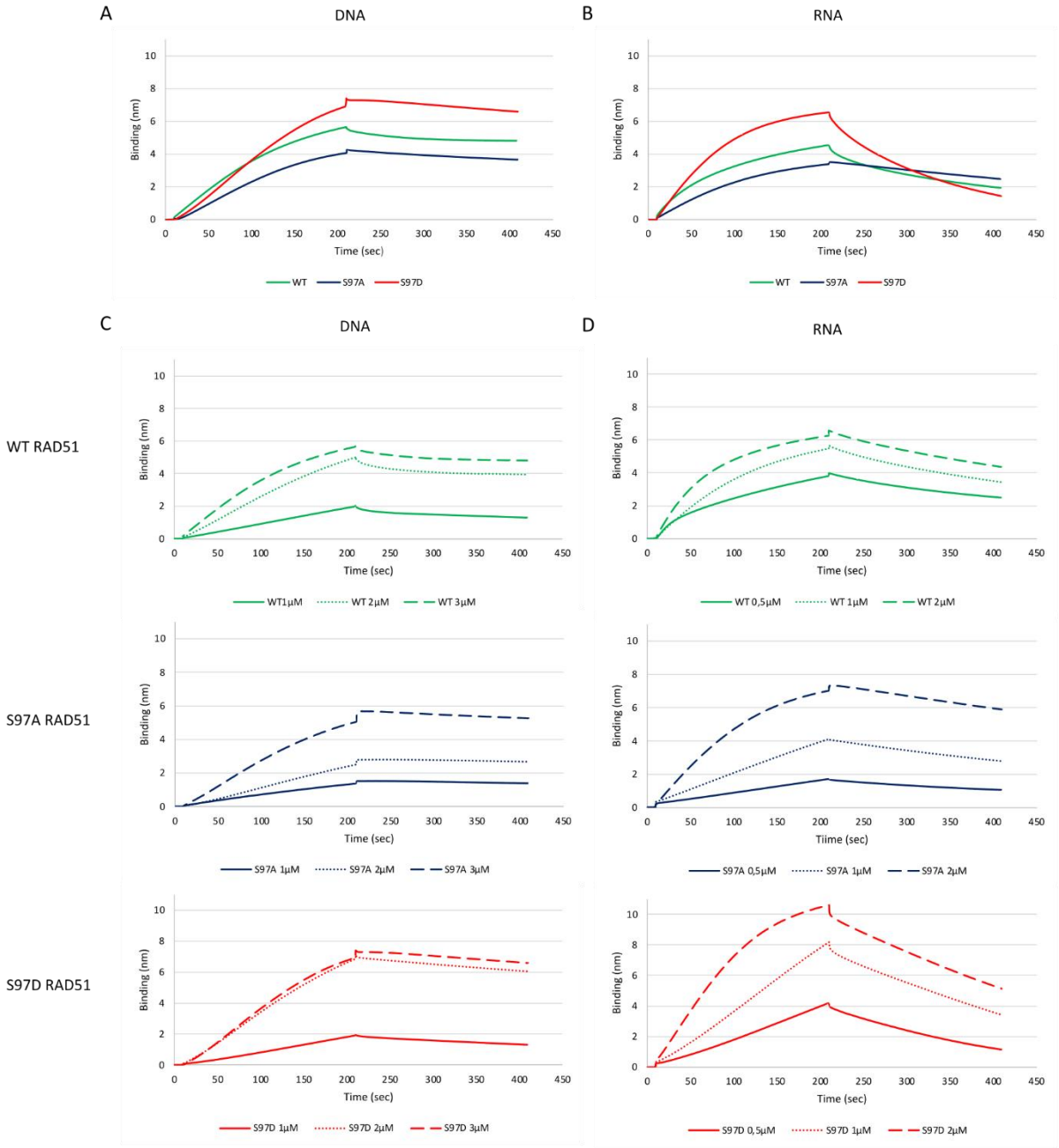

E

Estimated KD values (∝M)	DNA	RNA
WT RAD51	3.84 +/- 0.12	0.53 +/- 0.008
S97A RAD51	0.34 +/- 0.2	0.32 +/- 0.12
S97D RAD51	3.63 +/- 0.97	1.73 +/- 0.17

Figure 7: RAD51 phosphorylation mimetic on Ser97 affects its binding to RNA
A, B: 3 μM of WT**,** S97D and S97A RAD51 recombinant proteins were used to evaluate the effect of RAD51 phosphorylation on its binding to 33 nt sized single strand DNA or RNA, in 2 mM ATP final concentration, by using the Blitz technology.
C,D: Different concentrations, from 0.5 to 3 μM*,* of WT, S97A and S97D RAD51 recombinant proteins were used to characterize their DNA and RNA binding parameters.
E: Resulting KD values estimations of WT, S97A and S97D RAD51, binding affinity to DNA and RNA determined from n=4 experiments. Data are means +/- sd.

Supplemental Figures
Aurora A mediated new phosphorylation of RAD51 is observed in Nuclear Speckles

Mohamad Alaouid, Parfait Kenfack Ymbe, Vanessa Philippot-Ménil, Gwennina Cueff, Alexandre Demeyer, Damien Marquis, Nizar Ayadi, Fabrice Fleury, Houda Benhelli-Mokrani*

From Nantes Université, US2B, DNA repair team, UMR 6286 CNRS, 44000 Nantes, France

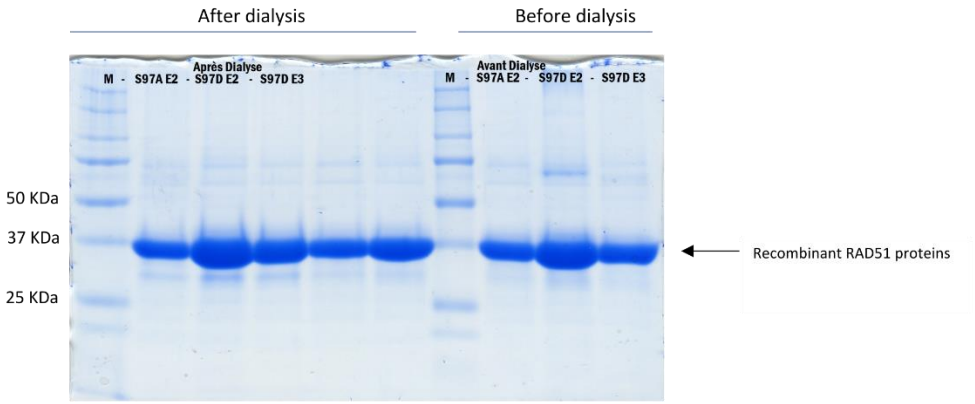

Supplemental Figure 1: Coomassie Gels of WT, S97A and S97D RAD51 recombinant proteins
Coomassie blue stained SDS-PAGE showing the recombinant mutant RAD51 proteins.
S97A E2 means S97A-RAD51 Elution N°2. S97D E2 means S97D-RAD51 Elution N°2. S97D E3 means S97D-RAD51 Elution N°3.

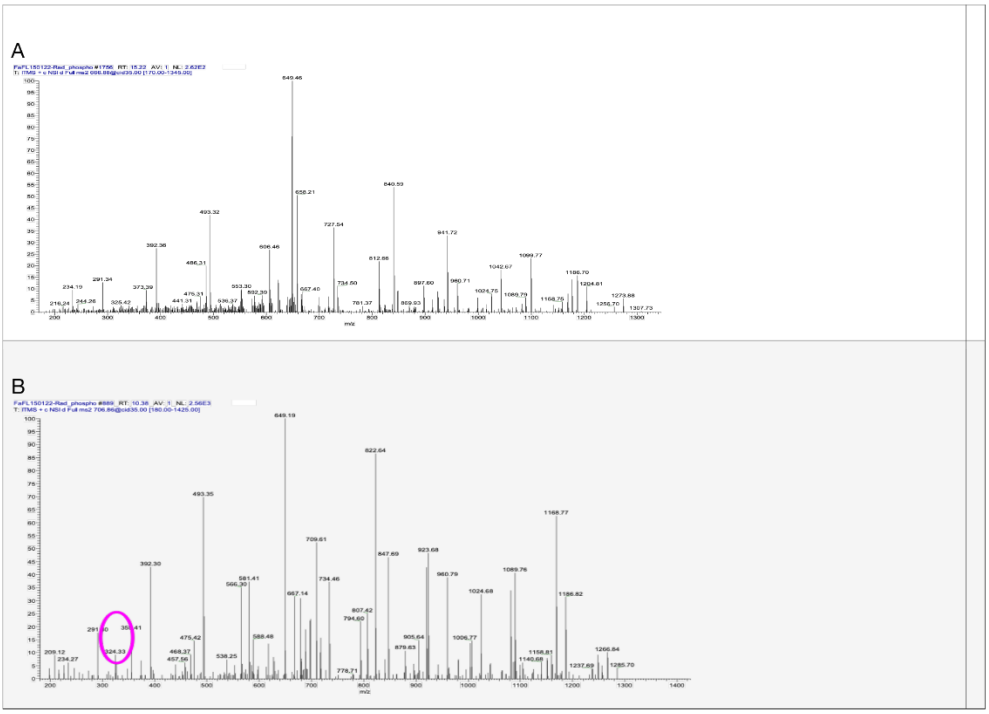

Supplemental figure 2: Mass spectra of the control and Aurora A-phosphorylated RAD51
A: mass spectra of the non phosphorylated RAD51 recombinant protein. B: mass spectra of the Aurora A phosphorylated RAD51 recombinant protein. The purple circle identified the phosphorylated residue.

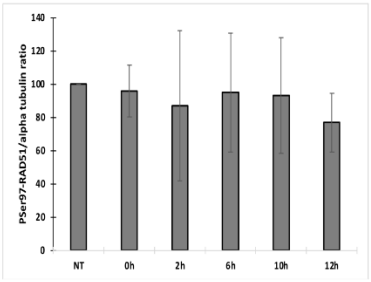

Supplemental Figure 3: PSer97RAD51/tubulin ratio throughout cell cycle progression
The PSer97/tubulin ratio was calculated during the cell cycle progression, from n=3 experiments.

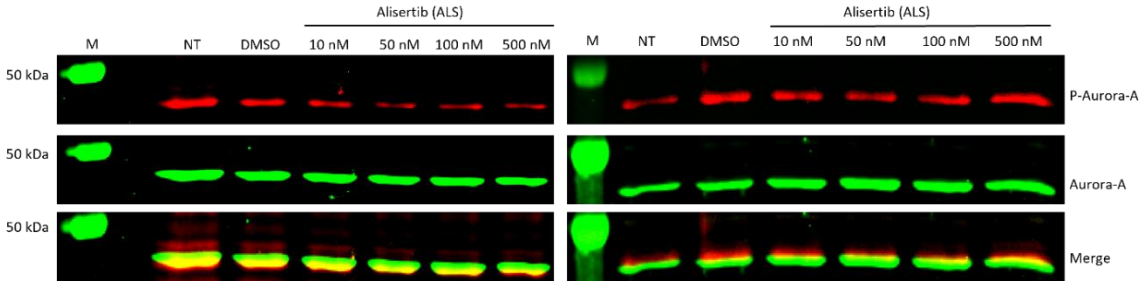

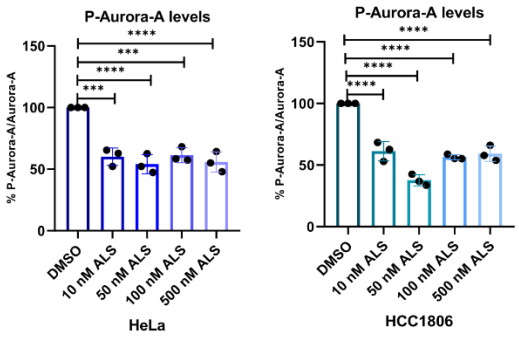

Supplemental Figure 4: Alisertib efficacy on phosphoThr288Aurora A
Different Alisertib concentrations were used in HeLa and HCC1806 cell lines, for 24 h treatment. Whole cell extracts were used to perform WB and evaluate the effect on the pThr288, auto-phosphorylated form of Aurora A kinase. Statistical analysis using paired t test were performed, n=3. p value (α= 0,05: *, α= 0,001: **, α= 0,001: ***).

Chapter 2- preliminary results

1. Modifying Ser97 through computational phosphorylation or mutation using Pymol can change how it interacts with other residues.

In an attempt to understand the differences in outcomes of our Blitz, D-Loop, and polymerization experiments, we performed an *in silico* comparison study to compare the different versions of S97 (S97A, S97D, and PSer97) in both the presynaptic (PDB: 5H1B) and postsynaptic (PDB: 5H1C) structures of RAD51. For a reminder, RAD51's presynaptic filament encases and slides along ssDNA, forming the nucleoprotein filament (NPF). The postsynaptic filament, on the other hand, forms by invading the NPF into homologous dsDNA. This comparison allowed us to investigate how modifying Ser97 could impact its interaction with neighboring residues [182]. Additionally, we investigated whether phosphorylation of Ser97 produces similar interaction profile as a phosphorylation mimic mutation (S97D).

In the presynaptic structure (5H1B), the unmodified Ser97 interacts *via* hydrogen bonds with residues Histidine 93 (H93) and Glutamine 94 (Q94). When Ser97 is phosphorylated (PSer97), the interactions are altered. In the monomers N-1 and N+1, PSer97 only forms hydrogen bonds with H93, while in the monomer N, PSer97 Showed an interaction with Glutamic acid 98 (E98), along with H93 and Q94 (Figure 31 A and B). The changing of Ser97 to Ala. or Asp. showed a different pattern of interactions, where A97 and D97 forming hydrogen bonds with H93 only in the monomer N+1. In the other monomers, A97 and D97 did not form any hydrogen bonds (Figure 31 C and D).

In the postsynaptic structure (5H1C), unmodified Ser97 formed hydrogen bonds with H93, Q94, and E98 in all monomers. When Ser97 is phosphorylated (PSer97), the interactions varied depending on the monomer. In the monomer N-1, PSer97 only forms a hydrogen bond with H93, while in the monomers N and N+1, PSer97 interacts with H93, Q94, and E98 (Figure 32 A and B). The S97A and S97D mutants again show a different pattern, with A97 or D97 forming a hydrogen bond with H93 only in the monomers N-1 (Figure 32 C and D).

These results suggest that the modification of Ser97 can significantly alter the interactions of RAD51's Ser97 with other residues, potentially affecting its function in DNA repair. The differential interactions observed in the presynaptic and postsynaptic structures suggest that the phosphorylation state of Ser97 may play a role in the transition between these states. Further studies are needed to fully elucidate the functional implications of these findings.

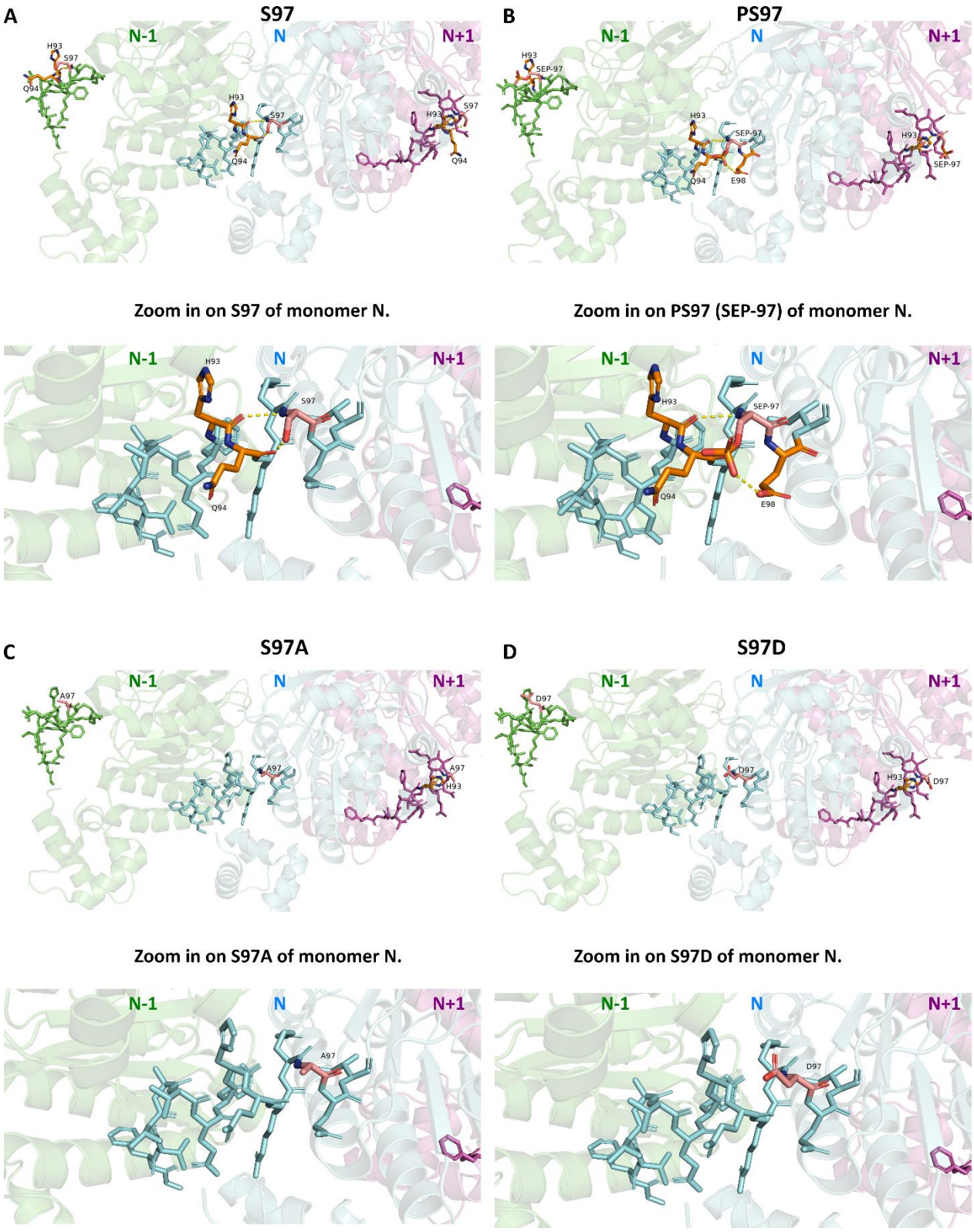

Figure 31 *In silico* modeling of S97 in the presynaptic structure.

The modulation of S97 within the RAD51 prestsynaptic complex: A) unmodified serine 97 (S97). B) phosphorylated serine 97 (SEP97). C) mutate serine 97 to alanine 97. D) mutate serine 97 to aspartic acid 97. In the cartoon, the upper panels show three RAD51 monomers from left to right as N-1, N, and N+1 in green, cyan, and magenta, respectively. The sticks represent the residues of the linker domain and are colored to match each monomer color. The residue S97, or its modified versions, are depicted in pink and the residues that interact with them are shown in orange. The hydrogen bonds are represented by dashed lines. The down panels are a zoomed-in view of monomer N. Histidine 93 (H93), Glutamine 94 (Q94), and Glutamic acid 98

(E98). The presynaptic structure of RAD51 was obtained from (PDB: 5H1B) and was modified using open-source Pymol.

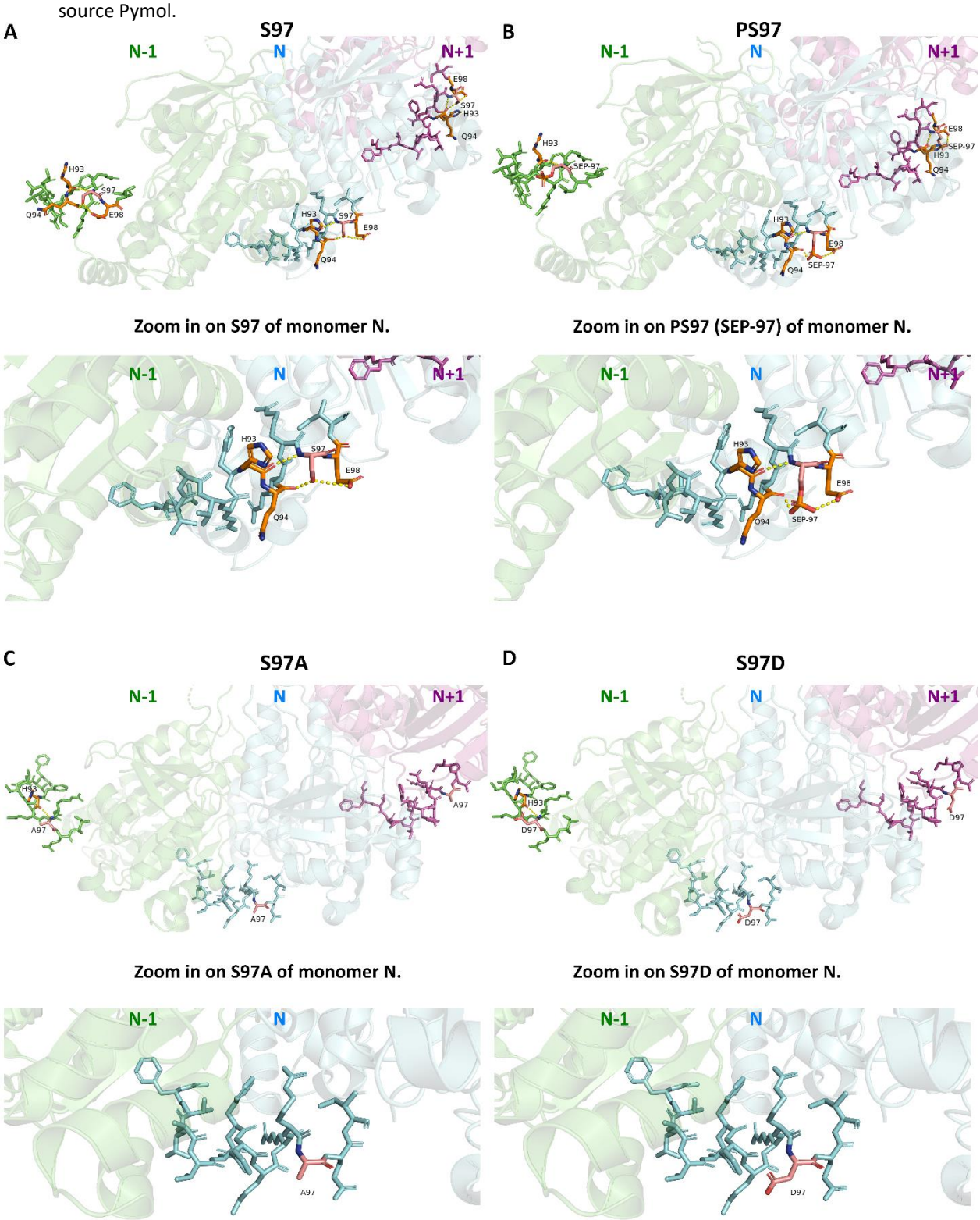

Figure 32 *In silico* modeling of S97 in the postsynaptic structure.

The modulation of S97 within the RAD51 postsynaptic complex: A) unmodified serine 97 (S97). B) phosphorylated serine 97 (SEP97). C) mutate serine 97 to alanine 97. D) mutate serine 97 to aspartic acid 97. In the cartoon, the upper panels show three RAD51 monomers from left to right as N-1, N, and N+1 in green, cyan, and magenta, respectively. The sticks represent the residues of the linker domain and are colored to match each monomer color. The residue S97, or its modified versions, are depicted in pink and the residues

that interact with them are shown in orange. The hydrogen bonds are represented by dashed lines. The down panels are a zoomed-in view of monomer N. Histidine 93 (H93), Glutamine 94 (Q94), and Glutamic acid 98 (E98). The presynaptic structure of RAD51 was obtained from (PDB: 5H1C) and was modified using open-source Pymol.

2. *In silico* Kinase prediction

Because the cell lines we used did not respond in the same way to AURKA inhibition we decided to investigate kinase redundancy - the concept that multiple kinases can perform similar functions. To explore this hypothesis, we conducted an *in silico* study to identify other possible kinases that could phosphorylate RAD51 at its Ser97. First, we performed a prediction of Kinase-specific phosphorylation site analysis using GPS 5 and the Kinase Predictor V2 tool of Kinexus PhosphoNET. The highest-scoring kinases, which are also known to be implicated in DDR, were then docked with RAD51 as described in the materials and methods. Furthermore, as detailed in the upcoming results, the kinases whose active site was shown to interact with Ser97 of RAD51 were later tested *in vitro* or *in cellulo*.

2.a- Prediction of potential kinases responsible for phosphorylating RAD51 at Ser97

As mentioned previously, the web service Group-based Prediction System (GPS) is used to predict the potential kinases that could phosphorylate Ser97. GPS uses three thresholds, high, medium, and low, to predict phosphorylation sites and responsible kinases. The threshold value is used to determine the significance or reliability of a prediction. A higher threshold value determines the confidence level in predicting phosphorylation events [343]. We perform the prediction at a high threshold to achieve the best level of confidence in kinase predicting.

The highest-scoring kinases that were predicted to phosphorylate Ser97 were CK1 and VRK2. They had the same score of 48.439. ROCK1 (40.325), MAP3K2 (25.451), and PLK2 (23.064) were also predicted to phosphorylate Ser97, while regarding the Aurora kinases family, only AURKB was predicted with a low score of 0.077. Interestingly, the updated version of GPS (GPS 6) released this year [379] predicted only one kinase, CK1, that could phosphorylate Ser97 with a score of 0.1366. It also predicted only five phosphorylation sites on RAD51, including Ser97, Thr225, Ser14, Ser233, and Thr309.

Moreover, 50 kinases that may potentially phosphorylate Ser97 were found using the Kinase Predictor V2 program from Kinexus PhosphoNET. As previously mentioned in the materials and methods, the maximum score that this tool can provide is 1000. The data from this prediction showed that PKG1 had the highest score of 359, followed by PKG2 with a score of 341; while

ROCK1, which had the highest score in GPS 5 prediction, was ranked as kinase 26 with a score of 310. VRK1, but not VRK2, was predicted with a score of 301. AURKC and AURKA received 298 and 293 scores, respectively, while AURKB was not anticipated. Furthermore, neither CK1 nor PLK2 or 1 were predicted by the Kinase Predictor V2 tool (Table 4).

Kinase name	Uniprot. ID	Score	Kinase prediction tools
CK1	P48729	48.439	**GPS 5**
VRK2	Q86Y07	48.439	
ROCK1	Q13464	40.325	
MAP3K2	Q9Y2U5	25.451	
PLK2	Q9NYY3	23.064	
AURKB (STK12)	Q96GD4	0.077	
PKG1 (PRKG1)	Q13976	359	**Kinase Predictor V2**
PKG2 (PRKG2)	Q13237	341	
MSK1 (RPS6KA5)	O75582	340	
ROCK1	Q13464	310	
ROCK2	O75116	307	
VRK1	Q99986	301	
AURC (STK13)	Q9UQB9	298	
AURA (STK15)	O14965	293	

Table 4 The potential kinases predicted to phosphorylate Ser97

This table shows some kinases predicted to phosphorylate RAD51 on Ser97 using GPS 5 and kinase predictor V2. Kinases were selected based on the highest score or relevance to DDR.

We chose VRK1, AURKs, and PLK1 for docking with RAD51 due to their strong prediction scores and/or link to DNA damage response, as discussed more below.

2.b- Serines 14 and 97 of the docked RAD51 are located within or very close of the interaction interface with PLK1 and AURKA, respectively.

To validate our docking methodology (Materials and Methods), we docked RAD51 with PLK1 and AURKA, which have been demonstrated *in vitro* to phosphorylate RAD51 at Ser14 and Ser97, respectively.

The PDB's 3D structures of RAD51 lack its first 15 amino acids. Our investigation aims to determine if Ser14 interacts with PLK1 or is part of their interface. Thus, we used AlphaFold's predicted RAD51 structure to dock it with PLK1. Additionally, we docked RAD51 with AURKA to search if Ser97's will be located in its catalytic site.

The kinase domain of PLK1 is located in its NTD (residues 13−345, defined by limited proteolysis) [380]. During G2, AURKA activates PLK1 with the help of the Bora protein. Bora facilitates the recognition of PLK1 by AURKA, which then phosphorylates PLK1 at Thr210 in its activation loop.

This pathway plays a crucial role in regulating the timing of mitotic entry and is necessary for re-entry into mitosis after a DNA damage response arrest [91,381]. The analysis of the docked PLK1-RAD51 complex revealed a protein-protein interface that consisted of 27 RAD51 residues and 31 PLK1 residues. Interestingly, Ser14 of RAD51 and Thr210 of PLK1 were located at the interaction interface (Figure 33A, C, E).

Moreover, PLK1 and RAD51 interact through 15 hydrogen bonds and 3 salt bridges. Residues around Ser14, including Glu16 and Glu18 of RAD51, formed hydrogen bonds and salt bridges with Lys264 and Lys257 of PLK1, respectively (Figure 33C, G). Thus our docking procedure was successful because it agrees with the *in cellulo* verified role of PLK1 in S14 RAD51 phosphorylation (As discussed earlier in section 3.2.1 b).

Furthermore, AURKA's activity is controlled by the autophosphorylation of Thr288, located in a flexible part of its kinase domain called the activation segment (residues 274–299) [382–384]. Based on our molecular docking data, there were 28 residues observed across the interface of RAD51. Although Ser97 was not directly within this interface, it was in close proximity to Thr90, Glu91, Phe92, His93, and Arg96, which were all located inside the interface. A total of 23 residues were observed with the AURKA interface, including three with the activation segment of AURKA (Val279, His280, and Arg286) (Figure 33B, D, F).

Our data have also revealed that AURKA physically interacts with RAD51 through 11 hydrogen bonds and 4 salt bridges. Some of them were formed between residues near Ser97, such as Arg96, which interacted by a hydrogen bond with Gln127 of AURKA (Figure 33D, H).

Collectively, these findings validate our docking methodology and indicate its effectiveness in docking RAD51 with the predicted Kinases that may also phosphorylate its Ser97.

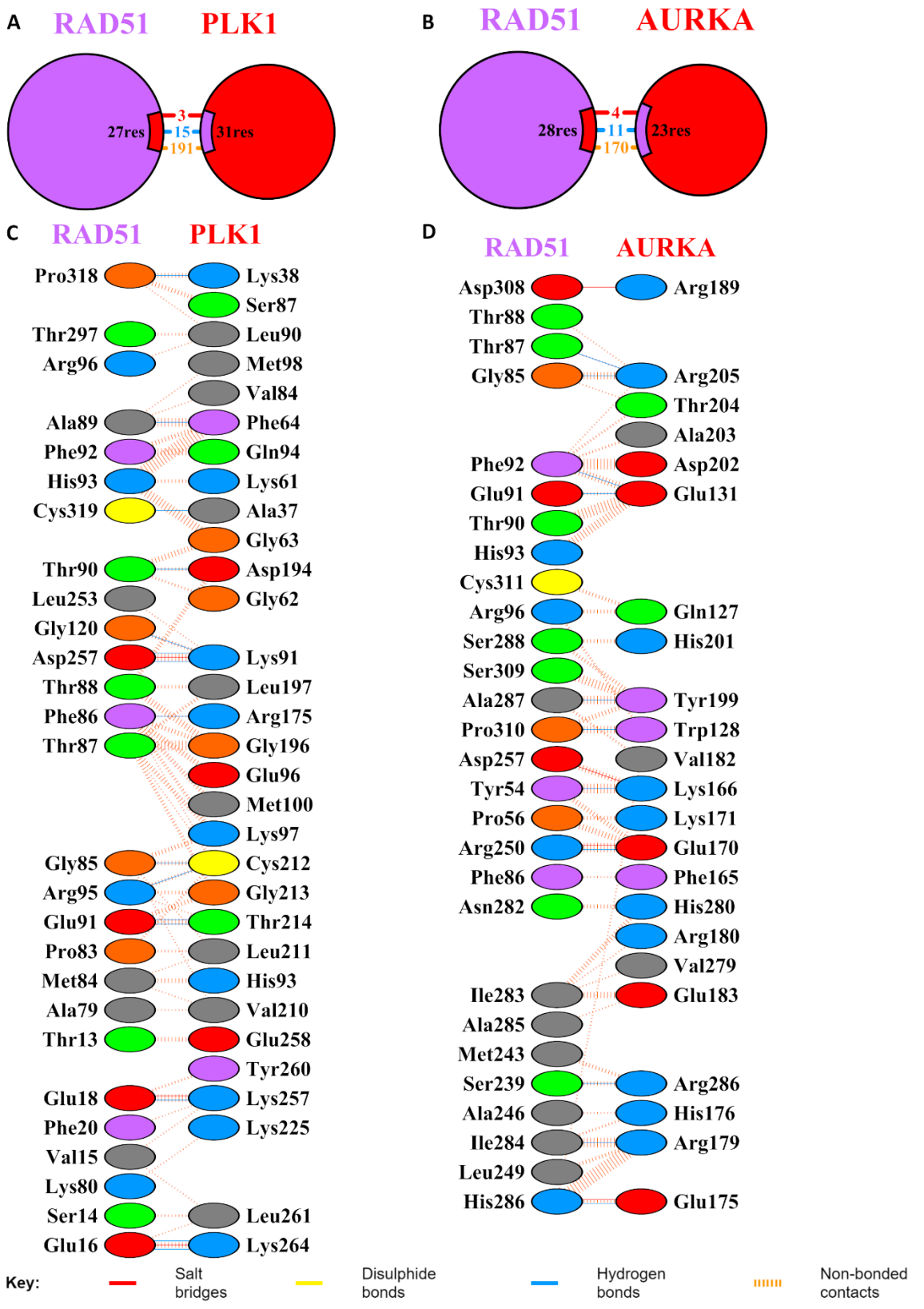

The number of H-bond lines between any two residues indicates the number of potential hydrogen bonds between them. For non-bonded contacts, which can be plentiful, the width of the striped line is proportional to the number of atomic contacts.

Residue colours: Positive (H,K,R); negative (D,E); S,T,N,Q = neutral; A,V,L,I,M = aliphatic; F,Y,W = aromatic; P,G = Pro&Gly; C = cysteine.

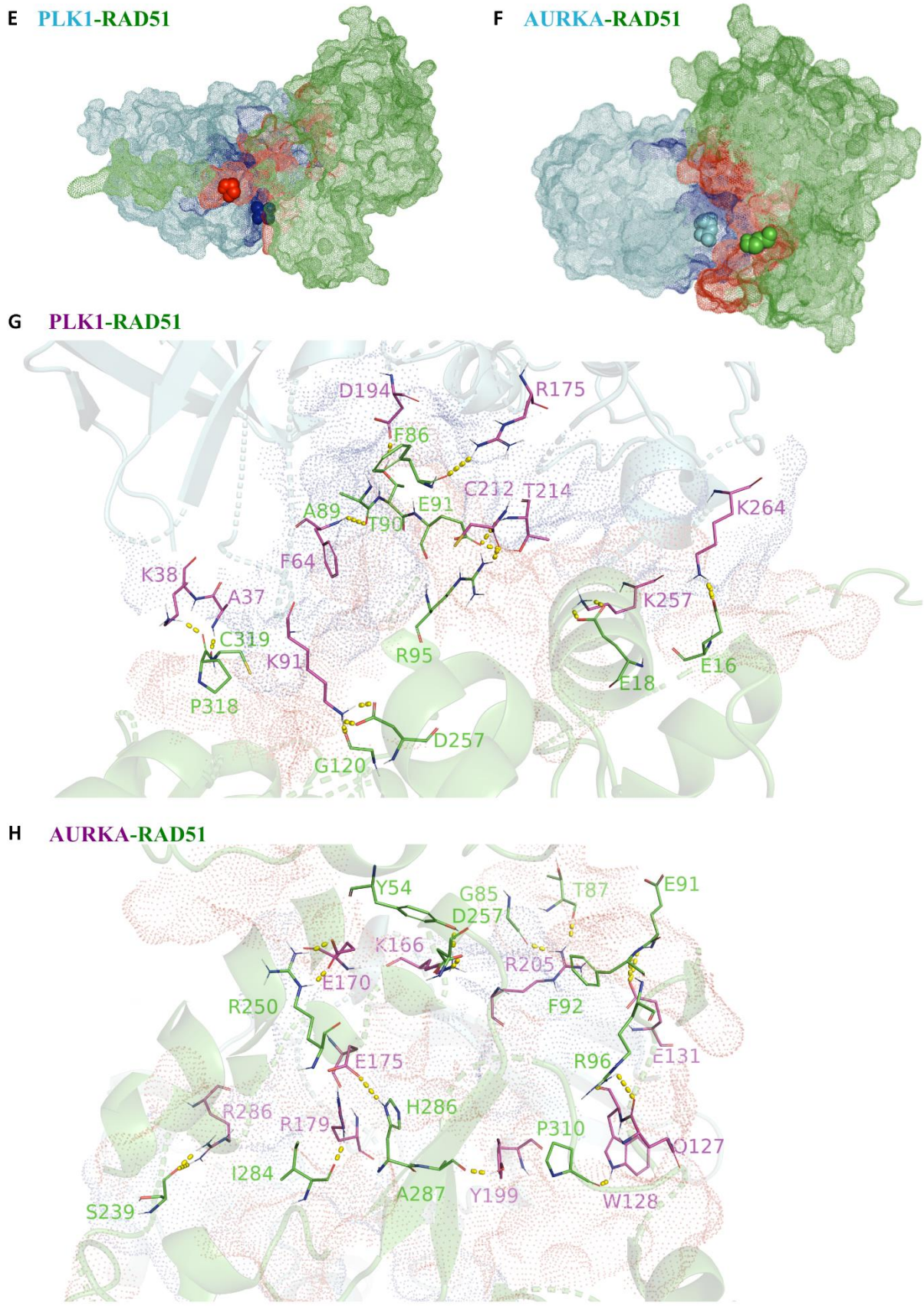

Figure 33 Molecular docking of PLK1 and AURKA with RAD51.

A, B) Schematic diagram that shows how proteins interact with each other. The lines connecting the proteins are colored differently to represent the various types of interactions. Red lines represent salt bridges, yellow lines represent Disulphide bonds, blue lines represent hydrogen bonds, and orange lines represent non-

bonded contacts. Circles are proportional to the surface area of the corresponding protein, and the black wedges represent the extent of the interface region on each protein. C,D) Residue interactions across interface. The color codes are as described in (A,B). E,F) Models of probable interactions between kinases (cyan surface) and RAD51 (green surface). The interface residues are represented by blue dot surface (Kinases) and by red dot surface (RAD51). The red sphere in (E) represents Ser14 of RAD51 inside the protein-protein interface, while the bleu sphere represents the active residue of PLK1 (T210V) also it located inside interaction interface. In addition, the green sphere in (F) represents Ser97 of RAD51 close to the protein-protein interface, while the cyan sphere represents the active residue of AURKA (Thr288). It is also located very close to the interaction interface. G,H) The polar interactions (sticks) between kinases residues (magenta) and RAD51 residues (green) are highlighted. The green labels represent RAD51 residues, while the magenta labels represent Kinase residues.

2.c- Ser97 of RAD51 is located within the interface of docked RAD51 with VRK1 and AURKB

VRK1:

VRK1 (Vaccinia-related kinase 1) is a nuclear protein composed of 396 amino acids that mostly binds to chromatin. The kinase domain, made up of residues 1-300, is located at the N-terminal (residues 1-332) region [385]. The docking data revealed that 42 VRK1 residues, the majority of which belonged to the catalytic site, interacted with 42 RAD51 residues *via* 4 salt bridges, 31 hydrogen bonds, and 325 non-bonded interactions (Figure 34).

Ser97 made non-bonded contacts within the interface with Ala6, Ala7, and Gln8 of VRK1. Additionally, Arg96 formed a salt bridge with Glu60 of VRK1. Furthermore, residues surrounding Ser97, including Glu98, interacted with VRK1's Gln8, Ala9, and Gly10 through hydrogen bonds. Besides, Ile99, Ile100, and Gln101 bonded with Ala7, Gly10, and Ala6 of VRK1, respectively (Figure 34 & Figure 35A). Therefore, VRK1 may be a potential candidate for the phosphorylation of RAD51 Ser97.

AURKB:

Currently, only one 3D structure of human AURKB is available in the PDB database. This structure displays AURKB's interaction with the Inner Centromere Protein (INCENP), which is another component of the Chromosomal Passenger Complex (CPC) where AURKB plays a central role. Unfortunately, due to this interaction, the activation segment of AURKB, which includes the phosphorylation site Thr232, is not visible in structure [386]. Nevertheless, it is worth noting that the kinase domain of AURKB is made up of residues (76-251) [387].

We revealed that AURKB and RAD51 interacted through 2 salt bridges, 23 hydrogen bonds, and 349 non-bonded contacts formed by 43 RAD51 residues and 42 AURKB residues, primarily in the catalytic site. One of the hydrogen bonds was observed between Ser97 and Gln121. Additionally,

Arg96 had non-bonded contacts with Met249, and Thr90 formed 4 hydrogen bonds with Phe219, Lys106, and Asn205 of AURKB (Figure 34 & Figure 35B).

We examined the interaction between the Alphafold predicted structure of AURKB (AF-Q96GD4-F1-model_v4) and RAD51 to check if Thr232 of AURKB and RAD51 Ser97 were within the protein-protein interface (The outcomes are not displayed here). Our results showed that 30 RAD51 residues interacted with 35 AURKB residues through 5 salt bridges, 29 hydrogen bonds, and 240 non-bonded contacts. Ser97 was found to be within the interface and had a non-bonded connection with Arg123 of AURKB. Moreover, Gln94 and Glu98, located around Ser97, formed five hydrogen bonds and two salt bridges with five residues of AURKB (Ser43, Arg44, His131, Asn142, and Tyr143). Furthermore, residues of AURKB close to Thr232, including Arg230 and Lys231, interacted *via* salt bridges and hydrogen bonds with Glu145 and Asp184 of RAD51, respectively.

AURKC

AURKC is a meiosis kinase activated by autophosphorylation on Thr195, located within the catalytic domain comprising residues (8-249) [387]. According to the docking results, 29 residues of AURKC were found in the interface with RAD51, mostly belonging to the catalytic domain.

Moreover, It was found that RAD51 interacted with AURKC through 28 residues, all of which were located in the C-terminal domain, except for Tyr54, Pro56, Thr90, Phe92, and Arg96. Of these, only Tyr54 formed a hydrogen bond with Arg61 of AURKC. The remaining hydrogen bonds and salt bridges were formed by the C-terminal RAD51 residues, resulting in 13 hydrogen bonds and 3 salt bridges in total (Figure 34 & Figure 35C).

Taken together, our docking data indicate that both VRK1 and AURKB are potent potential candidates for RAD51 phosphorylation at Ser97. More experiments, however, are required to validate these *in silico* results. In light of these findings, we conducted some experiments involving these two proteins, which will be discussed more below.

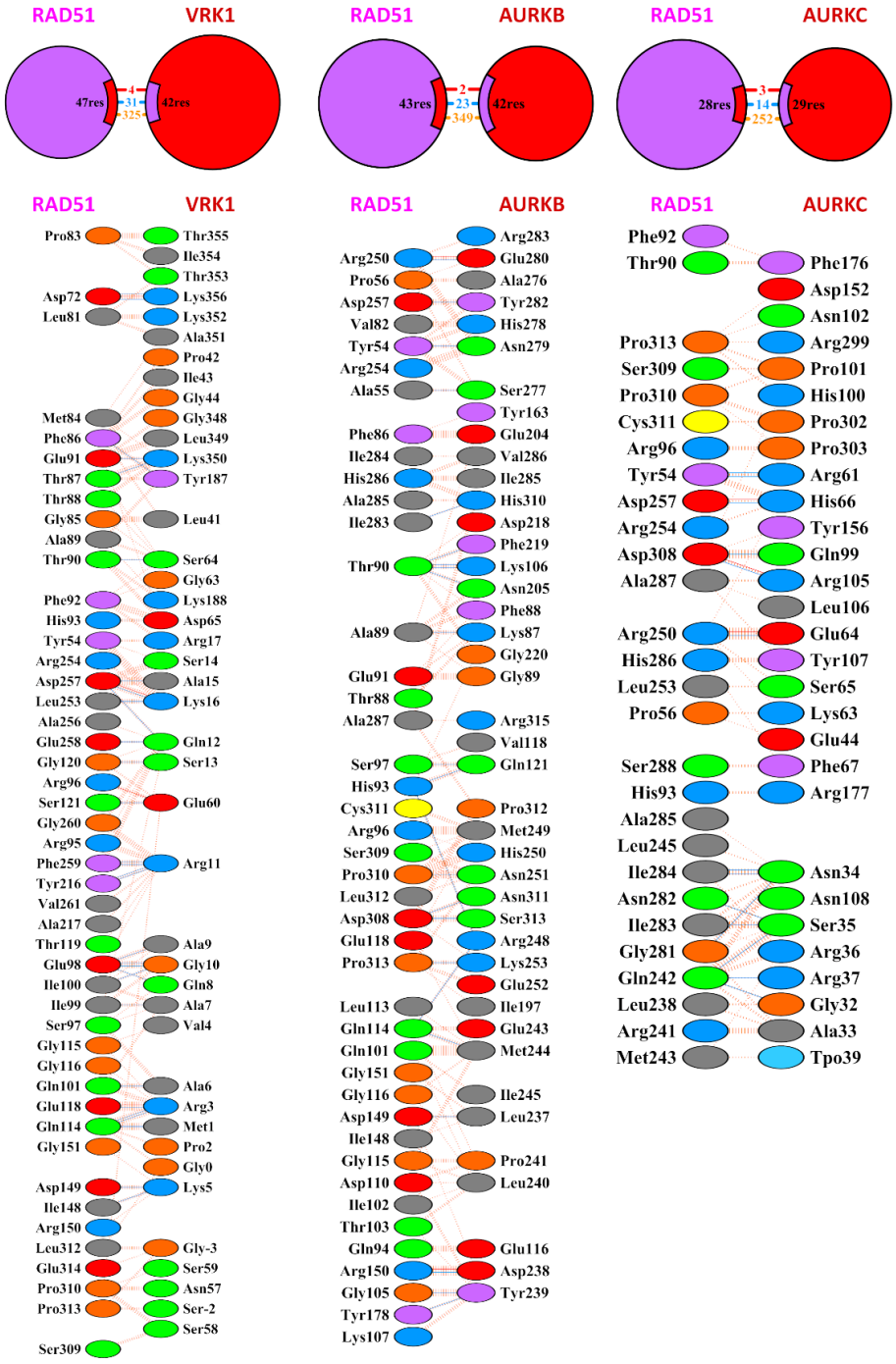

Figure 34 Analyzing the interactions between residues in a protein-protein interface.

The images above display schematic diagrams of protein interactions, with differently colored lines representing different types of interactions. The images below show residue interactions across the interface. Red lines represent salt bridges, yellow lines represent Disulphide bonds, blue lines represent hydrogen bonds, and orange lines represent non-bonded contacts.

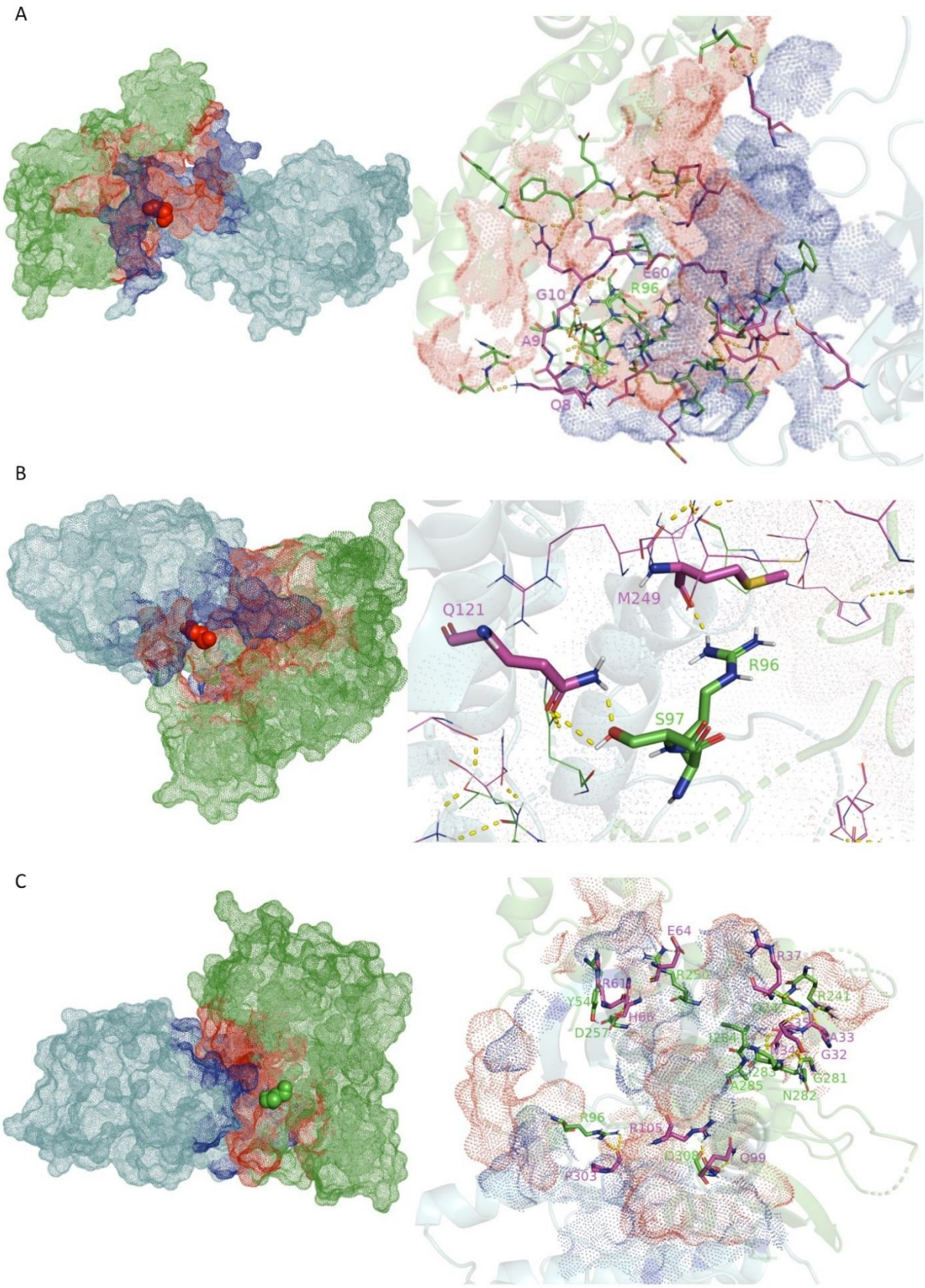

Figure 35 Protein-protein docking analysis shows the probable interaction of RAD51 with VRK1, AURKB and AURKC.

A) VRK1 with RAD51. B) AURKB with RAD51. C) AURKC with RAD51. The left panels show Models of the potential interaction between VRK1 and Aurora B and C kinase proteins (cyan surface) and RAD51 (green

surface). Kinase interactions with RAD51 are illustrated by blue dot surfaces and red dot surfaces for RAD51. The red sphere represents its location in the interaction interface while the green sphere represents Ser97 of RAD51 when it is located outside the protein-protein interface. The polar contacts (sticks) between kinase residues (magenta) and RAD51 (green) are highlighted in the right panel. The green labels indicate RAD51 residues, while the magenta labels indicate Kinases' residues. The yellow dash lines represent hydrogen bonds. In order to simplify the visualization of the hydrogen bonds between VRK1 and AURKB in panels A and B, only two of the RAD51 interface residues were labeled as interacting with the kinases. The remaining residues for both the kinases and RAD51 were represented by magenta and green lines, respectively.

3. AURKB phosphorylates RAD51 *in vitro*

To verify the *in silico* findings suggesting that AURKB may phosphorylate RAD51 on its Ser97 residue, we performed an *in vitro* kinase assay. Recombinant RAD51 was combined with recombinant AURKB and ATP. The membrane was then incubated with the Ser97 antibody for a western blot. Our results showed that AURKB did phosphorylate RAD51 on Ser97 (Figure 36). However, to corroborate this finding, the experiment must be repeated, and the P-site identification have to be validated using MS analysis.

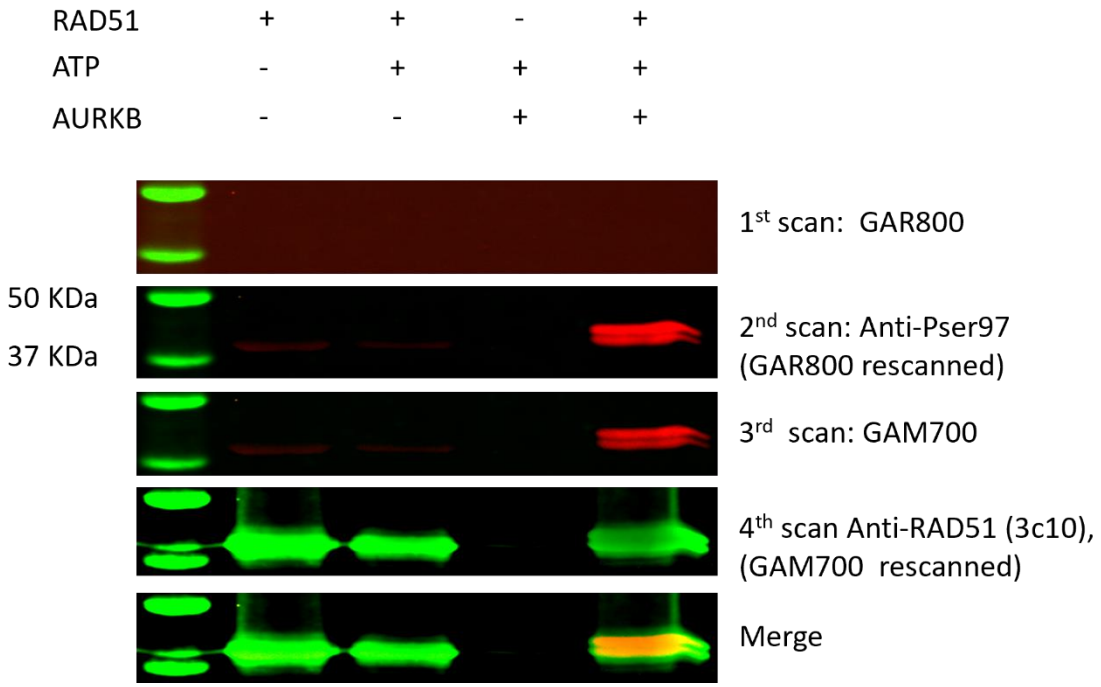

Figure 36 AURKB phosphorylate RAD51 *in vitro*

Western blot after *in vitro* phosphorylation of recombinant RAD51 by AURKB. GAR800 and GAM700 represent secondary goat anti-rabbit and goat anti-mouse antibodies, respectively.

4. The PSer97 levels were lower in cells that had VRK1 knocked down.

In order to determine if VRK1 plays a role in phosphorylating Ser97-RAD51 in cells, we conducted an experiment where we used si-RNA to knock down VRK1.

After 72 hours of siRNA transfection, VRK1 levels decreased by 70%, indicating effective knock down of VRK1 gene. We observed that the levels of phosphorylated Ser97 reduced by 30% when the ratio of PSer97-RAD51 on RAD51 was calculated. Alternatively, the levels of PSer97 on alpha-tubulin decreased more significantly by 70% when we measured the ratio of PSer97 on α-tubulin. However, there was a 55% significant reduction in RAD51 levels observed in response to VRK1 depletion (Figure 37 A and B).

Taken together, the simultaneous decrease in PSer97 and RAD51 levels makes it challenging to attribute the reduction in PSer97 to VRK1 depletion directly. Further experiments are needed to clarify the specific mechanisms underlying these alterations.

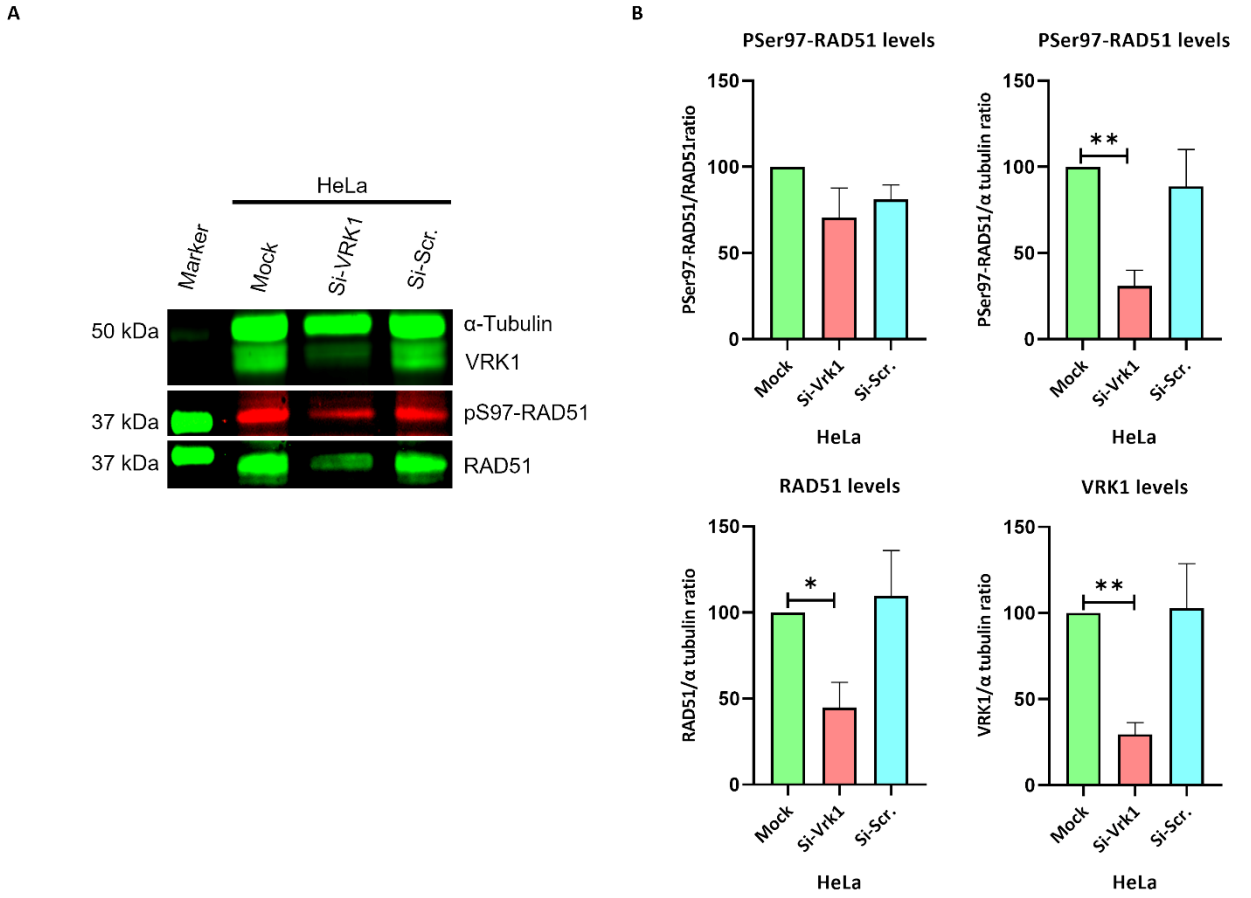

Figure 37 the knock-down of VRK1 affect pSer97-RAD51 levels

A) Whole-cell extracts of HeLa and HCC1806 cells were transfected with si-VRK1 for 24 hours and analyzed by Western blot. The experiment was performed for n=3. B) Protein levels were quantified by densitometric analysis and normalized using α-tubulin. Asterisks represent significance: * for P ≤ 0.05 and ** for P ≤ 0.01.

Discussion:

Here in this work, we have identified that Serine 97, which is in the Subunit Rotation Motif (SRM) of RAD51's linker domain, can be phosphorylated *in vitro* by AURKA. Additionally, we verified the presence of this phosphorylated form in living cells by employing antibodies specifically generated against PSer97-RAD51. Our results are the first report of a phosphorylation modification in the linker domain of RAD51, specifically in its SRM.

The SRM is a highly flexible region located immediately following the polymerization motif (PM) and before the central ATPase domain [193]. It should be noted that this motif influences the quaternary structures of the archaeal RadA and Rad51 proteins, and it is essential for the enzymatic activity of RecA family proteins. Additionally, it has been suggested that the SRM might be flexible enough to enable the rotation of the RadA/Rad51 filaments 360 degrees axially [190]. Moreover, our modeling of the 3D structure of the RAD51 filament showed that the residues of this motif, including Ser97, remained visible on the surface of the filament, which raises the interesting possibility that the SRM functions as an anchor platform for interactions with other RAD51 partners.

- Nucleic acids affinity, polymerization, and D-loop activity of WT and mutants RAD51.

We observed that S97D, the phosphomimetic, and S97A, the non-phosphorylatable mutants of RAD51, have a greater ability to form D-loops than WT RAD51. The S97D-RAD51 activity was more than two times higher than the WT RAD51, whereas the S97A-RAD51 was approximately 50% higher. This indicates that modification of Serine 97 residue significantly affects the recombinase activity of RAD51.

Previous studies from our lab highlighted the phosphorylation impacts on the recombinase activity of RAD51. *Chabot et al.,* in their experiment, used the BRC4-28 peptide to inhibit the polymerization of RAD51 [388,389]. They then compared the activity of the RAD51 WT protein to that of the *in vitro-phosphorylated* RAD51 (tyrosine residues Y159, Y191, Y205, and Y315) by active c-MET kinase. Interestingly, they found that the presence or absence of the BRC4-28 peptide did not affect the D-loop activity of phosphorylated RAD51. However, for the non-phosphorylated RAD51, the D-loop activity decreased by 40% in the presence of BRC4-28. This suggests that the presynaptic filament formed during the D-loop assay is more stable and less sensitive to the BRC4-28 peptide when RAD51 is phosphorylated [326].

Moreover, *Alligand et al.*, investigated the functional effects of mono or di-phosphomimetic mutations at cABL-mediated phosphorylation sites (Y54 and Y315) on RAD51 recombinase activity. Their DNA strand exchange and D-loop experiment results demonstrated that the recombinase activity was not impacted by any RAD51 mono-phosphomimetic modifications (RAD51-Y54E and RAD51-Y315E). However, interestingly, they noticed that the di-phosphomimetic modification (RAD51 Y54/315E) significantly reduced or even completely inhibited the recombinase activity [312].

Moreover, because that to mimic protein phosphorylation, using charged amino acids like aspartate and glutamate may not accurately represent phosphotyrosine. *Subramanyam et al.*, used a nonnatural amino acid called p-carboxymethyl-l-phenylalanine (pCMF), which more closely resembles a phosphorylated tyrosine residue than aspartate or glutamate. They observed that tyrosine 54 phosphorylation ($RAD51^{Y54pCMF}$) stimulates the activity of human RAD51 recombinase through altered nucleoprotein filament dynamics. However, the nucleoprotein filament generated by $RAD51^{Y54pCMF}$ differs from the nucleoprotein filament formed by unmodified RAD51. According to solution and single-molecule FRET analyses, the difference between two nucleoprotein filaments is manifested in the greater amounts of $RAD51^{Y54pCMF}$ necessary to generate stable nuclei on ssDNA. In contrast to $RAD51^{Y54pCMF}$, $RAD51^{Y315pCMF}$ exhibited similar DNA strand exchange activity to the unmodified protein [390]. These prior research efforts add to our understanding that phosphorylation can have various effects on RAD51 activity.

Our polymerization assay, in the absence of nucleic acids, showed that both S97A and S97D mutants displayed a statistically significant decrease in polymerization state, thus mutations at Ser97 affect RAD51's ability to polymerize. These results may appear inconsistent with those that indicated an increase in RAD51 D-loop activity due to the modification on Ser97. However, in looking at the experiment conditions, we can see that the polymerization assay did not take into consideration the other factors that RAD51 needs to perform nucleofilament, including the presence of ssDNA and ATP.

Drawing from the current understanding, in the process of homologous recombination, RAD51 ATPase forms nucleoprotein filaments when it polymerizes on ssDNA. ATP binding keeps the nucleoprotein filament in a ready state for strand pairing and exchange. After strand exchange, ATP hydrolysis allows the filament to be disassembled [207]. Thus, the recombinase activity which we measured in D-loop required several steps to be achieved including RAD51 self-association (polymerization), DNA binding, and ATP binding or hydrolysis.

Moreover, *Subramanyam et al.*, observed that RAD51^{Y54pCMF} did not bind to DNA at a low concentration of 250 nM. They suggest that this may be due to reduced oligomerization of the phosphomimetic protein caused by a distorted monomer/monomer interface. Where Y54 is located near the protomers' interface in the N-terminal domain of RAD51. As a result, RAD51 oligomerization will be delayed until greater protein concentrations are attained [390]. In our case, Ser97 located in the SRM which plays a critical role in controlling the quaternary structures of RecA family proteins including RAD51 [190].

Therefore, we believe that the interactions between RAD51 monomers may be impacted by modifications to Ser97 residue, such as the introduction of phosphomimetic or non-phosphorylatable residues, which could explain the significant decline of the polymerization level of the S97D and S97A mutants. Interestingly, we observed that when using 10 mM of BS3, the phosphomimetic mutant (S97D) formed significantly fewer polymers than the non-phosphorylatable mutant (S79A). This is supported by *Subramanyam et al*.'s explanation that the negative charge of the phosphomimetic mutant (Y54E) can deform the interface of RAD51's protomers [390]. Therefore, an instability of protomer-protomer interaction of S97D mutant would favor the dissociation of the nucleofilament. In this context our ssDNA and ssRNA binding analysis clearly showed that the dissociation kinetic phase is more rapid for S97D than WT RAD51.

Furthermore, the reduced self-association capacity of Ser97 mutants of RAD51 could suggest that they are less likely to forming extensive protein complexes than the WT RAD51. This emphasizes the significant role of Ser97 in RAD51-RAD51 interaction and filament formation, indicating that phosphorylation at Ser97 may have a distinctive function in cellular processes compared to the WT RAD51.

Thanks to our results using Blitz technology, we showed that RAD51 could bind to ssRNA. Remarkably, we noticed that the WT RAD51 protein showed a stronger affinity to ssRNA than to ssDNA. This was evident from the lower dissociation constant (KD) of 0.53 µM for ssRNA, compared to 3.84 µM for ssDNA.

As far as we know, there has only been one reported study on the binding of RAD51 to RNA. This study demonstrated that RAD51 promotes the recruitment of TERRA (Telomeric-repeat-containing RNA), a type of lncRNA transcribed from chromosome ends [391,392]. TERRA plays a role in regulating telomere maintenance and homology-directed DNA repair [392–394]. They found that TERRA is associated with RAD51 *in cellulo* based on their study in HeLa cells using native RNA

immunoprecipitation with anti-RAD51 antibodies [391]. Moreover, by using electrophoretic mobility shift assays (EMSAs), the researchers conducted an experiment where they incubated purified recombinant RAD51 with fluorescently labeled TERRA or telomeric DNA oligonucleotides. They then resolved the reactions by using agarose-gel electrophoresis. The results demonstrated that RAD51 had a three-fold higher affinity for the TERRA oligonucleotide compared to the corresponding telomeric DNA sequence. The TERRA oligonucleotide required a lower protein concentration to obtain shifted oligonucleotide–RAD51 complexe [391]. Their results suggest that RAD51 could bind to RNA, with higher affinity than DNA which is in agreement with the results that we had.

Concerning the mutants of RAD51, on the one hand, the S97D phosphomimetic mutant of RAD51, was found to have a weaker affinity for ssDNA compared to ssRNA, with KD values of 3.63 µM and 1.73 µM, respectively. Interestingly, compared to the WT RAD51, the S97D mutant showed lower affinity for ssRNA, suggesting that the phosphomimetic mutation on Ser97 decreased ssRNA binding. In contrast, the S97D mutant exhibited similar affinity for ssDNA as the WT RAD51, implying that Ser97 phosphorylation did not significantly alter ssDNA binding.

On the other hand, the non-phosphorylatable S97A mutant showed similar affinities for ssDNA and ssRNA, with KD values of 0.34 µM and 0.32 µM, respectively. Furthermore, the S97A displayed a similar affinity to ssRNA as the WT RAD51, suggesting that the absence of phosphorylation at Ser97 did not affect ssRNA binding. Notably, the S97A mutant exhibited a stronger affinity for ssDNA compared to both the WT RAD51 and the S97D mutant, indicating that the lack of polar group (as in the case S97A) at Ser97 enhanced ssDNA binding (Just to remind you, a table of KD values is shown in Figure 7 of Chapter 1 of the results).

Consequently, a total analysis of these findings reveals that while the S97D mutant had a lower affinity for ssRNA in comparison to the WT RAD51, the S97A mutant maintained a similar binding affinity for ssRNA as the WT. Furthermore, the S97A mutant displayed an increase in ssDNA binding, suggesting that Ser97 phosphorylation may play a role in modulating RAD51's nucleic acid binding preferences, with a specific impact on ssDNA binding. Additionally, we have to keep in mind that *in cellulo*, the effect of pSer97 on RAD51's ability to bind to DNA and RNA could be modified by RAD51 partners.

Our *in silico* analysis has revealed that the interaction profile of S97 varies between presynaptic and postsynaptic structures. We have observed that phosphorylation on S97 leads to an

interaction profile similar to that of the postsynaptic structure, indicating the importance of this residue in regulating RAD51 activity. Additionally, we found that S97 interacts with H93 and Q94 in both structures. On the other hand, the substitution of S97 with alanine or aspartic acid resulted in no interaction with the neighbouring residues. These notes could help us in understanding why S97A and S97D exhibited similar behaviour in the D-loop and polymerization assays. Interestingly, our analysis revealed that the substitution of S97 with D97 did not exhibit the same interaction profile as PS97. This raises the question of how well the phosphomimetic mutant S97D represents phosphoserine.

- Characterization of PSer97-RAD51 *in cellulo.*

As previously stated, employing specific antibodies against PSer97-RAD51 allowed us to detect its presence in living cells. Additionally, thanks subcellular fractionation analyses, performed under controlled circumstances, we revealed that PSer97 was found in both nuclear and chromatin-linked fractions; however, it was more abundant in the latter. Interestingly, we did not observe PSer97 in the cytoplasmic fraction, suggesting it exhibits a unique nuclear localization. Conversely, RAD51 was predominantly found in the cytoplasm which is consistent with previous reports that have indicated cytoplasmic distribution of RAD51 under normal conditions [335,395].

Moreover, Thanks to immunofluorescence and confocal microscopy analysis, we observed that PSer97 presented as a granular pattern. This pattern is distinguished by a pan-nuclear distribution with nucleolar exclusion and some foci of different sizes scattered throughout the nucleus.

During our investigation, we examined whether PSer97 foci would colocalize with γH2AX, a well-known marker of DSBs that is also known to colocalize with RAD51. Unexpectedly, we discovered that there was no colocalization between PSer97 and γH2AX. This unexpected observation led us to label different nuclear organelles in an attempt to determine the location of this new form of RAD51. We found a strong colocalization between PSer97 and Sc35, a splicing factor and a familiar Nuclear Speckles (NS) marker [396]. We also confirmed this finding by co-immunoprecipitating Sc35 with a commercial anti-RAD51 antibody, demonstrating the presence of RAD51 in the same structure as Sc35 within NS. However, additional biochemical approaches, such as nuclear speckle isolation, could be employed to determine the presence of RAD51 within them.

It's interesting to note that, in line with our findings, *Morozumi et al*.'s biochemical analyses demonstrated that RAD51 interacts physically and functionally with a component of spliceosome

known as PSF, a splicing factor, which exhibits multiple functions in RNA processing, transcription, and DNA recombination [397].

The NS, also known as splicing speckles or interchromatin granule clusters (IGC), are dynamic membrane-less bodies seen in mammalian cells' nucleoplasm. They are rich in RNA-binding proteins (RBPs), which mostly belong to various subsets of pre-mRNA splicing factors and have high overlap with spliceosome-associated proteins [398–400]. Moreover, *Matsui et al.* reported a relationship between the NS and HR. They found that USP42, a nuclear speckles protein, promotes HR by enhancing the interaction of BRCA1 with the MRN complex. This interaction, in turn, helps resolve the DSB-induced R-loop and promotes DNA-end resection [401].

Thereby, because nuclear speckles are known to be important in pre-mRNA splicing, we wanted to know if PSer97 had a role in splicing modulation. To investigate that, we used Pladiennolide B (plaB), a known splicing inhibitor, to suppress splicing in cells. However, our western blot findings revealed that there were no changes in PSer97 levels after splicing inhibition.

Furthermore, immunofluorescence studies showed that PSer97 maintained its location in NS even after splicing was hindered. However, the Pearson Correlation Coefficient (PCC) values showed a significant decrease in the plaB-treated cells (0.468 and 0.388 for HeLa and HCC1806, respectively) compared to the control (0.608 and 0.555 for HeLa and HCC1806, respectively). The PCC values obtained after PlaB treatment suggest a moderate colocalization [402]. However, it is worth noting that PSer97 still colocalizes with Sc35, and the change in the strength of this colocalization could be due to the dynamic change in the NS after PlaB treatment. This observation is in line with our own findings and with other research. Where it is know, that PlaB targets the SF3b1 subunit of the spliceosome, which is responsible for splicing pre-mRNA. When plaB inhibits splicing, the unspliced pre-mRNAs accumulate in the NS. PlaB treatment also alters the shape and the number of the NS, resulting in an increase in their size and a decrease in their numbers [403,404].

Another study found that injecting oligonucleotides or antibodies that suppressed pre-mRNA splicing *in vitro* into living cells caused significant alterations in the organization of splicing factors. Using immunofluorescence, they saw that the NS became more uniform in shape, reduced in quantity, and increased in size [405].

We used transient transfection of WT RAD51 and its mutants during our tests. The first obvious observation was that exogenous RAD51 location differed depending on the cell line type. In HeLa

cells, it localized in the nucleus, while in HCC1806, it remained in the cytoplasm. This difference in RAD51 localization in HeLa and HCC1806 cell lines could be explained in the context of its nucleocytoplasmic distribution. A preceding study discovered that a BRCA2 mutation, which is associated with cancer, prevents it from binding to a partner protein called DSS1. The binding between BRCA2 and DSS1 is crucial for the nuclear localization of BRCA2. This is because it hides the nuclear export signal (NES) in BRCA2. As a result, point mutations that impair BRCA2-DSS1 binding cause BRCA2 and its cargo, RAD51, to be present in the cytoplasm instead of the nucleus [199]. While there is no direct evidence of BRCA2 mutations in HCC1806 cells, a study suggests that around 10% of patients with TNBC - which is the same cancer type as HCC1806 - have harmful inherited mutations in BRCA1 or BRCA2 [406,407]. Therefore, this is just a hypothesis that could help us understand the difference in exogenous RAD51 distribution between HeLa and HCC1806. However, more studies are required to examine it.

The second apparent observation was that WT and the S97D exogenous RAD51 affected the NS similarly. Where compared to NT, transfected cells with WT and S97D showed a significant decrease in the NS number, and they became larger in size. Indeed, we observed such changes in the shape and number of NS after inhibiting the splicing by PlaB treatment; therefore, it is unclear whether the overexpression of RAD51 and its phosphomimetic mutant could affect the splicing. This hypothesis requires further investigation.

Furtheremore, in the third visible observation we noticed that the impact of the non-phosphorylatable mutant (S97A) varied depending on the cell line. In HeLa cells with nuclear localization of S97A, we detected a significant reduction in the number of NS compared to other transfected cells. We even observed some cells without NS. In contrast, in HCC1806 cells with cytoplasmic localization of S97A, there was no effect on NS, and it showed approximately the same NS number compared to the NT cells. Thus, we can conclude that the absence of phosphorylation on Ser97 in the nucleus is unfavorable to nuclear speckles. This implies that PSer97 could play a critical role in NS formation and /or organization.

During study the synchronized HeLa cells we observed that the level of PSer97-RAD51 remains approximately stable at different stages of the cell cycle. In contrast, the level of RAD51 itself changed with a peak in the late S/G2 phases, which agrees with previous studies that showed that RAD51 protein increases during the cell cycle's S/G2 phases [408].

The stable level of the phosphorylated form of RAD51 at Ser97 throughout the cell cycle could be explained by several hypotheses. This could suggest that the phosphorylation of RAD51 at Ser97 is a constitutive event that occurs independently of the cell cycle stage. The stable level of PSer97-RAD51 could also indicate that the phosphorylation and dephosphorylation rates of RAD51 at Ser97 are balanced, resulting in a constant level of this phosphorylated form.

Alternatively, the stable level of PSer97-RAD51 could be necessary for maintaining a pool of RAD51 ready to respond to DNA damage or replication stress at any cell cycle stage.

However, further research is needed to fully understand how RAD51 and PSer97-RAD51 levels during cell cycle affect RAD51's DNA repair function.

- Exploring the Kinase implicated in cellular Ser97-RAD51 Phosphorylation.

We investigated the kinase involved in Ser97 phosphorylation in cells. Our findings indicate that overexpression of AURKA resulted in increased levels of PSer97 in both HeLa and HCC1806 cell lines. Statistical analysis revealed that the increase was significant only in the HCC1806 cell line. Additionally, when AURKA was inhibited using alisertib, an AURKA inhibitor, PSer97 levels significantly decreased only in HCC1806 cells.

A previous study, on the other hand, demonstrated that the production of DNA double-strand breaks suppresses AURKA function. Because mitosis is slowed down, cells are able to repair damaged DNA [117]. This may offer another hypothesis to explain our findings, which indicate a drop in PSer97-RAD51 following camptothecin treatment. However, it is yet unclear if DNA repair pathway employ this particular phosphorylated RAD51 form. Therefore, extensive testing will be required to shed light on this topic.

Recently, *Damodaran et al*. reported a subcellular localization of AURKA in nuclear speckles, where they found that overexpressed GFP-AURKA was colocalized with Sc35. They also identified AURKA as a novel splicing kinase, where they observed that inhibiting its kinase activity disrupted alternative splicing [409]. Additionally, systems-level study conducted by *Berchtold, D. et al.* has identified AURKA as a regulator of membrane-less organelles in human cells, including nuclear speckles [410].

Looking at these Data in light of ours strongly supports AURKA's involvement in phosphorylating RAD51's Ser97 in cells. However, although AURKA may be involved in this cellular phosphorylation event, the mechanism by which it mediates this phosphorylation remains unclear. Furthermore,

our cell line-dependent findings highlight probable redundancy. As a result, other kinases could phosphorylate the RAD51 Ser97 residue.

We conducted a kinase prediction analysis to test the redundancy of kinases that could phosphorylate Ser97. Using a kinase prediction tools, we identified multiple kinases with high prediction scores that are known to be involved in the DNA damage response. We then used molecular docking to investigate direct interactions between their active sites and Ser97. Our analysis revealed that Vaccinia-Related Kinase 1 (VRK1) and Aurora Kinase B (AURKB) showed the most promise, as docking data of these two kinases showed that Ser97 was found to be in the RAD51-kinase interface.

To test these kinases, we depleted VRK1 using si-VRK1 and observed a decrease in PSer97 levels by an average of 70%. However, that decrease in PSer97 was accompanied by a significant decrease in RAD51 levels (55 %). Thus, it is challenging to determine from this experiment whether the decline in PSer97 was due to a decrease in RAD51 levels or a reduction in Ser97 phosphorylation rate.

Based on our current knowledge, there is no apparent connection between VRK1 and RAD51 or HRR. However, according to *Campillo-Marcos et al.*'s review, VRK1 is an initiating kinase located in chromatin and could be activated independently of the type of DNA damage. It is implicated in regulating histone modifications like acetylation and phosphorylation and also in creating DDR-induced foci such as 53BP1, γH2AX, and NBS1 [411,412].

VRK1 is well known for regulating Cajal Bodies (CBs) dynamics and protects coilin, a protein that is a marker of CBs, from proteasomal degradation [413]. The CBs are membrane-less subnuclear organelles enriched with proteins that play essential roles in RNA metabolism, such as splicing and small nuclear RiboNucleoProtein (snRNP) assembly (reviewed in [414]). Interestingly, several studies have shown colocalization between the CB protein, coilin, and the Sc35 protein of nuclear speckles, despite the two structures being distinct [415,416].

Concerning AURKB, we conducted a kinase *in vitro* assay, and we showed that AURKB was able to phosphorylate RAD51. Finally, western blot analysis confirmed that this AURKB-mediated phosphorylated RAD51 could be detected with anti-PSer97 antibodies, indicating that RAD51 was indeed phosphorylated on Ser97 by AURKB. That being said, it is important to validate these preliminary results using MS analysis.

Interestingly, *Moura, D. et al.*, reported that the proteins VRK1 and AURKB can combine to form a stable complex, which is only a small part of each kinase present in the cell. In addition, they demonstrated that each kinase can inhibit the activity of the other [417].

Perspectives:

In our research, we have discovered a new form of RAD51 that is phosphorylated on its Ser97. However, in order to fully understand the biological significance of PSer97-RAD51, it is crucial to create a CRISPR/Cas9 cell model with RAD51 S97 mutations. This will enable us to precisely manipulate the RAD51 S97 residue and investigate its role in DNA repair and the cellular response to genotoxic stress.

Additionally, the presence of PSer97-RAD51 in the Nuclear Speckles could suggests a potential connection between DNA repair and alternative splicing. Further investigation is required to explore the relationship between PSer97-RAD51 and RNA processing and to determine the impact of PSer97-RAD51 on alternative splicing.

Moreover, the impact of PSer97 phosphorylation on the stability of RAD51 is an important area for future research. Understanding how phosphorylation affects RAD51 stability will provide valuable insights into the regulation of RAD51 and its role in DNA repair.

Our results have also highlighted a possible kinase redundancy in the phosphorylation of RAD51. Further investigation is needed to determine the specific kinases involved in PSer97-RAD51 phosphorylation and to elucidate the regulatory mechanisms that control RAD51 phosphorylation.

Furthermore, while we have validated the presence of PSer97 in cancer cell lines, its presence in normal cells remains unknown. Investigating the presence of PSer97 in normal cells will provide important insights into the physiological role of PSer97-RAD51 and its potential as a therapeutic target or cancer marker.

References

1. Lindahl, T. Instability and decay of the primary structure of DNA. *Nature* **362**, 709–715 (1993).

2. Lindahl, T. & Barnes, D. E. Repair of endogenous DNA damage. *Cold Spring Harb Symp Quant Biol* **65**, 127–133 (2000).

3. Basu, A. K. DNA Damage, Mutagenesis and Cancer. *Int J Mol Sci* **19**, 970 (2018).

4. Schumacher, B., Pothof, J., Vijg, J. & Hoeijmakers, J. H. J. The central role of DNA damage in the ageing process. *Nature* **592**, 695–703 (2021).

5. De Bont, R. & van Larebeke, N. Endogenous DNA damage in humans: a review of quantitative data. *Mutagenesis* **19**, 169–185 (2004).

6. PENG, Y. & PEI, H. DNA alkylation lesion repair: outcomes and implications in cancer chemotherapy. *J Zhejiang Univ Sci B* **22**, 47–62 (2021).

7. Chatterjee, N. & Walker, G. C. Mechanisms of DNA damage, repair and mutagenesis. *Environ Mol Mutagen* **58**, 235–263 (2017).

8. Friedberg, E. C. A brief history of the DNA repair field. *Cell Research* **18**, 3–7 (2008).

9. Huang, R. & Zhou, P.-K. DNA damage repair: historical perspectives, mechanistic pathways and clinical translation for targeted cancer therapy. *Sig Transduct Target Ther* **6**, 1–35 (2021).

10. Li, F., Jiang, T., Li, Q. & Ling, X. Camptothecin (CPT) and its derivatives are known to target topoisomerase I (Top1) as their mechanism of action: did we miss something in CPT analogue molecular targets for treating human disease such as cancer? *Am J Cancer Res* **7**, 2350–2394 (2017).

11. Chakarov, S., Petkova, R., Russev, G. C. & Zhelev, N. DNA damage and mutation. Types of DNA damage. *BioDiscovery* **11**, e8957 (2014).

12. Krokan, H. E. & Bjørås, M. Base Excision Repair. *Cold Spring Harb Perspect Biol* **5**, a012583 (2013).

13. Sokhansanj, B. A. & Wilson, D. M., III. Estimating the Effect of Human Base Excision Repair Protein Variants on the Repair of Oxidative DNA Base Damage. *Cancer Epidemiology, Biomarkers & Prevention* **15**, 1000–1008 (2006).

14. Petruseva, I. O., Evdokimov, A. N. & Lavrik, O. I. Molecular Mechanism of Global Genome Nucleotide Excision Repair. *Acta Naturae* **6**, 23–34 (2014).

15. Schärer, O. D. Nucleotide Excision Repair in Eukaryotes. *Cold Spring Harb Perspect Biol* **5**, a012609 (2013).

16. Hsieh, P. & Yamane, K. DNA mismatch repair: Molecular mechanism, cancer, and ageing. *Mech Ageing Dev* **129**, 391–407 (2008).

17. Jiricny, J. The multifaceted mismatch-repair system. *Nat Rev Mol Cell Biol* **7**, 335–346 (2006).

18. Dall'Agnese, G. *et al.* Role of condensates in modulating DNA repair pathways and its implication for chemoresistance. *Journal of Biological Chemistry* **299**, (2023).

19. Cooke, M. S., Evans, M. D., Dizdaroglu, M. & Lunec, J. Oxidative DNA damage: mechanisms, mutation, and disease. *The FASEB Journal* **17**, 1195–1214 (2003).

20. Borrego-Soto, G., Ortiz-López, R. & Rojas-Martínez, A. Ionizing radiation-induced DNA injury and damage detection in patients with breast cancer. *Genet Mol Biol* **38**, 420–432 (2015).

21. Desouky, O., Ding, N. & Zhou, G. Targeted and non-targeted effects of ionizing radiation. *Journal of Radiation Research and Applied Sciences* **8**, 247–254 (2015).

22. Abbotts, R. & Wilson, D. M. Coordination of DNA Single Strand Break Repair. *Free Radic Biol Med* **107**, 228–244 (2017).

23. Leccia, M.-T., Lebbe, C., Claudel, J.-P., Narda, M. & Basset-Seguin, N. New Vision in Photoprotection and Photorepair. *Dermatol Ther (Heidelb)* **9**, 103–115 (2019).

24. Técher, H. & Pasero, P. The Replication Stress Response on a Narrow Path Between Genomic Instability and Inflammation. *Frontiers in Cell and Developmental Biology* **9**, (2021).

25. Zeman, M. K. & Cimprich, K. A. Causes and consequences of replication stress. *Nat Cell Biol* **16**, 2–9 (2014).

26. Saxena, S. & Zou, L. Hallmarks of DNA replication stress. *Molecular Cell* **82**, 2298–2314 (2022).

27. Brown, T. A. Mutation, Repair and Recombination. in *Genomes. 2nd edition* (Wiley-Liss, 2002).

28. Bębenek, A. & Ziuzia-Graczyk, I. Fidelity of DNA replication-a matter of proofreading. *Curr Genet* **64**, 985–996 (2018).

29. Tiwari, V. & Wilson, D. M. DNA Damage and Associated DNA Repair Defects in Disease and Premature Aging. *Am J Hum Genet* **105**, 237–257 (2019).

30. Errors in DNA Replication | Learn Science at Scitable. http://www.nature.com/scitable/topicpage/dna-replication-and-causes-of-mutation-409.

31. Singh, V., Fedeles, B. I. & Essigmann, J. M. Role of tautomerism in RNA biochemistry. *RNA* **21**, 1–13 (2015).

32. Mai, S., Marquetand, P., Richter, M., González-Vazquez, J. & González, L. A singlet and triplet excited-state dynamics study of the keto and enol tautomers of cytosine. *ChemPhysChem* **14**, 2920–2931 (2013).

33. Bouchal, T., Durník, I., Illík, V., Réblová, K. & Kulhánek, P. Importance of base-pair opening for mismatch recognition. *Nucleic Acids Research* **48**, 11322–11334 (2020).

34. Tubbs, A. & Nussenzweig, A. Endogenous DNA Damage as a Source of Genomic Instability in Cancer. *Cell* **168**, 644–656 (2017).

35. Minko, I. G. *et al.* Catalysts of DNA Strand Cleavage at Apurinic/Apyrimidinic Sites. *Sci Rep* **6**, 28894 (2016).

36. Thompson, P. S. & Cortez, D. New Insights into Abasic Site Repair and Tolerance. *DNA Repair (Amst)* **90**, 102866 (2020).

37. Chen, H., Yao, L., Brown, C., Rizzo, C. J. & Turesky, R. J. Quantitation of Apurinic/Apyrimidinic Sites in Isolated DNA and in Mammalian Tissue with a Reduced Level of Artifacts. *Anal. Chem.* **91**, 7403–7410 (2019).

38. Kitsera, N., Rodriguez-Alvarez, M., Emmert, S., Carell, T. & Khobta, A. Nucleotide excision repair of abasic DNA lesions. *Nucleic Acids Research* **47**, 8537–8547 (2019).

39. Shi, K. *et al.* Structural basis for recognition of distinct deaminated DNA lesions by endonuclease Q. *Proceedings of the National Academy of Sciences* **118**, e2021120118 (2021).

40. Lewis, C. A., Crayle, J., Zhou, S., Swanstrom, R. & Wolfenden, R. Cytosine deamination and the precipitous decline of spontaneous mutation during Earth's history. *Proceedings of the National Academy of Sciences* **113**, 8194–8199 (2016).

41. Alseth, I., Dalhus, B. & Bjørås, M. Inosine in DNA and RNA. *Current Opinion in Genetics & Development* **26**, 116–123 (2014).

42. Nieminuszczy, J. & Grzesiuk, E. Bacterial DNA repair genes and their eukaryotic homologues: 3. AlkB dioxygenase and Ada methyltransferase in the direct repair of alkylated DNA. *Acta Biochimica Polonica* **54**, 459–468 (2007).

43. Weston, A. & Poirier, M. C. Carcinogen–DNA Adduct Formation and DNA Repair. in *Encyclopedia of Toxicology (Third Edition)* (ed. Wexler, P.) 705–712 (Academic Press, 2014). doi:10.1016/B978-0-12-386454-3.00593-5.

44. Hossain, Md. A., Lin, Y. & Yan, S. Single-Strand Break End Resection in Genome Integrity: Mechanism and Regulation by APE2. *Int J Mol Sci* **19**, 2389 (2018).

45. Lin, Y. *et al.* APE1 senses DNA single-strand breaks for repair and signaling. *Nucleic Acids Research* **48**, 1925–1940 (2020).

46. Tounekti, O., Kenani, A., Foray, N., Orlowski, S. & Mir, L. M. The ratio of single- to double-strand DNA breaks and their absolute values determine cell death pathway. *Br J Cancer* **84**, 1272–1279 (2001).

47. Cao, H. *et al.* Hotspots of single-strand DNA “breakome” are enriched at transcriptional start sites of genes. *Frontiers in Molecular Biosciences* **9**, (2022).

48. Puc, J., Aggarwal, A. K. & Rosenfeld, M. G. Physiological functions of programmed DNA breaks in signal-induced transcription. *Nat Rev Mol Cell Biol* **18**, 471–476 (2017).

49. Domingo-Prim, J., Bonath, F. & Visa, N. RNA at DNA Double-Strand Breaks: The Challenge of Dealing with DNA:RNA Hybrids. *Bioessays* **42**, e1900225 (2020).

50. Cannan, W. J. & Pederson, D. S. Mechanisms and Consequences of Double-strand DNA Break Formation in Chromatin. *J Cell Physiol* **231**, 3–14 (2016).

51. Jeggo, P. A. & Löbrich, M. DNA double-strand breaks: their cellular and clinical impact? *Oncogene* **26**, 7717–7719 (2007).

52. Xue, C. & Greene, E. C. DNA repair pathway choices in CRISPR-Cas9 mediated genome editing. *Trends Genet* **37**, 639–656 (2021).

53. Rogakou, E. P., Pilch, D. R., Orr, A. H., Ivanova, V. S. & Bonner, W. M. DNA Double-stranded Breaks Induce Histone H2AX Phosphorylation on Serine 139 *. *Journal of Biological Chemistry* **273**, 5858–5868 (1998).

54. Rybak, P. *et al.* Low level phosphorylation of histone H2AX on serine 139 (γH2AX) is not associated with DNA double-strand breaks. *Oncotarget* **7**, 49574–49587 (2016).

55. Solier, S. & Pommier, Y. The apoptotic ring: a novel entity with phosphorylated histones H2AX and H2B and activated DNA damage response kinases. *Cell Cycle* **8**, 1853–1859 (2009).

56. Atkinson, J., Bezak, E. & Kempson, I. Imaging DNA double-strand breaks — are we there yet? *Nat Rev Mol Cell Biol* **23**, 579–580 (2022).

57. Suh, J.-S. & Kim, T.-J. A novel DNA double-strand breaks biosensor based on fluorescence resonance energy transfer. *Biomaterials Research* **27**, 15 (2023).

58. Manchester, K. L. Theodor Boveri and the origin of malignant tumours. *Trends in Cell Biology* **5**, 384–387 (1995).

59. Kuchenbaecker, K. B. *et al.* Risks of Breast, Ovarian, and Contralateral Breast Cancer for BRCA1 and BRCA2 Mutation Carriers. *JAMA* **317**, 2402–2416 (2017).

60. Beatty, G. L. & Gladney, W. L. Immune escape mechanisms as a guide for cancer immunotherapy. *Clin Cancer Res* **21**, 687–692 (2015).

61. Moon, J. *et al.* DNA Damage and Its Role in Cancer Therapeutics. *International Journal of Molecular Sciences* **24**, 4741 (2023).

62. Buck, J., Bowden, N. & Endersby, R. Chapter 12 - Cancer therapies inducing DNA damage. in *Epigenetics and DNA Damage* (ed. Jasiulionis, M. G.) vol. 33 205–225 (Academic Press, 2022).

63. Zhang, C., Xu, C., Gao, X. & Yao, Q. Platinum-based drugs for cancer therapy and anti-tumor strategies. *Theranostics* **12**, 2115–2132 (2022).

64. Liu, S. & Wang, Y. Mass spectrometry for the assessment of the occurrence and biological consequences of DNA adducts. *Chem Soc Rev* **44**, 7829–7854 (2015).

65. Todd, R. C. & Lippard, S. J. Structure of duplex DNA containing the cisplatin 1,2-{Pt(NH3)2}2+-d(GpG) cross-link at 1.77Å resolution. *Journal of Inorganic Biochemistry* **104**, 902–908 (2010).

66. Kartalou, M. & Essigmann, J. M. Mechanisms of resistance to cisplatin. *Mutation Research/Fundamental and Molecular Mechanisms of Mutagenesis* **478**, 23–43 (2001).

67. Torigoe, T. *et al.* Cisplatin Resistance and Transcription Factors. *Current Medicinal Chemistry - Anti-Cancer Agents* **5**, 15–27.

68. PubChem. Camptothecin. https://pubchem.ncbi.nlm.nih.gov/compound/24360.

69. Staker, B. L. *et al.* Structures of Three Classes of Anticancer Agents Bound to the Human Topoisomerase I–DNA Covalent Complex. *J. Med. Chem.* **48**, 2336–2345 (2005).

70. Sordet, O., Khan, Q. A., Kohn, K. W. & Pommier, Y. Apoptosis induced by topoisomerase inhibitors. *Curr Med Chem Anticancer Agents* **3**, 271–290 (2003).

71. Pommier, Y. *et al.* Repair of and checkpoint response to topoisomerase I-mediated DNA damage. *Mutation Research/Fundamental and Molecular Mechanisms of Mutagenesis* **532**, 173–203 (2003).

72. Morris, E. J. & Geller, H. M. Induction of neuronal apoptosis by camptothecin, an inhibitor of DNA topoisomerase-I: evidence for cell cycle-independent toxicity. *J Cell Biol* **134**, 757–770 (1996).

73. Pommier, Y. DNA Topoisomerase I Inhibitors: Chemistry, Biology and Interfacial Inhibition. *Chem Rev* **109**, 2894–2902 (2009).

74. Martino, E. *et al.* The long story of camptothecin: From traditional medicine to drugs. *Bioorganic & Medicinal Chemistry Letters* **27**, 701–707 (2017).

75. Apellániz, D. *et al.* MCM2-7 complex: a review. *Odontoestomatología* **20**, 4–11 (2018).

76. Ding, L. *et al.* The Roles of Cyclin-Dependent Kinases in Cell-Cycle Progression and Therapeutic Strategies in Human Breast Cancer. *International Journal of Molecular Sciences* **21**, 1960 (2020).

77. Sur, S. & Agrawal, D. K. Phosphatases and Kinases Regulating CDC25 Activity in the Cell Cycle: Clinical Implications of CDC25 Overexpression and Potential Treatment Strategies. *Mol Cell Biochem* **416**, 33–46 (2016).

78. Rizzato, M. *et al.* Master mitotic kinases regulate viral genome delivery during papillomavirus cell entry. *Nat Commun* **14**, 355 (2023).

79. Tavernier, N. *et al.* Bora phosphorylation substitutes in trans for T-loop phosphorylation in Aurora A to promote mitotic entry. *Nat Commun* **12**, 1899 (2021).

80. Jantscher, F., Pirker, C., Mayer, C.-E., Berger, W. & Sutterluety, H. Overexpression of Aurora-A in primary cells interferes with S-phase entry by diminishing Cyclin D1 dependent activities. *Molecular Cancer* **10**, 28 (2011).

81. Barr, A. R. & Gergely, F. Aurora-A: the maker and breaker of spindle poles. *Journal of Cell Science* **120**, 2987–2996 (2007).

82. Zheng, D. *et al.* Emerging roles of Aurora-A kinase in cancer therapy resistance. *Acta Pharmaceutica Sinica B* (2023) doi:10.1016/j.apsb.2023.03.013.

83. Yan, M. *et al.* Aurora-A Kinase: A Potent Oncogene and Target for Cancer Therapy. *Medicinal Research Reviews* **36**, 1036–1079 (2016).

84. Wang, R. *et al.* Selective targeting of non-centrosomal AURKA functions through use of a targeted protein degradation tool. *Commun Biol* **4**, 640 (2021).

85. Taguchi, S. ichi *et al.* Degradation of human Aurora-A protein kinase is mediated by hCdh1. *FEBS Lett* **519**, 59–65 (2002).

86. Walter, A. O., Seghezzi, W., Korver, W., Sheung, J. & Lees, E. The mitotic serine/threonine kinase Aurora2/AIK is regulated by phosphorylation and degradation. *Oncogene* **19**, 4906–4916 (2000).

87. Rajeev, R., Singh, P., Asmita, A., Anand, U. & Manna, T. K. Aurora A site specific TACC3 phosphorylation regulates astral microtubule assembly by stabilizing γ-tubulin ring complex. *BMC Molecular and Cell Biology* **20**, 58 (2019).

88. Terada, Y., Uetake, Y. & Kuriyama, R. Interaction of Aurora-A and centrosomin at the microtubule-nucleating site in Drosophila and mammalian cells. *J Cell Biol* **162**, 757–763 (2003).

89. Stefani, A. *et al.* Unweaving the mitotic spindle: A focus on Aurora kinase inhibitors in lung cancer. *Frontiers in Oncology* **12**, (2022).

90. Zorba, A. *et al.* Molecular mechanism of Aurora A kinase autophosphorylation and its allosteric activation by TPX2. *eLife* **3**, e02667 (2014).

91. Macůrek, L. *et al.* Polo-like kinase-1 is activated by aurora A to promote checkpoint recovery. *Nature* **455**, 119–123 (2008).

92. Combes, G., Alharbi, I., Braga, L. G. & Elowe, S. Playing polo during mitosis: PLK1 takes the lead. *Oncogene* **36**, 4819–4827 (2017).

93. Gheghiani, L., Loew, D., Lombard, B., Mansfeld, J. & Gavet, O. PLK1 Activation in Late G2 Sets Up Commitment to Mitosis. *Cell Rep* **19**, 2060–2073 (2017).

94. Willems, E. *et al.* The functional diversity of Aurora kinases: a comprehensive review. *Cell Division* **13**, 7 (2018).

95. Vugt, M. A. T. M. van, Brás, A. & Medema, R. H. Polo-like Kinase-1 Controls Recovery from a G2 DNA Damage-Induced Arrest in Mammalian Cells. *Molecular Cell* **15**, 799–811 (2004).

96. Chabalier-Taste, C. *et al.* Polo-like kinase 1 mediates BRCA1 phosphorylation and recruitment at DNA double-strand breaks. *Oncotarget* **7**, 2269–2283 (2016).

97. Gelot, C. *et al.* Polθ is phosphorylated by PLK1 to repair double-strand breaks in mitosis. *Nature* **621**, 415–422 (2023).

98. Cancers | Free Full-Text | Proteins from the DNA Damage Response: Regulation, Dysfunction, and Anticancer Strategies. https://www.mdpi.com/2072-6694/13/15/3819.

99. Nakad, R. & Schumacher, B. DNA Damage Response and Immune Defense: Links and Mechanisms. *Frontiers in Genetics* **7**, (2016).

100. Sefer, A. *et al.* Structural dynamics of DNA strand break sensing by PARP-1 at a single-molecule level. *Nat Commun* **13**, 6569 (2022).

101. Smith, J., Tho, L. M., Xu, N. & Gillespie, D. A. The ATM-Chk2 and ATR-Chk1 pathways in DNA damage signaling and cancer. *Adv Cancer Res* **108**, 73–112 (2010).

102. Bolderson, E., Richard, D. J., Zhou, B.-B. S. & Khanna, K. K. Recent Advances in Cancer Therapy Targeting Proteins Involved in DNA Double-Strand Break Repair. *Clin Cancer Res* **15**, 6314–6320 (2009).

103. Yue, X., Bai, C., Xie, D., Ma, T. & Zhou, P.-K. DNA-PKcs: A Multi-Faceted Player in DNA Damage Response. *Front Genet* **11**, 607428 (2020).

104. Burgess, R. C., Burman, B., Kruhlak, M. & Misteli, T. Activation of DNA damage response signaling by condensed chromatin. *Cell Rep* **9**, 1703–1717 (2014).

105. Podhorecka, M., Skladanowski, A. & Bozko, P. H2AX Phosphorylation: Its Role in DNA Damage Response and Cancer Therapy. *J Nucleic Acids* **2010**, 920161 (2010).

106. Huang, R.-X. & Zhou, P.-K. DNA damage response signaling pathways and targets for radiotherapy sensitization in cancer. *Sig Transduct Target Ther* **5**, 1–27 (2020).

107. Chao, W. C. H., Kulkarni, K., Zhang, Z., Kong, E. H. & Barford, D. Structure of the mitotic checkpoint complex. *Nature* **484**, 208–213 (2012).

108. Tong, Y. *et al.* Pin1 inhibits PP2A-mediated Rb dephosphorylation in regulation of cell cycle and S-phase DNA damage. *Cell Death Dis* **6**, e1640–e1640 (2015).

109. Bertoli, C., Skotheim, J. M. & de Bruin, R. A. M. Control of cell cycle transcription during G1 and S phases. *Nat Rev Mol Cell Biol* **14**, 518–528 (2013).

110. Knudsen, K. E. *et al.* RB-dependent S-phase response to DNA damage. *Mol Cell Biol* **20**, 7751–7763 (2000).

111. van Jaarsveld, M. T. M. *et al.* Cell-type-specific role of CHK2 in mediating DNA damage-induced G2 cell cycle arrest. *Oncogenesis* **9**, 1–7 (2020).

112. Smith, H. L., Southgate, H., Tweddle, D. A. & Curtin, N. J. DNA damage checkpoint kinases in cancer. *Expert Reviews in Molecular Medicine* **22**, e2 (2020).

113. Liu, K. *et al.* The role of CDC25C in cell cycle regulation and clinical cancer therapy: a systematic review. *Cancer Cell International* **20**, 213 (2020).

114. Kavanagh, J. N., Redmond, K. M., Schettino, G. & Prise, K. M. DNA Double Strand Break Repair: A Radiation Perspective. *Antioxidants & Redox Signaling* **18**, 2458–2472 (2013).

115. Xiao, Z. *et al.* Chk1 Mediates S and G2 Arrests through Cdc25A Degradation in Response to DNA-damaging Agents*. *Journal of Biological Chemistry* **278**, 21767–21773 (2003).

116. Chapter 12: DNA Damage and Repair – Chemistry. https://wou.edu/chemistry/courses/online-chemistry-textbooks/ch450-and-ch451-biochemistry-defining-life-at-the-molecular-level/chapter-12-dna-damage-repair-and-mutations/.

117. Krystyniak, A., Garcia-Echeverria, C., Prigent, C. & Ferrari, S. Inhibition of Aurora A in response to DNA damage. *Oncogene* **25**, 338–348 (2006).

118. Cazales, M. *et al.* CDC25B phosphorylation by Aurora-A occurs at the G2/M transition and is inhibited by DNA damage. *Cell Cycle* **4**, 1233–1238 (2005).

119. Visconti, R., Della Monica, R. & Grieco, D. Cell cycle checkpoint in cancer: a therapeutically targetable double-edged sword. *Journal of Experimental & Clinical Cancer Research* **35**, 153 (2016).

120. Cleveland, D. W., Mao, Y. & Sullivan, K. F. Centromeres and Kinetochores: From Epigenetics to Mitotic Checkpoint Signaling. *Cell* **112**, 407–421 (2003).

121. Fiore, B. D., Wurzenberger, C., Davey, N. E. & Pines, J. The Mitotic Checkpoint Complex Requires an Evolutionary Conserved Cassette to Bind and Inhibit Active APC/C. *Molecular Cell* **64**, 1144–1153 (2016).

122. Courtheoux, T. *et al.* Aurora A kinase activity is required to maintain an active spindle assembly checkpoint during prometaphase. *Journal of Cell Science* **131**, jcs191353 (2018).

123. Sitry-Shevah, D., Kaisari, S., Teichner, A., Miniowitz-Shemtov, S. & Hershko, A. Role of ubiquitylation of components of mitotic checkpoint complex in their dissociation from anaphase-promoting complex/cyclosome. *Proceedings of the National Academy of Sciences* **115**, 1777–1782 (2018).

124. Hunt, C. R. *et al.* Histone Modifications and DNA Double-Strand Break Repair after Exposure to Ionizing Radiations. *Radiat Res* **179**, 383–392 (2013).

125. Pandita, T. *et al.* Chromatin modifications and the DNA damage response to ionizing radiation. *Frontiers in Oncology* **2**, (2013).

126. Kouzarides, T. Acetylation: a regulatory modification to rival phosphorylation? *The EMBO Journal* **19**, 1176–1179 (2000).

127. Huyen, Y. *et al.* Methylated lysine 79 of histone H3 targets 53BP1 to DNA double-strand breaks. *Nature* **432**, 406–411 (2004).

128. Rass, E., Willaume, S. & Bertrand, P. 53BP1: Keeping It under Control, Even at a Distance from DNA Damage. *Genes* **13**, 2390 (2022).

129. Gómez-Cabello, D., Pappas, G., Aguilar-Morante, D., Dinant, C. & Bartek, J. CtIP-dependent nascent RNA expression flanking DNA breaks guides the choice of DNA repair pathway. *Nat Commun* **13**, 5303 (2022).

130. Bunting, S. F. *et al.* 53BP1 inhibits homologous recombination in Brca1-deficient cells by blocking resection of DNA breaks. *Cell* **141**, 243–254 (2010).

131. Ochs, F. *et al.* 53BP1 fosters fidelity of homology-directed DNA repair. *Nat Struct Mol Biol* **23**, 714–721 (2016).

132. Liu, T. & Huang, J. DNA End Resection: Facts and Mechanisms. *Genomics, Proteomics & Bioinformatics* **14**, 126–130 (2016).

133. Ranjha, L., Howard, S. M. & Cejka, P. Main steps in DNA double-strand break repair: an introduction to homologous recombination and related processes. *Chromosoma* **127**, 187–214 (2018).

134. Chang, H. H. Y., Pannunzio, N. R., Adachi, N. & Lieber, M. R. Non-homologous DNA end joining and alternative pathways to double-strand break repair. *Nat Rev Mol Cell Biol* **18**, 495–506 (2017).

135. Xu, Y. & Xu, D. Repair pathway choice for double-strand breaks. *Essays in Biochemistry* **64**, 765–777 (2020).

136. Fujita, H. *et al.* CHAMP1-POGZ counteracts the inhibitory effect of 53BP1 on homologous recombination and affects PARP inhibitor resistance. *Oncogene* **41**, 2706–2718 (2022).

137. Nambiar, T. S. *et al.* Stimulation of CRISPR-mediated homology-directed repair by an engineered RAD18 variant. *Nat Commun* **10**, 3395 (2019).

138. Mao, Z., Bozzella, M., Seluanov, A. & Gorbunova, V. DNA repair by nonhomologous end joining and homologous recombination during cell cycle in human cells. *Cell Cycle* **7**, 2902–2906 (2008).

139. Ray, U. & Raghavan, S. C. Understanding the DNA double-strand break repair and its therapeutic implications. *DNA Repair* **106**, 103177 (2021).

140. Chan, D. W., Ye, R., Veillette, C. J. & Lees-Miller, S. P. DNA-dependent protein kinase phosphorylation sites in Ku 70/80 heterodimer. *Biochemistry* **38**, 1819–1828 (1999).

141. Serrano-Benítez, A., Cortés-Ledesma, F. & Ruiz, J. F. "An End to a Means": How DNA-End Structure Shapes the Double-Strand Break Repair Process. *Frontiers in Molecular Biosciences* **6**, (2020).

142. Dueva, R. & Iliakis, G. Alternative pathways of non-homologous end joining (NHEJ) in genomic instability and cancer. *Translational Cancer Research* **2**, (2013).

143. Daley, J. M. *et al.* Specificity of end resection pathways for double-strand break regions containing ribonucleotides and base lesions. *Nat Commun* **11**, 3088 (2020).

144. Syed, A. & Tainer, J. A. The MRE11–RAD50–NBS1 Complex Conducts the Orchestration of Damage Signaling and Outcomes to Stress in DNA Replication and Repair. *Annual Review of Biochemistry* **87**, 263–294 (2018).

145. Uziel, T. *et al.* Requirement of the MRN complex for ATM activation by DNA damage. *EMBO J* **22**, 5612–5621 (2003).

146. Stiff, T. *et al.* Nbs1 is required for ATR-dependent phosphorylation events. *The EMBO Journal* **24**, 199 (2005).

147. Zhang, Y., Zhou, J. & Lim, C. U. The role of NBS1 in DNA double strand break repair, telomere stability, and cell cycle checkpoint control. *Cell Res* **16**, 45–54 (2006).

148. Zhu, X. D., Küster, B., Mann, M., Petrini, J. H. & de Lange, T. Cell-cycle-regulated association of RAD50/MRE11/NBS1 with TRF2 and human telomeres. *Nat Genet* **25**, 347–352 (2000).

149. Paull, T. T. & Gellert, M. The 3′ to 5′ Exonuclease Activity of Mre11 Facilitates Repair of DNA Double-Strand Breaks. *Molecular Cell* **1**, 969–979 (1998).

150. Deng, S. K., Gibb, B., de Almeida, M. J., Greene, E. C. & Symington, L. S. RPA Antagonizes Microhomology-Mediated Repair of DNA Double-Strand Breaks. *Nat Struct Mol Biol* **21**, 405–412 (2014).

151. Mah, L.-J., El-Osta, A. & Karagiannis, T. C. γH2AX: a sensitive molecular marker of DNA damage and repair. *Leukemia* **24**, 679–686 (2010).

152. Brochier, C. & Langley, B. Chromatin Modifications Associated with DNA Double-strand Breaks Repair as Potential Targets for Neurological Diseases. *Neurotherapeutics* **10**, 817–830 (2013).

153. Sullivan, M. R. & Bernstein, K. A. RAD-ical New Insights into RAD51 Regulation. *Genes (Basel)* **9**, 629 (2018).

154. Daza-Martin, M., Densham, R. M. & Morris, J. R. BRCA1-BARD1: the importance of being in shape. *Molecular & Cellular Oncology* **6**, e1656500 (2019).

155. Pathways and assays for DNA double-strand break repair by homologous recombination. *ABBS* 879–889 (2019) doi:10.1093/abbs/gmz076.

156. Gelot, C., Le-Guen, T., Ragu, S. & Lopez, B. S. Double-Strand Break Repair. in *Genome Stability: From Virus to Human Application* 337–351 (2016). doi:10.1016/B978-0-12-803309-8.00020-3.

157. Bhargava, R., Onyango, D. O. & Stark, J. M. Regulation of Single-Strand Annealing and its Role in Genome Maintenance. *Trends in Genetics* **32**, 566–575 (2016).

158. Do, A. T., Brooks, J. T., Le Neveu, M. K. & LaRocque, J. R. Double-strand break repair assays determine pathway choice and structure of gene conversion events in drosophila melanogaster. *G3: Genes, Genomes, Genetics* **4**, 425–432 (2014).

159. Prentiss, M., Prévost, C. & Danilowicz, C. Structure/function relationships in RecA protein-mediated homology recognition and strand exchange. *Crit Rev Biochem Mol Biol* **50**, 453–476 (2015).

160. Lin, Z., Kong, H., Nei, M. & Ma, H. Origins and evolution of the recA/RAD51 gene family: Evidence for ancient gene duplication and endosymbiotic gene transfer. *Proc Natl Acad Sci U S A* **103**, 10328–10333 (2006).

161. Chintapalli, S. V. *et al.* Reevaluation of the evolutionary events within recA/RAD51 phylogeny. *BMC Genomics* **14**, 240 (2013).

162. Andriuskevicius, T., Kotenko, O. & Makovets, S. Putting together and taking apart: assembly and disassembly of the Rad51 nucleoprotein filament in DNA repair and genome stability. *Cell Stress* **2**, 96–112 (2018).

163. Shinohara, A. *et al.* Cloning of human, mouse and fission yeast recombination genes homologous to RAD51 and recA. *Nat Genet* **4**, 239–243 (1993).

164. Bonilla, B., Hengel, S. R., Grundy, M. K. & Bernstein, K. A. RAD51 Gene Family Structure and Function. *Annual Review of Genetics* **54**, 25–46 (2020).

165. Amunugama, R., Groden, J. & Fishel, R. The HsRAD51B–HsRAD51C stabilizes the HsRAD51 nucleoprotein filament. *DNA Repair* **12**, 723–732 (2013).

166. Jiang, S., Lin, T., Xie, Q. & Wang, L. Network Analysis of RAD51 Proteins in Metazoa and the Evolutionary Relationships With Their Archaeal Homologs. *Frontiers in Genetics* **9**, (2018).

167. Gaasbeek, E. J. *et al.* Functional Characterization of Excision Repair and RecA-Dependent Recombinational DNA Repair in Campylobacter jejuni. *J Bacteriol* **191**, 3785–3793 (2009).

168. Tsuzuki, T. *et al.* Targeted disruption of the Rad51 gene leads to lethality in embryonic mice. *Proc Natl Acad Sci U S A* **93**, 6236–6240 (1996).

169. Yoshida, K. *et al.* The mouse RecA-like gene Dmc1 is required for homologous chromosome synapsis during meiosis. *Mol Cell* **1**, 707–718 (1998).

170. Yoo, S. & McKee, B. D. Functional analysis of the Drosophila Rad51 gene (spn-A) in repair of DNA damage and meiotic chromosome segregation. *DNA Repair (Amst)* **4**, 231–242 (2005).

171. Takanami, T., Mori, A., Takahashi, H., Horiuchi, S. & Higashitani, A. Caenorhabditis elegans Ce-rdh-1/rad-51 functions after double-strand break formation of meiotic recombination. *Chromosome Res* **11**, 125–135 (2003).

172. Symington, L. S. Role of RAD52 epistasis group genes in homologous recombination and double-strand break repair. *Microbiol Mol Biol Rev* **66**, 630–670, table of contents (2002).

173. Game, J. C. & Mortimer, R. K. A genetic study of X-ray sensitive mutants in yeast. *Mutation Research/Fundamental and Molecular Mechanisms of Mutagenesis* **24**, 281–292 (1974).

174. Takahashi, E.-I. *et al.* Chromosome Mapping of the Human (RECA) and Mouse (Reca) Homologs of the Yeast RAD51 and Escherichia coli recA Genes to Human (15q15.1) and Mouse (2F1) Chromosomes by Direct R-banding Fluorescence in Situ Hybridization. *Genomics* **19**, 376–378 (1994).

175. Matos-Rodrigues, G., Guirouilh-Barbat, J., Martini, E. & Lopez, B. S. Homologous recombination, cancer and the 'RAD51 paradox'. *NAR Cancer* **3**, zcab016 (2021).

176. Heeke, A. L. *et al.* Prevalence of Homologous Recombination-Related Gene Mutations Across Multiple Cancer Types. *JCO Precis Oncol* **2018**, PO.17.00286 (2018).

177. Ameziane, N. *et al.* A novel Fanconi anaemia subtype associated with a dominant-negative mutation in RAD51. *Nat Commun* **6**, 8829 (2015).

178. Depienne, C. *et al.* RAD51 Haploinsufficiency Causes Congenital Mirror Movements in Humans. *Am J Hum Genet* **90**, 301–307 (2012).

179. Trouillard, O. *et al.* Congenital Mirror Movements Due to RAD51: Cosegregation with a Nonsense Mutation in a Norwegian Pedigree and Review of the Literature. *Tremor Other Hyperkinet Mov (N Y)* **6**, 424 (2016).

180. Luo, W. *et al.* Variants in Homologous Recombination Genes EXO1 and RAD51 Related with Premature Ovarian Insufficiency. *The Journal of Clinical Endocrinology & Metabolism* **105**, e3566–e3574 (2020).

181. Wu, Y., He, Y., Moya, I. A., Qian, X. & Luo, Y. Crystal Structure of Archaeal Recombinase RadA: A Snapshot of Its Extended Conformation. *Molecular Cell* **15**, 423–435 (2004).

182. Xu, J. *et al.* Cryo-EM structures of human RAD51 recombinase filaments during catalysis of DNA-strand exchange. *Nat Struct Mol Biol* **24**, 40–46 (2017).

183. Sun, Y., McCorvie, T. J., Yates, L. A. & Zhang, X. Structural basis of homologous recombination. *Cell. Mol. Life Sci.* **77**, 3–18 (2020).

184. Pellegrini, L. *et al.* Insights into DNA recombination from the structure of a RAD51–BRCA2 complex. *Nature* **420**, 287–293 (2002).

185. Aihara, H., Ito, Y., Kurumizaka, H., Yokoyama, S. & Shibata, T. The N-terminal domain of the human Rad51 protein binds DNA: structure and a DNA binding surface as revealed by NMR1 1Edited by P. E. Wright. *Journal of Molecular Biology* **290**, 495–504 (1999).

186. Kurumizaka, H. *et al.* A Possible Role of the C-terminal Domain of the RecA Protein: A GATEWAY MODEL FOR DOUBLE-STRANDED DNA BINDING*. *Journal of Biological Chemistry* **271**, 33515–33524 (1996).

187. Yuan, Z.-M. *et al.* Regulation of Rad51 Function by c-Abl in Response to DNA Damage *. *Journal of Biological Chemistry* **273**, 3799–3802 (1998).

188. Galkin, V. E. *et al.* The Rad51/RadA N-Terminal Domain Activates Nucleoprotein Filament ATPase Activity. *Structure* **14**, 983–992 (2006).

189. Subramanyam, S., Jones, W. T., Spies, M. & Spies, M. A. Contributions of the RAD51 N-terminal domain to BRCA2-RAD51 interaction. *Nucleic Acids Research* **41**, 9020–9032 (2013).

190. Chen, L.-T. *et al.* Crystal structure of the left-handed archaeal RadA helical filament: identification of a functional motif for controlling quaternary structures and enzymatic functions of RecA family proteins. *Nucleic Acids Research* **35**, 1787–1801 (2007).

191. Shin, D. S. *et al.* Full-length archaeal Rad51 structure and mutants: mechanisms for RAD51 assembly and control by BRCA2. *The EMBO Journal* **22**, 4566–4576 (2003).

192. Han, W., Shen, Y. & She, Q. Nanobiomotors of archaeal DNA repair machineries: current research status and application potential. *Cell & Bioscience* **4**, 32 (2014).

193. Chen, L.-T. *et al.* Structural and Functional Analyses of Five Conserved Positively Charged Residues in the L1 and N-Terminal DNA Binding Motifs of Archaeal RadA Protein. *PLOS ONE* **2**, e858 (2007).

194. Demeyer, A., Benhelli-Mokrani, H., Chénais, B., Weigel, P. & Fleury, F. Inhibiting homologous recombination by targeting RAD51 protein. *Biochimica et Biophysica Acta (BBA) - Reviews on Cancer* **1876**, 188597 (2021).

195. Matsuo, Y., Sakane, I., Takizawa, Y., Takahashi, M. & Kurumizaka, H. Roles of the human Rad51 L1 and L2 loops in DNA binding. *The FEBS Journal* **273**, 3148–3159 (2006).

196. Tombline, G. & Fishel, R. Biochemical Characterization of the Human RAD51 Protein: I. ATP HYDROLYSIS *. *Journal of Biological Chemistry* **277**, 14417–14425 (2002).

197. Morrison, C. *et al.* The Essential Functions of Human Rad51 Are Independent of ATP Hydrolysis. *Mol Cell Biol* **19**, 6891–6897 (1999).

198. Sun, H. *et al.* CRIP1 cooperates with BRCA2 to drive the nuclear enrichment of RAD51 and to facilitate homologous repair upon DNA damage induced by chemotherapy. *Oncogene* **40**, 5342–5355 (2021).

199. Jeyasekharan, A. D. *et al.* A cancer-associated BRCA2 mutation reveals masked nuclear export signals controlling localization. *Nat Struct Mol Biol* **20**, 1191–1198 (2013).

200. Jumper, J. *et al.* Highly accurate protein structure prediction with AlphaFold. *Nature* **596**, 583–589 (2021).

201. Varadi, M. *et al.* AlphaFold Protein Structure Database: massively expanding the structural coverage of protein-sequence space with high-accuracy models. *Nucleic Acids Research* **50**, D439–D444 (2022).

202. Waterhouse, A. M., Procter, J. B., Martin, D. M. A., Clamp, M. & Barton, G. J. Jalview Version 2—a multiple sequence alignment editor and analysis workbench. *Bioinformatics* **25**, 1189–1191 (2009).

203. Danilowicz, C. *et al.* The differential extension in dsDNA bound to Rad51 filaments may play important roles in homology recognition and strand exchange. *Nucleic Acids Research* **42**, 526–533 (2014).

204. Bianco, P. R., Tracy, R. B. & Kowalczykowski, S. C. DNA strand exchange proteins: a biochemical and physical comparison. *Front Biosci* **3**, D570-603 (1998).

205. Hilario, J., Amitani, I., Baskin, R. J. & Kowalczykowski, S. C. Direct imaging of human Rad51 nucleoprotein dynamics on individual DNA molecules. *Proceedings of the National Academy of Sciences* **106**, 361–368 (2009).

206. Mani, A., Braslavsky, I., Arbel-Goren, R. & Stavans, J. Caught in the act: the lifetime of synaptic intermediates during the search for homology on DNA. *Nucleic Acids Research* **38**, 2036–2043 (2010).

207. Appleby, R., Bollschweiler, D., Chirgadze, D. Y., Joudeh, L. & Pellegrini, L. A metal ion-dependent mechanism of RAD51 nucleoprotein filament disassembly. *iScience* **26**, 106689 (2023).

208. Li, X. *et al.* Rad51 and Rad54 ATPase activities are both required to modulate Rad51-dsDNA filament dynamics. *Nucleic Acids Res* **35**, 4124–4140 (2007).

209. Lord, C. J. & Ashworth, A. RAD51, BRCA2 and DNA repair: a partial resolution. *Nat Struct Mol Biol* **14**, 461–462 (2007).

210. Yu, D. S. *et al.* Dynamic Control of Rad51 Recombinase by Self-Association and Interaction with BRCA2. *Molecular Cell* **12**, 1029–1041 (2003).

211. Špírek, M. *et al.* Human RAD51 rapidly forms intrinsically dynamic nucleoprotein filaments modulated by nucleotide binding state. *Nucleic Acids Res* **46**, 3967–3980 (2018).

212. Reitz, D., Chan, Y.-L. & Bishop, D. K. How strand exchange protein function benefits from ATP hydrolysis. *Current Opinion in Genetics & Development* **71**, 120–128 (2021).

213. Sharma, R., Davies, A. G. & Wälti, C. Directed assembly of 3-nm-long RecA nucleoprotein filaments on double-stranded DNA with nanometer resolution. *ACS Nano* **8**, 3322–3330 (2014).

214. Zhao, L., Xu, J., Zhao, W., Sung, P. & Wang, H.-W. Chapter Seven - Determining the RAD51-DNA Nucleoprotein Filament Structure and Function by Cryo-Electron Microscopy. in *Methods in Enzymology* (eds. Spies, M. & Malkova, A.) vol. 600 179–199 (Academic Press, 2018).

215. Ogawa, T., Yu, X., Shinohara, A. & Egelman, E. H. Similarity of the Yeast RAD51 Filament to the Bacterial RecA Filament. *Science* **259**, 1896–1899 (1993).

216. Candelli, A. *et al.* Visualization and quantification of nascent RAD51 filament formation at single-monomer resolution. *Proceedings of the National Academy of Sciences* **111**, 15090–15095 (2014).

217. Subramanyam, S., Kinz-Thompson, C. D., Gonzalez, R. L. & Spies, M. Observation and Analysis of RAD51 nucleation dynamics at single-monomer resolution. *Methods Enzymol* **600**, 201–232 (2018).

218. Modesti, M. *et al.* Fluorescent Human RAD51 Reveals Multiple Nucleation Sites and Filament Segments Tightly Associated along a Single DNA Molecule. *Structure* **15**, 599–609 (2007).

219. Forget, A. L., Loftus, M. S., McGrew, D. A., Bennett, B. T. & Knight, K. L. The human Rad51 K133A mutant is functional for DNA double-strand break repair in human cells. *Biochemistry* **46**, 3566–3575 (2007).

220. Yu, X. & Egelman, E. H. Structural data suggest that the active and inactive forms of the RecA filament are not simply interconvertible. *J Mol Biol* **227**, 334–346 (1992).

221. Reymer, A., Frykholm, K., Morimatsu, K., Takahashi, M. & Nordén, B. Structure of human Rad51 protein filament from molecular modeling and site-specific linear dichroism spectroscopy. *Proceedings of the National Academy of Sciences* **106**, 13248–13253 (2009).

222. Xu, J. *et al.* Mechanisms of distinctive mismatch tolerance between Rad51 and Dmc1 in homologous recombination. *Nucleic Acids Research* **49**, 13135–13149 (2021).

223. Esashi, F., Galkin, V. E., Yu, X., Egelman, E. H. & West, S. C. Stabilization of RAD51 nucleoprotein filaments by the C-terminal region of BRCA2. *Nat Struct Mol Biol* **14**, 468–474 (2007).

224. Chen, Z., Yang, H. & Pavletich, N. P. Mechanism of homologous recombination from the RecA–ssDNA/dsDNA structures. *Nature* **453**, 489–494 (2008).

225. Ragunathan, K., Joo, C. & Ha, T. Real-Time Observation of Strand Exchange Reaction with High Spatiotemporal Resolution. *Structure* **19**, 1064–1073 (2011).

226. Dutreix, M., Fulconis, R. & Viovy, J.-L. The Search for Homology: A Paradigm for Molecular Interactions? *Complexus* **1**, 89–99 (2003).

227. Adzuma, K. No sliding during homology search by RecA protein. *J Biol Chem* **273**, 31565–31573 (1998).

228. Yancey-Wrona, J. E. & Camerini-Otero, R. D. The search for DNA homology does not limit stable homologous pairing promoted by RecA protein. *Curr Biol* **5**, 1149–1158 (1995).

229. Shen, P. & Huang, H. V. Homologous recombination in Escherichia coli: dependence on substrate length and homology. *Genetics* **112**, 441–457 (1986).

230. Tsai, Y.-C., Wang, Y., Urena, D. E., Kumar, S. & Chen, J. Heterology tolerance and recognition of mismatched base pairs by human Rad51 protein. *DNA Repair* **10**, 363–372 (2011).

231. Shivashankar, G. V., Feingold, M., Krichevsky, O. & Libchaber, A. RecA polymerization on double-stranded DNA by using single-molecule manipulation: The role of ATP hydrolysis. *Proceedings of the National Academy of Sciences* **96**, 7916–7921 (1999).

232. Solinger, J. A., Kiianitsa, K. & Heyer, W.-D. Rad54, a Swi2/Snf2-like Recombinational Repair Protein, Disassembles Rad51:dsDNA Filaments. *Molecular Cell* **10**, 1175–1188 (2002).

233. Mazina, O. M. & Mazin, A. V. Human Rad54 Protein Stimulates DNA Strand Exchange Activity of hRad51 Protein in the Presence of Ca2+* ♦. *Journal of Biological Chemistry* **279**, 52042–52051 (2004).

234. San Filippo, J., Sung, P. & Klein, H. Mechanism of Eukaryotic Homologous Recombination. *Annual Review of Biochemistry* **77**, 229–257 (2008).

235. Zhong, A. X., Chen, Y. & Chen, P.-L. BRCA1 the Versatile Defender: Molecular to Environmental Perspectives. *International Journal of Molecular Sciences* **24**, 14276 (2023).

236. Chen, Y. *et al.* BRCA1 is a 220-kDa nuclear phosphoprotein that is expressed and phosphorylated in a cell cycle-dependent manner. *Cancer Res* **56**, 3168–3172 (1996).

237. Saurin, A. J., Borden, K. L. B., Boddy, M. N. & Freemont, P. S. Does this have a familiar RING? *Trends in Biochemical Sciences* **21**, 208–214 (1996).

238. Wu, L. C. *et al.* Identification of a RING protein that can interact in vivo with the BRCA1 gene product. *Nat Genet* **14**, 430–440 (1996).

239. Brzovic, P. S., Rajagopal, P., Hoyt, D. W., King, M. C. & Klevit, R. E. Structure of a BRCA1-BARD1 heterodimeric RING-RING complex. *Nat Struct Biol* **8**, 833–837 (2001).

240. Yun, M. H. & Hiom, K. CtIP-BRCA1 modulates the choice of DNA double-strand-break repair pathway throughout the cell cycle. *Nature* **459**, 460–463 (2009).

241. Isono, M. *et al.* BRCA1 Directs the Repair Pathway to Homologous Recombination by Promoting 53BP1 Dephosphorylation. *Cell Reports* **18**, 520–532 (2017).

242. Wu, Q. *et al.* Structure of BRCA1-BRCT/Abraxas Complex Reveals Phosphorylation-Dependent BRCT Dimerization at DNA Damage Sites. *Mol Cell* **61**, 434–448 (2016).

243. Zhao, W. *et al.* BRCA1–BARD1 promotes RAD51-mediated homologous DNA pairing. *Nature* **550**, 360–365 (2017).

244. Wang, B. *et al.* Abraxas and RAP80 Form a BRCA1 Protein Complex Required for the DNA Damage Response. *Science* **316**, 1194–1198 (2007).

245. Chen, L., Nievera, C. J., Lee, A. Y.-L. & Wu, X. Cell Cycle-dependent Complex Formation of BRCA1·CtIP·MRN Is Important for DNA Double-strand Break Repair*. *Journal of Biological Chemistry* **283**, 7713–7720 (2008).

246. Sadeghi, F. *et al.* Molecular contribution of BRCA1 and BRCA2 to genome instability in breast cancer patients: review of radiosensitivity assays. *Biological Procedures Online* **22**, 23 (2020).

247. Roy, R., Chun, J. & Powell, S. N. BRCA1 and BRCA2: different roles in a common pathway of genome protection. *Nat Rev Cancer* **12**, 68–78 (2011).

248. Christou, C. M. & Kyriacou, K. BRCA1 and Its Network of Interacting Partners. *Biology* **2**, 40–63 (2013).

249. Le, H. P., Heyer, W.-D. & Liu, J. Guardians of the Genome: BRCA2 and Its Partners. *Genes* **12**, (2021).

250. Oliver, A. W., Swift, S., Lord, C. J., Ashworth, A. & Pearl, L. H. Structural basis for recruitment of BRCA2 by PALB2. *EMBO Rep* **10**, 990–996 (2009).

251. Carreira, A. *et al.* The BRC repeats of BRCA2 modulate the DNA-binding selectivity of RAD51. *Cell* **136**, 1032–1043 (2009).

252. Davies, O. R. & Pellegrini, L. Interaction with the BRCA2 C-terminus Protects RAD51–DNA Filaments from Disassembly by BRC Repeats. *Nat Struct Mol Biol* **14**, 475–483 (2007).

253. Holthausen, J. T. *et al.* Effect of the BRCA2 CTRD domain on RAD51 filaments analyzed by an ensemble of single molecule techniques. *Nucleic Acids Research* **39**, 6558–6567 (2011).

254. Carreira, A. & Kowalczykowski, S. C. Two classes of BRC repeats in BRCA2 promote RAD51 nucleoprotein filament function by distinct mechanisms. *Proceedings of the National Academy of Sciences of the United States of America* **108**, 10448 (2011).

255. Scott, D. E., Marsh, M., Blundell, T. L., Abell, C. & Hyvönen, M. Structure-activity relationship of the peptide binding-motif mediating the BRCA2:RAD51 protein–protein interaction. *FEBS Letters* **590**, 1094–1102 (2016).

256. Esashi, F. *et al.* CDK-dependent phosphorylation of BRCA2 as a regulatory mechanism for recombinational repair. *Nature* **434**, 598–604 (2005).

257. Halder, S. *et al.* Double-stranded DNA binding function of RAD51 in DNA protection and its regulation by BRCA2. *Molecular Cell* **82**, 3553-3565.e5 (2022).

258. Hanamshet, K., Mazina, O. M. & Mazin, A. V. Reappearance from Obscurity: Mammalian Rad52 in Homologous Recombination. *Genes* **7**, 63 (2016).

259. Kagawa, W. *et al.* Crystal Structure of the Homologous-Pairing Domain from the Human Rad52 Recombinase in the Undecameric Form. *Molecular Cell* **10**, 359–371 (2002).

260. Koike, M., Yutoku, Y. & Koike, A. The C-terminal region of Rad52 is essential for Rad52 nuclear and nucleolar localization, and accumulation at DNA damage sites immediately after irradiation. *Biochem Biophys Res Commun* **435**, 260–266 (2013).

261. Sugiyama, T. & Kantake, N. Dynamic Regulatory Interactions of Rad51, Rad52, and Replication Protein-A in Recombination Intermediates. *Journal of Molecular Biology* **390**, 45–55 (2009).

262. Hanamshet, K. & Mazin, A. V. The function of RAD52 N-terminal domain is essential for viability of BRCA-deficient cells. *Nucleic Acids Research* **48**, 12778–12791 (2020).

263. Feng, Z. *et al.* Rad52 inactivation is synthetically lethal with BRCA2 deficiency. *Proceedings of the National Academy of Sciences* **108**, 686–691 (2011).

264. Yang, Q., Li, Y., Sun, R. & Li, J. Identification of a RAD52 Inhibitor Inducing Synthetic Lethality in BRCA2-Deficient Cancer Cells. *Frontiers in Pharmacology* **12**, (2021).

265. Bhowmick, R., Minocherhomji, S. & Hickson, I. D. RAD52 Facilitates Mitotic DNA Synthesis Following Replication Stress. *Molecular Cell* **64**, 1117–1126 (2016).

266. Heyer, W.-D., Li, X., Rolfsmeier, M. & Zhang, X.-P. Rad54: the Swiss Army knife of homologous recombination? *Nucleic Acids Res* **34**, 4115–4125 (2006).

267. Pazin, M. J. & Kadonaga, J. T. SWI2/SNF2 and Related Proteins: ATP-Driven Motors That Disrupt-Protein–DNA Interactions? *Cell* **88**, 737–740 (1997).

268. Thomä, N. H. *et al.* Structure of the SWI2/SNF2 chromatin-remodeling domain of eukaryotic Rad54. *Nat Struct Mol Biol* **12**, 350–356 (2005).

269. Petukhova, G., Stratton, S. & Sung, P. Catalysis of homologous DNA pairing by yeast Rad51 and Rad54 proteins. *Nature* **393**, 91–94 (1998).

270. Crickard, J. B., Moevus, C. J., Kwon, Y., Sung, P. & Greene, E. C. Rad54 Drives ATP Hydrolysis-Dependent DNA Sequence Alignment during Homologous Recombination. *Cell* **181**, 1380-1394.e18 (2020).

271. Mason, J. M. *et al.* RAD54 family translocases counter genotoxic effects of RAD51 in human tumor cells. *Nucleic Acids Research* **43**, 3180–3196 (2015).

272. Liu, T., Wan, L., Wu, Y., Chen, J. & Huang, J. hSWS1·SWSAP1 is an evolutionarily conserved complex required for efficient homologous recombination repair. *J Biol Chem* **286**, 41758–41766 (2011).

273. Miller, K. A., Sawicka, D., Barsky, D. & Albala, J. S. Domain mapping of the Rad51 paralog protein complexes. *Nucleic Acids Res* **32**, 169–178 (2004).

274. Masson, J. Y. *et al.* Identification and purification of two distinct complexes containing the five RAD51 paralogs. *Genes Dev* **15**, 3296–3307 (2001).

275. Chun, J., Buechelmaier, E. S. & Powell, S. N. Rad51 Paralog Complexes BCDX2 and CX3 Act at Different Stages in the BRCA1-BRCA2-Dependent Homologous Recombination Pathway. *Molecular and Cellular Biology* **33**, 387–395 (2013).

276. Greenhough, L. A. *et al.* Structure and function of the RAD51B–RAD51C–RAD51D–XRCC2 tumour suppressor. *Nature* **619**, 650–657 (2023).

277. Matsuzaki, K., Kondo, S., Ishikawa, T. & Shinohara, A. Human RAD51 paralogue SWSAP1 fosters RAD51 filament by regulating the anti-recombinase FIGNL1 AAA+ ATPase. *Nat Commun* **10**, 1407 (2019).

278. Sarwar, R. *et al.* Upregulation of RAD51 expression is associated with progression of thyroid carcinoma. *Exp Mol Pathol* **102**, 446–454 (2017).

279. Wang, Z. *et al.* The Emerging Roles of Rad51 in Cancer and Its Potential as a Therapeutic Target. *Frontiers in Oncology* **12**, (2022).

280. Hine, C. M., Seluanov, A. & Gorbunova, V. Use of the Rad51 promoter for targeted anti-cancer therapy. *Proceedings of the National Academy of Sciences* **105**, 20810–20815 (2008).

281. Orhan, E., Velazquez, C., Tabet, I., Sardet, C. & Theillet, C. Regulation of RAD51 at the Transcriptional and Functional Levels: What Prospects for Cancer Therapy? *Cancers* **13**, 2930 (2021).

282. Birney, E. *et al.* Identification and analysis of functional elements in 1% of the human genome by the ENCODE pilot project. *Nature* **447**, 799–816 (2007).

283. Sana, J., Faltejskova, P., Svoboda, M. & Slaby, O. Novel classes of non-coding RNAs and cancer. *Journal of Translational Medicine* **10**, 103 (2012).

284. Majidinia, M. *et al.* MicroRNAs, DNA damage response and ageing. *Biogerontology* **21**, 275–291 (2020).

285. Li, Y., Tong, Y., Liu, J. & Lou, J. The Role of MicroRNA in DNA Damage Response. *Frontiers in Genetics* **13**, (2022).

286. Chen, S. *et al.* MiR-34s negatively regulate homologous recombination through targeting RAD51. *Arch Biochem Biophys* **666**, 73–82 (2019).

287. Piotto, C., Biscontin, A., Millino, C. & Mognato, M. Functional validation of miRNAs targeting genes of DNA double-strand break repair to radiosensitize non-small lung cancer cells. *Biochimica et Biophysica Acta (BBA) - Gene Regulatory Mechanisms* **1861**, 1102–1118 (2018).

288. Mani, C. *et al.* Prexasertib treatment induces homologous recombination deficiency and synergizes with olaparib in triple-negative breast cancer cells. *Breast Cancer Res* **21**, 104 (2019).

289. Mani, C. *et al.* Racial differences in RAD51 expression are regulated by miRNA-214-5P and its inhibition synergizes with olaparib in triple-negative breast cancer. *Breast Cancer Research* **25**, 44 (2023).

290. Statello, L., Guo, C.-J., Chen, L.-L. & Huarte, M. Gene regulation by long non-coding RNAs and its biological functions. *Nat Rev Mol Cell Biol* **22**, 96–118 (2021).

291. Gazy, I. *et al.* TODRA, a lncRNA at the RAD51 Locus, Is Oppositely Regulated to RAD51, and Enhances RAD51-Dependent DSB (Double Strand Break) Repair. *PLOS ONE* **10**, e0134120 (2015).

292. Shen, L. *et al.* LncRNA lnc-RI regulates homologous recombination repair of DNA double-strand breaks by stabilizing RAD51 mRNA as a competitive endogenous RNA. *Nucleic Acids Res* **46**, 717–729 (2018).

293. Zhang, X. *et al.* LncRNA CACClnc promotes chemoresistance of colorectal cancer by modulating alternative splicing of RAD51. *Oncogene* **42**, 1374–1391 (2023).

294. Ramazi, S. & Zahiri, J. Post-translational modifications in proteins: resources, tools and prediction methods. *Database* **2021**, baab012 (2021).

295. Jin, J. Interplay between ubiquitylation and SUMOylation: Empowered by phase separation. *J Biol Chem* **294**, 15235–15236 (2019).

296. Wei, W. & Lin, H.-K. The key role of ubiquitination and sumoylation in signaling and cancer: a research topic. *Front Oncol* **2**, 187 (2012).

297. Guo, H. J., Rahimi, N. & Tadi, P. Biochemistry, Ubiquitination. in *StatPearls* (StatPearls Publishing, 2023).

298. Koo, S.-Y. *et al.* Ubiquitination Links DNA Damage and Repair Signaling to Cancer Metabolism. *International Journal of Molecular Sciences* **24**, 8441 (2023).

299. Pickart, C. M. Mechanisms underlying ubiquitination. *Annu Rev Biochem* **70**, 503–533 (2001).

300. Inano, S. *et al.* RFWD3-Mediated Ubiquitination Promotes Timely Removal of Both RPA and RAD51 from DNA Damage Sites to Facilitate Homologous Recombination. *Molecular Cell* **66**, 622-634.e8 (2017).

301. Kang, J. W. *et al.* PUMA facilitates EMI1-promoted cytoplasmic Rad51 ubiquitination and inhibits DNA repair in stem and progenitor cells. *Signal Transduction and Targeted Therapy* **6**, (2021).

302. Luo, K. *et al.* A phosphorylation–deubiquitination cascade regulates the BRCA2–RAD51 axis in homologous recombination. *Genes Dev.* **30**, 2581–2595 (2016).

303. Flotho, A. & Melchior, F. Sumoylation: a regulatory protein modification in health and disease. *Annu Rev Biochem* **82**, 357–385 (2013).

304. Hariharasudhan, G. *et al.* TOPORS-mediated RAD51 SUMOylation facilitates homologous recombination repair. *Nucleic Acids Research* **50**, 1501–1516 (2022).

305. Lee, E. J. *et al.* Hepatocyte Growth Factor Improves the Therapeutic Efficacy of Human Bone Marrow Mesenchymal Stem Cells via RAD51. *Molecular Therapy* **26**, 845–859 (2018).

306. Cohen, P. The origins of protein phosphorylation. *Nat Cell Biol* **4**, E127–E130 (2002).

307. Lim, G., Chang, Y. & Huh, W.-K. Phosphoregulation of Rad51/Rad52 by CDK1 functions as a molecular switch for cell cycle–specific activation of homologous recombination. *Science Advances* **6**, eaay2669 (2020).

308. Chen, G. *et al.* Radiation-induced Assembly of Rad51 and Rad52 Recombination Complex Requires ATM and c-Abl*. *Journal of Biological Chemistry* **274**, 12748–12752 (1999).

309. Slupianek, A. *et al.* Targeting RAD51 phosphotyrosine-315 to prevent unfaithful recombination repair in BCR-ABL1 leukemia. *Blood* **118**, 1062–1068 (2011).

310. Popova, M. *et al.* Detection of c-Abl kinase-promoted phosphorylation of Rad51 by specific antibodies reveals that Y54 phosphorylation is dependent on that of Y315. *FEBS Lett* **583**, 1867–1872 (2009).

311. Subramanyam, S., Ismail, M., Bhattacharya, I. & Spies, M. Tyrosine phosphorylation stimulates activity of human RAD51 recombinase through altered nucleoprotein filament dynamics. *Proc Natl Acad Sci U S A* **113**, E6045–E6054 (2016).

312. Alligand, B., Le Breton, M., Marquis, D., Vallette, F. & Fleury, F. Functional effects of diphosphomimetic mutations at cAbl-mediated phosphorylation sites on Rad51 recombinase activity. *Biochimie* **139**, 115–124 (2017).

313. Li, Y. *et al.* Arg tyrosine kinase is involved in homologous recombinational DNA repair. *Biochemical and Biophysical Research Communications* **299**, 697–702 (2002).

314. Yata, K. *et al.* Plk1 and CK2 act in concert to regulate Rad51 during DNA double strand break repair. *Mol Cell* **45**, 371–383 (2012).

315. Yata, K. *et al.* BRCA2 Coordinates the Activities of Cell-Cycle Kinases to Promote Genome Stability. *Cell Reports* **7**, 1547–1559 (2014).

316. Ehlén, Å., Sessa, G., Zinn-Justin, S. & Carreira, A. The phospho-dependent role of BRCA2 on the maintenance of chromosome integrity. *Cell Cycle* **20**, 731–741.

317. Bergoglio, V. *et al.* DNA synthesis by Pol η promotes fragile site stability by preventing under-replicated DNA in mitosis. *J Cell Biol* **201**, 395–408 (2013).

318. Wassing, I. E. *et al.* The RAD51 recombinase protects mitotic chromatin in human cells. *Nat Commun* **12**, 5380 (2021).

319. Graber-Feesl, C. L., Pederson, K. D., Aney, K. J. & Shima, N. Mitotic DNA Synthesis Is Differentially Regulated between Cancer and Noncancerous Cells. *Mol Cancer Res* **17**, 1687–1698 (2019).

320. Min, J., Wright, W. E. & Shay, J. W. Alternative Lengthening of Telomeres Mediated by Mitotic DNA Synthesis Engages Break-Induced Replication Processes. *Mol Cell Biol* **37**, e00226-17 (2017).

321. Peng, B. *et al.* PARP1 and CHK1 coordinate PLK1 enzymatic activity during the DNA damage response to promote homologous recombination-mediated repair. *Nucleic Acids Research* **49**, 7554–7570 (2021).

322. Sørensen, C. S. *et al.* The cell-cycle checkpoint kinase Chk1 is required for mammalian homologous recombination repair. *Nat Cell Biol* **7**, 195–201 (2005).

323. Parsels, L. A. *et al.* Gemcitabine sensitization by Chk1 inhibition correlates with inhibition of a Rad51 DNA damage response in pancreatic cancer cells. *Molecular cancer therapeutics* **8**, 45 (2009).

324. Bahassi, E. M. *et al.* The checkpoint kinases Chk1 and Chk2 regulate the functional associations between hBRCA2 and Rad51 in response to DNA damage. *Oncogene* **27**, 3977–3985 (2008).

325. Yang, Z., Waldman, A. S. & Wyatt, M. D. Expression and regulation of RAD51 mediate cellular responses to chemotherapeutics. *Biochem Pharmacol* **83**, 741–746 (2012).

326. Chabot, T. *et al.* New Phosphorylation Sites of Rad51 by c-Met Modulates Presynaptic Filament Stability. *Cancers (Basel)* **11**, E413 (2019).

327. Haaf, T., Golub, E. I., Reddy, G., Radding, C. M. & Ward, D. C. Nuclear foci of mammalian Rad51 recombination protein in somatic cells after DNA damage and its localization in synaptonemal complexes. *Proc Natl Acad Sci U S A* **92**, 2298–2302 (1995).

328. Tashiro, S., Walter, J., Shinohara, A., Kamada, N. & Cremer, T. Rad51 Accumulation at Sites of DNA Damage and in Postreplicative Chromatin. *Journal of Cell Biology* **150**, 283–292 (2000).

329. Tashiro, S. *et al.* S phase specific formation of the human Rad51 protein nuclear foci in lymphocytes. *Oncogene* **12**, 2165–2170 (1996).

330. Tarsounas, M., Davies, D. & West, S. C. BRCA2-dependent and independent formation of RAD51 nuclear foci. *Oncogene* **22**, 1115–1123 (2003).

331. Mladenov, E., Anachkova, B. & Tsaneva, I. Sub-nuclear localization of Rad51 in response to DNA damage. *Genes Cells* **11**, 513–524 (2006).

332. Weis, K. Regulating Access to the Genome: Nucleocytoplasmic Transport throughout the Cell Cycle. *Cell* **112**, 441–451 (2003).

333. Thumser-Henner, P., Nytko, K. J. & Rohrer Bley, C. Mutations of BRCA2 in canine mammary tumors and their targeting potential in clinical therapy. *BMC Veterinary Research* **16**, 30 (2020).

334. Tarsounas, M., Davies, A. A. & West, S. C. RAD51 localization and activation following DNA damage. *Philosophical Transactions of the Royal Society of London. Series B: Biological Sciences* (2004) doi:10.1098/rstb.2003.1368.

335. Gildemeister, O. S., Sage, J. M. & Knight, K. L. Cellular Redistribution of Rad51 in Response to DNA Damage. *J Biol Chem* **284**, 31945–31952 (2009).

336. Popova, M., Henry, S. & Fleury, F. Posttranslational Modifications of Rad51 Protein and Its Direct Partners: Role and Effect on Homologous Recombination Mediated DNA Repair. in (2011). doi:10.5772/21409.

337. Garcin, E. B. *et al.* Differential Requirements for the RAD51 Paralogs in Genome Repair and Maintenance in Human Cells. *PLoS Genet* **15**, e1008355 (2019).

338. Shah, N. B. & Duncan, T. M. Bio-layer Interferometry for Measuring Kinetics of Protein-protein Interactions and Allosteric Ligand Effects. *J Vis Exp* 51383 (2014) doi:10.3791/51383.

339. Liu, J., Sneeden, J. & Heyer, W.-D. In vitro assays for DNA pairing and recombination-associated DNA synthesis. *Methods Mol Biol* **745**, 363–383 (2011).

340. Cretu, C. *et al.* Structural Basis of Splicing Modulation by Antitumor Macrolide Compounds. *Molecular Cell* **70**, 265-273.e8 (2018).

341. Pederiva, C., Böhm, S., Julner, A. & Farnebo, M. Splicing controls the ubiquitin response during DNA double-strand break repair. *Cell Death Differ* **23**, 1648–1657 (2016).

342. The UniProt Consortium. UniProt: the Universal Protein Knowledgebase in 2023. *Nucleic Acids Research* **51**, D523–D531 (2023).

343. Wang, C. *et al.* GPS 5.0: An Update on the Prediction of Kinase-specific Phosphorylation Sites in Proteins. *Genomics Proteomics Bioinformatics* **18**, 72–80 (2020).

344. Datta, A. *et al.* Phosphoproteomic Identification of Vasopressin-Regulated Protein Kinases in Collecting Duct Cells. *Br J Pharmacol* **178**, 1426–1444 (2021).

345. Desta, I. T., Porter, K. A., Xia, B., Kozakov, D. & Vajda, S. Performance and Its Limits in Rigid Body Protein-Protein Docking. *Structure* **28**, 1071-1081.e3 (2020).

346. Comeau, S. R., Gatchell, D. W., Vajda, S. & Camacho, C. J. ClusPro: a fully automated algorithm for protein–protein docking. *Nucleic Acids Res* **32**, W96–W99 (2004).

347. Kozakov, D. *et al.* The ClusPro web server for protein-protein docking. *Nat Protoc* **12**, 255–278 (2017).

348. Nelson, W. G. & Kastan, M. B. DNA strand breaks: the DNA template alterations that trigger p53-dependent DNA damage response pathways. *Molecular and Cellular Biology* **14**, 1815–1823 (1994).

349. Wang, J. Y. J. Cell death response to dna damage. *Yale Journal of Biology and Medicine* **92**, 771–779 (2019).

350. Krystyniak, A., Garcia-Echeverria, C., Prigent, C. & Ferrari, S. Inhibition of Aurora A in response to DNA damage. *Oncogene* **25**, 338–348 (2006).

351. Tarsounas, M., Davies, D. & West, S. C. BRCA2-dependent and independent formation of RAD51 nuclear foci. *Oncogene* **22**, 1115–1123 (2003).

352. Karanam, K., Kafri, R., Loewer, A. & Lahav, G. Quantitative Live Cell Imaging Reveals a Gradual Shift between DNA Repair Mechanisms and a Maximal Use of HR in Mid S Phase. *Molecular Cell* **47**, 320–329 (2012).

353. Orthwein A, Noordermeer SM, Wilson MD, Landry S, Enchev RI, Sherker A, Munro M, Pinder J, Salsman J, Dellaire G, Xia B, Peter M, D. D. E. 2015 D. 9. A mechanism for the suppression of homologous recombination in G1 cells. *Nature* **528 (7582)**, 422–6.

354. Francesca Storici1, Katarzyna Bebenek1, Thomas A. Kunkel1, Dmitry A. Gordenin1, and M. A. R. RNA-templated DNA repair. *Nature* **447**, 338–341 (2007).

355. Nowacka-Zawisza, M. *et al.* Loss of heterozygosity for chromosomal regions 15q14-21.1, 17q21.31, and 13q12.3-13.1 and its relevance for prostate cancer. *Medical Oncology* **32**, (2015).

356. Wijnhoven, S. W. P., Kool, H. J. M., Van Teijlingen, C. M. M., Van Zealand, A. A. & Vrieling, H. Loss of heterozygosity in somatic cells of the mouse: An important step in cancer initiation? *Mutation Research - Fundamental and Molecular Mechanisms of Mutagenesis* **473**, 23–36 (2001).

357. Alligand, B., Le Breton, M., Marquis, D., Vallette, F. & Fleury, F. Functional effects of diphosphomimetic mutations at cAbl-mediated phosphorylation sites on Rad51 recombinase activity. *Biochimie* **139**, 115–124 (2017).

358. Chabot, T. *et al.* New phosphorylation sites of rad51 by c-met modulates presynaptic filament stability. *Cancers* **11**, (2019).

359. Popova, M. *et al.* Detection of c-Abl kinase-promoted phosphorylation of Rad51 by specific antibodies reveals that Y54 phosphorylation is dependent on that of Y315. *FEBS Letters* **583**, 1867–1872 (2009).

360. Chandler, D. S., Singh, R. K., Caldwell, L. C., Bitler, J. L. & Lozano, G. Genotoxic stress induces coordinately regulated alternative splicing of the p53 modulators MDM2 and MDM4. *Cancer Research* **66**, 9502–9508 (2006).

361. Muñoz, M. J. *et al.* DNA Damage Regulates Alternative Splicing through Inhibition of RNA Polymerase II Elongation. *Cell* **137**, 708–720 (2009).

362. Qi, F. *et al.* Significance of alternative splicing in cancer cells. *Chinese medical journal* **133**, 221–228 (2020).

363. Climente-González, H., Porta-Pardo, E., Godzik, A. & Eyras, E. The Functional Impact of Alternative Splicing in Cancer. *Cell Reports* **20**, 2215–2226 (2017).

364. Pederiva, C., Böhm, S., Julner, A. & Farnebo, M. Splicing controls the ubiquitin response during DNA double-strand break repair. *Cell Death and Differentiation* **23**, 1648–1657 (2016).

365. Katzenberger, R. J., Marengo, M. S. & Wassarman, D. A. ATM and ATR Pathways Signal Alternative Splicing of Drosophila TAF1 Pre-mRNA in Response to DNA Damage. *Molecular and Cellular Biology* **26**, 9256–9267 (2006).

366. Matsuoka, S. *et al.* ATM and ATR substrate analysis reveals extensive protein networks responsive to DNA damage. *Science* **316**, 1160–1166 (2007).

367. Shkreta, L. & Chabot, B. The RNA splicing response to DNA damage. *Biomolecules* **5**, 2935–2977 (2015).

368. Dunn, K. W., Kamocka, M. M., & McDonald, J. H. A practical guide to evaluating colocalization in biological microscopy. *American journal of physiology. Cell physiology, 300(4), C723–C742. https://doi.org/10.1152/ajpcell.00462.2010* **300**, 2011 (2011).

369. Zinchuk, V., Wu, Y. & Grossenbacher-Zinchuk, O. Bridging the gap between qualitative and quantitative colocalization results in fluorescence microscopy studies. *Scientific Reports* **3**, 1–5 (2013).

370. Mcdonald, J. H. & Dunn, K. W. Statistical tests for measures of colocalization in biological microscopy. *Journal of Microscopy* **252**, 295–302 (2013).

371. Rogakou, E. P., Pilch, D. R., Orr, A. H., Ivanova, V. S. & Bonner, W. M. DNA double-stranded breaks induce histone H2AX phosphorylation on serine 139. *Journal of Biological Chemistry* **273**, 5858–5868 (1998).

372. Van Alphen, R. J., Wiemer, E. A. C., Burger, H. & Eskens, F. A. L. M. The spliceosome as target for anticancer treatment. *British Journal of Cancer* **100**, 228–232 (2009).

373. Feretzaki, M. *et al.* RAD51-dependent recruitment of TERRA lncRNA to telomeres through R-loops. *Nature* **in press**, (2020).

374. Chen, L. T. *et al.* Crystal structure of the left-handed archaeal RadA helical filament: Identification of a functional motif for controlling quaternary structures and enzymatic functions of RecA family proteins. *Nucleic Acids Research* **35**, 1787–1801 (2007).

375. Sourisseau, T. *et al.* Aurora-A expressing tumour cells are deficient for homology-directed DNA double strand-break repair and sensitive to PARP inhibition. *EMBO Molecular Medicine* **2**, 130–142 (2010).

376. Carvalho, T., Martins, S., Rino, J., Marinho, S. & Carmo-Fonseca, M. Pharmacological inhibition of the spliceosome subunit SF3b triggers exon junction complex-independent nonsense-mediated decay. *Journal of Cell Science* **130**, 1519–1531 (2017).

377. Damodaran, A. P. *et al.* Aurora-A phosphorylates splicing factors and regulates alternative splicing. *bioRxiv* (2020) doi:10.1101/2020.11.04.368498.

378. Sciarrillo, R. *et al.* The role of alternative splicing in cancer: From oncogenesis to drug resistance. *Drug Resistance Updates* **53**, (2020).

379. Chen, M. *et al.* GPS 6.0: an updated server for prediction of kinase-specific phosphorylation sites in proteins. *Nucleic Acids Research* **51**, W243–W250 (2023).

380. Kothe, M. *et al.* Structure of the Catalytic Domain of Human Polo-like Kinase 1,. *Biochemistry* **46**, 5960–5971 (2007).

381. Seki, A., Coppinger, J. A., Jang, C.-Y., Yates, J. R. & Fang, G. Bora and the kinase Aurora a cooperatively activate the kinase Plk1 and control mitotic entry. *Science* **320**, 1655–1658 (2008).

382. Nowakowski, J. *et al.* Structures of the Cancer-Related Aurora-A, FAK, and EphA2 Protein Kinases from Nanovolume Crystallography. *Structure* **10**, 1659–1667 (2002).

383. Bayliss, R., Sardon, T., Vernos, I. & Conti, E. Structural Basis of Aurora-A Activation by TPX2 at the Mitotic Spindle. *Molecular Cell* **12**, 851–862 (2003).

384. Tavernier, N., Sicheri, F. & Pintard, L. Aurora A kinase activation: Different means to different ends. *Journal of Cell Biology* **220**, e202106128 (2021).

385. Valbuena, A. *et al.* Identification of a dominant epitope in human vaccinia-related kinase 1 (VRK1) and detection of different intracellular subpopulations. *Archives of Biochemistry and Biophysics* **465**, 219–226 (2007).

386. Elkins, J. M., Santaguida, S., Musacchio, A. & Knapp, S. Crystal Structure of Human Aurora B in Complex with INCENP and VX-680. *J. Med. Chem.* **55**, 7841–7848 (2012).

387. Goldenson, B. & Crispino, J. D. The aurora kinases in cell cycle and leukemia. *Oncogene* **34**, 537–545 (2015).

388. Nomme, J. *et al.* Design of potent inhibitors of human RAD51 recombinase based on BRC motifs of BRCA2 protein: modeling and experimental validation of a chimera peptide. *J Med Chem* **53**, 5782–5791 (2010).

389. Nomme, J. *et al.* Inhibition of filament formation of human Rad51 protein by a small peptide derived from the BRC-motif of the BRCA2 protein. *Genes Cells* **13**, 471–481 (2008).

390. Subramanyam, S., Ismail, M., Bhattacharya, I. & Spies, M. Tyrosine phosphorylation stimulates activity of human RAD51 recombinase through altered nucleoprotein filament dynamics. *Proceedings of the National Academy of Sciences* **113**, E6045–E6054 (2016).

391. Feretzaki, M. *et al.* RAD51-dependent recruitment of TERRA lncRNA to telomeres through R-loops. *Nature* **587**, 303–308 (2020).

392. Azzalin, C. M., Reichenbach, P., Khoriauli, L., Giulotto, E. & Lingner, J. Telomeric Repeat–Containing RNA and RNA Surveillance Factors at Mammalian Chromosome Ends. *Science* **318**, 798–801 (2007).

393. Redon, S., Zemp, I. & Lingner, J. A three-state model for the regulation of telomerase by TERRA and hnRNPA1. *Nucleic Acids Research* **41**, 9117–9128 (2013).

394. Arora, R. *et al.* RNaseH1 regulates TERRA-telomeric DNA hybrids and telomere maintenance in ALT tumour cells. *Nat Commun* **5**, 5220 (2014).

395. Mladenov, E., Anachkova, B. & Tsaneva, I. Sub-nuclear localization of Rad51 in response to DNA damage. *Genes to Cells* **11**, 513–524 (2006).

396. Faber, G. P., Nadav-Eliyahu, S. & Shav-Tal, Y. Nuclear speckles – a driving force in gene expression. *Journal of Cell Science* **135**, jcs259594 (2022).

397. Morozumi, Y., Takizawa, Y., Takaku, M. & Kurumizaka, H. Human PSF binds to RAD51 and modulates its homologous-pairing and strand-exchange activities. *Nucleic Acids Research* **37**, 4296–4307 (2009).

398. Spector, D. L. & Lamond, A. I. Nuclear Speckles. *Cold Spring Harb Perspect Biol* **3**, a000646 (2011).

399. Mintz, P. J., Patterson, S. D., Neuwald, A. F., Spahr, C. S. & Spector, D. L. Purification and biochemical characterization of interchromatin granule clusters. *The EMBO Journal* **18**, 4308–4320 (1999).

400. Ilık, İ. A. & Aktaş, T. Nuclear speckles: dynamic hubs of gene expression regulation. *The FEBS Journal* **289**, 7234–7245 (2022).

401. Matsui, M. *et al.* USP42 enhances homologous recombination repair by promoting R-loop resolution with a DNA–RNA helicase DHX9. *Oncogenesis* **9**, 60 (2020).

402. Zinchuk, V., Wu, Y. & Grossenbacher-Zinchuk, O. Bridging the gap between qualitative and quantitative colocalization results in fluorescence microscopy studies. *Sci Rep* **3**, 1365 (2013).

403. Kotake, Y. *et al.* Splicing factor SF3b as a target of the antitumor natural product pladienolide. *Nat Chem Biol* **3**, 570–575 (2007).

404. Carvalho, T., Martins, S., Rino, J., Marinho, S. & Carmo-Fonseca, M. Pharmacological inhibition of the spliceosome subunit SF3b triggers EJC-independent NMD. *Journal of Cell Science* jcs.202200 (2017) doi:10.1242/jcs.202200.

405. O'Keefe, R., Mayeda, A., Sadowski, C., Krainer, A. & Spector, D. Disruption of pre-mRNA splicing in vivo results in reorganization of splicing factors. *Journal of Cell Biology* **124**, 249–260 (1994).

406. Ye, F. *et al.* Insights Into the Impacts of BRCA Mutations on Clinicopathology and Management of Early-Onset Triple-Negative Breast Cancer. *Frontiers in Oncology* **10**, (2021).

407. Hartman, A.-R. *et al.* Prevalence of BRCA mutations in an unselected population of triple-negative breast cancer. *Cancer* **118**, 2787–2795 (2012).

408. Yoon, S.-W., Kim, D.-K., Kim, K. P. & Park, K.-S. Rad51 Regulates Cell Cycle Progression by Preserving G2/M Transition in Mouse Embryonic Stem Cells. *Stem Cells Dev* **23**, 2700–2711 (2014).

409. Damodaran, A. P. *et al.* Aurora-A phosphorylates splicing factors and regulates alternative splicing. 2020.11.04.368498 Preprint at https://doi.org/10.1101/2020.11.04.368498 (2020).

410. Berchtold, D., Battich, N. & Pelkmans, L. A Systems-Level Study Reveals Regulators of Membrane-less Organelles in Human Cells. *Molecular Cell* **72**, 1035-1049.e5 (2018).

411. Campillo-Marcos, I. & Lazo, P. A. Implication of the VRK1 chromatin kinase in the signaling responses to DNA damage: a therapeutic target? *Cell Mol Life Sci* **75**, 2375–2388 (2018).

412. Sanz-García, M., Monsalve, D. M., Sevilla, A. & Lazo, P. A. Vaccinia-related Kinase 1 (VRK1) Is an Upstream Nucleosomal Kinase Required for the Assembly of 53BP1 Foci in Response to Ionizing Radiation-induced DNA Damage *. *Journal of Biological Chemistry* **287**, 23757–23768 (2012).

413. Cantarero, L. *et al.* VRK1 regulates Cajal body dynamics and protects coilin from proteasomal degradation in cell cycle. *Sci Rep* **5**, 10543 (2015).

414. Mao, Y. S., Zhang, B. & Spector, D. L. Biogenesis and Function of Nuclear Bodies. *Trends Genet* **27**, 295–306 (2011).

415. Stepanova, I. S., Bogolyubov, D. S., Skovorodkin, I. N. & Parfenov, V. N. Cajal bodies and interchromatin granule clusters in cricket oocytes: composition, dynamics and interactions. *Cell Biol Int* **31**, 203–214 (2007).

416. Bogolyubov, D. S. & Bogolyubova, I. O. SC35 Splicing factor and coilin are colocalized within the "endobodies" in oocytes of the spider Araneus diadematus. *Cell Tiss. Biol.* **1**, 352–356 (2007).

417. Moura, D. S., Campillo-Marcos, I., Vázquez-Cedeira, M. & Lazo, P. A. VRK1 and AURKB form a complex that cross inhibit their kinase activity and the phosphorylation of histone H3 in the progression of mitosis. *Cell. Mol. Life Sci.* **75**, 2591–2611 (2018).

Appendices

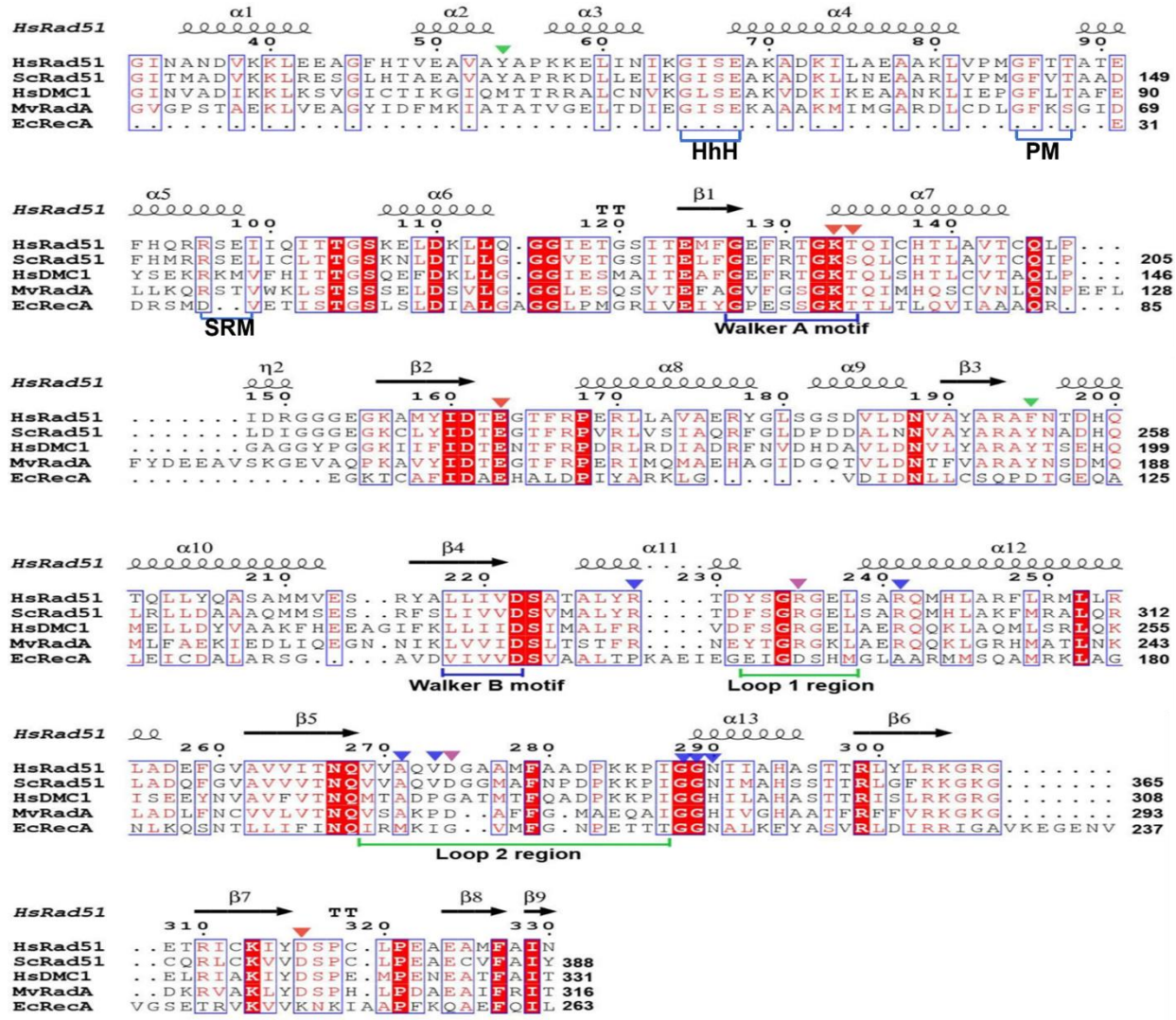

Appendix 1 Human RAD51 and its orthologs sequence alignment.

Sequence alignment of RecA family proteins from H. sapiens (HsRad51 and HsDmc1), S. cerevisiae (ScRad51), M. voltae (MvRadA), and E. coli (EcRecA). On top of the corresponding residues, the secondary structural elements of human RAD51 are identified. Functional motifs are indicated under their corresponding amino acid sequences: the putative dsDNA binding HhH motif, the polymerization motif (PM), the subunit rotation motif (SRM), the ATP-binding Walker A and B motifs, and the putative ssDNA-binding L1 and L2 loops. The essential residues for human RAD51 function are all labeled. The green triangles indicate Y54 and F195, which are situated at the interface between human RAD51 protomers. The red triangles indicate K133, T134, E163, and D316, which interact with AMP-PNP-Mg2+. The blue triangles point to R229, R241, A271, V273, G288, G289, and N290 residues involved in ssDNA binding. Lastly, the magenta triangles indicate R235 and D274, which are involved in dsDNA binding Figure is adapted from [182,190].

PDB code	Name	Organism	Method and Resolution	Ligands and Environments	Entry DOI
8BR2	CryoEM structure of the post-synaptic RAD51 NPF in the presence of ATP and Ca2+	*H. sapiens*	EM, 2.9 Å	CA ATP	iScience (2023) [PMID: 37216117
8BQ2	CryoEM structure of the pre-synaptic RAD51 NPF in the presence of ATP and Ca2+	*H. sapiens*	EM, 3.8 Å	CA ATP	iScience (2023) [PMID: 37216117
8BSC	CryoEM structure of the RAD51 NPF in the presence of ADP and Ca2+	*H. sapiens*	EM, 3.6 Å	CA ADP	iScience (2023) [PMID: 37216117
7EJC	human RAD51 presynaptic complex	*H. sapiens*	EM, 3.97 Å	J46 MG ANP	Nucleic Acids Res (2021) [PMID: 34871438
7EJE	human RAD51 post-synaptic complex	*H. sapiens*	EM, 3.98 Å	MG ANP	Nucleic Acids Res (2021) [PMID: 34871438
7C9A	Human RAD51 post-synaptic complexes mutant (V273P, D274G)	*H. sapiens*	EM, 4.2 Å	CA ANP	Nat Commun (2021) [PMID: 33446654
5NWL	Crystal structure of a human RAD51-ATP filament.	*H. sapiens*	X-ray, 3.93 Å	MG ATP	EMBO J (2018) [PMID: 29507080
5NP7	CryoEM structure of Human Rad51 on single-stranded DNA to 4.2A resolution.	*H. sapiens*	EM, 4.2 Å	ANP	Nucleic Acids Res (2016) [PMID: 27596592
5H1B	Human RAD51 presynaptic complex	*H. sapiens*	EM, 4.4 Å	MG ANP	Nat Struct Mol Biol (2017) [PMID: 27941862
5H1C	Human RAD51 post-synaptic complexes	*H. sapiens*	EM, 4.5 Å	MG ANP	Nat Struct Mol Biol (2017) [PMID: 27941862
5JZC	Helical filament	*H. sapiens*	EM, 4.2 Å		Nucleic Acids Res (2016) [PMID: 27596592
1N0W	Crystal structure of a RAD51-BRCA2 BRC repeat complex	*H. sapiens*	X-ray, 1.7 Å	CL EDO MG	Nature (2002) [PMID: 12442171
1B22	RAD51 (N-TERMINAL DOMAIN)	*H. sapiens*	NMR		J Mol Biol (1999) [PMID: 10390347
7qv8	Leishmania infantum BRC1 repeat in complex with LiRAD51	*L. infantum*	X-ray, 2.15 Å	MG ADP	Biochem J (2022) [PMID: 35502837
3lda	Yeast Rad51 H352Y Filament Interface Mutant	*S. cerevisiae*	X-ray, 2.5 Å	CL	Nucleic Acids Res (2010) [PMID: 20371520
1szp	A Crystal Structure of the Rad51 Filament	*S.cerevisiae*	X-ray, 3.25 Å	SO4	Nat Struct Mol Biol (2004) [PMID: 15235592

Appendix 2 Crystallography structures of RAD51 and its filaments in the Protein Data Bank (PDB).

In the PDB, there are currently 16 crystallography structures available for RAD51. Of these, 13 are for *Homo sapiens*, 2 are for *Saccharomyces cerevisiae*, and 1 is for *Leishmania infantum*.

Aurora A mediates the phosphorylation of RAD51 on Serine 97, which it is observed in Nuclear Speckles.

Mohamad Alaouid, Parfait Kenfack Ymbe, Vanessa Philippot-Ménil, Gwennina Cueff, Alexandre Demeyer, Damien Marquis, Nizar Ayadi, Fabrice Fleury, Houda Benhelli-Mokrani

DNA Repair team, US2B, CNRS UMR 6286,UFR Sciences & Technique, Nantes Université, NANTES, France

Mohamad.alaouid@univ-nantes.fr

Background

Based on previous research, DNA double-strand breaks (DSBs) are considered to be the most severe type of DNA damage, which can lead to chromosomal abnormalities and cell death if not repaired properly. However, under normal conditions, the cell undergoes a series of DNA damage response mechanisms to avoid genomic instability. Over-expression of RAD51, a DNA repair protein, has been linked to chemo-resistance in many cancers, making it a potential target for cancer therapy [1]. Therefore, it is essential to understand how to control RAD51 activity to achieve therapeutic purposes.

Phosphorylation is one of the post-translational modifications that cells use naturally to regulate protein functions. Recently, we identified a new phosphorylation site on RAD51's serine 97, which is mediated by Aurora A kinase. Using a specifically generated antibody, the presence of pSer97-RAD51 has been confirmed in cellular contexts, and its level show changes after Aurora A inhibition or overexpression.
Moreover, it has been observed that this novel RAD51 form is present throughout the cell cycle, with a peak in the G2/M phase.

Interestingly, the phosphorylation of Ser97 appears to be associated with the localization of RAD51 within Nuclear Speckles, which are involved in RNA maturation. This raises the exciting possibility that RAD51 may play a role in splicing modulation, which is particularly relevant in the context of splicing profile modulations linked with cancer therapy resistance.

The Serine 97 residue of RAD51 is phosphorylated by Aurora-A kinase

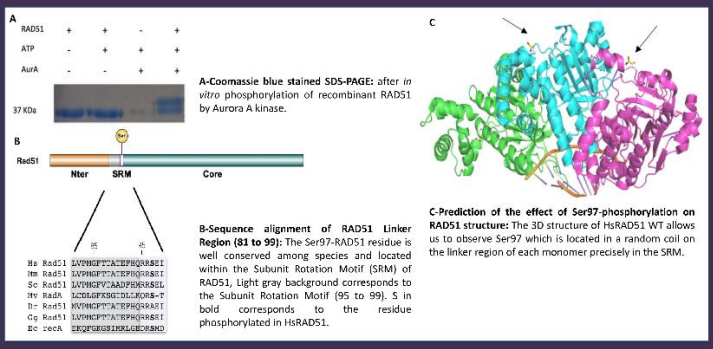

A-Coomassie blue stained SDS-PAGE: after *in vitro* phosphorylation of recombinant RAD51 by Aurora A kinase.

B-Sequence alignment of RAD51 Linker Region (81 to 99): The Ser97-RAD51 residue is well conserved among species and located within the Subunit Rotation Motif (SRM) of RAD51, Light gray background corresponds to the Subunit Rotation Motif (95 to 99). S in bold corresponds to the residue phosphorylated in HsRAD51.

C-Prediction of the effect of Ser97-phosphorylation on RAD51 structure: The 3D structure of HsRAD51 WT allows us to observe Ser97 which is located in a random coil on the linker region of each monomer precisely in the SRM.

in cellulo validation of PSer97-RAD51 presence

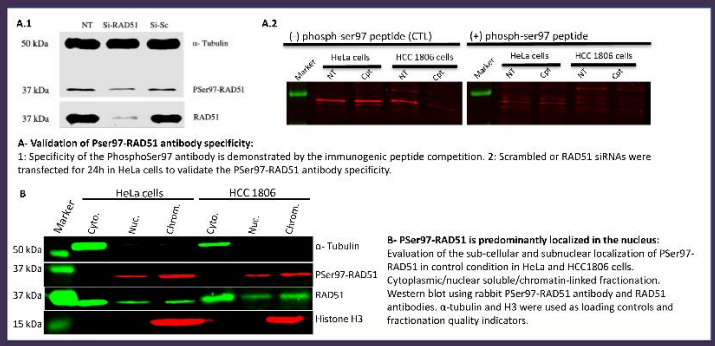

A- Validation of Pser97-RAD51 antibody specificity:
1: Specificity of the PhosphoSer97 antibody is demonstrated by the immunogenic peptide competition. 2: Scrambled or RAD51 siRNAs were transfected for 24h in HeLa cells to validate the PSer97-RAD51 antibody specificity.

B- PSer97-RAD51 is predominantly localized in the nucleus: Evaluation of the sub-cellular and subnuclear localization of PSer97-RAD51 in control condition in HeLa and HCC1806 cells. Cytoplasmic/nuclear soluble/chromatin-linked fractionation. Western blot using rabbit PSer97-RAD51 antibody and RAD51 antibodies. α-tubulin and H3 were used as loading controls and fractionation quality indicators.

PSer97-RAD51/RAD51 ratio is dynamic during the cell cycle progression

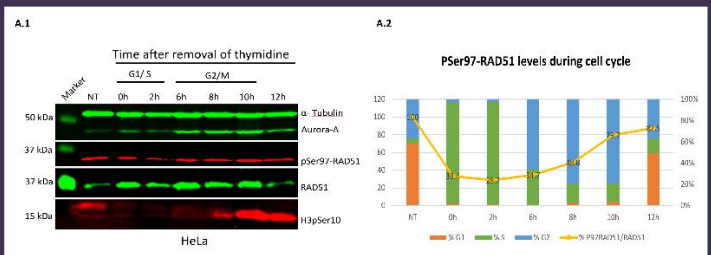

A-Cell Synchronization by Double Thymidine Block:
1: Western blot of PSer97-RAD51 protein levels for the total synchronized HeLa.
2: Densitometric analyses of western blot of total synchronized HeLa show the distribution of pS97-RAD51 during different cell cycle phases.

Aurora A inhibition or overexpression alters the levels of PSer97-RAD51

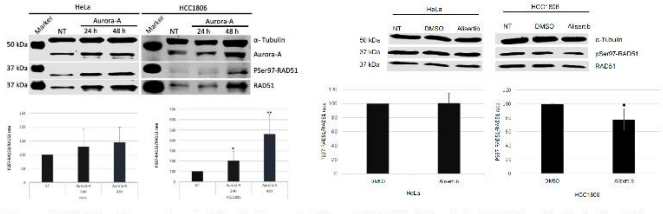

HeLa and HCC1806 cells were transfected with Aurora-A plasmid: (Up panel) western blots were done with whole cell extracts. (Down panel) the PSer97-RAD51/RAD51 ratio was calculated. Statistical analysis was done for n=3 experiments.

HeLa and HCC1806 cells treated with DMSO or Alisertib for 24 and 48 hours: (Up panel) western blots for the corresponding proteins. (Down panel) statistical analyses of Pser97-RAD51 and RAD51 was done for n=3 experiments.

PSer97-RAD51 foci are not localized in DNA damaged sites

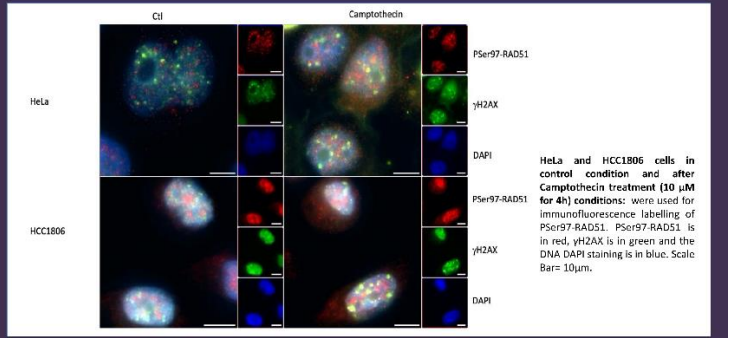

HeLa and HCC1806 cells in control condition and after Camptothecin treatment (10 µM for 4h) conditions: were used for immunofluorescence labelling of PSer97-RAD51. PSer97-RAD51 is in red, γH2AX is in green and the DNA DAPI staining is in blue. Scale Bar= 10µm.

PSer97-RAD51 nuclear foci are localized within Nuclear Speckles

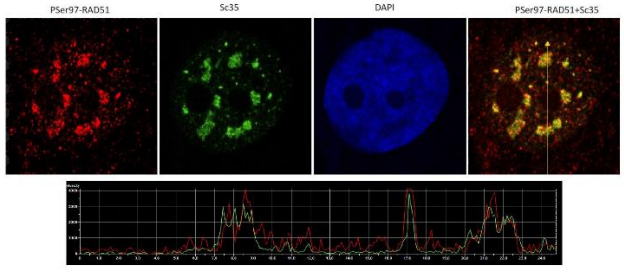

Line scan analysis showing the PSer97-RAD51 and Sc35 signal intensities along the arrow, (HeLa cells).

Conclusion & Perspectives

Our study reveals that Aurora A phosphorylates serine 97 residue of RAD51. Our findings demonstrate that PSer9-RAD51 is present in cells at all cell cycle stages and is mostly located in the nucleus as a chromatin-bound form. We also discovered that the overexpression of Aurora A significantly increases PSer97, and inhibiting Aurora A catalytic activity by Alisertib reduces PSer97 levels in a cell line-dependent manner, raising the question of kinase redundancy. Our research also reveals that RAD51 is present within the RNA maturation site, Nuclear speckles, which opens further avenues of investigation into the link between DNA repair and alternative splicing regulation.

However, to further investigate the biological role of pSer97-RAD51, it is crucial to create a CRISPR Ser97-RAD51 Knock-In cell line with a single-point mutation. This approach will allow for the study of the specific effects of Ser97 phosphorylation in RAD51 and its potential impact on DNA repair processes.

References:

1- *Liao, C., Talluri, S., Zhao, J., Mu, S., Kumar, S., Shi, J., Buon, L., Munshi, N.C. and Shammas, M.A.*, 2022. RAD51 Is Implicated in DNA Damage, Chemoresistance and Immune Dysregulation in Solid Tumors. *Cancers*, *14*(22), p.5697.
2- *Alaouid, M., Kenfack Ymbe, P., Philippot-Ménil, V., Cueff, G., Demeyer, A., Marquis, D., Ayadi, N., Fleury, F. and Benhelli-Mokrani, H.*, 2023. Aurora A mediated new phosphorylation of RAD51 is observed in Nuclear Speckles. Under revision at Review Commons, *EMBO*.

Titre: La caractérisation d'un nouveau site de phosphorylation de RAD51 sur le résidu sérine 97.

Mots clés : CDBs, RH, Phosphorylation de RAD51

Résumé : Dans les cellules, les cassures double brin de l'ADN (CDBs) constituent les types de dommages à l'ADN les plus dangereux. Si les CBDs s'accumulent à des niveaux élevés, ils peuvent entraîner des mutations potentiellement cancérigènes. La voie de réparation par Recombinaison Homologue (RH) est une voie de réparation fidèle que les cellules utilisent pour réparer ce type de dommage à l'ADN.
La recombinase RAD51 est une protéine essentielle impliquée dans cette voie. Des études suggèrent que la dérégulation de RAD51 contribue à la chimio-résistance résistance de nombreux cancers. L'étude de la phosphorylation est un facteur clé dans la compréhension de la régulation d'activité de RAD51.
Notre laboratoire a déjà montré *in vitro* que la kinase Aurora A peut phosphoryler le résidu Ser97 dans la Subunit Rotation Motif (SRM) du domaine de liaison de RAD51. Dans cette étude, nous avons révélé à l'aide d'études *in vitro* que la phosphorylation de RAD51 sur son Ser97 affecte sa capacité à médier l'invasion des brins complémentaires et l'auto-association de monomères de RAD51. De plus, nous avons constaté que RAD51 possède une affinité de liaison avec l'ARN et que la phosphorylation de Ser97 module cette affinité. nous avons confirmé la présence de PSer97-RAD51 dans les cellules à toutes les phases du cycle cellulaire et avons constaté qu'il est principalement localisé dans le noyau. Étonnamment, nous n'avons pas trouvé corrélation claire entre PSer97-RAD51 et la réponse aux dommages à l'ADN. En revanche PSer97-RAD51 est colocalisé avec les Nuclear Speckles (NS) ce qui suggère que cette phosphorylation nouvellement identifiée pourrait guider RAD51 à jouer un nouveau rôle. Cependant les mécanismes moléculaires expliquant la fonction précise de RAD51 phosphorylé dans le NS nécessitent des recherches plus approfondies.

Title: *In vitro* and *in cellulo* profiling of a novel phosphorylated form of RAD51 at serine 97.

Keywords : DSBs, HRR, RAD51 phosphorylation

Abstract: DNA double-strand breaks (DSBs) are the most genotoxic type of DNA damage that can occur inside cells. The accumulation of high levels of DSBs within the cell may promote cancer-causing mutations. The homologous recombination repair (HRR) pathway is an error-free repair mechanism that cells use to fix this kind of DNA damage.
RAD51 recombinase, a vital protein, is involved in this pathway. Studies indicate that the uncontrolled activity of RAD51 contributes to the therapy resistance observed in various types of cancer. The activity of RAD51 can be altered by phosphorylation, which is an important factor that has to be more investigated.
Based on prior *in vitro* results obtained in our lab, we demonstrated that Aurora A kinase phosphorylates RAD51 on Ser97 within the Subunit Rotation Motif (SRM) in its linker domain.
Using *in vitro* investigations, we observed that RAD51 phosphorylation at Ser97 alters its ability to facilitate complementary strand invasion and impacts the self-association of RAD51 monomers. Furthermore, we identified that RAD51 has RNA binding affinity, which is modulated by this Ser97 phosphorylation. Moreover, we confirmed the presence of PSer97-RAD51 in cells and revealed that it is present during all cell cycle phases. Furthermore, our findings showed that PSer97-RAD51 is mainly found in the nucleus and colocalized within the nuclear speckles (NS). We found no apparent relationship between PSer97-RAD51 and the response to DNA damage, implying that this newly discovered phosphorylation could direct RAD51 to a novel functional role. However, the precise role of this phosphorylated RAD51 remains unclear and requires further investigation.